RADIOSCIENCE LABORATORY

STANFORD ELECTRONICS LABORATORIES
DEPARTMENT OF ELECTRICAL ENGINEERING
STANFORD UNIVERSITY · STANFORD, CA 94305

NONLINEAR LONGITUDINAL RESONANCE INTERACTION OF ENERGETIC CHARGED PARTICLES AND VLF WAVES IN THE MAGNETOSPHERE

By

Slobodan Tkalcevic

May 1982

Technical Report E4-2311

Prepared Under

Division of Polar Programs of the National Science Foundation
Grants NSF-DPP80-22282 and DPP80-22540

Atmospheric Sciences Section of the National Science Foundation
Grant ATM80-18248

National Aeronautics and Space Administration
Grant NGL-05-020-008

ABSTRACT

This study treats the longitudinal resonance of waves and energetic electrons in the earth's magnetosphere, and the possible role this resonance may play in generating various magnetospheric phenomena. The first part of the study is concerned with the derivation of time-averaged nonlinear equations of motion for energetic particles longitudinally resonant with a whistler mode wave propagating with non-zero wave normal. It is shown that the wave magnetic forces can be neglected at lower particle pitch angles, while they become equal to or larger than the wave electric forces for $\alpha>30°$. The time-averaged equations of motion were used in test particle simulations which were done for a wide range of wave amplitudes, wave-normals, particle pitch angles, particle parallel velocities, and in an inhomogeneous medium such as the magnetosphere. It was found that there are two classes of particles, trapped and untrapped, and that the scattering and energy exchange for those two groups exhibit significantly different behavior. The trapped particles are characterized by a bounded phase variation (with respect to the wave) which is less then 2π, whereas the phase variation of untrapped particles is unbounded. It is also found that the trapping of the particles requires that the wave amplitude exceed a certain threshold value, and that the trapped electrons become space bunched due to the interaction. The full distribution simulations indicate that the expected particle precipitation is considerably smaller (one order of magnitude) compared to gyroresonance-induced precipitation for waves of comparable amplitude, which shows that the scattering efficiency of the longitudinal resonance is small. The amplitude threshold effect, together with the space bunching effect, was found to support one of the mechanisms suggested to explain whistler precursors.

ACKNOWLEDGMENTS

This research was supervised by Professors R. A. Helliwell and D. L. Carpenter. The author wishes to thank them for their guidance and support, and for many helpful discussions during the course of this work. I wish to express appreciation to Dr. C. G. Park who first interested me in problems of longitudinal resonance interaction.

I would also like to thank Drs. U. S. Inan and T. F. Bell for their cooperation and many valuable discussions. Thanks are also due to W. Terluin who drafted the figures, and to K. Dean and K. Feas who assisted with the typescript.

This research was supported in part by NASA under grant NGL-05-020-008, in part by the Division of Polar Programs of the National Science Foundation under grants DPP80-22282 and DPP80-22540, and in part by the Division of Atmospheric Sciences of NSF under grant ATM80-18248. Much of the computer modeling was done by remote job entry using the facilities of the National Center for Atmospheric Research which is sponsored by the National Science Foundation.

TABLE OF CONTENTS

TABLE OF CONTENTS (Cont.)

LIST OF TABLES

LIST OF TABLES (Cont.)

ILLUSTRATIONS

ILLUSTRATIONS (Cont.)

ILLUSTRATIONS (Cont.)

I. INTRODUCTION

A. ORGANIZATION OF MATERIAL

This study treats longitudinal resonance interactions between energetic electrons and VLF waves in the earth's magnetosphere. The aim was to derive suitable analytical methods for test particle studies, and then to use those methods to investigate various aspects of the longitudinal resonance process.

The first part of the study is concerned with the derivation of equations of motion and their applications to the longitudinal resonance for a wide range of magnetospheric parameters. The second part gives the results of the numerical simulation of wave-particle interactions. The numerical simulations are done using a test particle approach to determine the perturbations of pitch angle for various wave functions. Also investigated are the perturbations of the full particle distribution and the energy exchange process.

In conclusion the longitudinal resonance interaction is compared to the cyclotron resonance interaction, and is related to phenomena observed in the magnetosphere.

B. WAVE-PARTICLE INTERACTIONS IN THE MAGNETOSPHERE

The magnetosphere, a magnetized region extending from about 1000 km altitude up to distance of roughly 100,000 km from the earth, is filled with both 'cold' and 'hot' plasma; the cold plasma consists of electrons and protons with energies in the 0.1-1 eV range, while the hot plasma consists of energetic particles with higher energies in the range from 100 eV to tens of MeV. The cold plasma together with the earth's static magnetic field determines the wave propagation properties of the magnetosphere. The hot plasma is a source of energetic particles which participate in the wave-particle interactions that result in radio wave emissions. As seen from both ground and satellite observations the magnetosphere supports numerous modes of wave propagation. It can be shown that the hot plasma, due to its very low density, does not affect the wave dispersion properties of the magnetosphere, i.e. the dispersion of waves can be explained assuming that only cold plasma is present.

It is known that very-low-frequency waves can propagate in the magnetosphere with phase velocities much smaller than the velocity of light, and that those waves, called whistler-mode waves, can undergo interactions with energetic particles both through longitudinal resonance and cyclotron (gyro) resonance. In longitudinal resonance the particle parallel velocity is matched to the wave phase velocity, whereas in the cyclotron resonance the doppler-shifted frequency of the wave (shifted due to the particle parallel velocity) matches the gyrofrequency of the energetic particle. Both types of interactions may induce perturbations of the energetic particle distribution through

pitch angle scattering, and may also result in different types of radio wave emissions, wave amplification (growth) and wave attenuation. The purpose of this study is to investigate the longitudinal resonance interactions of energetic particles with whistler mode signals propagating at an oblique angle to the static magnetic field. The approach taken is to use a test particle analysis and to study how the resonance process depends on various parameters. The particle trajectories are then used to estimate other effects such as wave growth/damping and particle trapping and precipitation. The trajectory calculations were done using a set of nonlinear equations of motion which are averaged over one gyroperiod [Inan and Tkalcevic, 1982].

C. PREVIOUS WORK ON LONGITUDINAL RESONANCE

The longitudinal resonance process has been invoked by many authors to explain various magnetospheric wave phenomena. One of the early works considered the traveling-wave-tube type of process as a generation mechanism for VLF emissions [Gallet and Helliwell, 1959], and this process was also considered for amplification of whistler mode signals [Brice, 1961]. The traveling-wave-tube mechanism was also considered by Dowden [1962] as a possible mechanism of hiss generation. Bell [1964] derived linearized solutions for the trajectories of longitudinally resonant particles, but these have not been extended to cover the nonlinear regime. The various emission-generation theories have been reviewed by Brice [1964], including both Cerenkov radiation and the traveling wave amplification hypothesis. The Cerenkov mechanism

is a process in which charged particles radiate electromagnetic waves as they travel through a medium. The necessary condition for the existence of this type of radiation, called a coherence condition, is easily found, and is the same as the condition required for the longitudinal interaction between the wave and the particle. Therefore, it is evident that those two processes, the longitudinal resonance interactions and Cerenkov radiation, are based on the same physical principle.

The Cerenkov radiation mechanism has been suggested by many authors [Ellis, 1959,1960; Dowden, 1960; McKenzie, 1963] in order to explain VLF hiss. The problem of stability of whistler mode signals, i.e. the possibility of wave growth, accounting both for longitudinal and gyroresonance effects, was discussed by Kennel and Petschek [1966], Kennel and Thorne [1967], and also by Brinca [1972]. The work on radiation from moving charged particles, which includes Cerenkov radiation, includes the analysis done by Liemohn [1965], Mansfield [1967], and Seshadri [1967]. A good review of work done on Cerenkov radiation, along with additional analysis of the hiss power density spectrum, was given by Taylor and Shawhan [1974]. Their work gives examples of the power spectral density of hiss, both measured [Gurnett, 1966; Gurnett and Frank, 1972], and calculated [Jorgensen, 1968; Lim and Laaspere, 1972]. Swift and Kan [1975] showed that an electron beam can excite a whistler mode instability near the resonance cone through the longitudinal resonance interaction. Maggs [1976] and Kumagai at al. [1980] investigated beam amplification due to Cerenkov radiation from longitudinally resonant electrons, and considered this type of beam instability as a generating mechanism of VLF hiss. The whistler

precursor generation mechanism of Park and Helliwell [1977] was based on modifications of the particle distribution function achieved through longitudinal interaction between whistlers and energetic electrons.

Most of the above studies were primarily concerned with wave growth calculations using the wave dispersion relation. On the other hand, the detailed nonlinear motion of longitudinally resonant particles was studied only for the case of electrostatic waves [Nunn, 1971; 1973]. Palmadesso [1973] derived equations of motion for a case of oblique propagation, and used particle trajectories to estimate the nonlinear time dependent Landau damping rate of the wave.

D. CONTRIBUTIONS OF THE PRESENT WORK

The motion of electrons longitudinally resonant with a whistler mode wave propagating at an angle to the static magnetic field is represented by a simple set of equations motion which are averaged over the cyclotron period. It is shown that these nonlinear equations are a very accurate representation of the electron motion for a wide range of magnetospheric parameters.

Using the time-averaged nonlinear equations of motion in numerical simulations involving whistler mode signals propagating in an inhomogeneous medium it was found that the effects of wave magnetic forces can be neglected for low pitch angles, high wave normal angle, and/or high normalized wave frequency. At the higher pitch angles the wave magnetic forces become very important and it is necessary to

include the additional force terms as derived.

The sample calculations indicate that there are two classes of electrons, distinguished by the behavior of their phases with respect to the wave. In a case when the phase variation is bounded, i.e. less then 2π, the electron is said to be trapped, whereas unbounded phase variation characterizes the untrapped electrons. The scattering and corresponding energy exchange for the trapped and untrapped electrons exhibit significantly different characteristics.

It is also found that the trapping of electrons is easier under conditions of spatial amplitude variation of a narrowband signal rather than for a constant amplitude. Analysis was done for a constant amplitude CW signal, a CW signal amplified at the equator through gyroresonance, and also for a spatial amplitude variation of the pulse formed by a nonducted signal.

It is also shown that the longitudinal resonance process involves a wave amplitude threshold effect, i.e. the trapping of electrons is possible only if the amplitude of the wave parallel electric field $E_{\parallel}$ exceeds a certain value. The trapped electrons also become space bunched and temporarily increase the electron density over a particular range of parallel velocities.

The full distribution results show that the expected precipitation is small when compared to gyroresonance-induced precipitation for waves of comparable amplitude. In general, the results indicate that the longitudinal resonance scattering efficiency (scattering vs. amplitude) is considerably smaller, i.e. the efficiencies of the two processes differ by as much as an order of

magnitude.

The amplitude threshold effect was tested on whistler precursors, and it was found that the whistler amplitudes are well correlated with the occurrence of precursors, i.e. only whistlers with amplitudes above a certain threshold resulted in precursors. This provides support for the whistler precursor generation mechanism suggested by Park and Helliwell [1977], which involves longitudinal resonance interactions, and therefore it should exhibit a threshold effect as indicated by the measurements.

II. BASIC PHYSICS AND TIME AVERAGED EQUATIONS OF MOTION

A. MOTION OF CHARGED PARTICLES IN EARTH'S MAGNETIC FIELD

Motion of the charged energetic particles in the magnetosphere is governed by the earth's magnetic field. The earth's field in the inner magnetosphere can be approximated by the dipole model with the magnetic field strength B_o given as

$$B_o = 0.312 \cdot 10^{-4} (R_o/R)^3 \cdot (1 + 3\sin^2\lambda)^{1/2} \quad Wb/m^2 \qquad (2.1)$$

where λ is the geomagnetic latitude, R is geocentric radius, and R_o is the radius of the earth. The axis of the magnetic dipole is inclined with respect to the rotation axis by 11°.

The motion of a particle in the magnetosphere is uniquely described by either the parallel and perpendicular velocities of the particle, $v_\parallel$ and $v_\perp$ respectively, or by the parallel (perpendicular) velocity and pitch angle $\alpha = \arctan(v_\perp / v_\parallel)$. Fig. 2.1 shows a typical geometry with the definitions of $v_\parallel$, $v_\perp$, and α .

It can be shown that for a spatially changing magnetic field, such as the earth's magnetic field given by Eq.2.1, charged particles will bounce forth and back along the field line between the mirror points [Northrop, 1963; Buneman 1980]. This is so because the particle perpendicular velocity must change in order to satisfy adiabatic

invariants, while the total kinetic energy of the particle must remain constant. The first adiabatic invariant is the invariance of the orbital magnetic moment, given as

$$W_\perp/B = \text{constant} \qquad (2.2)$$

where $W_\perp$ is the perpendicular kinetic energy of the particle.

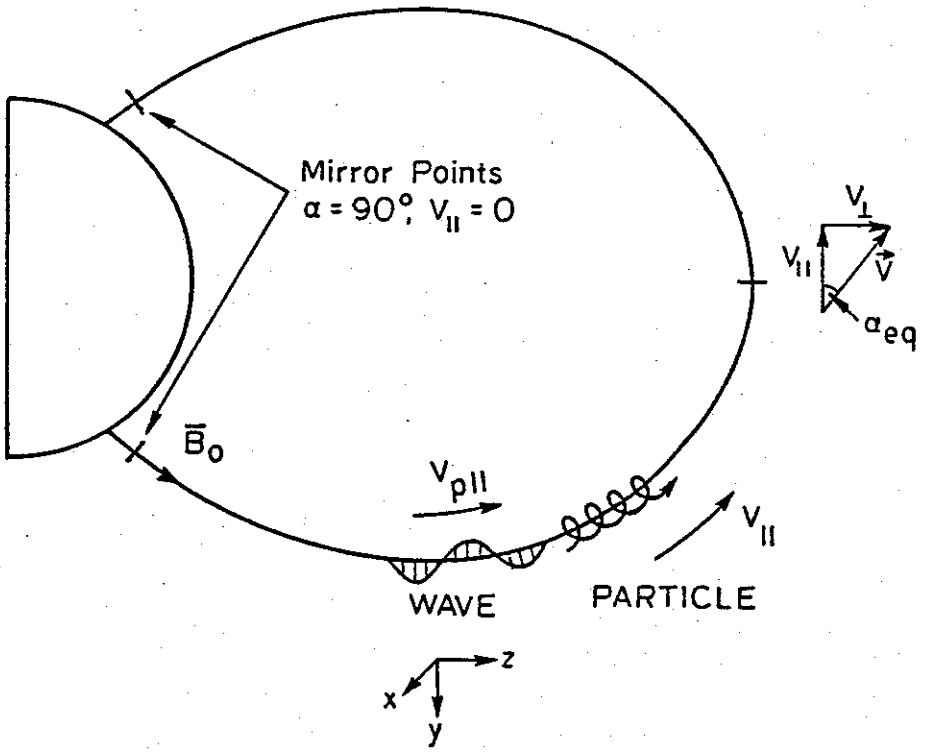

FIGURE 2.1 DIPOLE GEOMETRY AND SYMBOLS USED FOR PARTICLE IDENTIFICATION. Note that the z-axis is aligned with the magnetic field line and that both the wave and the particles travel in the +z direction. Particle orbits are described in terms of equatorial values of $v_\parallel$ and α.

The second adiabatic invariant requires that the magnetic flux through the circle described by the particle gyrating around the field line remains constant, or

$$r_H^2 \times B = \text{constant} \tag{2.3}$$

where r_H is the electron gyroradius.

Thus if the magnetic field $\overline{B}_o$ increases, the perpendicular kinetic energy $W_\perp$ must also increase according to Eq. 2.2. Furthermore, the parallel energy $W_\parallel$ of the particle must decrease so that the total energy $W_\parallel + W_\perp$ remains constant. Therefore, the particle pitch angle $\alpha = \arctan\left(\sqrt{\frac{W_\perp}{W_\parallel}}\right)$ increases as $\overline{B}$ increases up to the point where $\alpha = 90°$. At this point the parallel velocity of the particle has been reduced to zero, and the particle begins to travel in the opposite direction along the same field line. When the particle reaches the conjugate point where again $\alpha = 90°$, the process repeats. Hence the particle bounces back and forth along the magnetic field line between the two mirror points where $v_\parallel = 0$.

Finally, the motion of a particle trapped along a field line can be described by the following equations

$$\frac{dv_\parallel}{dt} = -\frac{v_\perp^2}{2B_o} \cdot \frac{dBo}{dz} \tag{2.4}$$

$$\frac{dv_\perp}{dt} = +\frac{v_\parallel\, v_\perp}{2B_o} \cdot \frac{dBo}{dz} \tag{2.5}$$

which can be derived from the first adiabatic invariant and the law of

energy conservation.

B. LONGITUDINAL RESONANCE

The bounce motion of the particles can be affected by resonant interactions between waves and the particles. The resonance condition is satisfied whenever the doppler-shifted frequency of the wave seen by the particle is equal to an integral multiple of the particle gyrofrequency, i.e.

$$\omega - k_{\parallel} v_{\parallel} = m\omega_H \qquad m = 0, \pm 1, \pm 2, \pm 3, \ldots \qquad (2.6)$$

where ω is the wave frequency, $k_{\parallel}$ is the wave number in the direction of the static magnetic field, and ω_H is the particle gyrofrequency.

The resonance condition given by Eq. 2.6 can be further divided into three subgroups according to different values of the parameter m. For $m>0$ we have the resonance condition for the m-th order gyroresonance; $m<0$ is the resonance condition for the m-th order anomalous gyroresonance; $m=0$ yields the resonance condition for the longitudinal or Landau resonance. The last condition is given as

$$\omega - k_{\parallel} v_{\parallel} = 0 \qquad (2.7)$$

or

$$v_{p\parallel} = v_{\parallel} \qquad (2.8)$$

where $v_{p\parallel}$ is the wave phase velocity measured in the direction of the static magnetic field.

Before discussing the longitudinal resonance we should note that this resonance ($m=0$) is fully separable from the gyroresonances ($m\neq 0$), since the longitudinal resonance is possible only when the wave and the particles travel in the same direction, while the gyroresonance condition is satisfied only if the wave and the particles travel in the opposite direction. This separability of the different resonances makes their analysis much simpler. It is still possible for the same particle to interact simultaneously in both resonances with two different waves that satisfy corresponding resonant conditions. In this report we shall limit ourselves to discussion of the longitudinal resonance, although a comparison with the gyroresonance mechanism is given later in the text.

The condition given in Eq. 2.8 is the necessary condition for the longitudinal resonance. However, in order for the particle and the wave to exchange energy through the particle trapping process, the parallel component of the wave electric field must have a non-zero value. Therefore, even if the particle parallel velocity matches the wave phase velocity there will be no energy exchange between the particle and the wave if $E_\parallel = 0$. The direction of the energy exchange (whether wave or particle gains energy) depends on the initial velocity of the particle $v_\parallel$. In the case when $v_\parallel$ is initially less than the phase velocity $v_{p\parallel}$ the particle will gain energy; if the initial $v_\parallel$ is larger than $v_{p\parallel}$ the particle will lose some of its energy. We shall now present a simple analytical model for the longitudinal resonance and trapping process similar to that given by Seshadri [1973].

Let us assume that the longitudinal component of the wave electric field, propagating in the homogeneous medium, is given by

$$E_{\parallel}(s,t) = E_{\parallel_o} \sin(k_{\parallel} \cdot s - \omega \cdot t) \tag{2.9}$$

where s is the space coordinate. Eq. 2.9 is written in the laboratory coordinate system, but it is useful to do the analysis in the wave frame which moves at the phase velocity $v_{p_{\parallel}}$. In this case a new space coordinate z is defined as

$$z = s - v_{p_{\parallel}} t \tag{2.10}$$

Now, Eq. 2.9 can be rewritten as

$$E_{\parallel}(s,t) = E_{\parallel_o} \sin\left[k_{\parallel}\left(s - \frac{\omega}{k_{\parallel}} t\right)\right] \tag{2.11}$$

and using Eq. 2.10 and $v_{p_{\parallel}} = \frac{\omega}{k_{\parallel}}$ Eq. 2.11 simplifies to

$$E_{\parallel}(z) = E_{\parallel_o} \sin(k_{\parallel} z) \tag{2.12}$$

The electric field given by the Eq. 2.12 is static in the wave frame and it is possible to derive a corresponding scalar potential $\Phi(z)$, by integrating $E_{\parallel}(\eta)$ where η is a dummy variable.

$$\Phi(z) = -\int_0^z E(\eta) \cdot d\eta \tag{2.13}$$

$$\Phi(z) = -\int_{o}^{z} E_{\parallel_o} \sin(k_\parallel \eta)\, d\eta \qquad (2.13a)$$

$$\Phi(z) = \frac{E_{\parallel_o}}{k_\parallel} (\cos(k_\parallel z) - 1) \qquad (2.13b)$$

Next we consider an electron (a similar derivation is possible for other types of charged particles) and its potential energy $W_p(z)$ which, in the wave frame is given by

$$W_p(z) = - e \cdot \Phi(z) \qquad (2.14)$$

$$W_p(z) = \frac{eE_{\parallel_o}}{k_\parallel} (1 - \cos(k_\parallel z)) = W_{p_{max}} (1 - \cos(k_\parallel z)) \qquad (2.14a)$$

The constant of the integration is chosen such that the minimum potential energy given by Eq. 2.14a is zero. Thus, the potential energy of the electron is a periodic function, as shown in Fig. 2.2.

It can be shown that the possibility of an electron being trapped depends on the initial kinetic energy of that electron measured in the wave frame. In a case when the initial kinetic energy of an electron, placed at z at the time t=0, is larger than the potential energy given by Eq. 2.14a, $W_{p_{max}}$, there is no net interaction between the wave and electron, regardless of the electron initial velocity. The electron simply slides up and down the potential well as it moves either forward or backward through the wave, and there is no net energy exchange when averaged over one wavelength.

However, if the kinetic energy of the electron in the wave frame, $W_k(t=0)$, is less than the potential energy given by Eq. 2.14a,

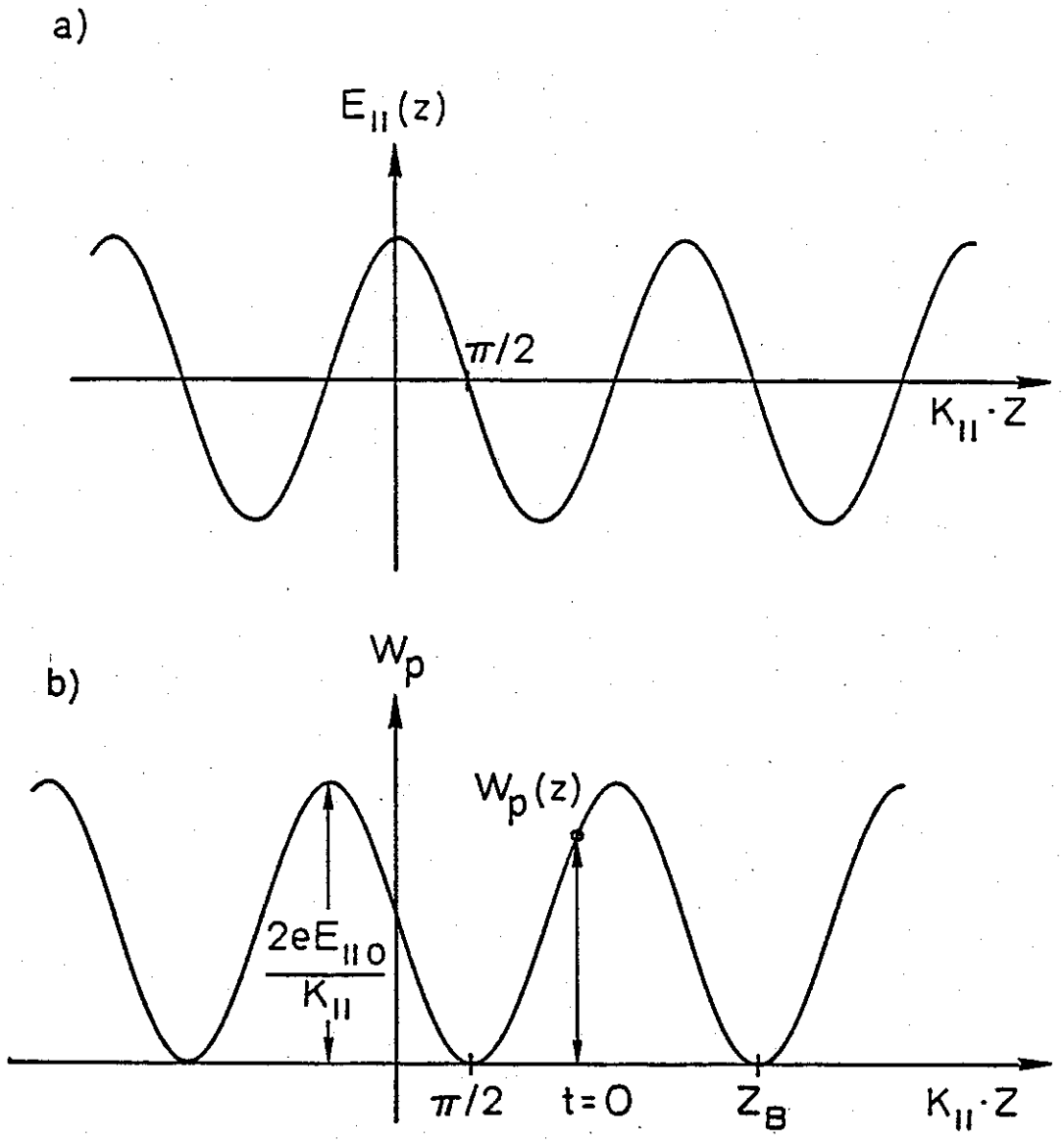

FIGURE 2.2 PARALLEL ELECTRIC FIELD AND THE CORRESPONDING POTENTIAL ENERGY. Both the parallel electric field $E_{\parallel}$ and potential energy W_p of the electron are periodic functions in a reference frame moving at at the parallel phase velocity $v_{p\parallel}$. In (b) z_B indicates the bottom of the potential well.

$W_{p_{max}}$ as shown in Fig. 2.2 the electron is trapped in the potential well. The trapping condition is then given as

$$\frac{1}{2} m (v_{\parallel} - v_{p\parallel})^2 < W_{p_{max}} \tag{2.15}$$

$$\frac{1}{2} m (v_{\parallel} - v_{p\parallel})^2 < \frac{eE_{\parallel o}}{k_{\parallel}} \tag{2.15a}$$

$$|v_{\parallel} - v_{p\parallel}| < \sqrt{\frac{2eE_{\parallel o}}{mk_{\parallel}}} \tag{2.15b}$$

Rewriting the inequality of Eq. 2.15b as

$$v_{p\parallel} - \sqrt{\frac{2eE_{\parallel o}}{mk_{\parallel}}} < v_{\parallel} < v_{p\parallel} + \sqrt{\frac{2eE_{\parallel o}}{mk_{\parallel}}} \tag{2.16}$$

we have a range of velocities for which it is possible to trap an electron. Therefore, all electrons with parallel velocities that satisfy Eq. 2.16 are trapped in the wave potential well. The trapping velocity bandwidth v_t is given as

$$v_t = \sqrt{\frac{2eE_{\parallel o}}{mk_{\parallel}}} \tag{2.17}$$

Furthermore, it can be shown that the total energy, ΔW, exchanged between the wave and electrons during the trapping process is

$$\Delta W = \int_{v_{p\parallel} - v_t}^{v_{p\parallel} + v_t} f(v_{\parallel}) \, \Delta E \, dv_{\parallel} \tag{2.18}$$

where $f(v_{\parallel})$ is the electron distribution function; ΔE is the amount of

energy exchanged through trapping of a single electron, and it is expressed as

$$\Delta E = \frac{1}{2} m (v_{p_\parallel} + \hat{v}_\parallel)^2 - \frac{1}{2} m v_\parallel^2 \qquad (2.19)$$

$$\Delta E = - m_e v_{p_\parallel} (v_\parallel - v_{p_\parallel}) \qquad (2.19a)$$

where $\hat{v}_\parallel$ is a time-varying periodic function describing the oscillation of an electron at the bottom of the potential well. Expanding $f(v_\parallel)$ in a Taylor series around $v_\parallel = v_{p_\parallel}$ we obtain

$$f(v_\parallel) = f(v_{p_\parallel}) + (v_\parallel - v_{p_\parallel}) \left. \frac{\partial f(v_\parallel)}{\partial v_\parallel} \right|_{v_\parallel = v_{p_\parallel}} \qquad (2.20)$$

and finally substituting Eq. 2.20 in Eq. 2.18 the total energy exchanged in the trapping process, ΔW, is given as

$$\Delta W = -\frac{2}{3} m v_{p_\parallel} v_t^3 f'(v_{p_\parallel}) \qquad (2.21)$$

The result derived in Eq. 2.21 shows that the net energy exchanged between the trapped electrons and the wave depends on the slope of the distribution function at a point where the electron velocity is equal to the phase velocity of the wave. In the case when the number of electrons moving faster is larger than the number of electrons moving slower than the phase velocity, the wave gains energy and its amplitude grows. Similarly, if the number of slow electrons is larger than the number of fast electrons, the amplitude of the wave is

reduced.

The above analysis, using a longitudinal plasma wave and one-dimensional distribution function $f(v_{\parallel})$, has demonstrated that it is possible to have wave damping in the absence of collisions, also known as Landau damping. It was also shown that the wave amplitude grows if the slope of the distribution function is positive. However, the expressions for the energy exchange were derived assuming that the particles are already trapped. It was also assumed that the medium is homogeneous, and that both the wave and the distribution function are one-dimensional.

In the magnetosphere Eq. 2.18 is still valid, but the trapping process is governed by the particle equations of motion. Thus in order to find the energy exchanged between a wave and particle (ΔE in Eq. 2.18) it is necessary to derive the equations of motion for a single particle when it is in longitudinal resonance with waves in the magnetosphere.

C. NONLINEAR EQUATIONS OF MOTION FOR LANDAU RESONANCE INTERACTIONS WITH A WHISTLER MODE WAVE

Now we consider an elliptically polarized wave propagating in the cold plasma of the magnetosphere with a static magnetic field $\overline{B}_o$. The wave frequency f is assumed to be less than the electron gyrofrequency f_H ; in that case there is only one propagating wave [Ratcliffe, 1959; Budden, 1961], which is called a whistler wave.

In the most general case all Cartesian components of the wave electric $\bar{E}_w$ and magnetic field $\bar{B}_w$ have non-zero values. All of these components can be expressed in terms of δ_z through the cold-plasma dispersion relation. Without any loss of generality the wave vector $\bar{k}$ is confined to the x-z plane, at an angle θ from the static magnetic field. The coordinate system used is shown in Fig. 2.3.

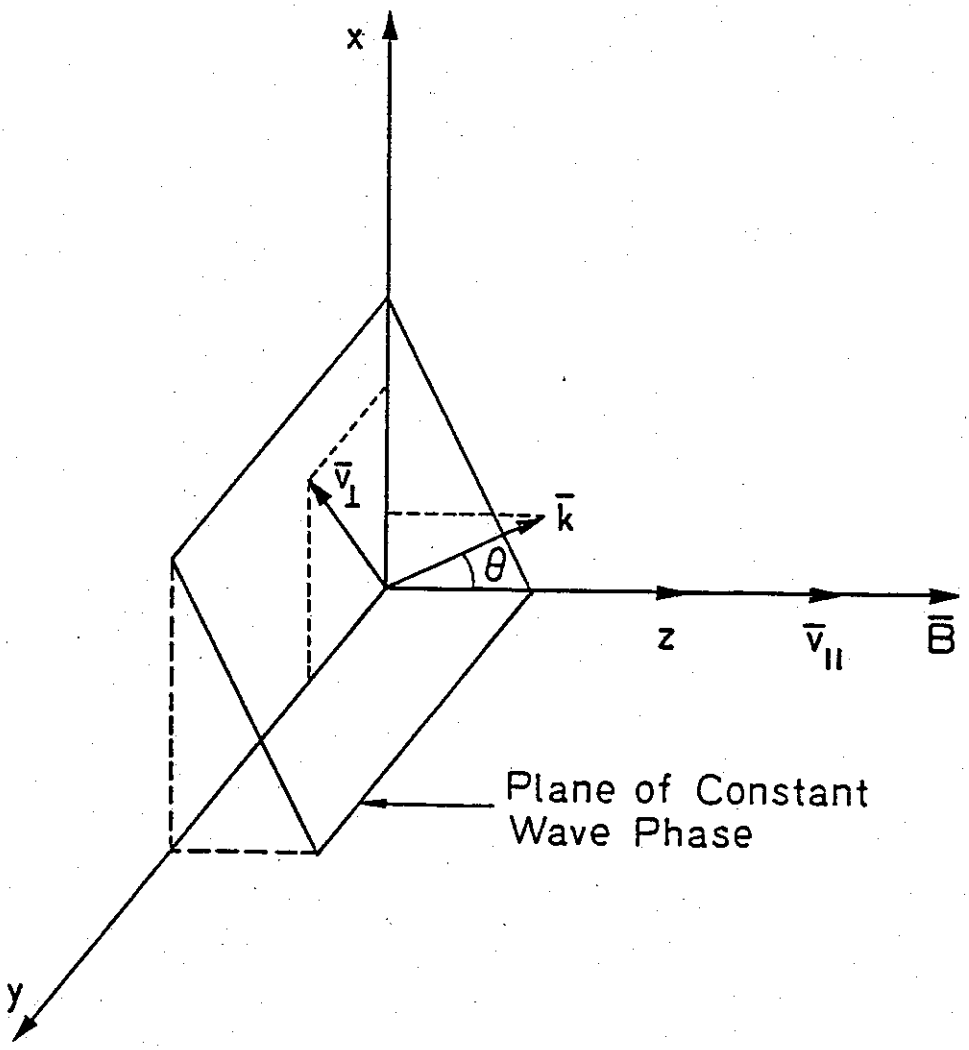

FIGURE 2.3 COORDINATE SYSTEM FOR THE EQUATIONS OF MOTION. The wave vector $\bar{k}$ is at an angle θ from the static magnetic field $\bar{B}_o$.

We also assume propagation as exp $i(\omega t - \bar{k}\cdot\bar{r})$. Using a plasma dispersion relation [Stix, 1962]

$$\begin{vmatrix} \varepsilon_\perp - n^2\cos^2\theta & -i\varepsilon_x & n^2\sin\theta\cos\theta \\ i\varepsilon_x & \varepsilon_\perp - n^2 & 0 \\ n^2\sin\theta\cos\theta & 0 & \varepsilon_\parallel - n^2\sin^2\theta \end{vmatrix} \begin{vmatrix} \mathcal{E}_x \\ \mathcal{E}_y \\ \mathcal{E}_z \end{vmatrix} = 0 \qquad (2.22)$$

all electric field components can be expressed in terms of $\mathcal{E}_z$ as follows

$$\mathcal{E}_z = E_\parallel \cos(\omega t - \bar{k}\cdot\bar{r}) \qquad (2.23)$$

$$\mathcal{E}_x = \frac{n^2\sin\theta - \varepsilon_\parallel}{n^2\sin\theta\cos\theta} E_\parallel \cos(\omega t - \bar{k}\cdot\bar{r}) \qquad (2.24)$$

$$\mathcal{E}_y = \frac{\varepsilon_x}{n^2 - \varepsilon_\perp}\frac{n^2\sin\theta - \varepsilon_\parallel}{n^2\sin\theta\cos\theta} E_\parallel \sin(\omega t - \bar{k}\cdot\bar{r}) \qquad (2.25)$$

where $\varepsilon_\parallel = 1 - \frac{\omega_p^2}{\omega^2}$, $\varepsilon_\perp = 1 - \frac{\omega_p^2}{\omega^2 - \omega_H^2}$, $\varepsilon_x = \frac{\omega_H}{\omega}\frac{\omega_p^2}{\omega^2 - \omega_H^2}$. The refractive index n can be derived from Eq. 2.22 as (QL approximation)

$$n^2 = 1 + \frac{f_p^2}{f(f_H\cos\theta - f)} \qquad (2.25a)$$

Using Maxwell's equation $\nabla \times \bar{E} = -\frac{\partial \bar{B}}{\partial t}$ the wave magnetic components are

$$\mathcal{B}_x = -\frac{k\cos\theta}{\omega}\mathcal{E}_y \qquad (2.26)$$

$$\mathcal{B}_y = \frac{k\cos\theta}{\omega}\,\mathcal{E}_x - \frac{k\sin\theta}{\omega}\,\mathcal{E}_z \qquad (2.27)$$

$$\mathcal{B}_z = \frac{k\sin\theta}{\omega}\,\mathcal{E}_y \qquad (2.28)$$

which can be also expressed in terms of $\mathcal{E}_z$ using Eqs. 2.23, 2.24, and 2.25.

The variation of the total electron velocity $\bar{v}$ is governed by the Lorentz force equation

$$m\frac{d\bar{v}}{dt} = q\,[\bar{E}_w + \bar{v} \times (\bar{B}_w + \bar{B}_o)] \qquad (2.29)$$

where m and q are electron mass and charge. For the case when $|\bar{B}_w| << |\bar{B}_o|$, the electron gyromotion can be assumed to be unaffected by the wave to the first order, so that the Cartesian components of the electron velocity vary as

$$v_z = v_{\parallel} \qquad (2.30)$$

$$v_x = v_\perp \cos(\omega_H t + \beta_o) \qquad (2.31)$$

$$v_y = v_\perp \sin(\omega_H t + \beta_o) \qquad (2.32)$$

where ω_H is the electron gyrofrequency and β_o is the initial cyclotron phase. Furthermore, as long as the wave field is much smaller than the earth's magnetic field, it is permissible first to derive the force applied to an electron by the wave fields and then to superimpose the

adiabatic variation of $v_\perp$ and $v_\parallel$. Therefore, the perturbation of the electron motion induced by the wave fields only is given by

$$m \frac{d\bar{v}}{dt} = q[\bar{E}_w + \bar{v} \times \bar{B}_w] \tag{2.33}$$

It is useful to examine each Cartesian component in Eq. 2.33 separately. These three components are given as

$$F_x = q[\mathcal{E}_x + v_y\mathcal{B}_z - v_z\mathcal{B}_y] \tag{2.34}$$

$$F_y = q[\mathcal{E}_y + v_z\mathcal{B}_x - v_x\mathcal{B}_z] \tag{2.35}$$

$$F_z = q[\mathcal{E}_z + v_x\mathcal{B}_y - v_y\mathcal{B}_x] \tag{2.36}$$

Before investigating those equations we simplify $\cos(\omega t - \bar{k}\cdot\bar{r})$, which can be expressed as

$$\cos(\omega t - k\cos\theta \cdot z - k\sin\theta \cdot x) \tag{2.37}$$

or letting $\gamma = \omega t - k\cos\theta\, z$ in Eq. 2.37 we have

$$\cos(\gamma - k\sin\theta\, x) \tag{2.38}$$

Eq. 2.38 can be further simplified using the fact that

$$x = \frac{v_\perp}{\omega_H}\sin(\omega_H t + \beta_o) \tag{2.39}$$

which is derived by integrating Eq. 2.31. Finally, replacing x in Eq. 2.38 by (2.39)

$$\cos(\omega t - \bar{k}\cdot\bar{r}) = \cos(\gamma - \eta \sin\phi) \qquad (2.40)$$

where $\phi = \omega_H t + \beta$ and $\eta = \dfrac{v_\perp k \sin\theta}{\omega_H}$.

Now, using the result derived in (2.40) we can rewrite three Cartesian components of the Lorentz force as

$$F_x = q\,[E_x \sin(\gamma - \eta\sin\phi) + v_\perp \sin\phi\ B_y \sin(\gamma - \eta\sin\phi) - v_\parallel B_z \cos(\gamma - \eta\sin\phi)] \qquad (2.41)$$

$$F_y = q\,[E_y \sin(\gamma - \eta\sin\phi) + v_\parallel B_x \sin(\gamma - \eta\sin\phi) - v_\perp \cos\phi\ B_z \sin(\gamma - \eta\sin\phi)] \qquad (2.42)$$

$$F_z = q\,[E_z \cos(\gamma - \eta\sin\phi) + v_\perp \cos\phi\ B_y \cos(\gamma - \eta\sin\phi) - v_\perp \sin\phi\ B_x \sin(\gamma - \eta\sin\phi)] \qquad (2.43)$$

Note that E_x, E_y, E_z, B_x, B_y, and B_z are the real magnitudes of the fields, with the phase differences taken separately into account through $\begin{matrix}\sin\\ \cos\end{matrix}$ $(\gamma - \eta\sin\phi)$ terms.

At this point we have three equations which can be used to describe the motion of particles in resonance with a whistler wave. However, it is desirable to reduce the number of required equations to simplify numerical simulations. In this case it is useful to combine

the x and y components of the Lorentz force in one perpendicular component. This is done by taking the time derivative of the square of the perpendicular velocity $v_\perp^2 = v_x^2 + v_y^2$

$$v_\perp^2 = v_x^2 + v_y^2 \Big/ \frac{d}{dt} \tag{2.44}$$

$$v_\perp \frac{dv_\perp}{dt} = v_x \frac{dv_x}{dt} + v_y \frac{dv_y}{dt} \tag{2.44a}$$

and multiplying it by $m/v_\perp$

$$m\frac{dv_\perp}{dt} = m\,\frac{v_x}{v_\perp}\,\frac{dv_x}{dt} + m\,\frac{v_y}{v_\perp}\,\frac{dv_y}{dt} \tag{2.45}$$

However, $\frac{v_x}{v_\perp} = \cos\phi$, $\frac{v_y}{v_\perp} = \sin\phi$, $m\,\frac{dv_\perp}{dt} = F_\perp$, $m\,\frac{dv_x}{dt} = F_x$, and $m\,\frac{dv_y}{dt} = F_y$, and (2.45) reduces to

$$F_\perp = \cos\phi\ F_x + \sin\phi\ \ F_y \tag{2.46}$$

Now, combining Eqs. 2.46, 2.41, and 2.42 the perpendicular force term is

$$\begin{aligned} F_\perp = \cos\phi\ \{q\,[E_x \sin(\gamma - \eta\sin\phi) + v_\perp \sin\phi\ \ B_y \sin(\gamma - \eta\sin\phi) \\ - v_\parallel\ B_z \cos(\gamma - \eta\sin\phi)]\} \\ + \sin\phi\ \{q\,[E_y \sin(\gamma - \eta\sin\phi) + v_\parallel\ B_x \sin(\gamma - \eta\sin\phi) \\ - v_\perp \cos\phi\ B_z \sin(\gamma - \eta\sin\phi)]\} \end{aligned} \tag{2.47}$$

The motion of a particle is now described in terms of the parallel and perpendicular forces, given respectively by Eqs. 2.43 and

2.47. If the $\begin{matrix}\sin\\ \cos\end{matrix}$ $(\gamma - \eta \sin \phi)$ terms in these equations are expanded (Appendix A), the result is an infinite series of harmonics at frequencies $n\omega_H$ with amplitudes given by $J_n(\eta)$. In a general formulation all terms must be kept and Eqs. 2.43 and 2.47 must be used as they stand. However, the equations can be considerably simplified when time averaged over one cyclotron period, T_H, because the higher order force terms ($n \geq 2$) vanish. Also, qualitatively, the $v_x B_y$ term should average out to zero since wave phase does not vary in the y-direction. In the next section we present the necessary conditions for the averaging to be valid, along with the time averaged equations of motion.

D. TIME AVERAGING OF EQUATIONS OF MOTION

Before averaging Eqs. 2.43 and 2.47 over one gyroperiod we have to make sure that the wave phase variations, as seen by the particles during one gyroperiod, are negligible. For the small field case this condition can be stated as

$$\omega - \bar{k}\cdot\bar{v} \ll \omega_H \qquad (2.48)$$

which would certainly be the case for the Landau resonance described by

$$\omega - \bar{k}\cdot\bar{v} \simeq 0 \qquad (2.49)$$

Note that Eq. 2.49 is the equivalent of Eq. 2.8.

We have stated condition (2.48) assuming small amplitude waves. This requires that the wave field be small enough that it cannot move the particle by a substantial fraction of a wavelength during a gyroperiod. This condition can be stated as

$$|a_p|\frac{1}{f_H^2} << \frac{c}{nf} \tag{2.50}$$

where a_p is the peak parallel acceleration, c is the speed of light, n is the refractive index, $f = \frac{\omega}{2\pi}$ is the wave frequency and $f_H = \frac{\omega_H}{2\pi}$ is the electron gyrofrequency. The peak value of the parallel acceleration a_p during a gyroperiod can be taken to be that for $\phi = \frac{3\pi}{2}$ and $\gamma - \eta \sin\phi = \frac{\pi}{2}$. From Eq. 2.43 we have

$$|a_p| = \left|\frac{q}{m} \left(E_z - v_y B_x\right)\right| \tag{2.51}$$

In a order to express E_z in terms of B_x, we have from Eq. 2.25

$$\mathcal{E}_y = \rho_z \mathcal{E}_z \tag{2.52}$$

where $\rho_z = i\frac{\varepsilon_x}{n^2-\varepsilon} \frac{n^2\sin\theta - \varepsilon_{\shortparallel}}{n^2\sin\theta\cos\theta} = \frac{\mathcal{E}_y}{\mathcal{E}_z}$. Substituting Eq. 2.52 in Eq. 2.26

$$B_x = -\frac{k\cos\theta}{\omega} \rho_z E_z \tag{2.53}$$

or

$$E_z = - \frac{B_x}{\rho_z} \frac{\omega}{k\cos\theta} \qquad (2.54)$$

Furthermore, for the near resonant particles $\frac{\omega}{k\cos\theta} = v_{p\parallel} = v_\parallel$ and Eq. 2.54 yields

$$E_z = - \frac{B_x}{\rho_z} v_\parallel \qquad (2.55)$$

Replacing the E_z in Eq. 2.51 with the above expression the peak acceleration $|a_p|$ is

$$|a_p| = \left|\frac{q}{m} \left(- \frac{B_x}{\rho_z} v_\parallel - v_\perp B_x\right)\right| \qquad (2.56)$$

$$|a_p| = \frac{q}{m} B_x v_\perp \left(1 + \frac{1}{|\rho_z| \tan\alpha}\right) \qquad (2.56a)$$

where $\tan\alpha = \frac{v_\perp}{v_\parallel}$.

The final step is to substitute (2.56a) in (2.50) in order to get the condition on wave intensity for which the averaging of equations (2.43) and (2.47) is valid;

$$B_x << B_u = \frac{m f_H^2 c}{q v_\perp n f} \frac{|\rho_z| \tan\alpha}{1 + |\rho_z| \tan\alpha} \qquad (2.57)$$

Thus B_u represents the upper limit on wave magnetic field intensity. Note that B_x is equal to the total transverse B_w for circularly polarized whistler waves. Assuming B_u to have a value much higher (> 100 times) than the typical field intensities for whistler mode waves in the magnetosphere [Burtis and Helliwell, 1975], as shown later

in the text, we shall now time average Eqs. 2.43 and 2.47 over one gyroperiod. In doing so we use the identities derived in Appendix A. The averaged equations of motion become

$$< m \frac{dv_z}{dt} > = < q \tilde{\mathcal{E}}_z > - < q v_y \mathcal{B}_x > \qquad (2.58)$$

$$< m \frac{dv_\perp}{dt} > = < q \tilde{\mathcal{E}}_y > - < q v_z \mathcal{B}_x > \qquad (2.59)$$

or

$$m \frac{dv_\parallel}{dt} = q E_z J_o(\eta) \left[1 - \frac{v_\perp \cos\theta}{\omega} \rho_z \frac{J_1(\eta)}{J_o(\eta)}\right] \sin(\omega t - k z \cos\theta) \qquad (2.60)$$

$$m \frac{dv_\perp}{dt} = - q\rho_z E_z J_1(\eta) \left[1 - \frac{v_\parallel k\cos\theta}{\omega}\right] \sin(\omega t - k z \cos\theta) \qquad (2.61)$$

Since the brackets on the left hand sides are dropped, $\frac{dv_\parallel}{dt}$ and $\frac{dv_\perp}{dt}$ should be understood to be the average rates of change of $v_\parallel$ and $v_\perp$, respectively.

Finally, for an inhomogeneous medium with $\bar{B}_o$ variable as in the magnetosphere, the adiabatic variations of $v_\parallel$ and $v_\perp$ can be superposed on the wave-induced perturbations as long as the variation of $\bar{B}_o$ in one wavelength is negligible. Thus the complete averaged nonlinear equations of motion become

$$\frac{dv_\parallel}{dt} = \frac{q}{m} E_z J_o(\eta) \left[1 - \frac{v_\perp k\cos\theta}{\omega} \rho_z \frac{J_1(\eta)}{J_o(\eta)}\right] \sin(\omega t - kz\cos\theta) - \frac{v_\perp}{2B_o} \frac{dB_o}{dz}$$

$$(2.62)$$

$$\frac{dv_\perp}{dt} = - \frac{q}{m} \rho_z E_z J_1(\eta) \left[1 - \frac{v_\parallel k\cos\theta}{\omega}\right]\sin(\omega t - kz\cos\theta) + \frac{v_\parallel v_\perp}{2B_o} \frac{dB_o}{dz}$$

(2.63)

We shall discuss the relative importance of the different terms in Eqs. 2.62 and 2.63 in the next section.

E. DISCUSSION OF FORCE EQUATIONS

Two terms of the parallel force are:

$$\langle q \mathcal{E}_z \rangle = q E_z J_o(\eta) \sin\gamma \qquad (2.64)$$

$$\langle q v_y \mathcal{B}_x \rangle = - q E_z J_1(\eta) \rho_z \tan\alpha \sin\gamma \qquad (2.65)$$

Also note that using (2.49)

$$\eta = v_\perp \frac{k \sin\theta}{\omega_H} = \frac{\omega}{\omega_H} \tan\theta \frac{k \cos\theta}{\omega} v_\perp \qquad (2.66)$$

$$\eta = \frac{\omega}{\omega_H} \tan\theta \tan\alpha \qquad (2.66a)$$

for near-resonant particles.

The term in (2.64) proportional to $qE_zJ_o(\eta)$ is similar to the qE_z term that would be present in the case of electrostatic waves. The

$J_o(\eta)$ represents the fact that the E_z field seen by the particle at different points in its transverse orbit is changing since E_z has a transverse phase variation given by k x sin θ . The term in (2.65) represents the effect of the q $\overline{v}$ x $\overline{B}$ force, and the fact that since the plane of rotation of the particle and the wave polarization ellipse are at an angle ($\frac{\pi}{2} - \theta$), there is a net longitudinal acceleration even after averaging over one gyroperiod. For cases in which (2.64) is the dominant term, the equations of motion for interaction with whistler mode waves are much the same as those for electrostatic waves [Nunn 1971, 1973].

Before comparing the relative magnitudes of (2.64) and (2.65) for the range of the parameters in the magnetosphere it should be noted that $\frac{dv_\perp}{dt}$, given by Eq. 2.61, becomes very small for near-resonant particles with $v_\parallel = v_{p_\parallel}$. In this case $1 - \frac{v_\parallel k\cos\theta}{\omega} = 1 - \frac{v_\parallel}{v_{p_\parallel}} \simeq 0$, and the perpendicular motion of the particles is primarily governed by the adiabatic term of Eq. 2.63. In the following figures we present the magnitudes of (2.64) and (2.65), as well as the longitudinal polarization ρ_z as a function of different parameters.

Figure 2.4 shows a plot of the longitudinal polarization ρ_z as a function of the wave normal angle θ , for different values of normalized frequency $\frac{\omega}{\omega_H}$. The results are computed by using the cold plasma dispersion relation [Stix, 1962]. The longitudinal polarization is $\rho_z = \frac{\mathcal{E}_y}{\mathcal{E}_z}$, as defined in (2.52). A plasma frequency f_p = 180 kHz, corresponding to 400 el/cc at the magnetic equator at L = 4, along with the equatorial gyrofrequency f_H = 13.65 kHz, were used in computing ρ_z . For $f_p >> f_H$ the value of ρ_z is not strongly dependent on f_p. Note from

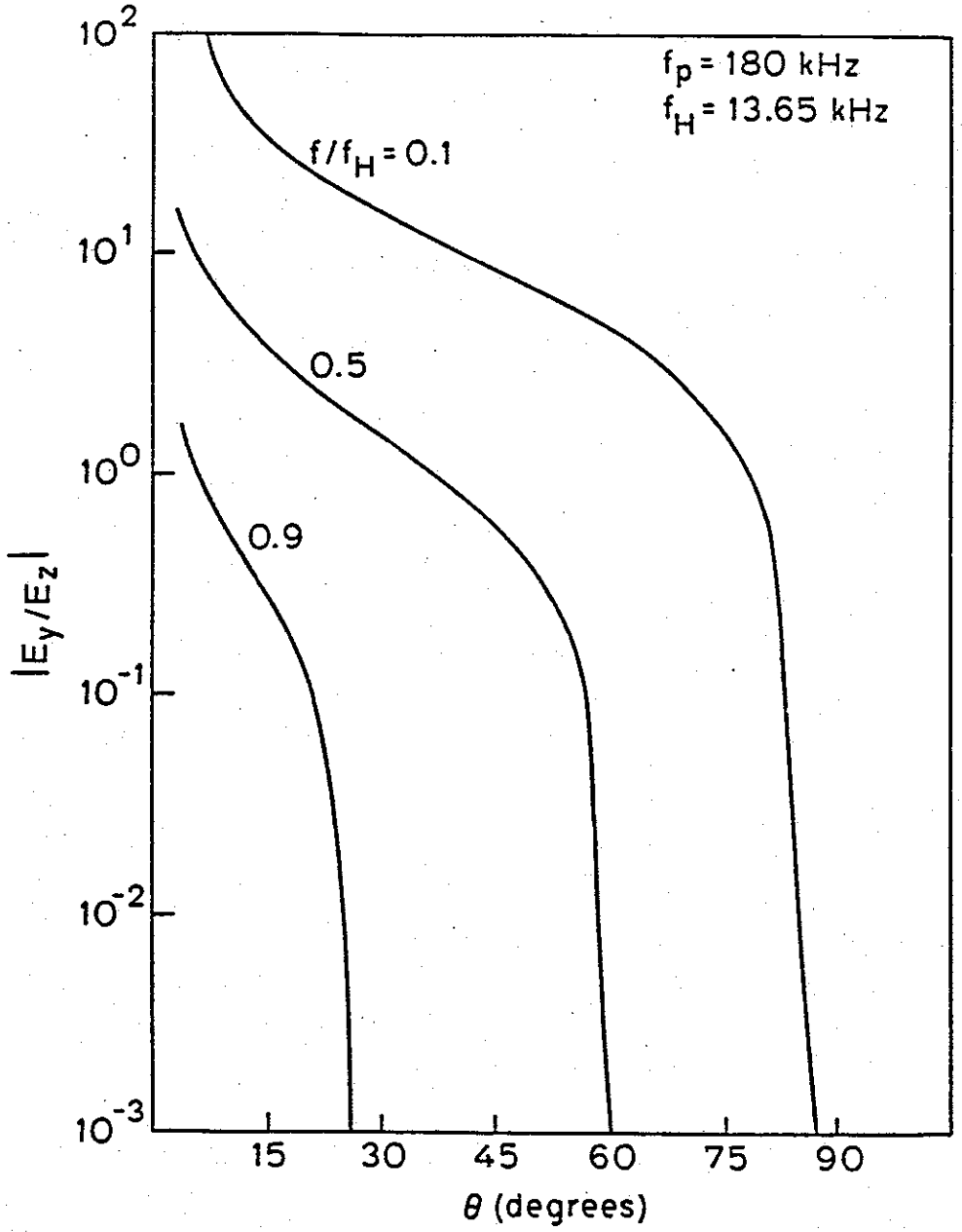

FIGURE 2.4 MAGNITUDE OF THE WAVE LONGITUDINAL POLARIZATION $|\rho_z| = |\mathcal{E}_y/\mathcal{E}_z|$ AS A FUNCTION OF WAVE NORMAL ANGLE θ. $|\rho_z|$ is shown for three different normalized frequencies.

Fig. 2.4 that ρ_z is in general higher at lower frequencies and decreases with increasing θ . Also recall that for longitudinal propagation, i.e., $\theta = 0°$, $E_z = 0$ and there is no interaction between the particles and the waves.

Figures 2.5, 2.6 and 2.7 compare the peak magnitudes of the two terms as given by (2.64) and (2.65) for various parameters. Figure 2.5 shows variation of both terms with pitch angle α , for various wave normal angles θ and $f = 0.5\ f_H$. It can be seen that the $\langle qv_y\mathcal{B}_x\rangle$ term is negligible for lower pitch angles, while it becomes equal to or larger than the $\langle q\mathcal{E}_z\rangle$ term for $\alpha>30°$. As long $\alpha<30°$, the $\langle q\mathcal{E}_z\rangle$ term alone can be used to compute the motion of the Landau resonant particles with less than 10% error.

Figure 2.6 shows the dependence on the wave normal angle for various pitch angles α and for $f = 0.5\ f_H$. The resonance cone angle for this frequency is $\simeq 60°$ as shown. This result indicates that for any pitch angle α , the $\langle qv_y\mathcal{B}_x\rangle$ term is more important at lower wave normal angles, but that there is a strong dependence on pitch angle as was also indicated in Figure 2.5. For θ approaching zero $J_1(\eta)$ goes to zero and ρ_z approaches infinity. As a result, the $\langle qv_y\mathcal{B}_x\rangle$ term will go to zero and may be approximated by $-qE_z\sin\gamma\tan^2\alpha(1 - f/f_H)/(2 + 2f/f_H)$ for small values of θ (Appendix A).

Finally, Figure 2.7 shows the variation of the terms with normalized frequency f/f_H. The curves are for $\alpha = 40°$ and three different values of wave normal angle θ. It can be seen that the magnetic field term is more important at lower frequencies, although the dependence on frequency is not as strong as that on θ and α .

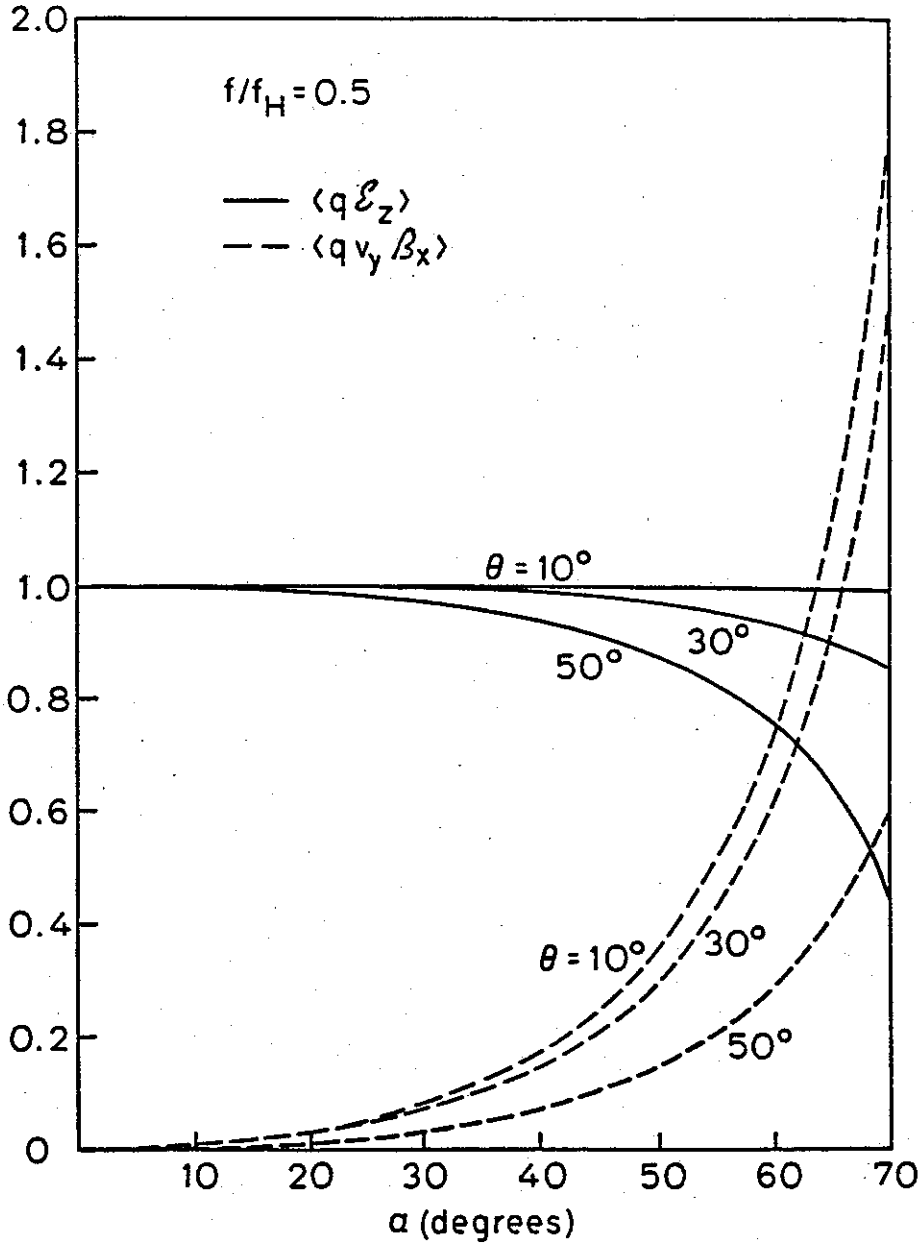

FIGURE 2.5 NORMALIZED PEAK MAGNITUDES OF THE $\langle qv_y\mathcal{B}_x\rangle$ AND $\langle q\mathcal{E}_z\rangle$ TERMS AS FUNCTIONS OF PITCH ANGLE α. The results shown are for $f = 0.5\ f_H$, and for three different wave normal angles θ .

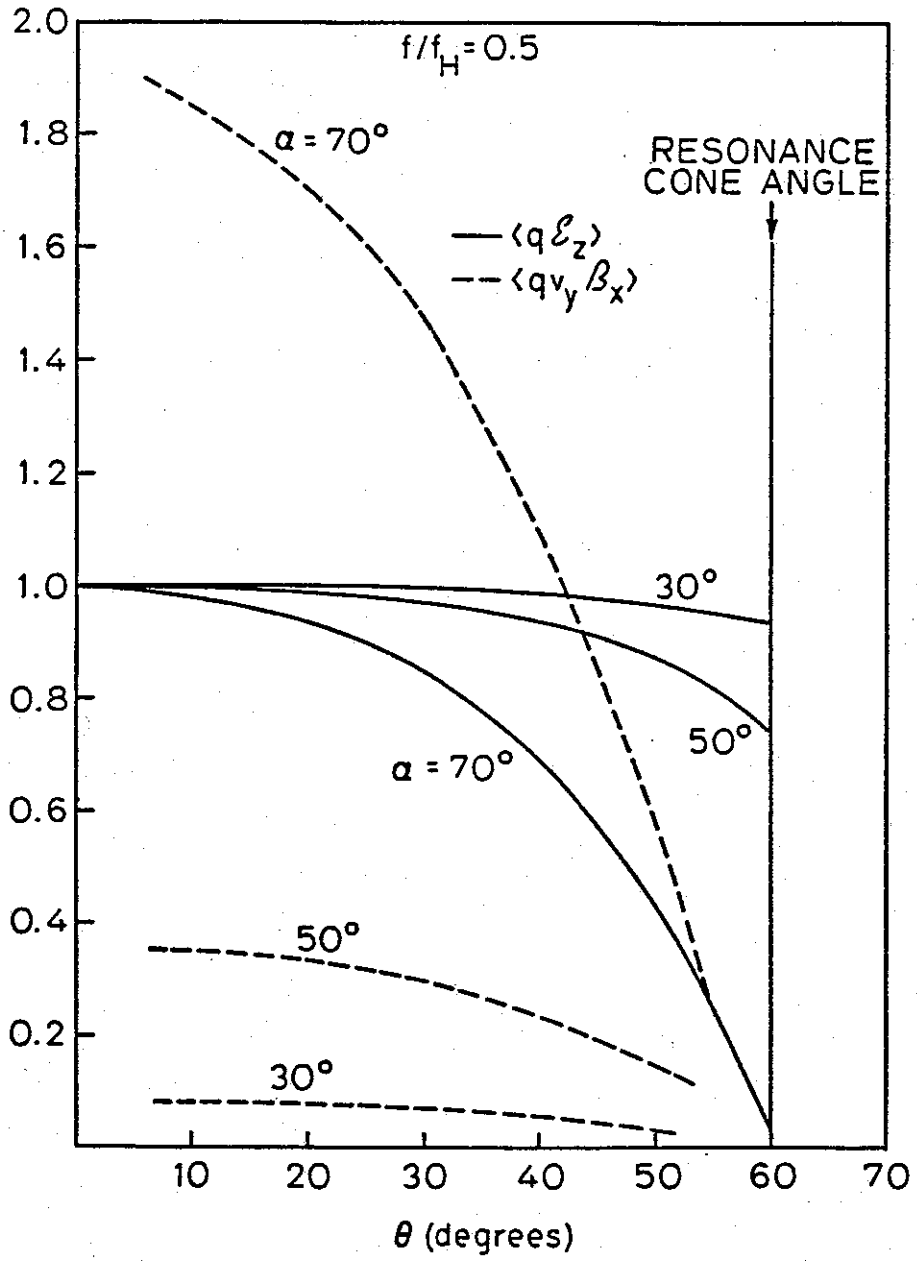

FIGURE 2.6 NORMALIZED PEAK MAGNITUDES OF THE $\langle q v_y \mathcal{B}_x \rangle$ AND $\langle q \mathcal{E}_z \rangle$ TERMS AS FUNCTIONS OF WAVE NORMAL ANGLE Θ. Both terms are calculated for three different pitch angles. The resonance cone angle for $f = 0.5\ f_H$ is $\simeq 60°$ as shown.

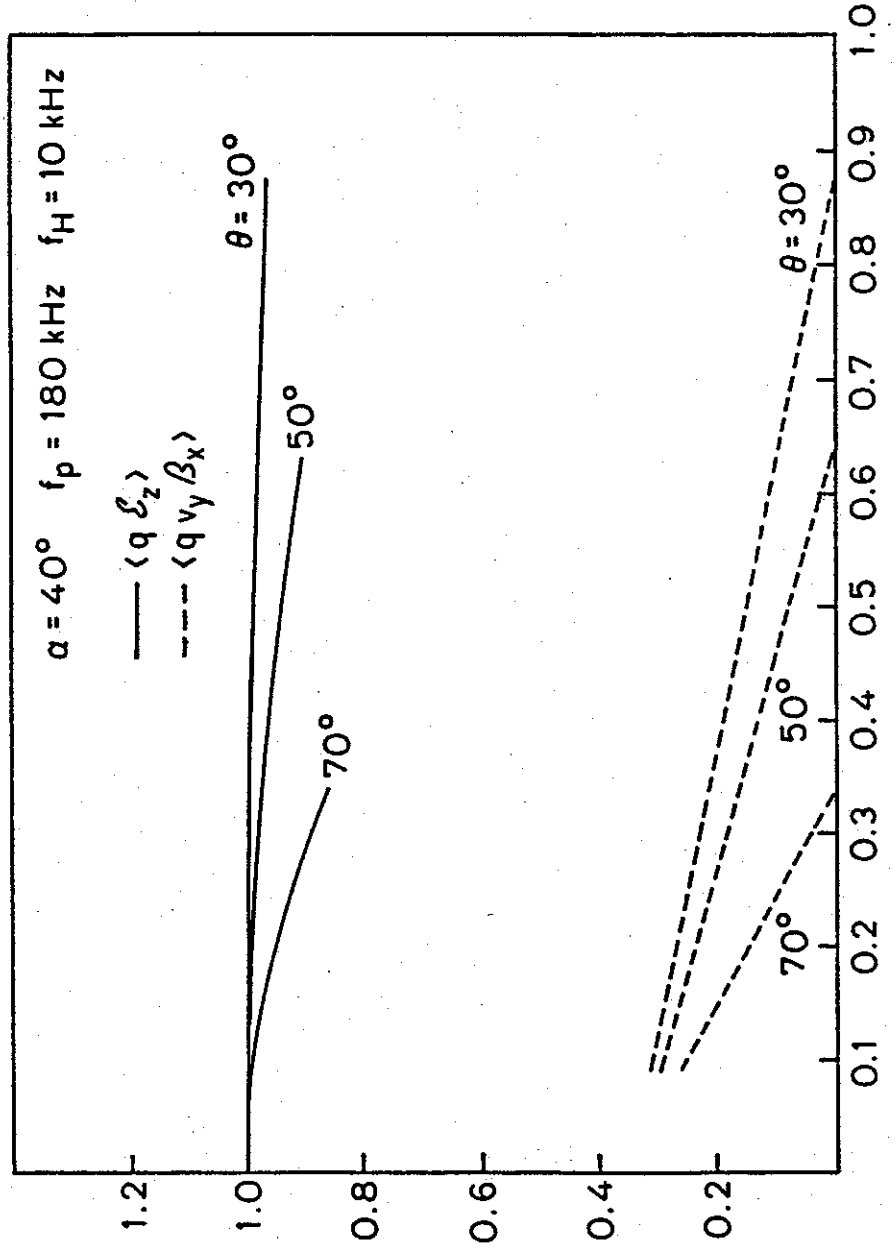

FIGURE 2.7 NORMALIZED PEAK MAGNITUDES OF THE $\langle qv_y\beta_x \rangle$ AND $\langle q\delta_z \rangle$ TERMS AS FUNCTIONS OF NORMALIZED FREQUENCY f/f_H. The results shown are for three different values of α and $\theta = 40^\circ$.

We can also use Fig. 2.4 to show that the upper limit on wave magnetic field intensity is really satisfied, as it was assumed when averaging the equations of motion. For the parameters of Fig. 2.4, and $f = 5$ kHz, $\alpha = 45°$, and $\theta = 30°$, $B_u = 1.3 \times 10^5$ pT, a value much larger than the typical field intensities in the 0.1 to 100 pT range for whistler mode waves. Therefore, the required small wave condition for the averaging over one gyroperiod is easily achieved in most cases.

We have presented a simple set of equations describing cyclotron averaged motion of Landau resonant particles in a whistler mode wave propagating at an angle to the static magnetic field. We have argued that for the parameters of the earth's magnetosphere and for $f < f_H$, as it is the case for the whistler mode waves, this would be a very accurate description of the near resonant particles. The fact that the equations are compact and simple makes them suitable for analytical as well as test particle computer simulation studies presented in the next chapters.

III. ANALYTICAL STUDY OF LONGITUDINAL RESONANCE INTERACTIONS

A. INTRODUCTION

In the preceding chapter we derived a set of equations of motion (Eqs.2.62, 2.63) for an electron interacting with a whistler mode wave through a longitudinal resonance process. Before using those equations in numerical simulations it is useful to have a semi-quantitative analysis of that interaction process, the purpose of which is to:

a) Determine, qualitatively, the effects of different parameters on the resonance process, and to

b) Provide a reference for the testing and explaining of numerical results.

From the equations of motion and the resonance condition it is evident that the most important factors that affect the interaction process are:

1) The magnitude of the wave parallel electric field $E_{\parallel}$

2) The magnitudes of Bessel terms in the equations of motion

3) The wave phase velocity $v_{p\parallel}$

4) The electron parallel velocity $v_{\parallel}$

The variations of Bessel terms have already been discussed in Section II.E.

In the following text we discuss the remaining parameters

starting with calculations of expected magnitudes of $E_{\parallel}$ in the magnetosphere. Next we calculate the wave phase velocity $v_{p\parallel}$ and analyze the resonance condition $v_{p\parallel} = v_{\parallel}$ for a wide range of magnetospheric parameters. We also stress the importance of the phase between a wave and the interacting electrons and examine its variations. Finally, we discuss the energy exchange between the wave and electrons through the longitudinal resonance interaction in an inhomogeneous medium such as the magnetosphere.

B. RELATION OF $E_{\parallel}$ TO $B_{\perp}$ AND MAGNITUDE OF $E_{\parallel}$ FOR WHISTLER MODE WAVES

Two equations of motion of an electron (Eqs.2.62, 2.63) are given in terms of the wave parallel electric field $E_{\parallel}$ (E_z). However, it is useful to relate $E_{\parallel}$ to the wave perpendicular magnetic field $B_{\perp}$ (B_y) because most often wave amplitudes are given and referred to in terms of $B_{\perp}$. We proceed now with a derivation of the quantitative relationship between $E_{\parallel}$ and $B_{\perp}$.

Using the plasma dispersion relation (Eq. 2.22) it follows that

$$n^2 \sin\theta \cos\theta \, E_x + (\varepsilon_{\parallel} - n^2 \sin^2\theta) \, E_z = 0 \qquad (3.1)$$

or

$$n^2 \sin\theta \cos\theta \, E_x = - \left(1 - \frac{\omega_p^2}{\omega^2} - n^2 \sin^2\theta\right) E_z \qquad (3.1a)$$

Furthermore, from Maxwell's equation $\nabla \times E = -\frac{\partial \bar{B}}{\partial t}$ we have

$$k \cos\theta \; E_x - k \sin\theta \; E_z = \omega B_y \qquad (3.2)$$

Note that we use only amplitudes of $\mathcal{E}_z$ and $\mathcal{B}_y$, E_z and B_y, because both $\mathcal{E}_z$ and $\mathcal{B}_y$ vary as $\cos(\omega t - \bar{k} \cdot \bar{r})$.

Now, substituting E_x from (3.2) in (3.1a) we have

$$n^2 \sin\theta \cos\theta \quad \left(\frac{\omega B_y + k \sin\theta E_z}{k \cos\theta} \right) = -\left(1 - \frac{\omega_p^2}{\omega^2} - n^2 \sin^2\theta\right) E_z \qquad (3.3)$$

or

$$\frac{n^2 \sin\theta \; \omega B_y}{k} + \left(n^2 \sin^2\theta + 1 - \frac{\omega_p^2}{\omega^2} \, n^2 \sin^2\theta \right) E_z = 0 \qquad (3.4)$$

Finally,

$$E_z = \frac{n^2 \sin\theta \; \omega}{k\left(\frac{\omega_p^2}{\omega^2} - 1\right)} \; B_y \qquad (3.5)$$

or

$$E_{\parallel} = \frac{c \; n \; \sin\theta}{f_p^{\,2}/f^2 - 1} \; B_{\perp} \qquad (3.6)$$

Equation 3.6 relates $E_{\parallel}$ to $B_{\perp}$ for whistler mode waves, and it can be further simplified if $f_p^{\,2} >> f \cdot f_H$ when it becomes possible to use the QL approximation for the refractive index. The refractive index is

then given as

$$n^2 = \frac{f_p^2}{f(f_H \cos\theta - f)} \qquad (3.7)$$

and substituting (3.7) for n in Eq. 3.6 the final result is

$$E_{\parallel} = \frac{c}{n} \frac{\sin\theta}{(f_H/f)\cos\theta - 1} B_{\perp}. \qquad (3.8)$$

Eq. 3.8 was also derived by Helliwell [1965]. It relates $E_{\parallel}$ to $B_{\perp}$ for whistler mode signals assuming that QL approximation for a refractive index is valid.

Equation 3.6 can be applied to any whistler mode signal, although it is possible to derive similar equations for some special cases of propagation. One such special case is a whistler mode signal propagating in the Gendrin mode. This mode of propagation is characterized by the Gendrin angle θ_G which can be found by setting $\frac{d}{d\theta}(n \cos\theta) = 0$. The resulting wave normal angle θ_G is

$$\cos\theta_G = 2\frac{f}{f_H} \qquad (3.9)$$

It clearly follows from Eq. 3.9 that the propagation in the Gendrin mode is possible only if $f < f_H/2$ and that θ_G varies from 0° to 90° as f/f_H decreases from 0.5 to 0. The interesting properties of propagation at the Gendrin angle are summarized as follows:

i) Substituting (3.9) in (3.7) the refractive index is

$$n_G(\theta_G) = \frac{f_p}{f} \tag{3.10}$$

ii) The phase velocity in the direction of $\overline{B}_o$ is

$$v_{p''_G} = \frac{v_p}{\cos\ \theta_G} = \frac{c}{2}\frac{f_H}{f_p} \tag{3.11}$$

iii) The group refractive index and velocity are

$$n_{g_G}(\theta_G) = n_G(\theta_G) = \frac{f_p}{f} \tag{3.12}$$

$$v_{g_G}(\theta_G) = v_p = c\ \frac{f}{f_p} \tag{3.13}$$

iv) The group ray refractive index and velocity are

$$n_{g_{r_G}}(\theta_G) = n_{g_G}(\theta_G)\ \cos\theta_G = 2\ \frac{f_p}{f_H} \tag{3.14}$$

$$v_{g_{r_G}} = v_{p''_G} = \frac{c}{2}\frac{f_H}{f_p} \tag{3.15}$$

Figure 3.1 illustrates the shape of the refractive index curve for $f/f < 0.5$, and also shows the Gendrin angle θ_G. The second angle indicated in Fig.3.1, θ_R, is the resonance cone angle where the refractive index becomes infinite.

Thus, waves propagating at the Gendrin angle have their wave packets traveling in the direction of $\overline{B}_o$ with the velocity v_{gr_G}, which is identical to the phase velocity in that direction $v_{p''_G}$, and both

velocities are independent of the wave frequency. This property makes Gendrin mode waves rather interesting for longitudinal resonance interactions since electrons in resonance with those waves, i.e. $v_{\parallel} = v_{p\parallel} = v_{gr}$, do not drift through the wave packet during the interaction as they do in the most general case when the wave phase and ray group velocities along the magnetic field line are different.

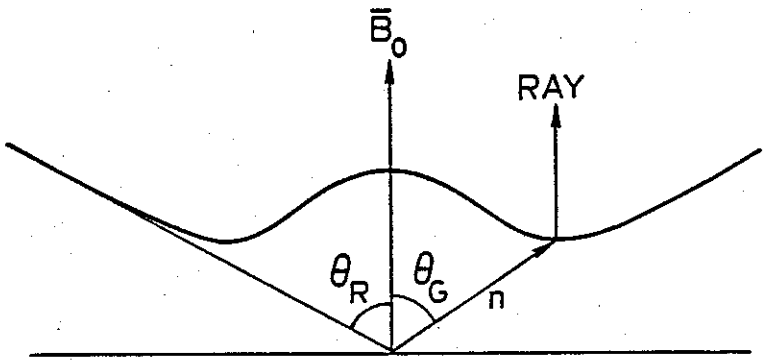

FIGURE 3.1. REFRACTIVE INDEX SURFACE FOR $f<f_H/2$. θ_R indicates the resonance cone where $n\to\infty$. θ_G is the Gendrin angle, for which the ray is aligned with the static magnetic field.

Returning to the derivation of the parallel electric field for the Gendrin mode waves we can substitute $n(\theta_G)$, $\cos\theta_G$ and $\sin\theta_G = \sqrt{1 - \cos^2\theta_G}$ for n, $\cos\theta$ and $\sin\theta$ in Eq. 3.8 assuming that $f_p^2/f \cdot f_H << 1$ is valid. The final result is then

$$E_{\parallel G} = c \cdot B_{\perp} \cdot \frac{f}{f_p} \sqrt{1 - \frac{4f^2}{f_H^2}} \qquad (3.16)$$

Note that Eq. 3.8 represents the most general expression for $E_{\parallel}$

(allowing for the QL approximation) and can also be used to compute $E_{\parallel G}$, whereas Eq. 3.16 is valid only for the Gendrin mode. At this point we can use Eqs. 3.8 and 3.16 to plot the magnitude of the parallel electric field $E_\parallel$ as a function of frequency. Three curves shown in Figure 3.2 are calculated for different values of the wave normal angle (30°, 50° and 70°), while the wave perpendicular magnetic field $B_\perp$ is taken to be 10 pT. This figure clearly shows the resonance cone effect; for a fixed wave frequency f the parallel electric field $E_\parallel$ increases as the wave normal angle increases and $E_\parallel$ approaches infinity as $\theta \to \theta_R$. The resonance cone angle θ_R can be found from Eq. 3.7 which yields (for the QL approximation) $\cos\theta_R = \frac{f}{f_H}$ and θ_R as a function of frequency is illustrated by the dashed line in Fig. 3.2. At this point we recall that an upper limit on the magnitude of $E_\parallel$ was already set during the derivation of equations of motion when they were time-averaged. Although this limit is not exceeded in most practical cases it is possible that those equations become invalid in a situation when $\theta - \theta_R < 0.5°$. In such a case it would be necessary to use the complete equations of motion (Eqs. 2.41, 2.42 and 2.43).

Figure 3.3 shows the wave parallel electric field $E_\parallel$ as a function of frequency and parametric in $B_\perp$ (10, 20 and 30 pT), while the wave normal angle θ for all curves is 30°. Figure 3.4 shows the wave parallel electric field $E_{\parallel G}$ for the Gendrin mode propagation as a function of frequency and parametric in $B_\perp$. The dashed curves show θ_G and θ_R as functions of frequency. By setting $\frac{d}{df} E_{\parallel G}(\theta_G) = 0$ it can be shown that $E_{\parallel_G}$ reaches a maximum at the frequency $f = 0.354\ f_H$ at which $\theta_G = 45°$. This result is interesting in the light of data on chorus

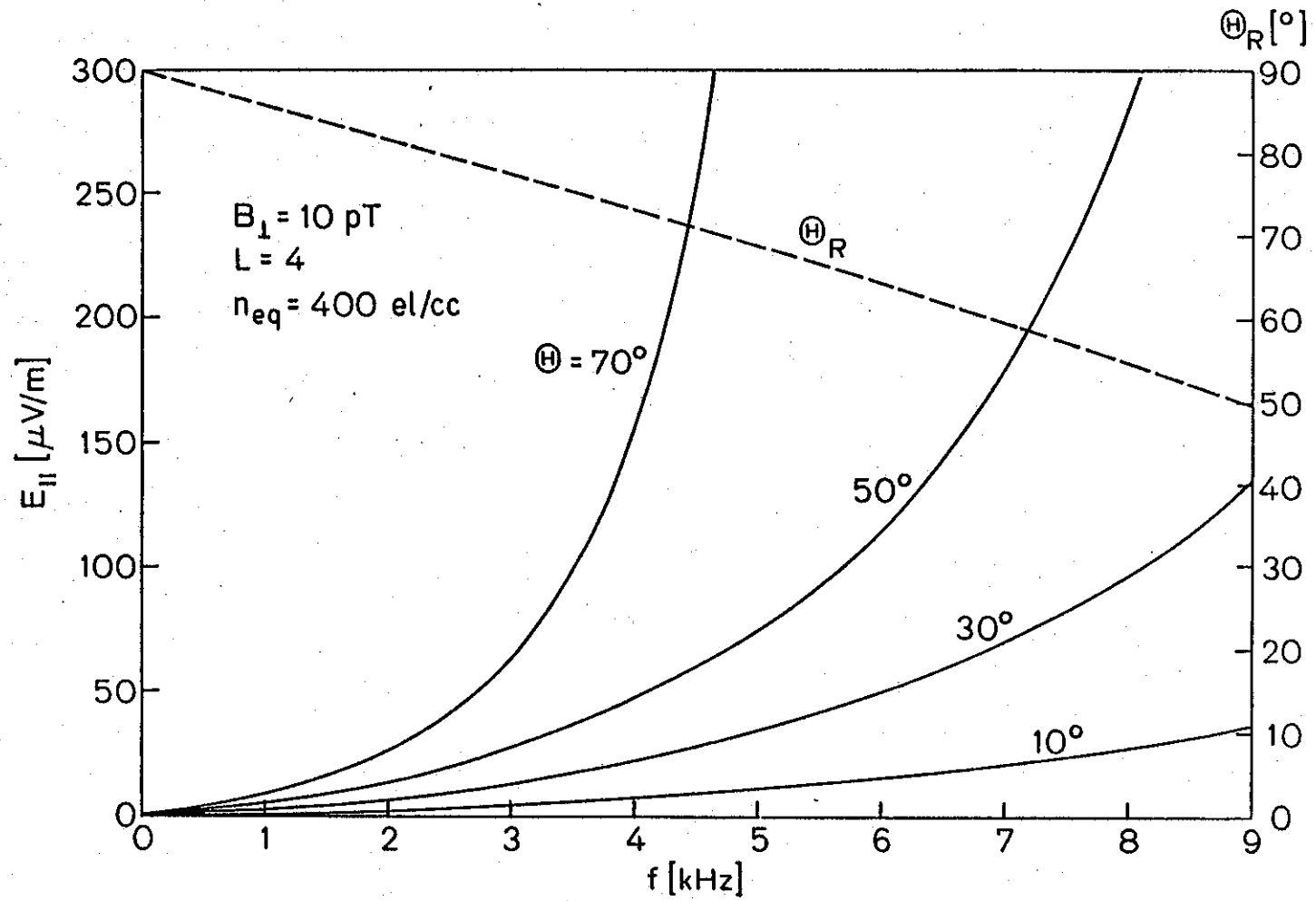

FIGURE 3.2 PARALLEL ELECTRIC FIELD $E_{\parallel}$ AS A FUNCTION OF FREQUENCY FOR A WHISTLER MODE SIGNAL WITH $B_\perp$ = 10 pT. Different solid curves represent different values of the wave normal angle θ. The dashed curve shows the resonance angle θ_R as a function of frequency.

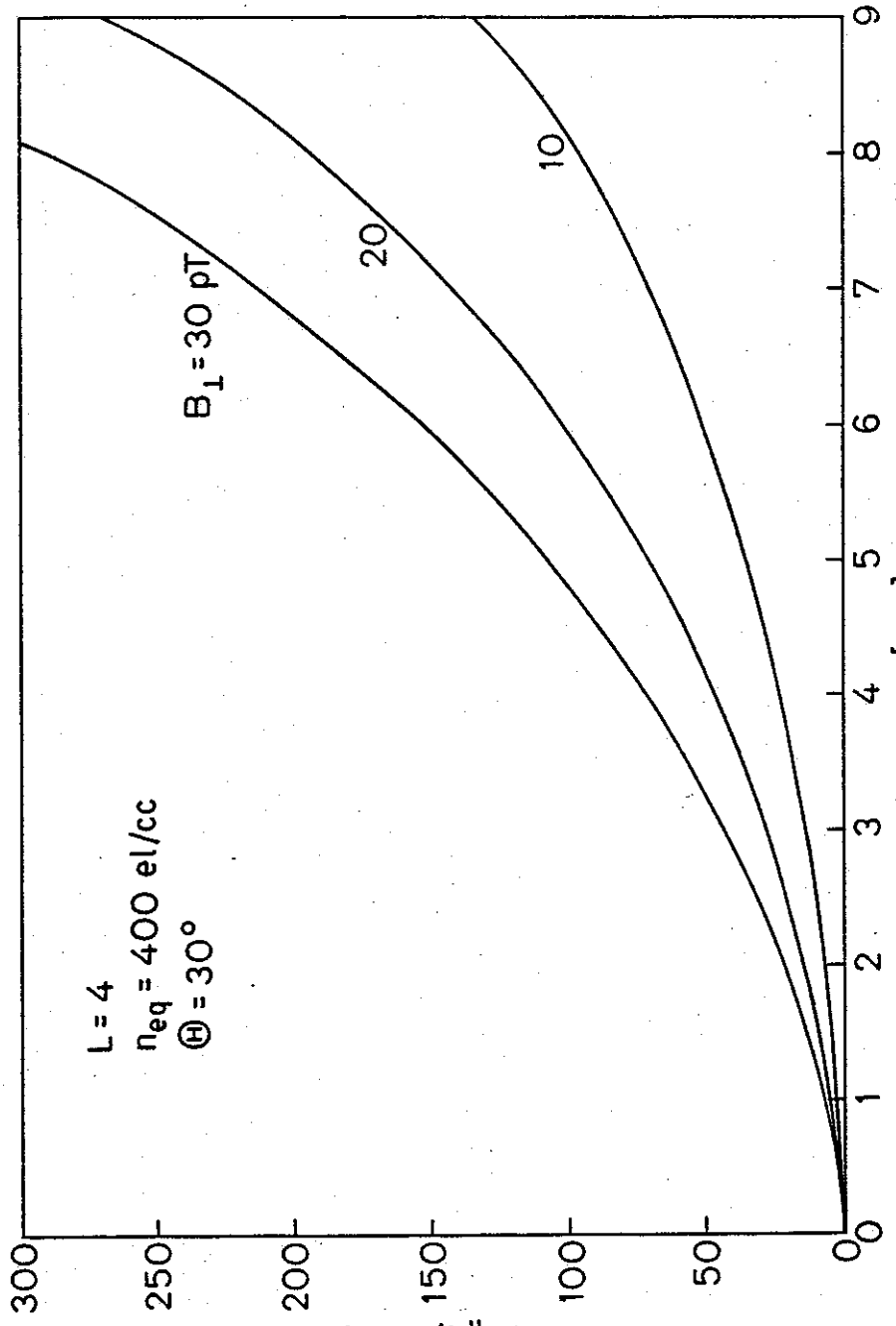

FIGURE 3.3 PARALLEL ELECTRIC FIELD $E_\parallel$ AS A FUNCTION OF FREQUENCY FOR A WHISTLER MODE SIGNAL, PARAMETRIC IN $B_\perp$.

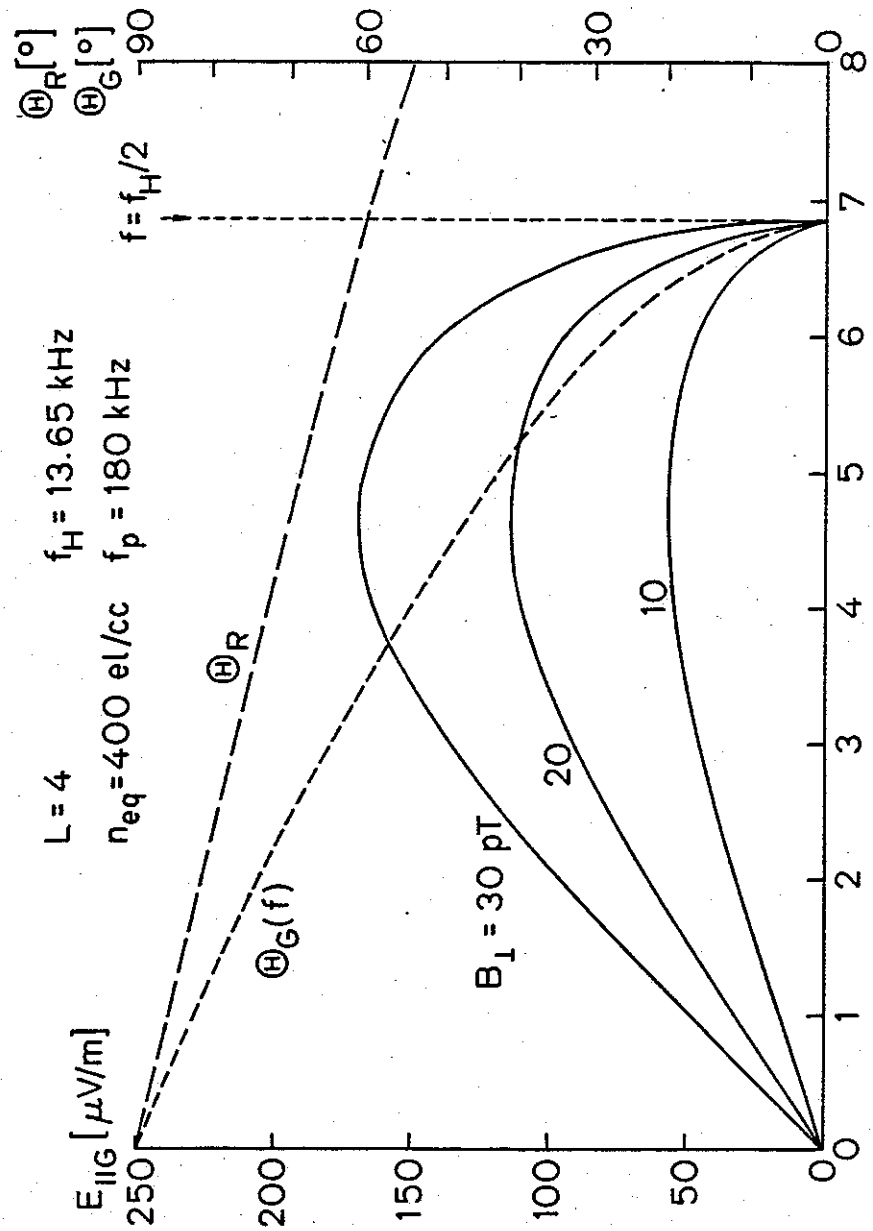

FIGURE 3.4 PARALLEL ELECTRIC FIELD $E_\parallel$ AS A FUNCTION OF FREQUENCY FOR A WHISTLER MODE WAVE PROPAGATING IN THE GENDRIN MODE. Note that $E_\parallel$ has a maximum at $f = 0.354\ f_H$. The two dashed curves indicate the resonance cone and Gendrin angles, θ_R and θ_G.

activity obtained by Burtis [1974]. It was found that in the equatorial region there are often observed two narrow bands of chorus. The upper band is commonly centered just above half the electron gyrofrequency, 0.5 f_H, while the lower band is centered near 0.35 f_H. Therefore, it may be speculated that the chorus lower band is made up of waves propagating in the Gendrin mode and that those waves are amplified through the strong longitudinal resonance due to their maximum $E_{\parallel G}$. This wave growth could then account for the observed peak of chorus activity.

Finally, Figure 3.5 shows $E_\parallel$ as a function of wave-normal angle θ; different curves in that figure correspond to different wave frequencies, while the $B_\perp$ is 10 pT. Again we see the resonance cone effect where $E_\parallel \to \infty$ as $\theta \to \theta_R$.

All of the above calculations were done at the equator of the the magnetic field line given by L = 4 and assuming n_{eq} = 400 el/cc. Similar calculations can be carried out for different L values and corresponding values of n_{eq}. Figure 3.6 shows the results of such calculations for a range of L values; corresponding values of n_{eq} used in those calculations are shown in Figure 3.7, with a plasmapause, characterized by the sharp decrease of electron density, located at L = 4. The wave parallel electric field $E_\parallel$ is also normalized by $B_\perp$ and given in μV/m/pT. From this figure it is evident that $E_\parallel$ for a given L value increases as the frequency of the signal increases, as already found before (see Fig. 3.2). Furthermore $E_\parallel$ is larger outside than inside the plasmapause, a fact which is directly related to lower electron density outside the plasmapause.

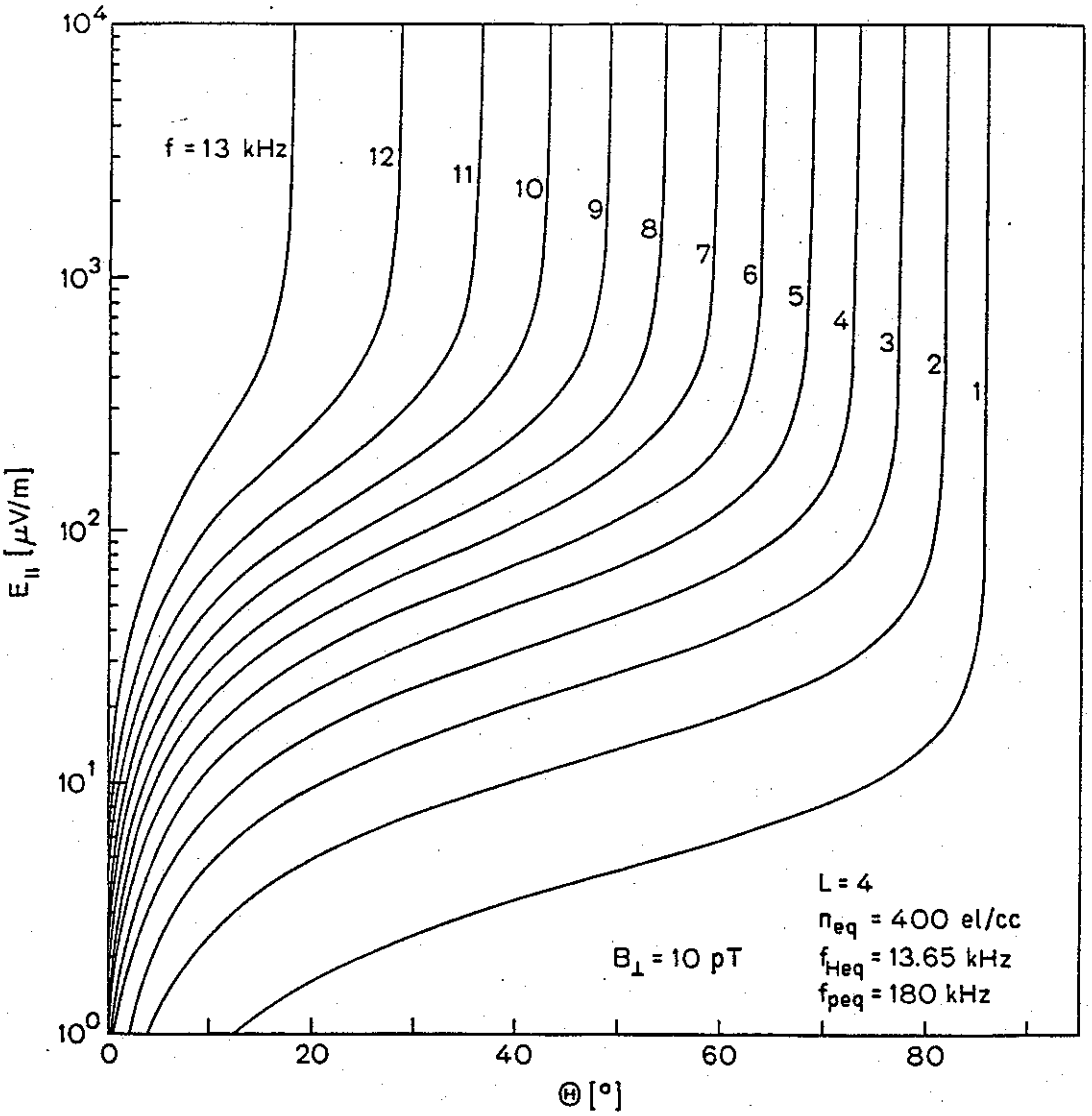

FIGURE 3.5 PARALLEL ELECTRIC FIELD $E_{\parallel}$ AS A FUNCTION OF WAVE NORMAL ANGLE θ. Different curves correspond to different wave frequencies. Note that $E_{\parallel} \to \infty$ as $\theta \to \theta_R$.

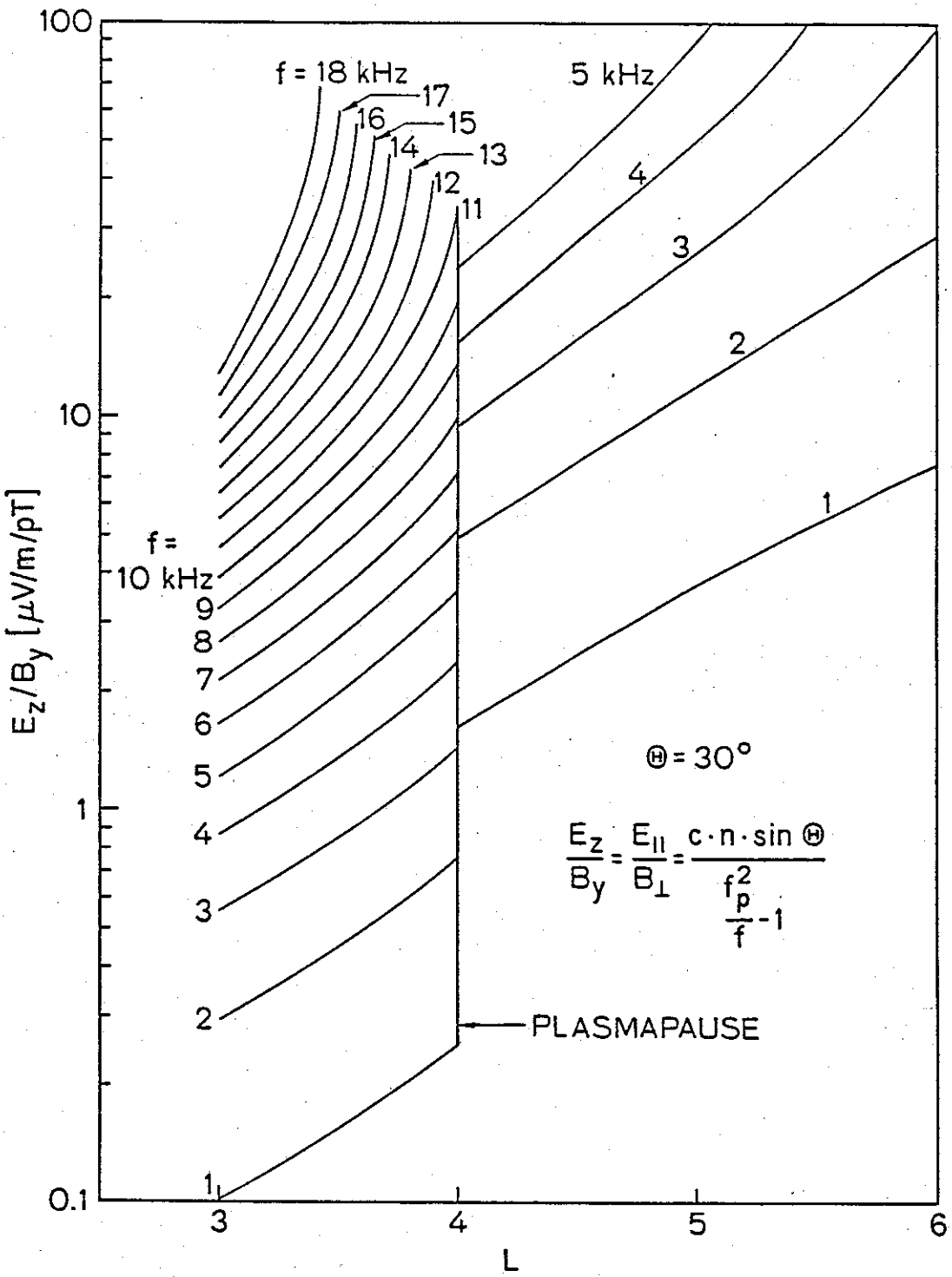

FIGURE 3.6 NORMALIZED PARALLEL ELECTRIC FIELD $E_{\parallel}/B_{\perp}$ AS A FUNCTION OF L VALUE. The normalized parallel electric field $E_{\parallel}/B_{\perp}$ is computed for different wave frequencies and the equatorial density profile shown in Fig. 3.7.

Summarizing, a stronger $E_{\parallel}$ (for a given $B_{\perp}$) can be achieved by increasing the wave frequency, or by raising the wave-normal angle, or both.

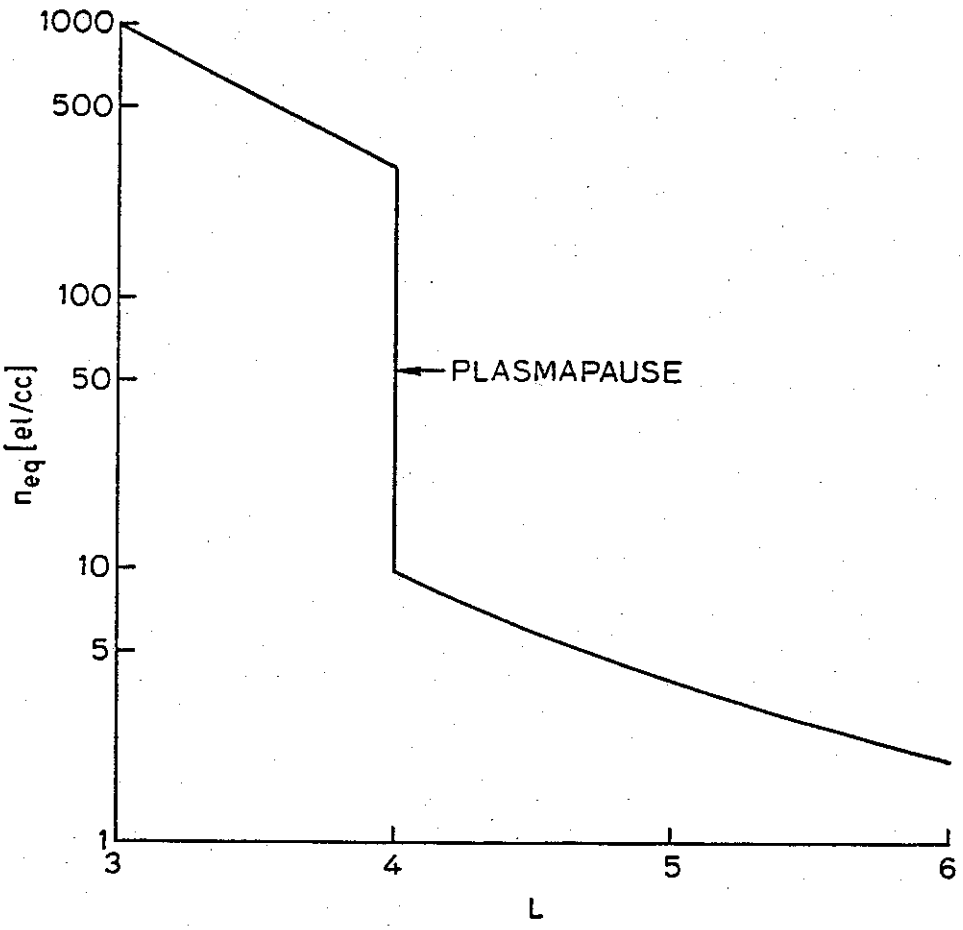

FIGURE 3.7 EQUATORIAL ELECTRON DENSITY AS A FUNCTION OF L VALUE. The plasmapause is located at L = 4.

An additional increase in $E_{\parallel}$ is also possible for waves propagating outside the plasmapause. However, waves with high wave-normal angles are usually associated with a non-ducted mode of wave propagation which in general is not field aligned, whereas in the ducted mode the wave normals are very nearly aligned with the magnetic field [Smith et al. 1960]. In the latter case guiding is based on the presence of linear field-aligned enhancement (or depression) of ionization referred to as a duct. Therefore, the effects of the longitudinal resonance involving ducted waves are limited by the low wave-normal angles of propagation at which magnitudes of the parallel electric field are low (see Fig. 3.2). There are other possibilities for wave guiding along the field line not limited to low wave-normal angle waves, such as when the plasmapause acts as a one-sided duct [Inan and Bell, 1978]. Still another possibility is to have a non-ducted wave which propagates in a field-aligned mode over a portion of the magnetospheric path. Although those waves usually remain field aligned only for a short period of time, their large $E_{\parallel}$ may be sufficient to cause a strong longitudinal resonance interaction.

The importance of field aligned propagation arises from the fact that electrons in the magnetosphere follow the earth's magnetic field as explained in Section II.A. Thus, if the ray path is not field aligned, or is only partially aligned, the interaction may be relatively weak.

C. RESONANCE CONDITION $v_{\parallel} = v_{p\parallel}$

Beside the equations of motion another important factor to be considered is the resonance condition $v_{\parallel} = v_{p\parallel}$ (Eq.2.8). As discussed above, this condition requires that the wave phase velocity in the direction of $\overline{B}_o$ match the particle velocity in that direction. However, for an inhomogeneous medium such is the magnetosphere, both the phase velocity $v_{p\parallel}$ and the electron parallel velocity $v_{\parallel}$ are variable and their variations depend on the magnetospheric model. Hence, in a case when the resonance condition is satisfied for a given wave and electron at some location in the magnetosphere, it will not in general hold at some other location. For that reason it is necessary to study how $v_{p\parallel}$ depends on different models used to represent electron density along the field line. It is also essential to examine variations of both phase and parallel velocities with latitude and to study variations of $v_{\parallel}$ for different pitch angles.

First, let us consider the phase velocity in the direction of $\overline{B}_o$ which is given as

$$v_{p\parallel} = \frac{c}{n \cdot \cos\theta} \qquad (3.17)$$

where n is the refractive index given by Eq. 3.7. Using Eq. 3.17 it is a simple task to calculate the phase velocity of a whistler mode wave for a wide range of parameters. Figure 3.8 shows the equatorial phase velocity as a function of L value; values of n_{eq} used here are again those of Fig. 3.6. Figures 3.9a,b show the phase velocity as a function

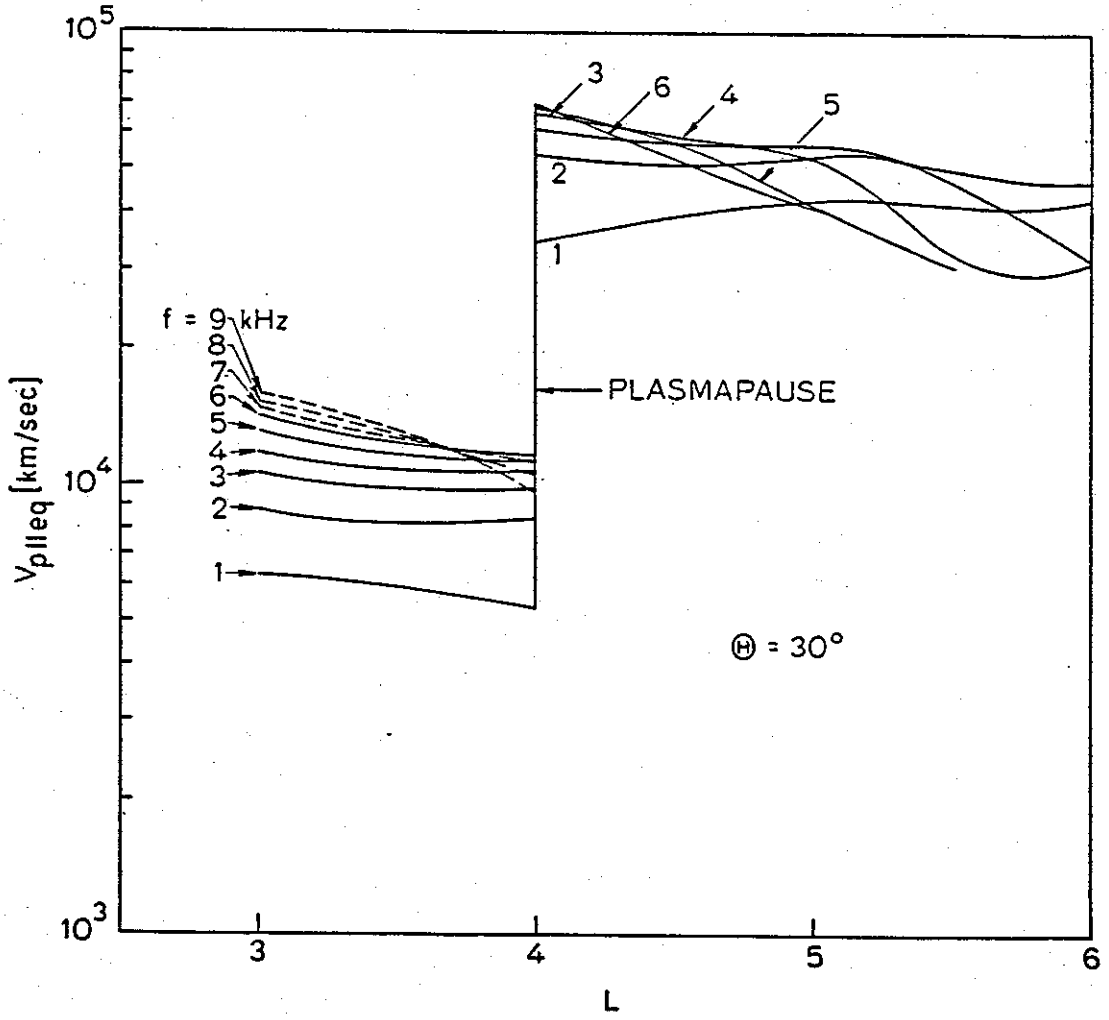

FIGURE 3.8 EQUATORIAL PARALLEL PHASE VELOCITY AS A FUNCTION OF L VALUE. Values of n_{eq} used to compute $v_{p_\parallel}$ are those of Fig. 3.7.

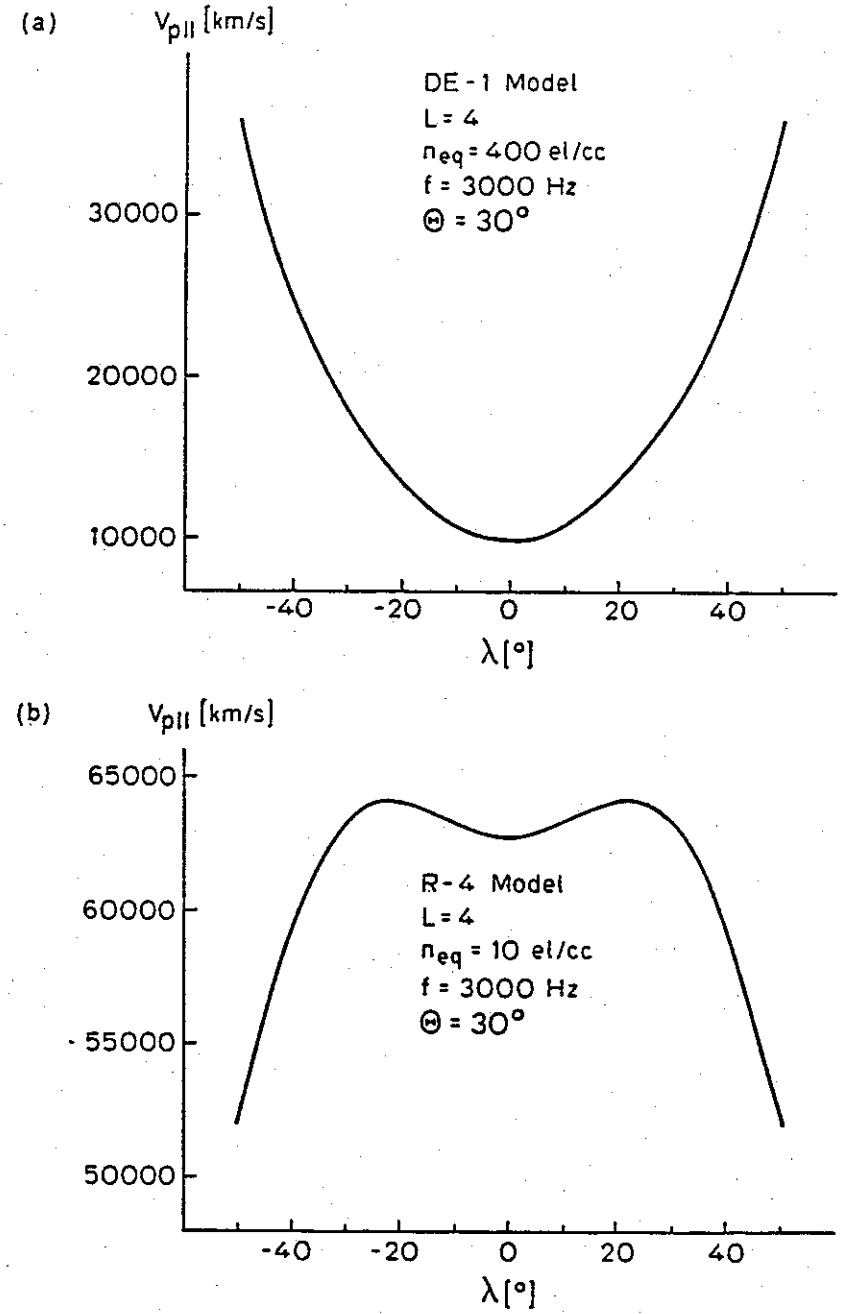

FIGURE 3.9 PARALLEL PHASE VELOCITY AS A FUNCTION OF LATITUDE FOR DIFFERENT MODELS OF THE DISTRIBUTION OF ELECTRON DENSITY ALONG THE FIELD LINE. In (a) electron density along the field line is represented by the diffusive equilibrium model DE-1, whereas in (b) the electron density is calculated the collisionless model R-4.

of latitude; Fig. 3.9a shows a typical shape of $v_{p\parallel}$ inside the plasmapause, while Fig. 3.9b shows $v_{p\parallel}$ outside the plasmapause. The difference between Figs. 3.9a and 3.9b reflects not only the assumed equatorial electron densities n_{eq} , but also the electron density distribution along the field line. Figure 3.9a is calculated using a diffusive equilibrium model [Park,1972], which is usually used inside the plasmapause. On the other hand, the electron density model of Fig. 3.9b is a collisionless model [Park, 1972] with the electron density along the field line approximated by

$$n = n_{eq}\left(\frac{1}{\cos^2\lambda}\right)^4 \qquad (3.18)$$

where λ is the latitude.

Evidently, from Fig. 3.9, the phase velocity of whistler mode waves outside the plasmapause exceeds that found inside. Therefore, the parallel velocity of an electron, which has to match the phase velocity of the wave, is also larger outside the plasmapause. Since the electrons are moving faster when interactions take a place outside the plasmapause the corresponding interaction times are shorter compared to interaction times inside the plasmapause. Thus, the effects of a stronger wave parallel electric field $E_\parallel$, related to propagation outside the plasmapause, tends to be offset by a reduced interaction time.

The parallel velocity as well as the wave phase velocity varies with latitude, as already shown in Section II.A, but the two variations are generally different. By combining the first adiabatic invariant and

the law of energy conservation we find that the parallel velocity is given by

$$v_{\parallel} = v_{\parallel eq}\sqrt{1+\tan^2\alpha_{eq} - \frac{\sqrt{4-3\cos^2\lambda}}{\cos^6\lambda}\tan^2\alpha_{eq}} \qquad (3.19)$$

where $v_{\parallel eq}$ is the electron equatorial parallel velocity, α_{eq} is the equatorial pitch angle and λ is latitude.

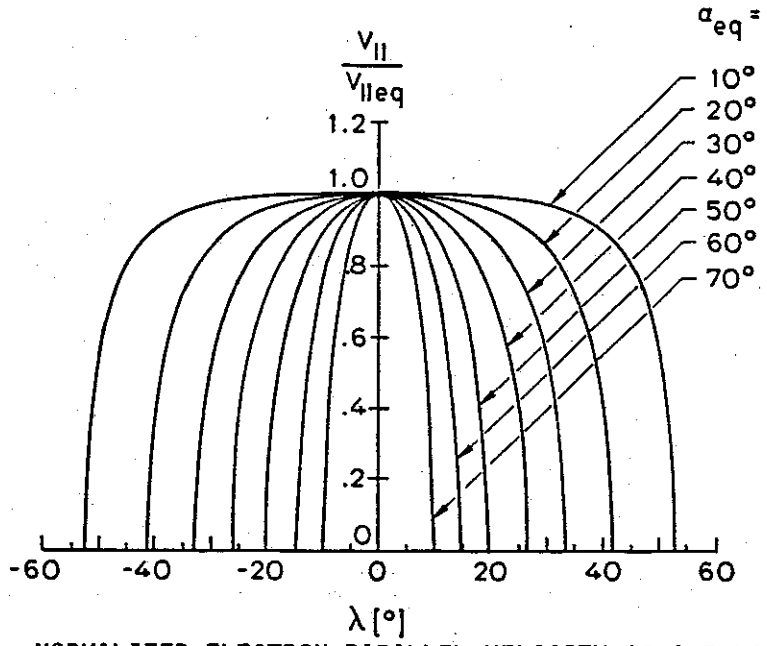

FIGURE 3.10 NORMALIZED ELECTRON PARALLEL VELOCITY AS A FUNCTION OF LATITUDE. Different curves correspond to different equatorial pitch angles. Note that the mirror point latitude, where $v_{\parallel} = 0$, decreases as the equatorial pitch angle increases.

Figure 3.10 shows the normalized parallel velocity as a function of latitude for different values of the equatorial pitch angle. This figure also shows mirror point latitudes where $v_{\parallel} = 0$. From Figs. 3.9 and 3.10 it is evident that the resonance condition for a given wave and electron may, or may not, be satisfied depending on the ratio of the equatorial phase and parallel velocities. Typical examples shown in

Fig. 3.11 are for three different ratios of the equatorial velocities. Note that the parallel velocities shown in Fig. 3.11 represent the unperturbed motion of electrons, i.e. Fig. 3.11 shows only adiabatic variations of $v_{\parallel}$. Although the adiabatic motion of electrons is altered by the wave-particle interaction, the electrons are identified in terms of their initial unperturbed equatorial parameters which simplifies the problem of comparing properties of different electrons.

Those different variations of $v_{p\parallel}$ and $v_{\parallel}$ with latitude and their effects on the interaction process, along with effects of other factors are further discussed in the chapters on numerical results.

D. PHASE BETWEEN WAVE AND ELECTRON IN LONGITUDINAL RESONANCE

In Chapter II it was shown that the electrons trapped in the wave potential well execute an oscillatory motion around the bottom of the potential well. In general the analytical solution of the equation of motion for that case is very complex, but it is possible to derive an approximate solution if the maximum amplitude of the oscillation remains relatively small. From Eq. 2.12 the parallel electric field $E_{\parallel}$, as seen by electrons in the wave frame, is given by

$$E_{\parallel} = E_{\parallel_0} \sin(k_{\parallel} \cdot z) \qquad (3.20)$$

Therefore, the force exerted on an electron is

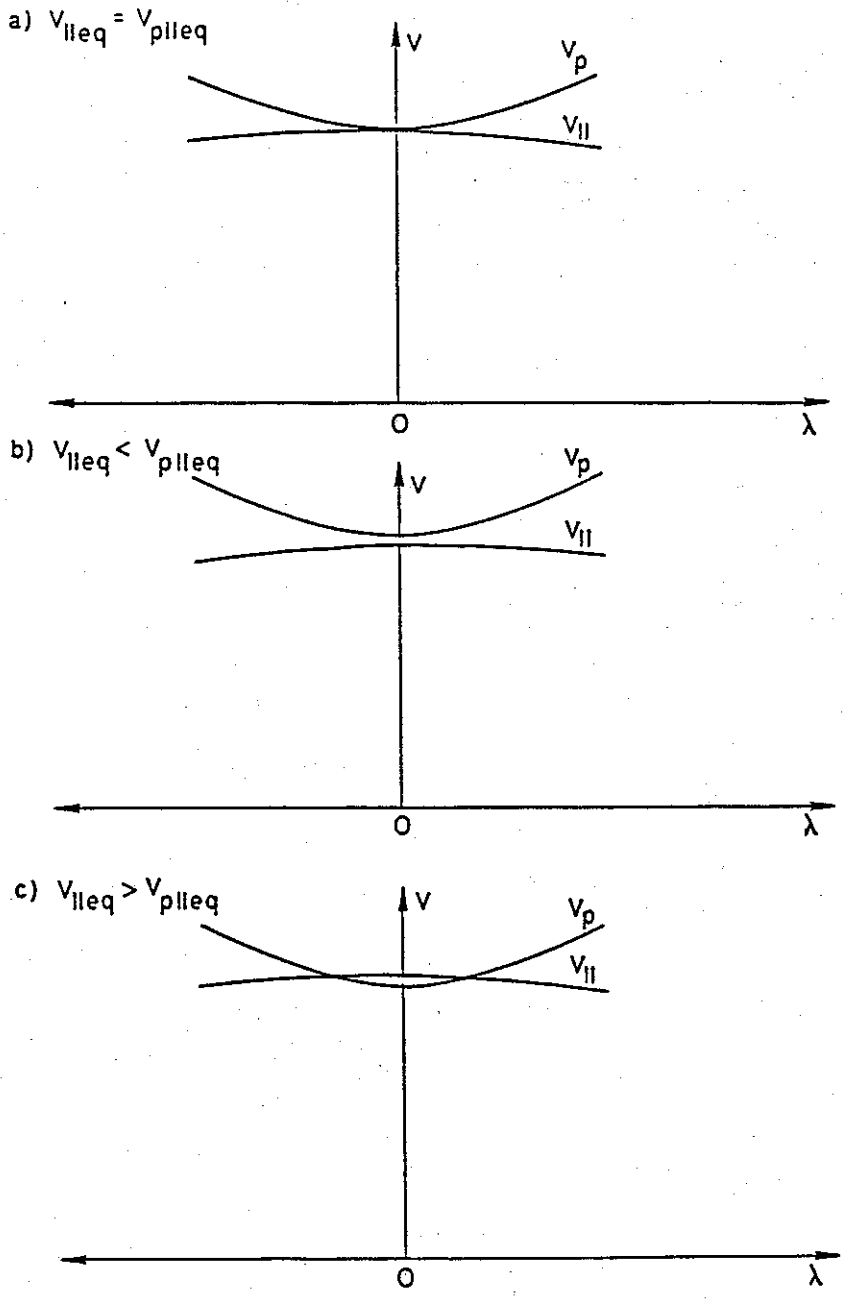

FIGURE 3.11 RELATION BETWEEN $v_\parallel$ AND $v_{p_\parallel}$ ALONG THE FIELD LINE. Depending on the ratio of $v_{\parallel eq}/v_{p_\parallel eq}$ there may be one (a), none (b), or two (c) latitudes at which the longitudinal resonance condition $v_\parallel = v_{p_\parallel}$ is satisfied.

$$m\frac{d^2z}{dt^2} = q\, E_{\parallel o}\sin(k_\parallel \cdot z) \qquad (3.21)$$

which, for a small amplitude oscillation where $\sin(k_\parallel \cdot z) \cong k_\parallel \cdot z$, can be written as

$$\frac{d^2z}{dt^2} = \frac{q}{m}\, E_{\parallel o} k_\parallel \cdot z \qquad (3.22)$$

The solution of Eq. 3.22 is

$$z = z_B \sin(\omega_t \cdot t) \qquad (3.23)$$

where z_B is the position of the bottom of the potential well as shown in Fig. 2.2, z is the position of the electron and ω_t is the period of oscillation given as $\omega_t = \sqrt{\frac{e\, E_{\parallel o}\, k_\parallel}{m}}$. It should be noted that although this oscillation period is computed for a homogeneous medium, this result can also be used in the case of a slowly varying medium such as the magnetosphere. Now, dividing Eq. 3.23 by the wavelength, we obtain the relative phase between the reference point at the potential well bottom and the electron. This relative phase is

$$\phi_r = \frac{z_B}{2\pi/k_\parallel} \sin(\omega_t \cdot t) \qquad (3.24)$$

$$\phi_r = \phi_B \sin(\omega_t \cdot t) \qquad (3.24a)$$

The relative phase between the wave and the trapped electron is also oscillatory in its nature and the phase variation is bounded such

that $\phi_B < 360°$. It should also be noted that the smallest amplitude of the phase oscillation- corresponds to the case of strongest trapping. On the other hand the relative phase variation for untrapped electrons is represented by constantly increasing ($v_{p\parallel} > v_\parallel$) or constantly decreasing ($v_{p\parallel} < v_\parallel$) phase as those electrons drift backward or forward through the wave, respectively.

All of the above computations, as already pointed out, are carried out in the wave frame which moves in the z direction at the phase velocity $v_{p\parallel}$. In order to determine the total phase variation let us again assume propagation as exp $i(\omega \cdot t - \bar{k} \cdot \bar{r})$. The instantaneous frequency ω_i can be found by taking the time derivative $\frac{d}{dt}(\omega \cdot t - \bar{k} \cdot \bar{r})$ which yields

$$\omega_i = \omega - \bar{k} \frac{d\bar{r}}{dt} \tag{3.25}$$

where ω_i is actually the Doppler shifted frequency of the wave as seen by an electron placed at a location defined by radius vector $\bar{r}$. It is possible to rewrite Eq. 3.18 in the same form as that of Eq. 2.6 by using $\frac{d\bar{r}}{dt} = v_\parallel$ and substituting $m \cdot \omega_H$ for ω_i. Equation 3.24 can now be used to examine a behavior of the total phase between a wave and an electron. First, rewriting (3.25) we have

$$\omega_i = \omega - k_\parallel \cdot v_\parallel \tag{3.26}$$

If $\omega_i = 0$ Eq. 3.26 reduces to Eq. 2.7, or

$$v_{p\parallel} = v_{\parallel} \tag{3.27}$$

which is the original longitudinal resonance condition. Therefore, if $v_{\parallel} = v_{p\parallel}$ the relative phase ϕ_r remains constant (Eq. 3.24a).

However, if an electron has a parallel velocity which does not match the wave phase velocity exactly the instantaneous (Doppler shifted) frequency ω_i has a non-zero value. In that case both the sign and the magnitude of ω_i depend on the difference between the parallel velocity and the phase velocity; when $v_{\parallel} < v_{p\parallel}$, ω_i is positive and its magnitude increases as $v_{\parallel}$ decreases assuming that $v_{p\parallel}$ is constant; in a case when $v_{\parallel} > v_{p\parallel}$ the instantaneous frequency ω_i is negative and its magnitude increases as $v_{\parallel}$ increases, again assuming a constant $v_{p\parallel}$.

When ω_i is known the total phase shift can be expressed as

$$\phi = \int_t \omega_i dt \tag{3.28}$$

or as

$$\phi = \int_s \frac{\omega_i}{v_{p\parallel}} ds \tag{3.29}$$

where we have used the identity $dt = \frac{ds}{v_{p\parallel}}$.

Finally, Table 3.1 summarizes qualitatively the behavior of the total phase shift as a function of $v_{p\parallel} - v_{\parallel}$.

The phase between the wave and the electron is a very important factor in the trapping process. It is eventually the phase that determines if a given wave will trap any electrons, although all other

resonance conditions may already be met, i.e the parallel velocity is close to the phase velocity and the parallel electric field is strong enough to pull the electron into the potential well. There is no trapping if the phasing is wrong, i.e. if electrons are accelerated when trapping would require deceleration or vice versa. The numerical results will show that a small difference in phase, less than 10°, can make a large difference in the behavior of electrons for which the resonance condition $v_{p\parallel} = v_{\parallel}$ is satisfied. Furthermore, the phase directly translates into the position of an electron within a wave packet (Eq. 3.24) and if there is any space bunching of electrons there must exist a corresponding phase bunching.

Velocity Conditions	$v_{p\parallel} - v_{\parallel} > 0$	$v_{p\parallel} - v_{\parallel} < 0$
Magnitude of Total Phase Shift	Positive and increases with time	Negative and decreases with time
Rate of Phase Change with Time	increases as $v_{p\parallel} - v_{\parallel}$ increases	increases as $v_{p\parallel} - v_{\parallel}$ decreases

Table 3.1 PHASE SHIFT PROPERTIES OF LONGIDUTINALLY RESONANT ELECTRON AS A FUNCTION OF PARALLEL VELOCITY CONDITIONS.

E. ENERGY EXCHANGE

In Chapter II we have discussed the energy exchange between the wave and trapped electrons in a homogeneous medium. For the case of an inhomogeneous medium the energy exchanged during a longitudinal interaction can be computed in a similar fashion. However, we shall see later when presenting numerical results that the longitudinal resonance in the magnetosphere may, or may not, involve trapping of electrons. It will also be shown that electrons in both cases, whether they are trapped or not, exchange their energy with a wave. The energy exchange process is quite different in those two cases, but it is still possible to use an equation similar to Eq.2.18 by using correct velocity limits for integration and an adequate value to represent the energy exchanged through the interaction with a single electron. It is then also essential to compare contributions from both groups of electrons (trapped and untrapped), and to determine whether there are situations where the contribution from either group is negligible.

Here we recall that in the case of a homogeneous medium the energy is exchanged only during the trapping process, i.e. only during the period when the electrons are accelerated/decelerated by the wave in order to match the phase and parallel velocities, and there is no net energy exchange after that process is finished, or alternatively, an electron has to be trapped in order to exchange its energy with a wave. There is still an instantaneous energy exchange after the trapping is completed because electrons oscillate at the bottom of the potential well, but when this instantaneous energy is averaged over one trapping

period there is no net effect. This is so because the electron's oscillatory motion is perfectly symmetric around the bottom of the potential well, shown by Eq. 3.20, whereas in the magnetosphere or any other inhomogeneous medium, the energy can also be exchanged after the electrons are trapped. This can be explained as follows; after an electron is trapped its parallel velocity is very close or equal to the wave phase velocity and it follows the phase velocity variations as long as that electron remains trapped. Thus, the perturbed parallel velocity is different from the parallel velocity that a particular electron would have in the absence of the wave. This difference, $\Delta v_{\parallel}$, is directly proportional to the phase velocity changes [Brice, 1960] and it is given as

$$\Delta v_{\parallel} = \left(\frac{\partial v_p}{\partial s} \right)_f ds + \left(\frac{\partial v_p}{\partial f} \right)_f df \qquad (3.30)$$

where, in general, phase velocity depends on both frequency and position. For the positive sign of $\Delta v_{\parallel}$ the electron gains energy, while for the negative sign the wave gains energy. We shall discuss further various aspects of Eq. 3.30 later in the text.

In the next chapters we present results of a test particle simulation of the wave-particle interaction and illustrate various aspects of the interaction as they were discussed in the above analysis.

IV. DESCRIPTION OF THE NUMERICAL SIMULATION

A. INTRODUCTION

In this chapter we detail procedures used in numerical simulations of the time-averaged equations of motion. The method used in this report is a test particle simulation. This approach uses a single particle to find wave induced perturbations of the particle trajectory, and it is feasible to test quantitatively the effects of various factors already considered in a qualitative analysis presented in Chapter III. The test particle approach can be further expanded to determine the perturbations of a full particle distribution by computing the effects of the wave on an adequate number of particles that are appropriately distributed in the phase-velocity space. However, there are restrictions imposed on the full distribution simulations because there is no feedback that should account for variations of the wave amplitude as particles and the wave exchange their energies. This feedback problem is treated in more detail in a discussion of the numerical results.

The actual listing of the particle code used in all simulations presented here is given in Appendix B. Next we outline the basic operation of the program.

B. COMPUTATION OF PROPAGATION AND ADIABATIC MOTION PARAMETERS

The representation of the static magnetic field along the field line is based on a centered magnetic dipole model described by Eq. 2.1. Values of B_o obtained from that equation are then used to compute local values of the gyrofrequency f_H, as well as to compute a normalized gradient of the magnetic field $\frac{1}{B_o}\frac{dB_o}{dz}$. At the same time a cold plasma density variation along the field line can be calculated using two different models. One model assumes diffusive equilibrium [Angerami and Thomas, 1964] with the electron density along the field line given as

$$N_{DE}(r) = \left[\sum_{i=1}^{n} \delta_i e^{G/S_i}\right]^{1/2} \qquad (4.1)$$

where the δ_i are the relative concentrations of the ionic species, n is the number of species, $G = r_b[1 - (r_b/r)]$, r_b is the geocentric distance (in kilometers) to the base of the DE model, $S_i = 1.506T(r_b/7370)^2(1/4^{i-1})$, and T is temperature at the base of the DE model (r = 1000 km). A second model is a collisionless model for which the density is given by Eq. 3.18. The input parameters needed to uniquely define the field line and propagation properties are L value, the equatorial cold plasma density n_{eq}, the wave frequency f, and the wave-normal angle θ. Given those parameters the program divides the entire field line in spatial segments 10 kilometers long and than computes, and stores, values of $v_{p\parallel}(z)$, $k_\parallel(z)$, and $\frac{1}{B_o}\frac{dB_o}{dz}$ for each segment; z is a distance between the equator and a particular 10 km

segment measured along the field line. The stored values of $\frac{1}{B_o}\frac{dB_o}{dz}$, as seen from Eqs. 2.62. and 2.63, are used to compute adiabatic terms in the equations of motion. All of the above computations can be done either for a general whistler mode wave or for the Gendrin mode wave. In the latter case the program also computes, and stores, values of $\theta_G(z)$ and $E_{\parallel G}(z)$. In addition the program also computes, and stores, values of wave phase change given as $\int_z k_\parallel dz$. In contrast to other parameters the values of $\int_z k_\parallel dz$ are not symmetric about the equator and depend on the latitude where the particles are started. This starting latitude, i.e location where particles start their motion along the field line, is also one of the input parameters.

C. NUMERICAL INTEGRATION OF THE EQUATIONS OF MOTION

Before we start with simulations each particle must be uniquely defined by an appropriate set of parameters. Those parameters then describe the particle's position in phase-velocity space. For particles in the magnetosphere the velocity coordinate is uniquely given by their equatorial parallel velocity $v_{\parallel oeq}$ and equatorial pitch angle, α_{oeq}. As particles move along the field line their corresponding equatorial parallel velocities can be computed with the help of Eq. 3.19. At the same time the local pitch angle is related to the equatorial pitch angle through

$$\sin\alpha = \sqrt{\frac{B_o(z)}{B_{oeq}}}\,\sin\alpha_{oeq} \qquad (4.2)$$

where $B_o(z)$ is the local value of the static magnetic field, and B_{oeq} is the equatorial magnetic field.

In this report a given particle is always identified in terms of the equatorial parameters which then simplifies the task of comparing properties of different particles. The conversion from local to equatorial values is made on the assumption of unperturbed particle motion.

In addition to the velocity $v_{\parallel oeq}$ and pitch angle α_{oeq} there is a third parameter, the initial phase ϕ_o, which determines the position of a particle with respect to the wave packet at the beginning of the interaction (this is a local, as opposed to an equatorial, quantity). In order to examine the dependence of the interaction results on the initial particle phase a simulation is actually done using twelve particles uniformly distributed in phase space; the parallel velocity and pitch angle are, however, identical for all twelve particles. This assembly of twelve particles uniformly distributed in phase is called a test sheet and is illustrated in Figure 4.1. It should be recalled that, as already emphasized in Section III.D, the phase between a particle and a wave is directly related to the particle's position in the z-axis direction. This is important because if particles are distributed in phase, i.e. space, the starting time t of the integration must be increased by $\Delta t = \frac{\lambda}{12 v_{p\parallel}}$ from particle to particle in order to maintain a correct phase separation between the particles in the sheet. This is especially important in particle phase (space) bunching calculations where particle positions determine the

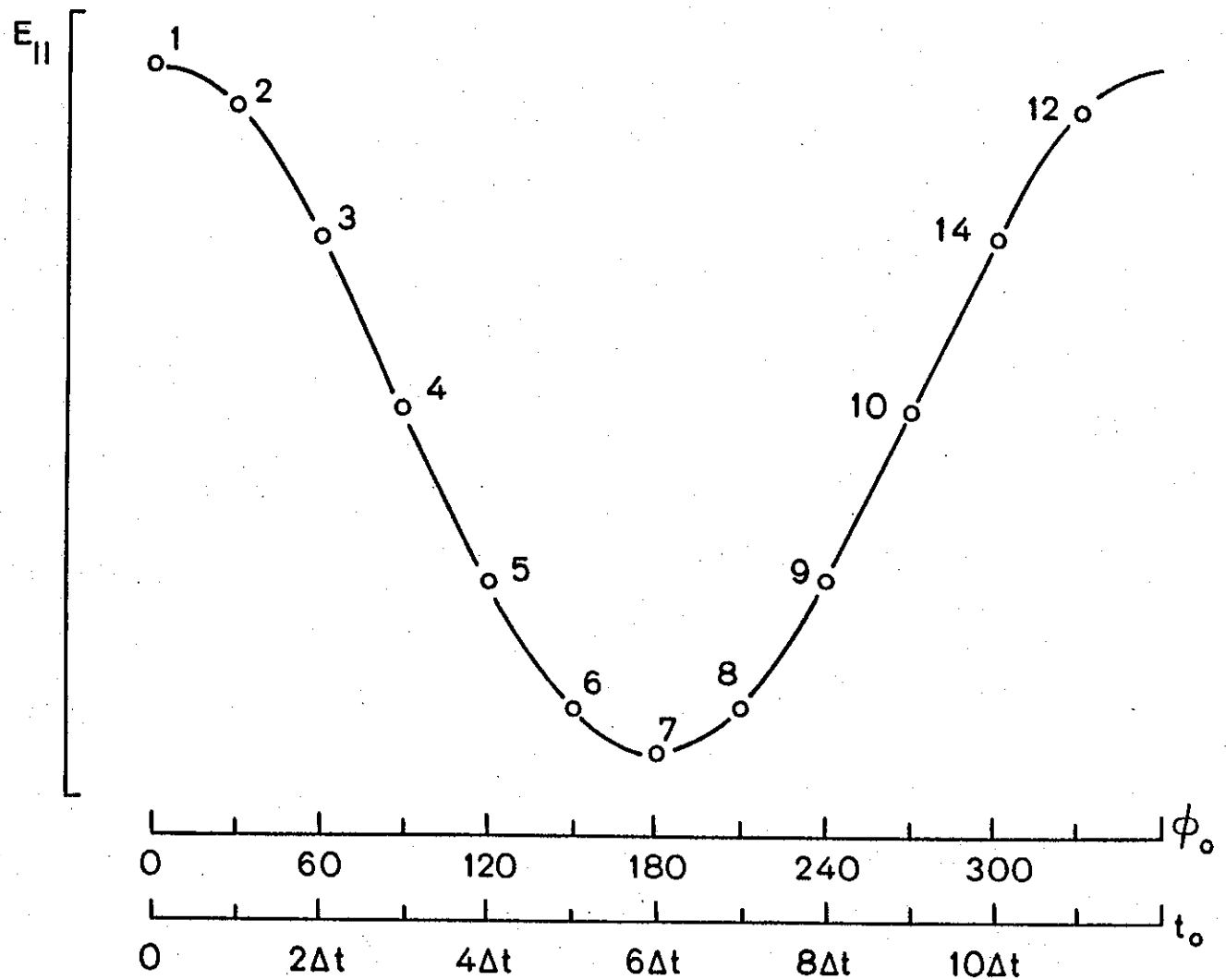

FIGURE 4.1 INITIAL UNIFORM DISTRIBUTION OF ELECTRONS FORMING A TEST SHEET. At the beginning of the simulation electrons are uniformly spaced in phase every 30° throughout one cycle of $E_{||}$. For explanation of different initial times t_o see text.

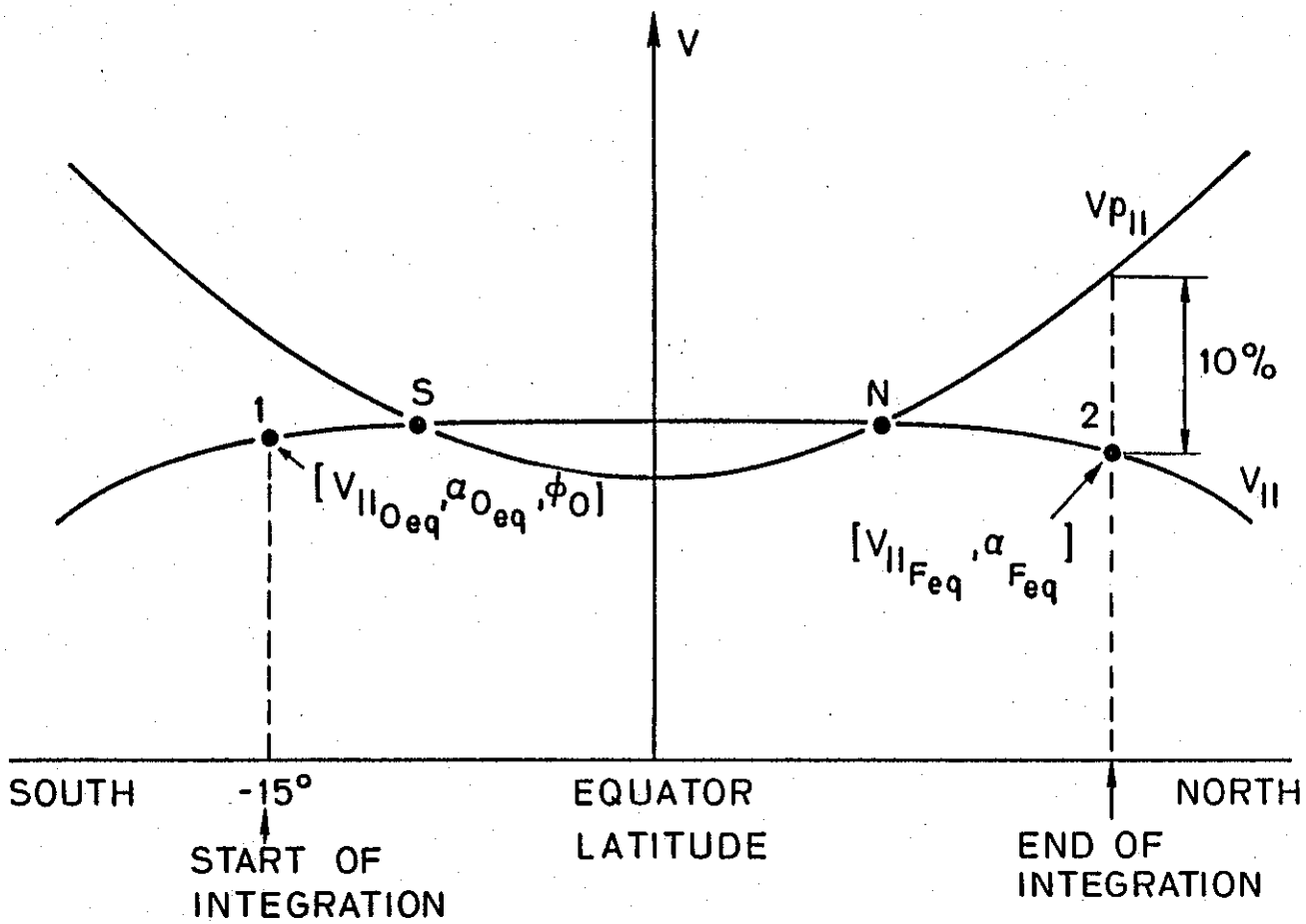

FIGURE 4.2 INTERACTION OF THE WAVE AND A TEST PARTICLE. Both the wave phase and particle parallel velocity vary with latitude, and, in general, the longitudinal resonance condition is satisfied at two locations along the field line.

extent of bunching.

After particles are injected at a given latitude their motion is altered due to the wave force which is computed by numerical integration of the equations of motion. A proper value of the starting latitude, for interactions with a monochromatic CW signal as illustrated in Fig. 4.2, was found experimentally by gradually increasing the distance between the first resonance location and the location of particle injection, and finding a latitude where further increase of this distance caused no significant changes of the final results. The actual integration of the equation of motions is done using a simple predictor-corrector method using temporal steps with $\Delta t = 0.001$ msec. This time step size was also found experimentally, and for smaller size step there were only insignificant fluctuations of the final results in all of the examples presented later in the text. The integration method itself consists in predicting a position of a given particle after elapse of one time increment using current values of force, i.e. using those forces acting on the particle at the beginning of the time increment. However, after the particle reaches a new position forces acting on it are also different, and it is necessary to recompute (correct) the particle's position by using the average force. This average force is found as a mean value of two forces, one at the beginning and one at the end of the time interval Δt. This newly computed position of the particle is then taken as a new starting point, and the whole process is repeated.

For a case of a monochromatic CW wave particles travel along the field line and reach the first resonance point (Fig. 4.2) where the wave

induced perturbations of particles trajectories become stronger and stronger. At this point further behavior of the particles is very dependent on the initial phase ϕ_o . Although all particles have their motion altered by the wave forces only a certain class of particles becomes trapped, i.e. only those with an appropriate phase, while other particles remain untrapped. However, in both cases the integration is continued until all particles reach their second resonant point on the other side of the equator. After that moment the wave induced perturbations become smaller and smaller as the difference between particles parallel velocities and the wave phase velocity increases. The end point of the integration is then defined as the location where the absolute difference between the two velocities exceeds 10%. This value was determined experimentally, and the particular latitude where the above condition occurs is called the detrapping latitude.

As the particle moves along the field line from the starting point toward a detrap point it has its adiabatic pitch angle variation modified by the wave. Finally, after the particle reaches its detrap point it will have certain α_F and $v_{\parallel F}$ which are then transformed into the corresponding equatorial values α_{Feq} and $v_{\parallel eq}$ by using (4.1) and (3.19). The difference $\alpha_{oeq} - \alpha_{Feq}$ gives the total pitch angle change, or scattering, while the difference $\Delta v_\parallel = v_{\parallel oeq} - v_{\parallel Feq}$ gives the total energy exchange through $1/2\ m\ \Delta v_\parallel^2$. The final scattering and the amount of transferred energy are given both for each individual particle and for a complete test particle sheet (mean value for 12 particles).

In the next chapters we study the scattering of particles and

the energy exchange process for different wave functions and a wide range of particle initial parameters.

V. NUMERICAL ANALYSIS OF THE INTERACTION

A. INTRODUCTION

In the previous chapters we have derived a set of equations of motion for longitudinally resonant electrons, and we have studied analytically various aspects of the resonance process. Those analytical studies are now complemented by the results of the numerical simulation analysis. Numerical results should further illuminate the physics of the interaction process, and enable us to compare the effects of various parameters on a quantitative basis, i.e. in terms of scattering and energy exchange efficiencies. The behavior of individual electrons and sheets is studied for a wide range of the parameters such as $E_{\parallel}$, n_{eq}, L, α_{eq}, ϕ_o, and for different wave functions, i.e. for different wave amplitude variations along the field line. In our calculations we have used three different types of wave functions as they are described below:

a) Monochromatic CW wave with a constant wave amplitude along the field line.

b) One-sided wave function characterized by a very weak wave on one side of the equator and a strong wave on the other side. The transition region between the above regions is taken to be 1000 km long and starting at the equator. Such a wave function can be created through a gyroresonance process.

c) Spatial amplitude pulse formed by a non-ducted wave when its ray path is partially field aligned.

In the following discussion we present results of the numerical simulations.

B. SCATTERING OF A SINGLE SHEET INTERACTING WITH CW SIGNAL

For a case of monochromatic CW signal the interaction geometry is already shown in Fig. 4.2, with electrons being injected at -15^{o} latitude. All electrons are identified in terms of their equatorial parameters, $v_{\parallel eq}$ and α_{eq}, with the initial phase ϕ_o being a third parameter. First, we consider scattering of a single sheet (12 electrons uniformly distributed in phase at the injection point) as a function of the initial equatorial parallel velocity $v_{\parallel eq_o}$. Other parameters for this example are listed in Table 5.1 below.

Field Line	L = 4
Equatorial Electron Density	n_{eq} = 400 el/cc
Equatorial Gyrofrequency	f_H = 13.65 kHz
Equatorial Plasmafrequency	f_p = 180 kHz
Wave Amplitude	$B_\perp$ = 10 pT
Wave Frequency	f = 3 kHz
Wave Normal Angle	$\theta = 30^{o}$
Equatorial Parallel Phase Velocity	$v_{p_{\parallel eq}} = 9.924\ 10^{6}$ m/s

Table 5.1 PARAMETER VALUES FOR THE EXAMPLE CASE

At this point we should note that we have used two approximations in numerical computations. First, it is assumed that the wave-normal angle is fixed, and second, the wave amplitude is also treated as though it has a constant value. However, it is well known that in the magnetosphere both wave-normal angle and wave amplitude change with location. The wave-normal angle changes as dictated by the guiding mechanisms [Helliwell, 1965] which is true for ducted waves, whereas wave-normals of nonducted waves can be found using ray-tracing analysis [Kimura, 1966, Burtis, 1974]. The wave amplitude variation arises from the inhomogeneity of the magnetosphere, and it is feasible to use a slowly-varying medium analysis to calculate those variations [Budden, 1961]. From ray-tracing and amplitude calculations it is obvious that both the wave-normal angle and the wave amplitude may change significantly along the field line, and affect the longitudinal resonance interaction. Nevertheless, if the interaction region is relatively small, the changes of wave properties are also small, and it is permissible to assume as a first order approximation that the wave-normal angle and wave amplitude are constant quantities. If there is a need for even more accurate analysis it is feasible to use ray-tracing along with WKB solution to derive exact solutions for both θ and B_1 , and then incorporate those results in the longitudinal resonance calculations.

The mean scattering, $\langle \Delta\alpha_{eq} \rangle$ ($\langle\ \rangle$ denotes averaging over the initial phases), of a single sheet of electrons as a function of sheet equatorial parallel velocity is illustrated in Figure 5.1. The wave

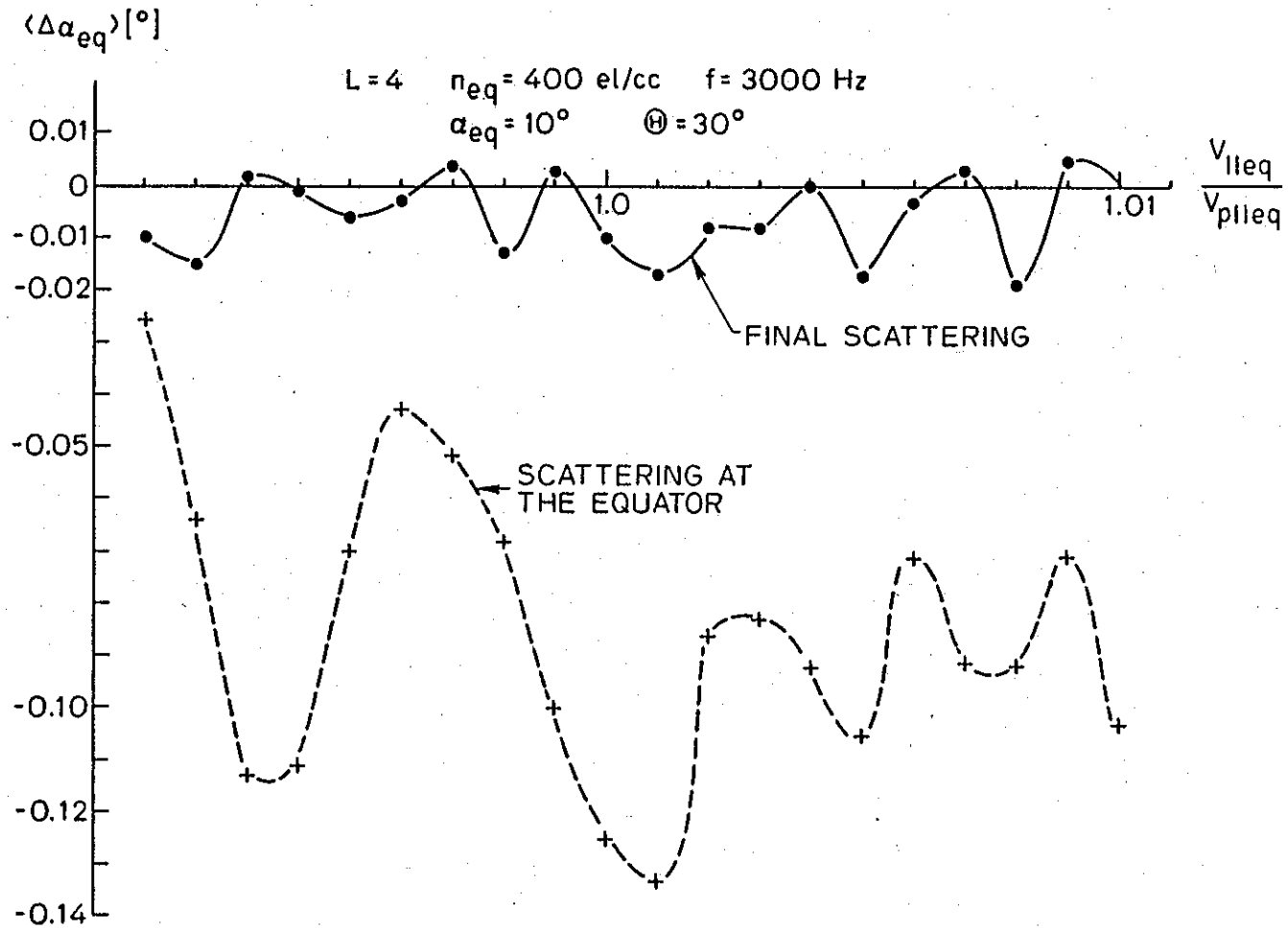

FIGURE 5.1 MEAN SCATTERING AS A FUNCTION OF PARALLEL VELOCITY. Electrons interacting with a CW signal exhibit a small final scattering (solid curve), whereas the cumulative scattering evaluated at the equator is significantly larger (dashed curve). The final scattering is computed at the end point of the integration which is defined in Fig. 4.2.

intensity $B_{\perp}$ = 10 pT corresponds to $E_{\parallel}$ = 15 μV/m. A solid curve shown in that figure indicates the mean final scattering of a sheet at the end point of the integration of equations of motion (as defined in Fig. 4.2), while the dashed curve represents the mean scattering of a sheet computed at the equator. Comparing the equatorial, i.e. cumulative scattering when electrons reach the equator, and the final scattering it is obvious that the final scattering is, on average, one order of magnitude smaller than the equatorial scattering. It is also clear from Fig. 5.1 that the equatorial scattering is negative, i.e. the mean equatorial pitch angle of twelve electrons forming a sheet is lowered. To explain those results shown in Fig. 5.1 it is useful to study trajectories of individual electrons. For example Figure 5.2 illustrates typical electron trajectories and energy variations calculated for interactions with a monochromatic CW signal. Four electrons shown in Fig. 5.1 belong to a test sheet specified by $v_{\parallel eq_o} = v_{p_{\parallel} eq}$, and $\alpha_{eq} = 10°$. A main difference between those electrons are their initial phases ϕ_o as indicated in Fig. 5.1 and defined in Fig. 4.1. The left column of Fig. 5.2 shows energies of the four electrons as a function of interaction time, while the right column of the same figure illustrates variations of both parallel and phase velocities as a function of latitude. Note that the time scale and the latitude scale cover the same portion of the field line. Next consider Fig. 5.2a where, as the electron approaches the equator, the parallel velocity becomes better matched to the wave phase velocity, and the wave effects become more cumulative. Those wave effects cause the oscillations of $v_{\parallel}$ and E, and as the electron comes closer to the

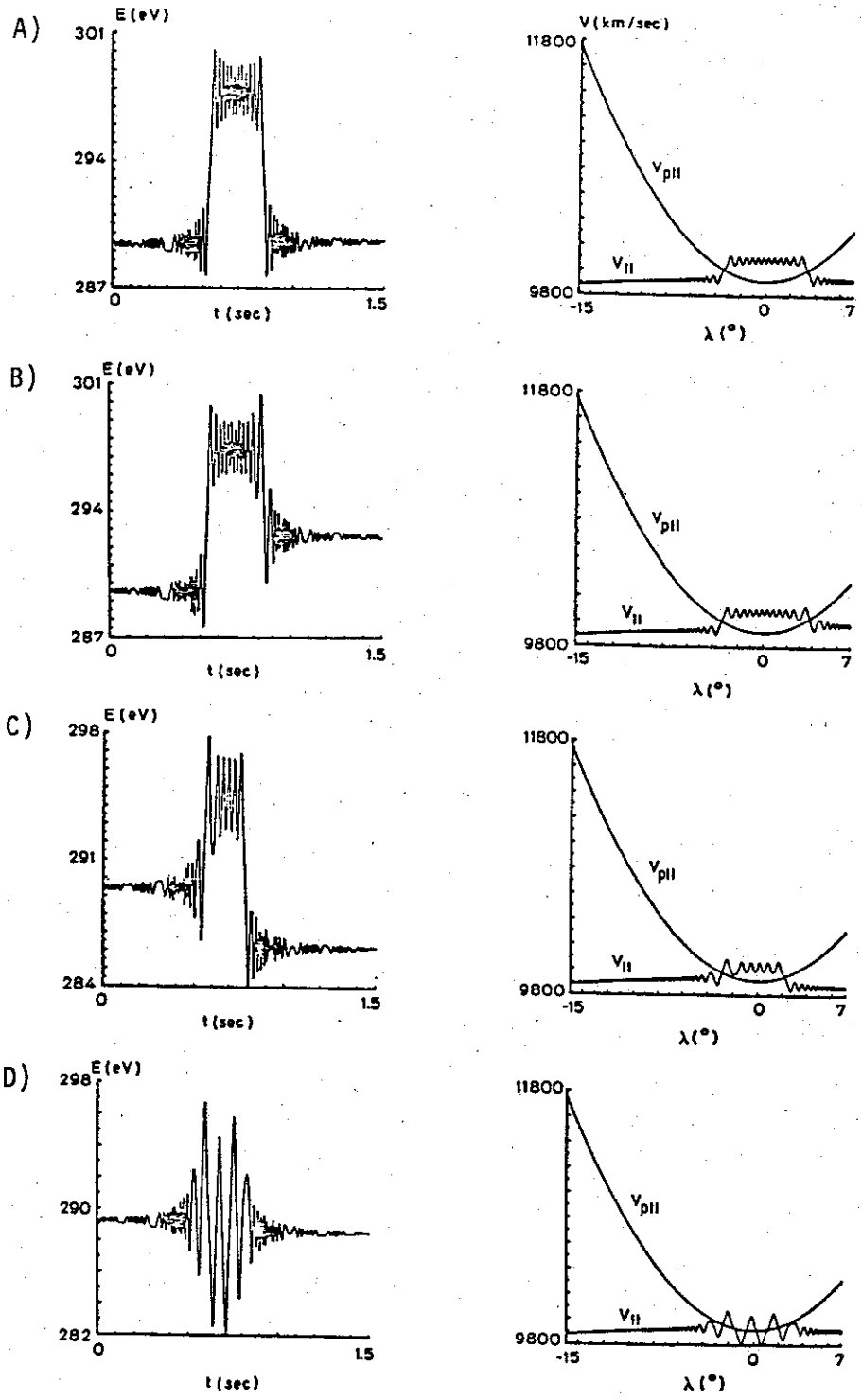

FIGURE 5.2 SINGLE ELECTRON TRAJECTORIES FOR $B_\perp$ = 10 pT. The electron energy and parallel velocity are shown as a function of latitude as it interacts with CW wave. The initial parallel velocity $v_{\parallel eoq} = v_{p\parallel eq}$, and $\alpha = 10^\circ$ for all electrons. The initial phase ϕ_o is 30° in (a), 90° in (b), 120° in (c), and 270° in (d).

equator the amplitudes of the oscillations increase. At the point $t = 0.52$ sec ($\lambda = -3.5°$) the parallel velocity of the electron equals the phase velocity, and that point is called the first resonance point. Electrons shown in Figs. 5.2b, 5.2c, and 5.2d exhibit similar behavior before they reach the first resonance point. However, after electrons travel beyond the first resonance only the top three electrons shown in Fig. 5.2 are accelerated by the wave in such a manner that their parallel velocities become larger than the phase velocity. It is also clear from Figs. 5.2a, 5.2b, and 5.2c that this increase of the parallel velocity is accompanied by an increase of the total energy of the electrons. After those electrons have traveled beyond the first resonance their motion, as they travel across the equator, is still affected by the wave, but the parallel velocity remains larger than the phase velocity. However, on the other side of the equator the phase velocity again starts to increase and the electrons approach their second resonance point. At this second resonance point the electrons are decelerated by the wave and consequently their energy is also decreased. Thus the electrons shown in Figs. 5.2a, 5.2b, and 5.2c are being accelerated at the first resonance point and then decelerated at the second resonance point. The amount of acceleration and deceleration in general depends on the actual phase between a given electron and the wave, and as a final result electron energy can be unchanged (Fig. 5.2a), increased (Fig. 5.2b) or decreased (Fig. 5.2c). Compared to those top three cases (Figs. 5.2a, 5.2b, 5.2c) a fourth electron trajectory illustrated in Fig. 5.2d is quite different. This electron became trapped after the first resonance interaction and its parallel

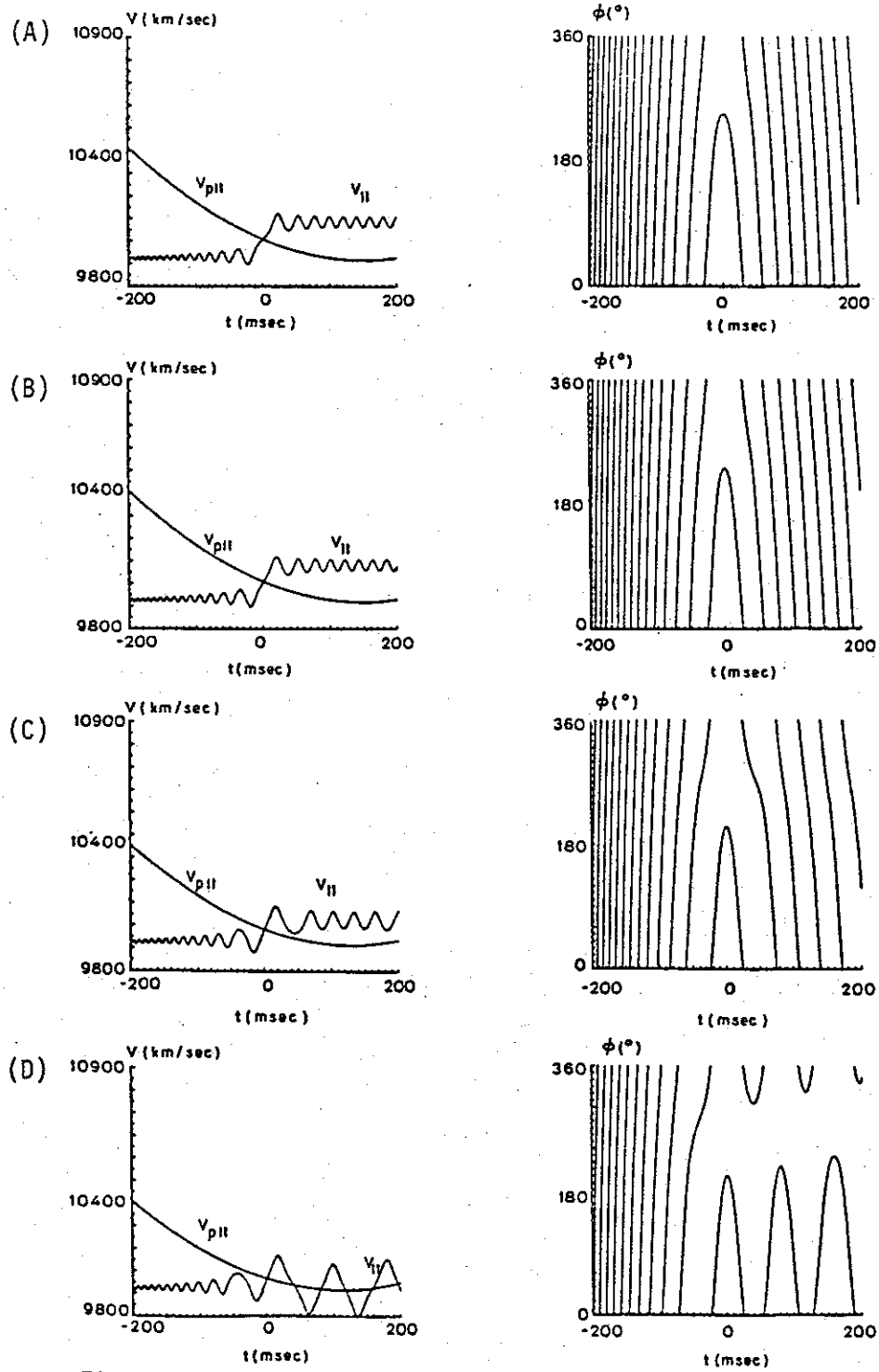

FIGURE 5.3 SINGLE ELECTRON TRAJECTORIES FOR $B_\perp$ = 10 pT. The electron parallel velocity $v_\parallel$ and phase ϕ as a function of time. Time t = 0 indicates occurrence of the first resonance. Other parameters are the same as those in Fig. 5.2.

velocity, as well as the total energy, shows oscillatory behavior which is characteristic of the trapped electrons.

Figure 5.3 is a time expanded view of the electron's behavior during a 400 msec window centered around the first resonance point at t = 0 msec. This figure shows both parallel velocity and electron phase behavior. From the phase diagrams it follows that the phase is increasing before the first resonance, with the rate of increase decreasing as electrons approach the first resonance point. This type of phase variation is consistent with that found analytically in Chapter III. At the resonance point the phase does not change, i.e. it becomes constant, and the first derivative is equal to zero, as indicated in Fig. 5.3. After the first resonance untrapped and trapped electrons undergo different phase variations. Untrapped electrons are associated with a constantly decreasing phase as a result of $v_{\parallel} > v_{p_{\parallel}}$, while trapped electrons exhibit an oscillatory phase behavior as they oscillate at the bottom of the potential well. Note that an electron is considered to be trapped if it executes at least one complete phase oscillation. Figure 5.3 also clearly illustrates significance of the phase between electrons and a wave. By comparing the phase behavior of the electrons shown in Figs. 5.3c and 5.3d, we see that the difference in their phases at the resonance point (t = 0 msec) is less then 5 degrees, but the electron of Fig.5.2c is not trapped, whereas the electron of Fig. 5.2d is trapped.

Those four sample trajectories are representative of typical perturbations of electron motion induced by the wave forces. Finally, to explain the results of Fig. 5.1 where the equatorial scattering is

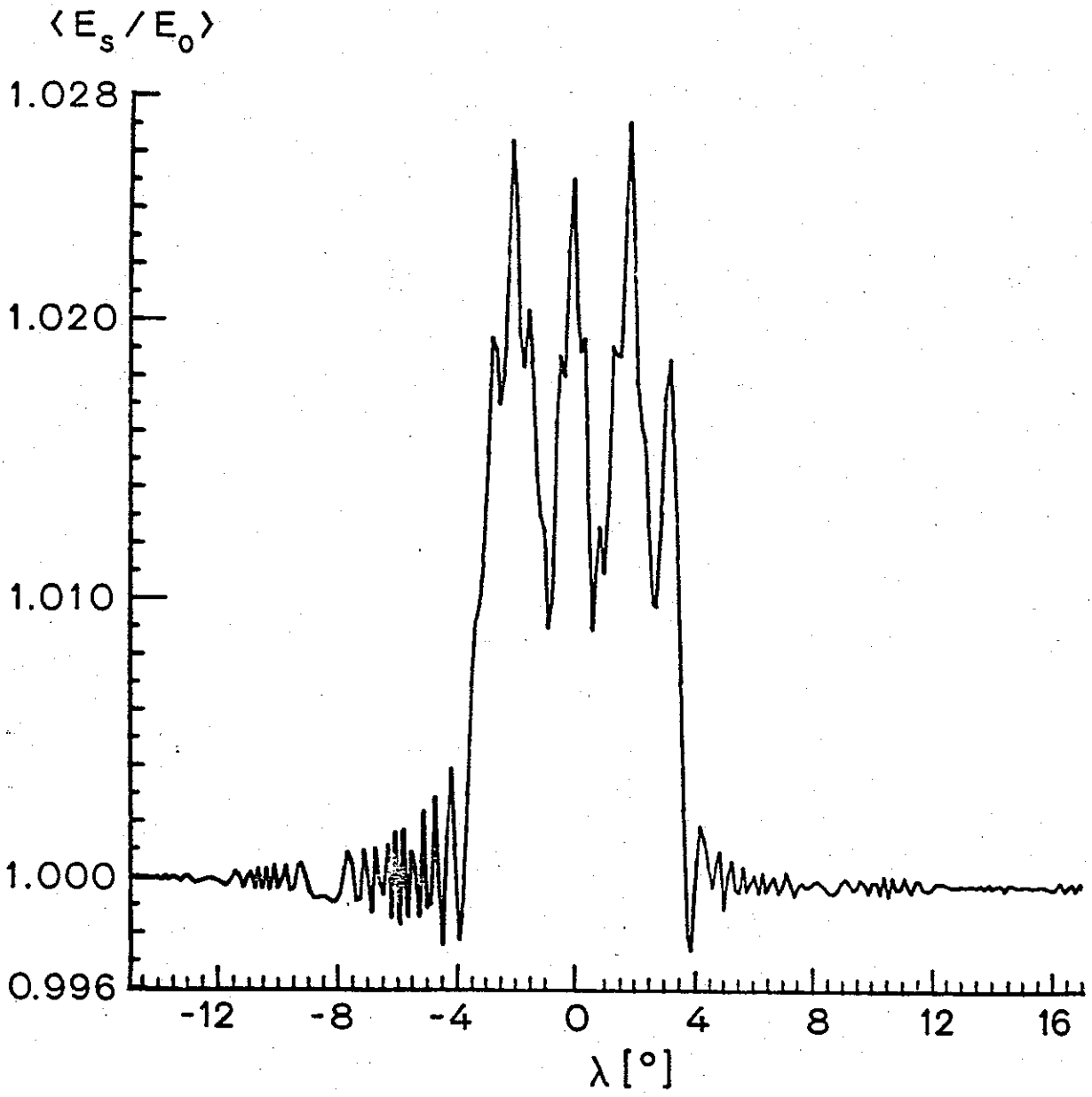

FIGURE 5.4 NORMALIZED ENERGY OF TEST SHEET AS A FUNCTION OF LATITUDE. The normalized energy of a test sheet (12 electrons) increases about 2.5% around the equator when those electrons interact with a CW signal. The sheet initial parallel velocity is $v_{\parallel eq} = v_{p\parallel eq}$ and $\alpha = 10^{\circ}$.

larger than the final scattering, the energies of all 12 electrons are added together and plotted as a function of latitude in Figure 5.4. From this figure it immediately follows that there is a region around the equator where the normalized total energy of the electron sheet is increased. This energy increase is on average about 2% of the initial total energy, and it is limited to latitudes between $-4°$ and $4°$. The jump in the energy is caused by the acceleration of untrapped electrons such as those shown in Figs. 5.2a, 5.2b, 5.2c, while the energy envelope oscillations are caused by trapped electrons such as that of Fig. 5.2d. In the particular example there were 7 untrapped electrons and 5 trapped electrons. Beyond $\lambda = 4°$ the total energy of the sheet returns almost to the initial level. Here we recall that an increase of the electron energy yields a decrease of the pitch angle, while a decrease of the electron energy yields an increase of the pitch angle. Bearing this relation in mind it is then easy to explain the results of Fig. 5.1 by translating energy variations shown in Fig. 5.4 into pitch angle variations. This transformation immediately reveals that the equatorial scattering is negative and larger than the final scattering, again as indicated in Fig. 5.1. It also explains why the final scattering can be both positive or negative because the final energy can be either larger or smaller than the initial energy. The final scattering appears, due to its randomness, as though it resulted from an incoherent interaction. On the other hand the equatorial scattering appears to be much less random implying a larger degree of coherence. This indicates that coherence of this particular type of longitudinal interaction is position dependent, and it is necessary to examine electron trajectories

rather than to rely only on scattering results.

The energy gained by the electrons is extracted from the wave which means that the wave amplitude must be reduced around the equator. For test particle studies involving only twelve particles this attenuation of the wave amplitude is negligible, but it should be considered in full distribution computations where significant loss of the wave energy will cause a strong wave attenuation and consequently weaken the interaction process.

From Fig. 5.3d it follows that the trapping period is about 82 msec. Because the medium inhomogeneity is very small around the equator this trapping period can be also computed using a relation derived for the homogeneous medium

$$T_t = \frac{1}{2\pi}\sqrt{\frac{m}{eE_{\parallel} k_{\parallel}}} \qquad (5.1)$$

Using (5.1) with $k_{\parallel} = 1.9\ 10^{-3}$ and $E_{\parallel} = 15\ \mu V/m$, the trapping period is computed to be 81.5 msec, which is in very good agreement with the numerical result. It is also easy to check the oscillation period of $v_{\parallel}$ for untrapped electrons. For example consider the electron shown in Fig. 5.2b and its parallel velocity at t = 100 msec. The period of parallel velocity oscillation at that point is about 20 msec, which may also be found by computing the doppler shifted frequency of the wave $\omega_i = \omega - k_{\parallel}v_{\parallel}$. Taking $\omega = 2\pi \cdot 3000$ rad/sec, $k_{\parallel} = 1.9\ 10^{-3}$, and $v_{\parallel} =$ 10100 km/sec yields $\omega_i = 331$ rad/sec; the equivalent oscillation period is of about 19 msec which is in a good agreement with numerical results.

As mentioned earlier results shown in Figs. 5.2, 5.3, and 5.4

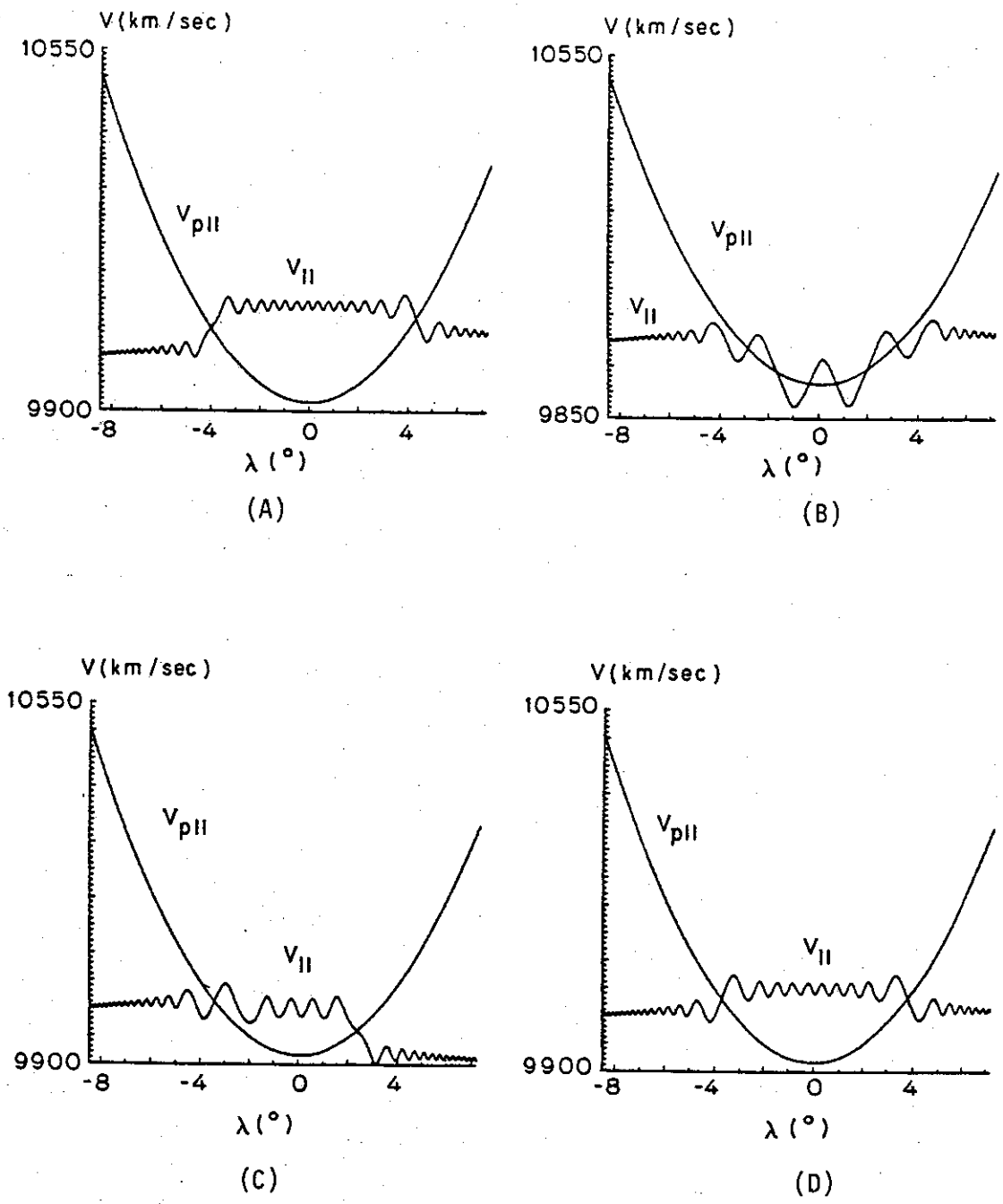

FIGURE 5.5 SINGLE ELECTRON TRAJECTORIES FOR $B_{\perp}$ = 10 pT. Electron parallel velocities as functions of latitude for a case when the initial parallel velocity is $v_{\parallel s}$= 1.050 $v_{p\parallel eq}$. The pitch angle and initial phases of electrons are the same as those in Fig. 5.2.

are calculated for a sheet with initial equatorial parallel velocity $v_{\parallel eq_o}$ equal to the equatorial phase velocity $v_{p\parallel eq}$ of a wave. For purposes of comparison, Figure 5.5 shows the parallel velocity behavior of four electrons, from a sheet with $v_{\parallel eq_o} = 1.050\ v_{p\parallel eq}$, and again as a function of latitude. The motion of the electrons is similar to that shown in Fig. 5.2. The possibility of trapping, or not trapping, depends on the initial phase ϕ_o of each individual electron, and the final scattering can be both positive and negative.

The above results suggest that the longitudinal resonance interaction with a monochromatic CW signal is confined to a relatively small region around the equator. The controlling factor in the interaction is the variation of phase ϕ which determines if electrons become trapped or not, and affects the amount of exchanged energy.

C. SCATTERING OF A SINGLE SHEET INTERACTING WITH CW WAVES AMPLIFIED AT THE EQUATOR THROUGH THE CYCLOTRON RESONANCE

Next we consider the scattering of single electron sheet interacting with a monochromatic CW wave whose amplitude is increased through the gyroresonance process. The amplification process of CW waves takes place close to the equator [Helliwell, 1967], and in our calculations the growth region is taken to be 1000 km long. The wave amplitude, before it reaches the equatorial growth region, is 0.1 pT.

Figures 5.6 and 5.7 illustrate the scattering of a single sheet as a function of the initial parallel velocity $v_{\parallel eq_o}$. In all

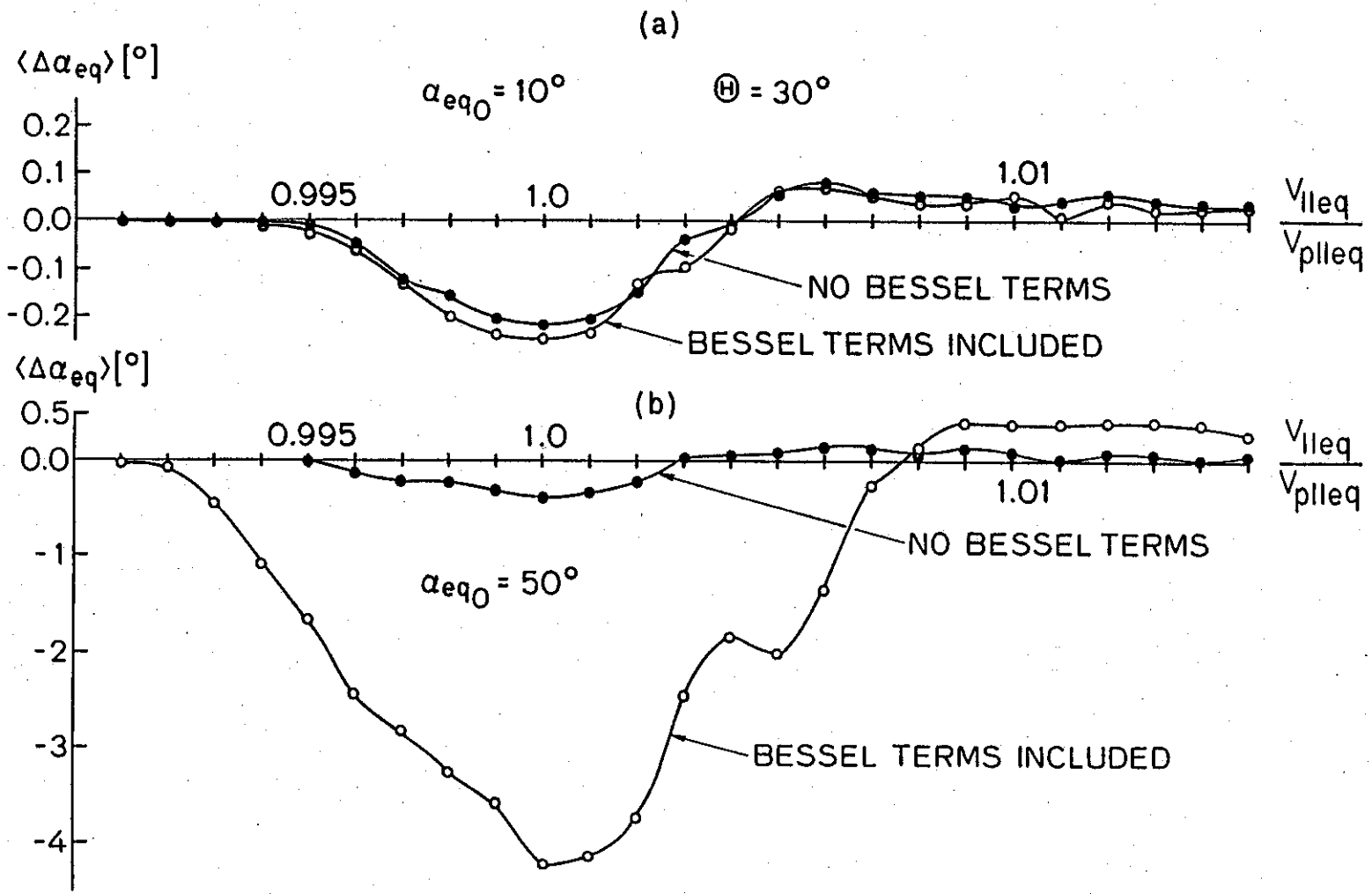

FIGURE 5.6 MEAN SCATTERING AS A FUNCTION OF PARALLEL VELOCITY. The mean scattering is computed for longitudinal resonance interactions with a CW signal which is amplified after it crosses the equator. The results indicate that the wave magnetic forces become important at larger pitch angles; then it is necessary to include Bessel terms in the equations of motion.

computations the wave amplitude is $B_\perp$ = 10 pT, or $E_\parallel$ = 15 μV/m, while the equatorial pitch angle is taken to be 10°, 30°, 50°, and 70°. The total sheet scattering is computed twice for each parallel velocity increment; once it is computed using complete averaged equations of motion, and once using only the qE term of Eq.2.61 as though the wave is electrostatic, i.e. it is assumed that $J_o(\eta) = 1$ and $J_1(\eta) = 0$. As discussed earlier, the effects of the Bessel terms, i.e. the effects of the wave magnetic field forces, should become significant at larger pitch angles, while at lower pitch angles the difference between the two computational methods is expected to be small. From Fig. 5.6a, which is calculated using $\alpha_{eq} = 10°$, it is evident that the two methods produce very similar results, as expected. On the other hand, as the pitch angle increases the difference between the results becomes much larger and for $\alpha_{eq} = 70°$ there is almost no scattering if we exclude the Bessel terms from the equations of motion (Fig. 5.7b), whereas the scattering calculated using the complete equations is about −6° at $v_{\parallel eq} = v_{p\parallel eq}$. Those examples confirm the results of Chapter II, where it was found that the Bessel terms will be a very important factor in governing the motion of electrons with high pitch angles. This is especially true for the $J_1(\eta)$ term, which represents effects of the wave magnetic force, as already indicated in Figs. 2.5, 2.6 and 2.7.

As discussed earlier the longitudinal resonance interaction depends strongly on the wave amplitude. This wave amplitude dependence is depicted in Figure 5.8. Three different curves shown in that figure represent scattering of sheets with three different initial parallel velocities $v_{\parallel eq_o}$. A sheet with $v_{\parallel eq_o} = v_{p\parallel eq}$ has the optimal parallel

velocity as required by the resonance condition. Two other sheets with $v_{\parallel eq_o} = 0.995\ v_{p\parallel eq}$ and $v_{\parallel eq_o} = 1.005\ v_{p\parallel eq}$ are slightly off the resonance when they encounter the wave growth region at the equator; the first is slower and the second is faster than the phase front of the wave, respectively. The effects of different sheet velocities are best illustrated by considering the amount of pitch angle scattering for a given wave amplitude. The particle sheet with $v_{\parallel eq} = v_{p\parallel eq}$ is scattered about -0.1° when interacting with a relatively weak wave with $B_\perp = 5$ pT. On the other hand, the other two sheets require a wave with $B_\perp = 18$ pT to achieve the same amount of scattering. Below $B_\perp = 18$ pT scattering of the sheet with $v_{\parallel eq} = 0.995\ v_{p\parallel eq}$ is small and negative, whereas scattering of the sheet with $v_{\parallel eq} = 1.005\ v_{p\parallel eq}$ is also small, but positive. We recall from Section III.E that the direction of energy exchange depends on the relative magnitudes of the parallel and phase velocities; if an electron is faster than a wave it is decelerated and loses its kinetic energy; if an electron is slower than a wave it is accelerated and gains kinetic energy. An increase, or decrease, of the kinetic energy is accomplished by changing the parallel velocity of the electron through the resonance process. If the parallel velocity of an electron is increased, its equatorial pitch angle becomes smaller, or equivalently, if the parallel velocity of an electron is decreased, its equatorial pitch angle becomes larger. It is this type of process that explains the behavior of the two sheets with $v_{\parallel eq_o} = 0.995\ v_{p\parallel eq}$ and $v_{\parallel eq_o} = 1.005\ v_{p\parallel eq}$ for $B_\perp < 18$ pT. It may be wondered why a sheet with $v_{\parallel eq_o} = v_{p\parallel eq}$ does not show similar behavior, and what is happening when $B_\perp > 18$ pT in the other two cases. The answers may be found by

examining trajectories of individual test electrons. From those results it was found that for weak waves all electrons remain untrapped regardless of their initial parallel velocities. As long as the electron is not trapped, i.e as long as the electron parallel velocity does not follow the phase velocity variation, the longitudinal interaction is generally limited to two relatively small regions around the two resonance points. In our case the interaction is further limited to only one side of the equator where the wave amplitude is sufficiently strong. Next, as the wave amplitude increases beyond the equator the interaction becomes stronger, and from the trajectory calculations, it is evident that some electrons become trapped. This transition between the untrapped and trapped mode of the longitudinal interaction is characterized by a significant increase in the scattering. The amplitude threshold at which the trapped mode scattering overtakes the untrapped mode scattering depends on the initial parallel velocity $v_{\parallel eq_o}$, as shown in Fig. 5.8. The threshold amplitude for $v_{\parallel eq_o} = v_{p\parallel eq}$ is as low as $B_\perp = 3$ pT, with a relatively smooth transition between the two interaction regimes. The amplitude threshold in the two other cases is about $B_\perp = 18$ pT with a much sharper transition between two interaction regimes.

The individual particle trajectories are illustrated in Figures 5.9, 5.10, and 5.11. Figure 5.9 shows parallel velocities and phases of four electrons with $v_{\parallel eq_o} = v_{p\parallel eq}$, $\alpha = 10°$, and different initial phases ϕ_o, as functions of latitude and time, respectively. The wave amplitude is $B_\perp = 10$ pT. As in the case for a CW signal the parallel velocity variation of those electrons is controlled by the phase

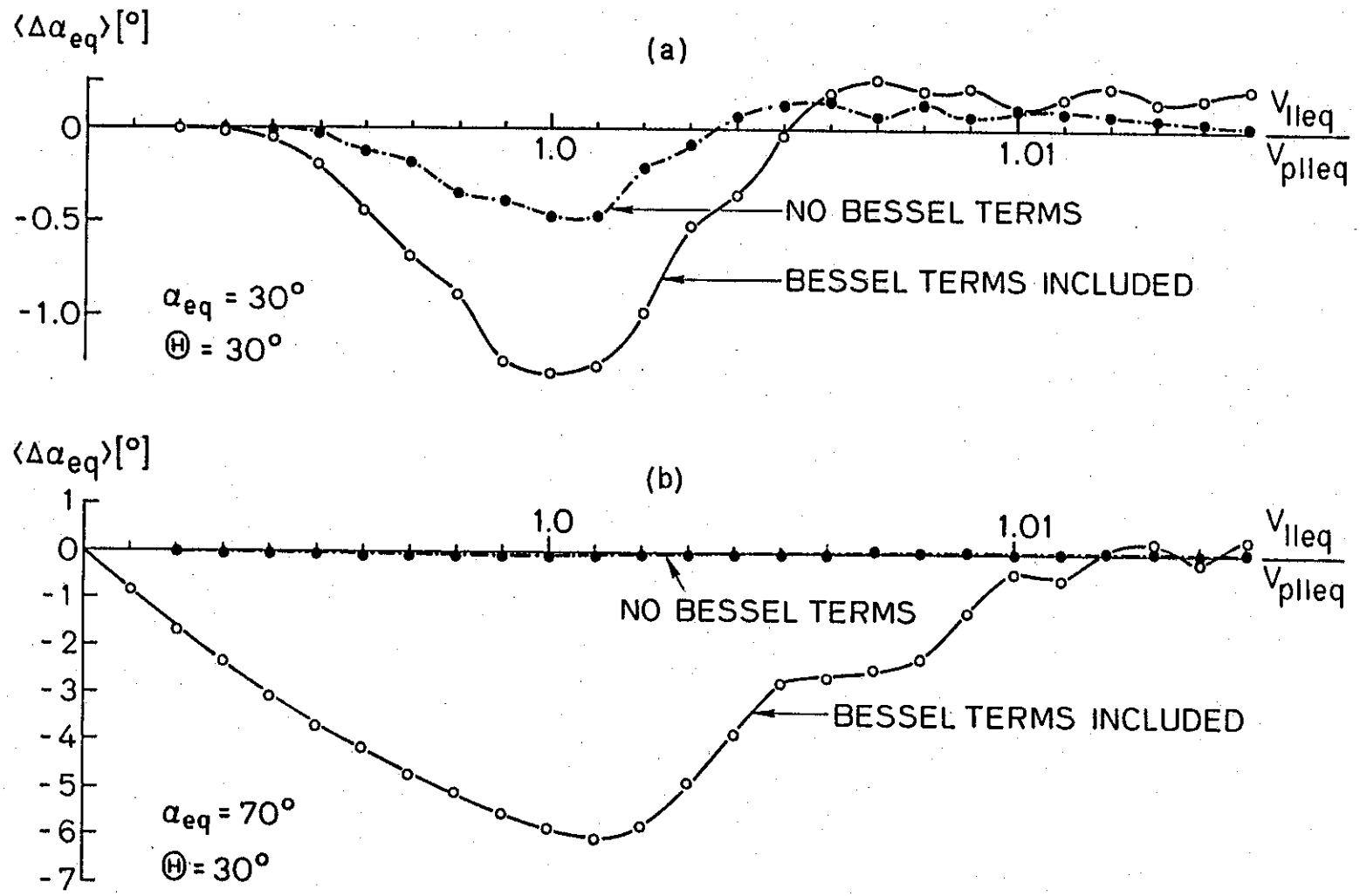

FIGURE 5.7 MEAN SCATTERING AS A FUNCTION OF PARALLEL VELOCITY. The format is the same as Fig. 5.6, except that α_{eq}= 30° in (a), and α_{eq}= 70° in (b).

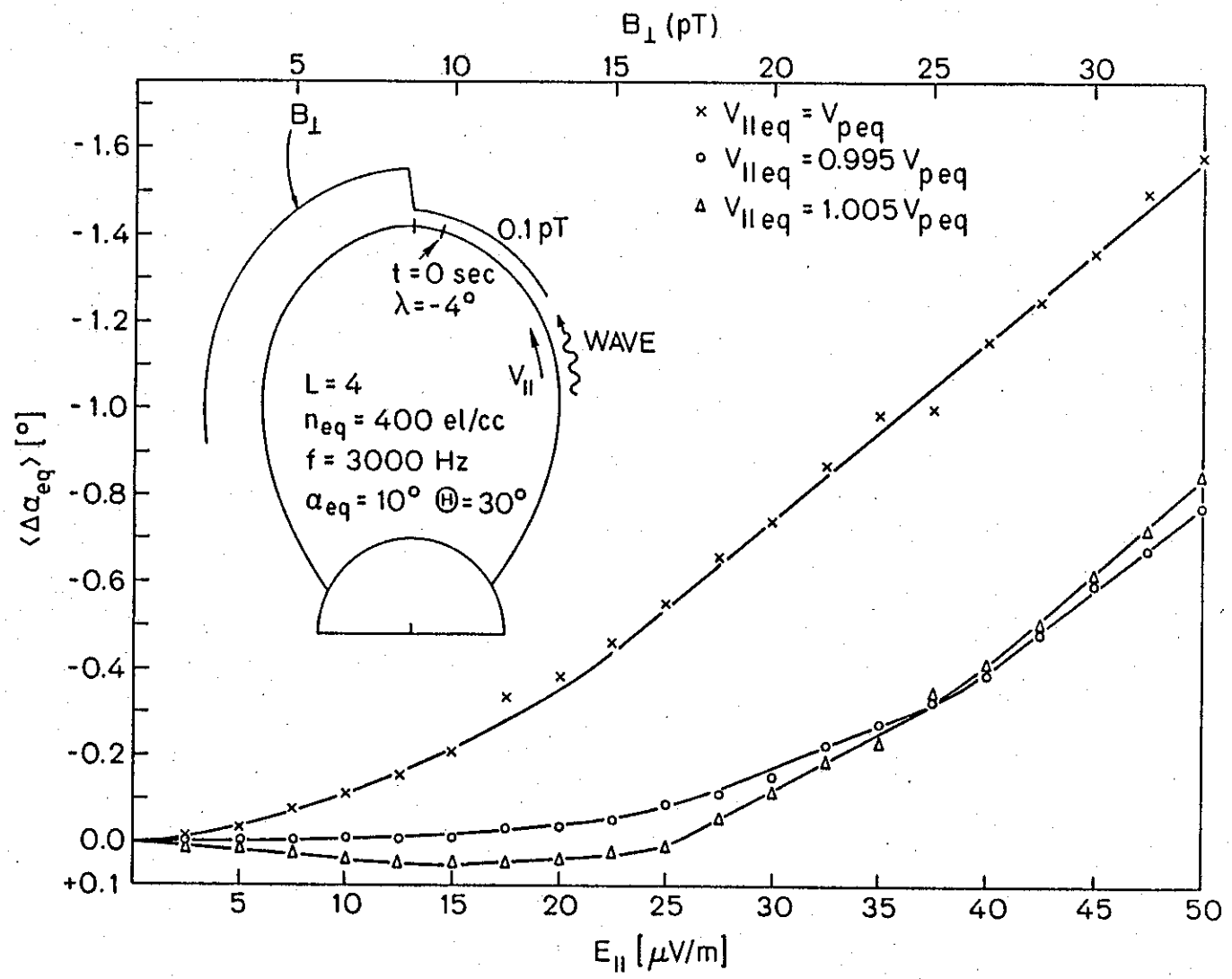

FIGURE 5.8 MEAN SCATTERING AS A FUNCTION OF WAVE AMPLITUDE FOR THE AMPLIFIED CW SIGNAL. The behavior of the mean scattering indicates the presence of an amplitude threshold effect, i.e. significant scattering is possible only if the wave amplitude exceeds a certain value. The threshold amplitude increases as the absolute difference between the initial parallel and phase velocity becomes larger.

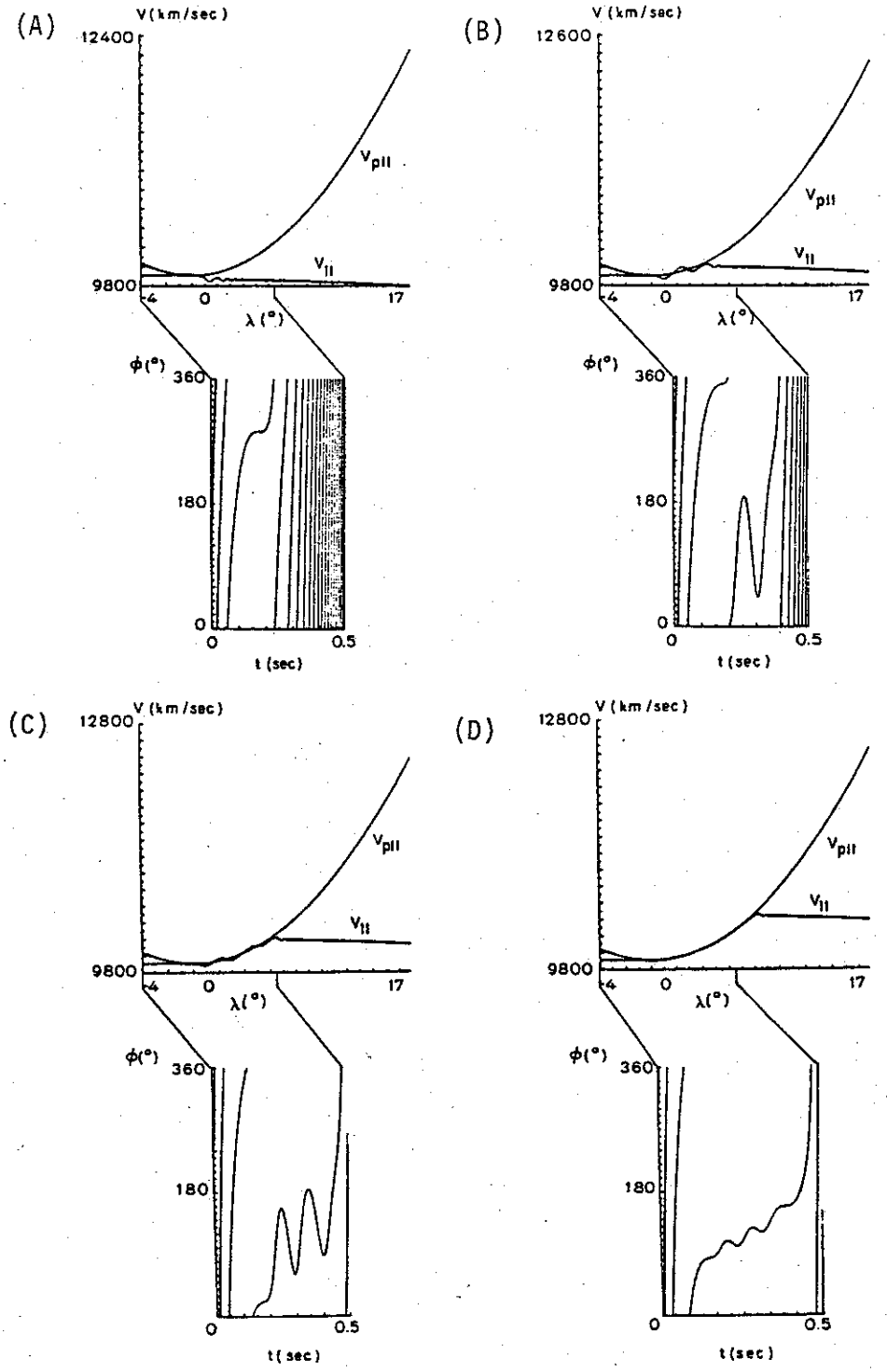

FIGURE 5.9 SINGLE ELECTRON TRAJECTORIES FOR $B_{\perp}$ = 10 pT. Parallel velocity and phase behavior for electrons with $v_{\parallel eq} = v_{peq}$ and $\alpha = 10^{\circ}$ interacting with variable amplitude CW signal. The initial electron phase is 0° in (a), 120° in (b), 150° in (c), and 300° in (d).

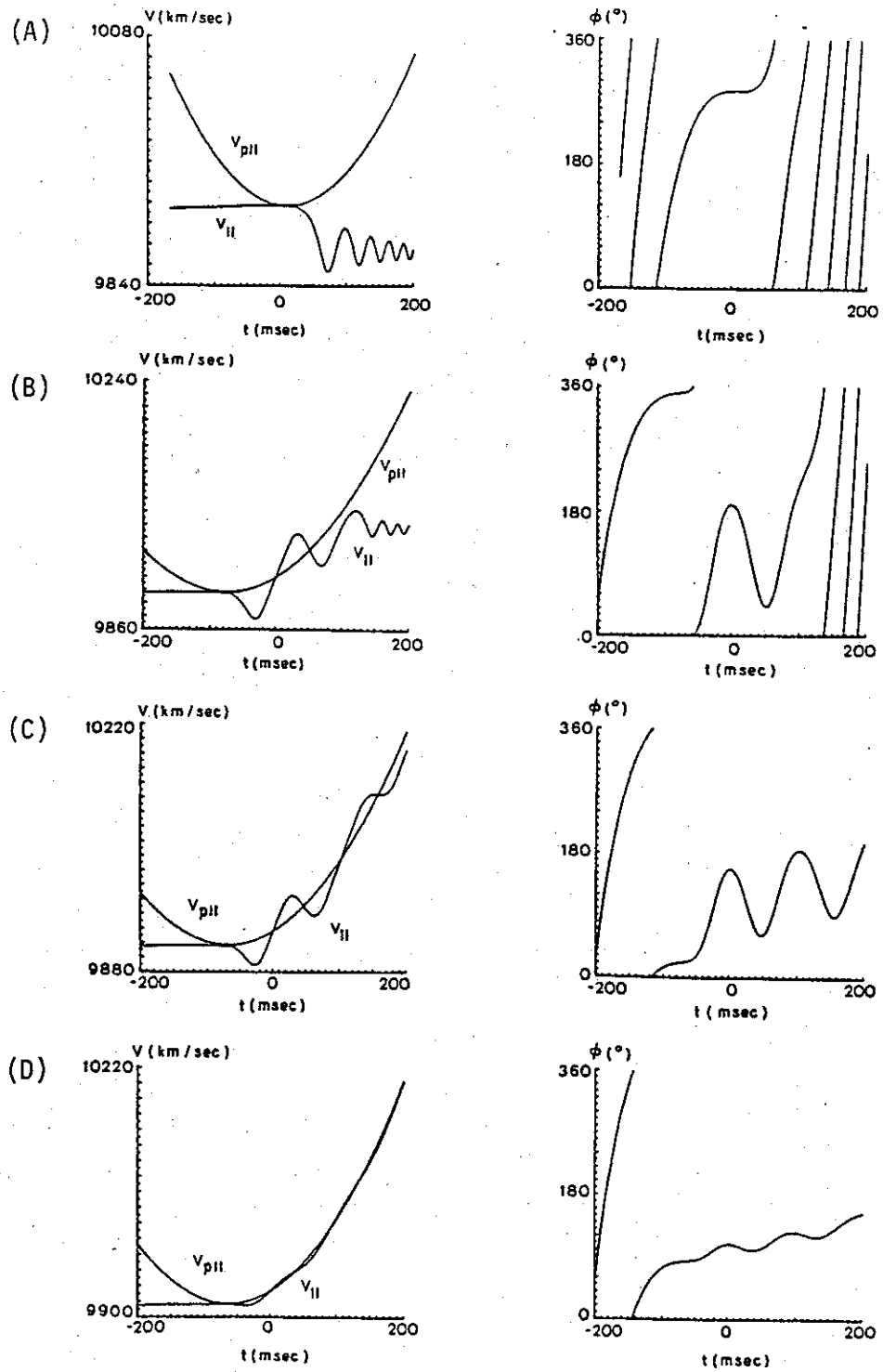

FIGURE 5.10 SINGLE ELECTRON TRAJECTORIES FOR $B_{\perp}$ = 10 pT. Shown here are the parallel velocity and phase variations around the first resonance point at t=0. Other parameters are same as those in Fig. 5.9.

variation. For example, the electron trajectory of Fig. 5.9a indicates absence of trapping because of an improper phase, whereas the number of oscillations for trapped electrons in the other three cases also depends on the phase at the moment when the parallel velocity equals the wave phase velocity. Figure 5.10 depicts a time expanded view of the electron trajectories around the first resonance point. Before analysing those trajectories we recall from section II.B that the variation of $E_{\parallel}$ is described, in the wave frame, as cos $k_{\parallel} z$, and that the bottom of the potential well is at Z_B as shown in Figure 2.2. In Figure 5.10 the time t = 0 indicates the first resonance where $v_{\parallel} = v_{p_{\parallel}}$. The phase at this point is a crucial factor governing the further motion of a particular electron. For example, the phase of electron shown in Fig. 5.10a is such that it is strongly decelerated and by the time of phase reversal, i.e. electron acceleration, the parallel and wave phase velocity are too different for trapping to be possible. Observing the phase of the electron in Fig. 5.10b at t = 0 we find this phase to be significantly smaller than the phase in Fig. 5.10a. Due to this different phase the second electron is less decelerated, eventually becomes trapped, and executes one oscillation at the bottom of the potential well. For the next two electrons shown in Figs. 5.10c and 5.10d the phases at t = 0 are even smaller resulting in an increasing number of oscillations. We note that the amplitudes of both velocity and phase oscillations decrease as the phase at t = 0 decreases. In the example shown in Fig. 5.10d the phase at t = 0 is very close to the optimal 90° which then results in the strongest trapping. As discussed earlier the 90° phase indicates that an electron is exactly at the

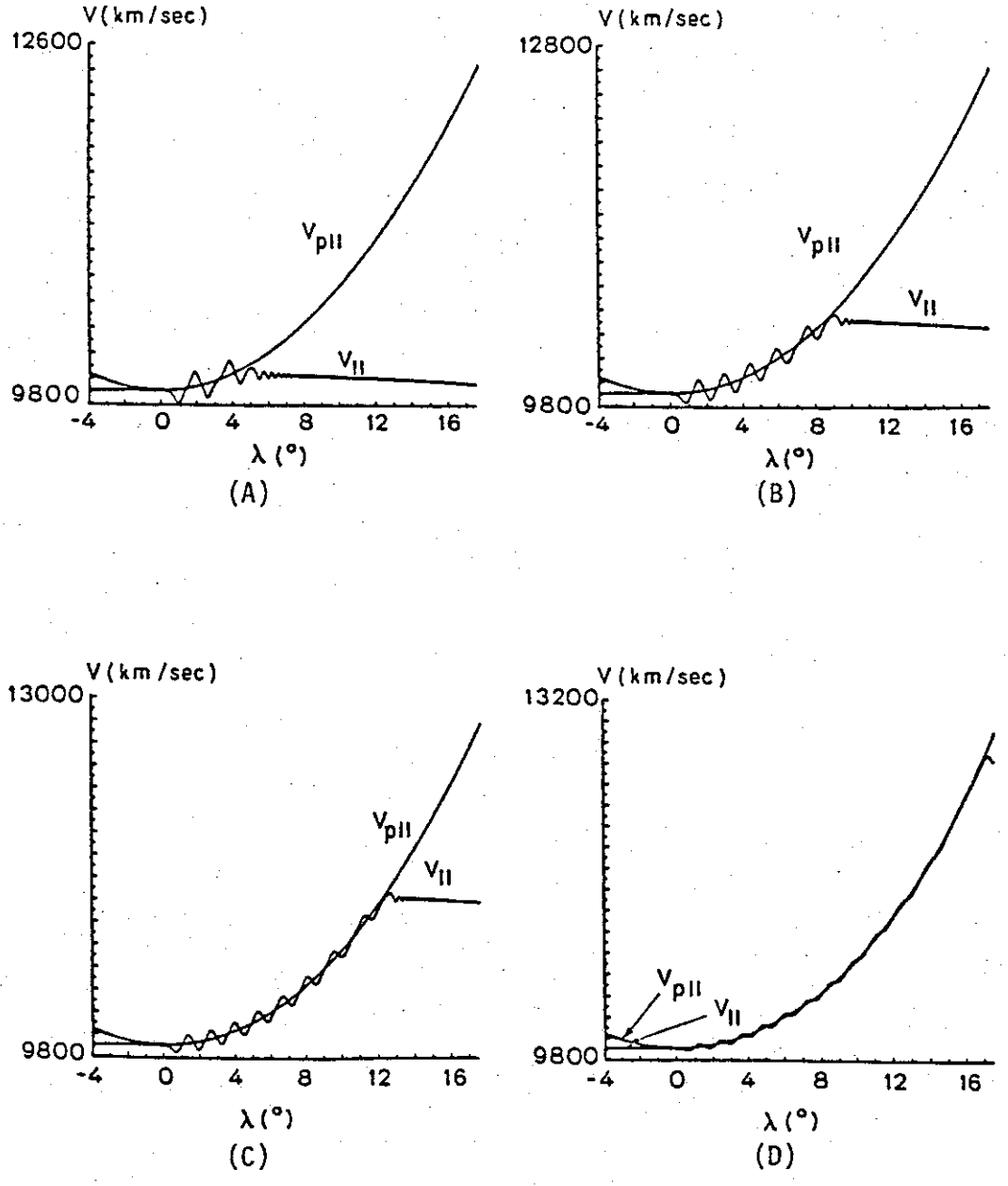

FIGURE 5.11 SINGLE ELECTRON TRAJECTORIES FOR B = 30 pT. The electron parameters are same as those in Fig. 5.9.

bottom of the potential well. To illustrate the effects of wave amplitude Figure 5.11 shows the same four electrons, but the wave amplitude is increased to $B_\perp$ = 30 pT. In this case even the first electron becomes trapped, and the other three electrons now remain trapped for longer periods of time.

Figure 5.12 shows the scattering of individual electrons as a function of their initial phases ϕ_o for three different wave amplitudes. This figure confirms the importance of phase as a controlling factor in the longitudinal resonance interaction. Figure 5.12 shows that it is possible to achieve a significant increase of the scattering efficiency by changing the inital phase ϕ_o from 0° to 180°. We summarize the results of the above analysis in Figure 5.13 which shows the normalized total energy of a single sheet as a function of latitude. The initial equatorial parallel velocity equals the equatorial phase velocity and wave amplitude is $B_\perp$ = 10 pT. Before electrons reach the equator the wave amplitude is very small and there are no significant changes of the sheet energy. After the equator crossing the wave amplitude starts to increase and electrons become trapped. As long as those electrons remain trapped their parallel velocities increase and so does the total energy of the electron sheet. As the electrons move away from the equator some of them become detrapped, but the energy increase continues up to the point where the last electron becomes detrapped. At that point the energy of a sheet has reached its maximum and remains constant. From Figure 5.13 we see that the particular sheet has gained about 4.6% over the initial energy. The energy gain region is between $\lambda = 1°$ and $\lambda = 7°$. Recall that this energy increase must be accompanied

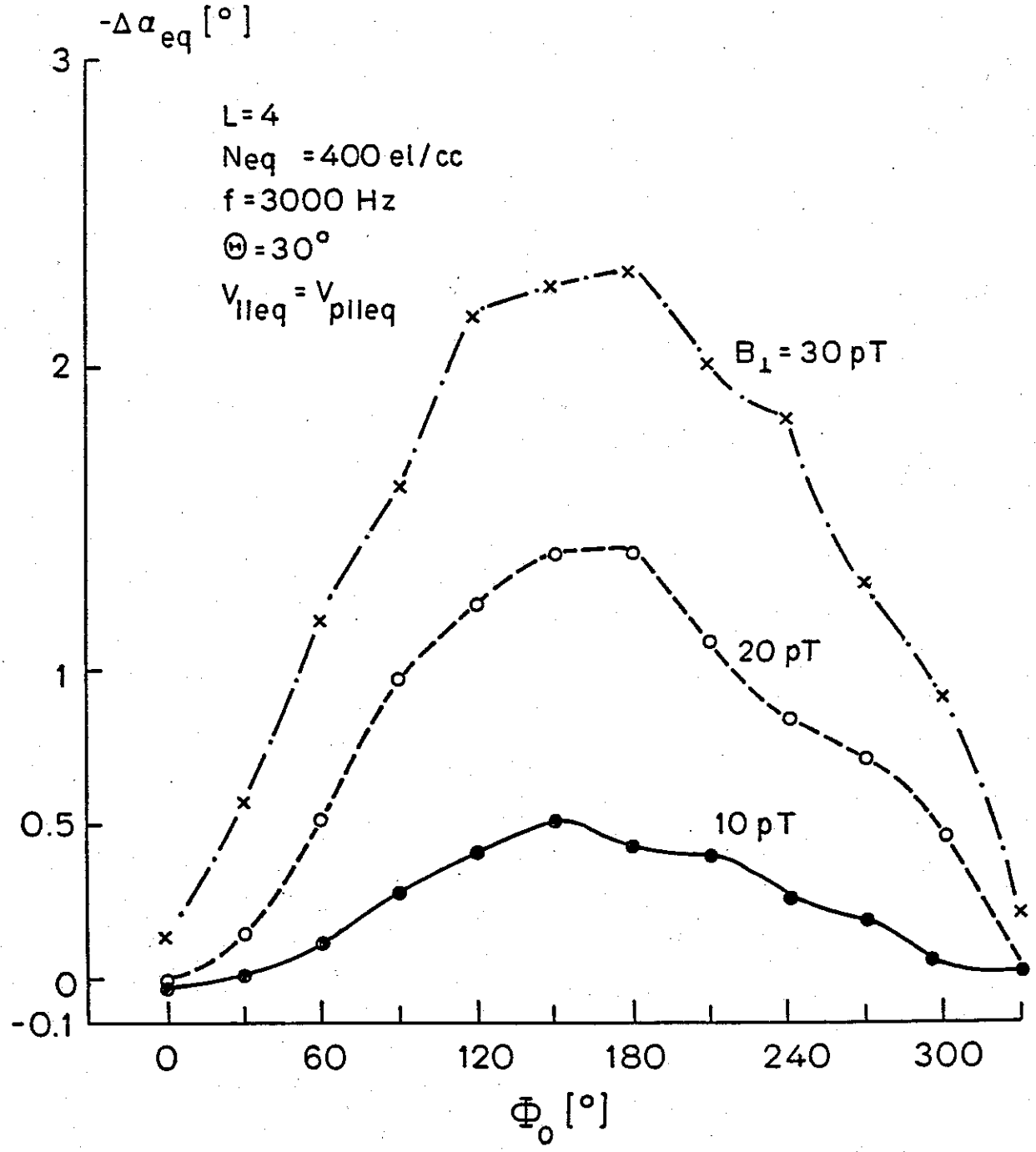

FIGURE 5.12 TOTAL SCATTERING, $\Delta\alpha_{eq}$, VERSUS INITIAL PHASE FOR DIFFERENT WAVE AMPLITUDES. The initial pitch angle is $\alpha_{eq} = 10^{\circ}$.

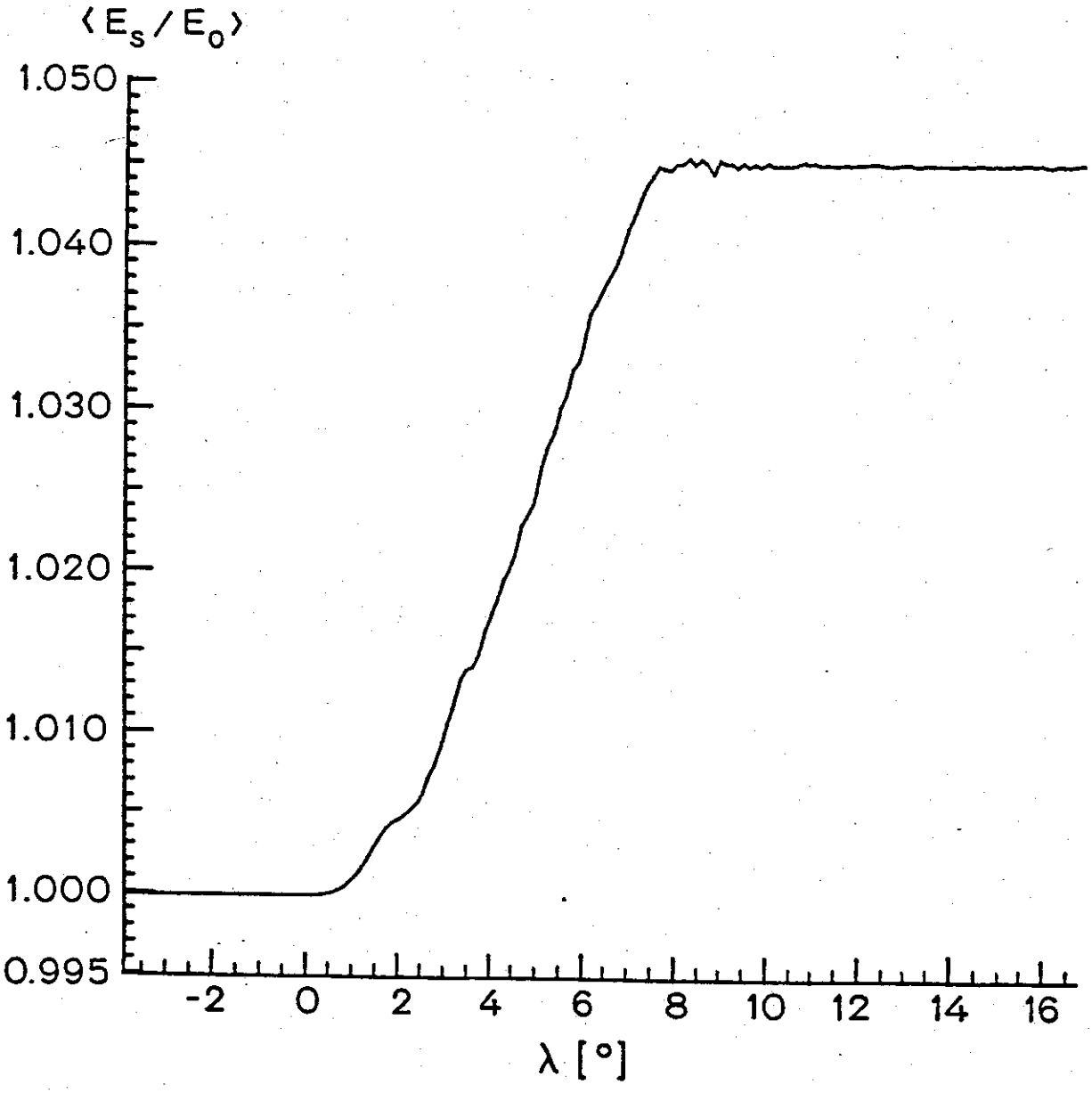

FIGURE 5.13 NORMALIZED ENERGY OF TEST SHEET AS A FUNCTION OF LATITUDE. The energy of the test sheet is increased as it interacts with the variable amplitude CW signal.

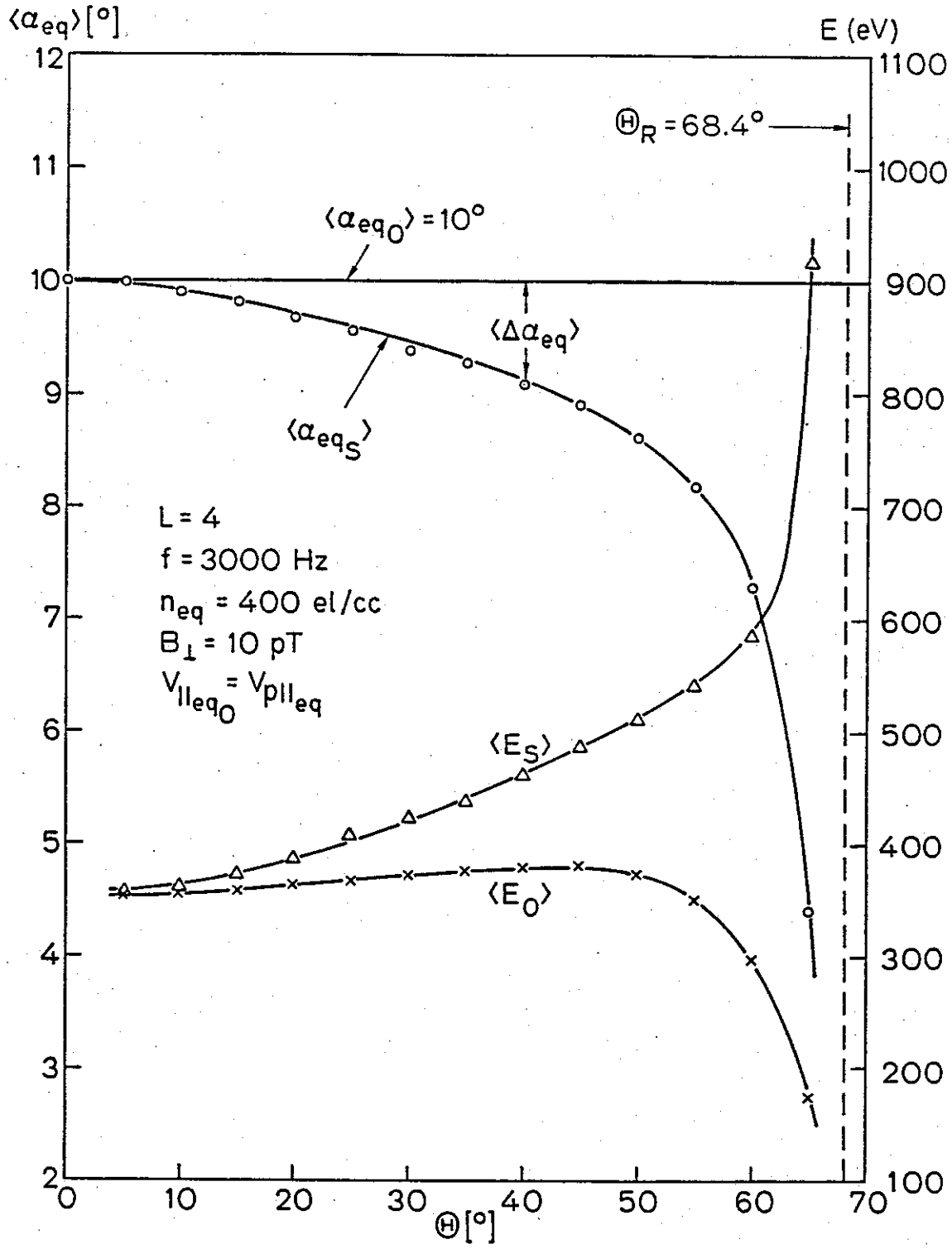

FIGURE 5.14 MEAN SCATTERING AS A FUNCTION OF WAVE NORMAL ANGLE. The difference $\langle E_S \rangle - \langle E_O \rangle$ represents the amount of energy gained by electrons.

by wave attenuation which is not considered in the test particle studies, i.e there is no feedback to account for wave amplitude changes. The feedback effects can be neglected in a test particle simulation where the number of electrons is small, but they must be considered in a full distribution analysis.

Next we take into account the scattering efficiency dependence on the wave-normal angle. Figure 5.14 shows $\langle \Delta\alpha_{eq} \rangle$ *vs.* θ for $B_\perp = 10$ pT, $\alpha_{eq} = 10°$ and $v_{\parallel eq_o} = v_{p\parallel eq}$. The wave function corresponds to one given in Fig. 5.3. Also shown are the initial energy of the sheet, $\langle E_o \rangle$ and the final energy $\langle E_S \rangle$. We have found earlier that the main effect of the wave-normal angle increase is seen through an increase of $E_\parallel$. Thus, as the wave normal increases the longitudinal interactions become more effective, as indicated in Fig. 5.14. Furthermore, when the wave-normal approaches the resonance cone electrons are scattered by as much as -5.5°, and the sheet energy is increased about five times. For such a strong interaction the wave amplitude would most likely be heavily attenuated, although to find the exact solution it is necessary to include a previously discussed feedback term. The inclusion of the feedback term would than probably diminish the scattering effects as the wave amplitude becomes smaller with the increasing scattering.

In Chapter II we discussed the possibility of space bunching of electrons through the longitudinal resonance process. Figure 5.15 shows the phases of nine electrons from a sheet with $v_{\parallel eq_o} = v_{p\parallel eq}$, $\alpha_{eq} = 10°$ and interacting with a 30 pT wave. Three remaining electrons are omitted from this figure because they are very weakly trapped as already illustrated in Fig. 5.12. Initially all electrons are uniformly

distributed in phase space and maintain this phase separation as they approach the equator. At the equator they reach a wave growth region and trapping takes place. As electrons become trapped around t = 0.21 sec their maximum phase separation is reduced to about 150°, and can be as small as 50° at the moment when all electrons reach the bottom of potential well nearly simultaneously at t = 0.21, t = 0.24, and t = 0.27 sec. Thus the original spacing between the electrons is reduced and we have a case of space bunching. In this particular example 9 out of 12 electrons are bunched in about a half of the original separation. Thus, the density increase is roughly 9/12 × 360/150, or about 180% of the initial density for $v_{\parallel eq_o} = v_{p\parallel eq}$. For other velocities the density increase is smaller because the resonance condition is not satisfied exactly at the equator. Note that after a few initial oscillation periods electrons go out of phase and start to reach the bottom of the potential well at different times. It is possible to have a new synchronization later in time, as occurs at t = 0.54 and t = 0.565 sec (Fig. 5.15). This problem may be understood as though we have 9 harmonic oscillators with slightly different periods of oscillation caused by different phases at the moment those electrons entered the trap.

Figure 5.16 shows $\langle \Delta\alpha_{eq} \rangle$ *vs.* $v_{\parallel}$,and $\langle \Delta E \rangle$ *vs.* $v_{\parallel}$ for interactions taking place inside and outside the plasmapause. Those results clearly show that interactions outside the plasmapause result in less scattering, but in more energy exchange, than those interactions inside the plasmapause. This interesting result may be explained as follows; as n_{eq} drops outside the plasmapause the wave phase velocity

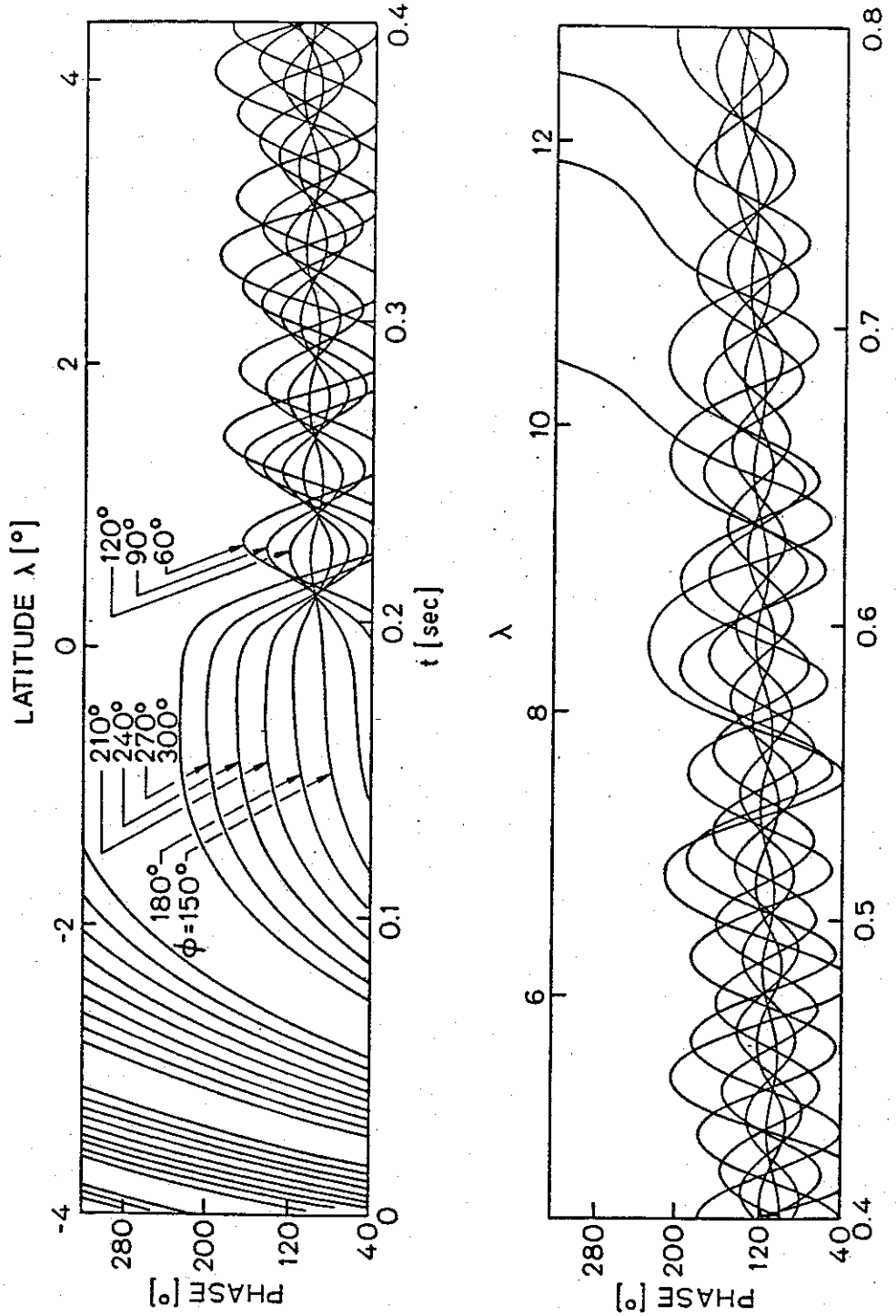

FIGURE 5.15 PHASE BUNCHING DUE TO THE LONGITUDINAL RESONANCE INTERACTIONS.

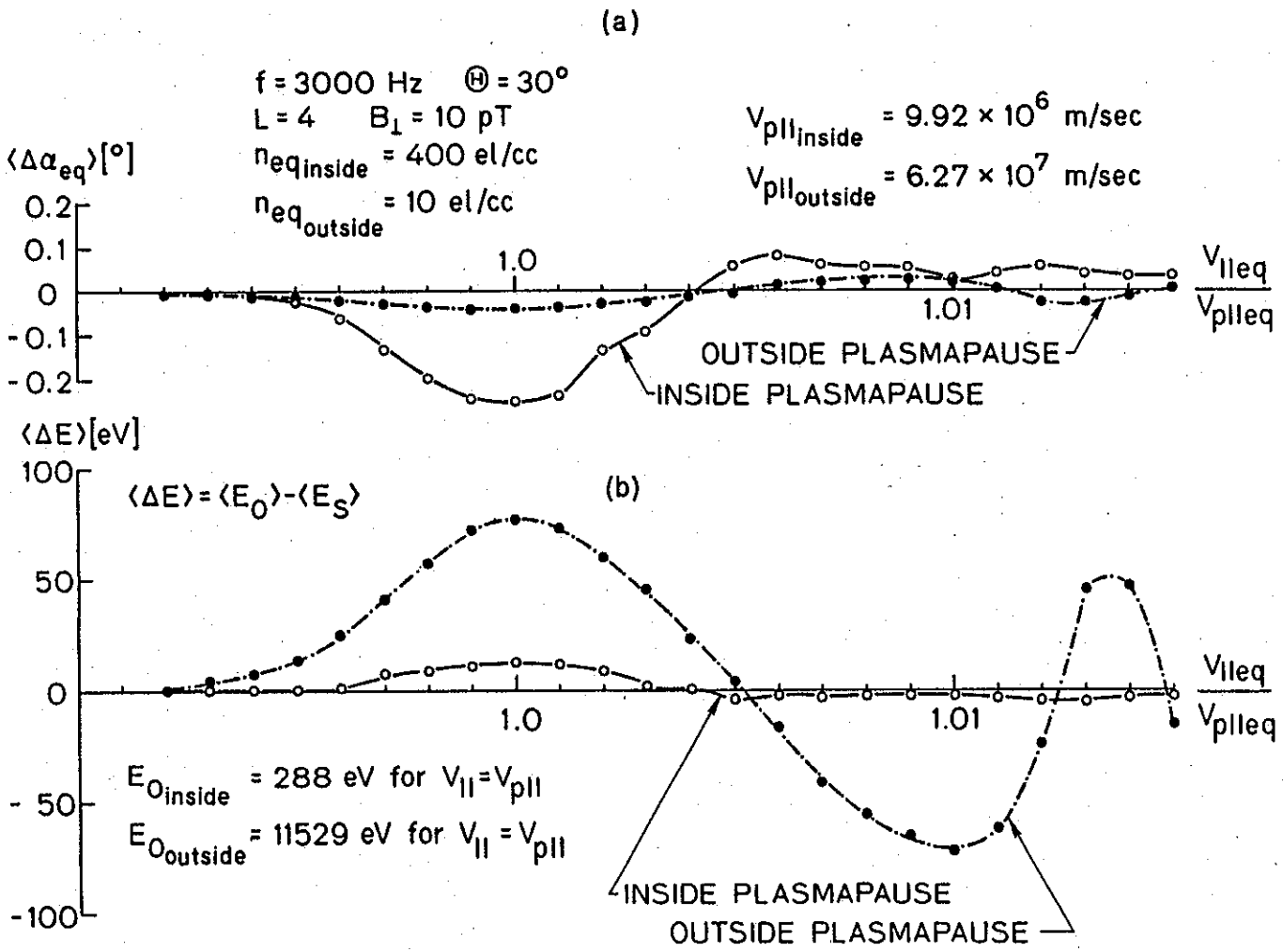

FIGURE 5.16 COMPARISON BETWEEN THE EFFECTS OF LONGITUDINAL RESONANCE INTERACTIONS INSIDE AND OUTSIDE THE PLASMAPAUSE. Shown in (a) is the mean scattering $\langle\alpha_{eq}\rangle$, while (b) depicts the corresponding energy exchange $\langle\Delta E\rangle$.

increases and the parallel resonant energy becomes higher. Higher energy electrons move faster through the wave and hence have a shorter time to be scattered. Note that although the resonant energy is about 288 eV for n_{eq} = 400 el/cc it is 11529 eV for n_{eq} = 10 el/cc. Because of that difference in resonant energies even a relatively small scattering outside the plasmapause results in energy changes that are larger compared to those found inside the plasmapause.

This concludes our discussion of single sheet scattering interacting with a one-sided wave function. In the next section we present results involving sheet scattering by a spatial pulse.

D. SCATTERING OF A SINGLE SHEET INTERACTING WITH A SPATIAL PULSE

In this section we examine the scattering of a single electron sheet as it moves through a spatial amplitude pulse formed by a non-ducted wave when its ray direction stays field aligned for a certain portion of the wave path. As depicted in Figure 5.17a the ray direction is field aligned between $\lambda = -10°$ and $\lambda = -7°$, which is equivalent to 1000 km in length. Other interaction parameters are specified in the same figure. The interaction is studied for a wide range of initial parallel velocities, $\Delta v_{\parallel}$, as illustrated in Figure 5.17b. The minimum parallel velocity is 1.012 $v_{p\parallel eq}$, the maximum parallel velocity is 1.106 $v_{p\parallel eq}$, and the parallel velocity increment is 0.001 $v_{p\parallel eq}$. The wave amplitude is assumed to be zero everywhere except for $-10° < \lambda < -7°$. The scattering results are shown in Figure 5.17. To explain those

results we can use Figure 5.17b as follows; when the initial parallel velocity is small, for example $v_{\parallel peq} = 1.012\ v_{p\parallel eq}$, the latitude of the first resonance point is also small, i.e. it is close to the equator. Hence, as those electrons travel up the field line toward the equator they encounter the spatial amplitude pulse but parallel and phase velocities are rather different resulting in a very weak interaction. As the initial parallel velocity of a sheet is increased the first resonance point moves away from the equator and closer to the amplitude pulse, and the two velocities become better matched. This better velocity match results in a stronger interaction and a negative scattering $<\Delta\alpha_{eq}>$. A negative sign of $<\Delta\alpha_{eq}>$ means that electrons are accelerated. This acceleration is consistent with the relative ratio of two velocities; namely, before electrons reach the first resonance point their velocity is less than the wave phase velocity in which case electrons are accelerated in order to match the phase velocity. However, further increase of the parallel velocity beyond $1.082\ v_{p\parallel eq}$ results in a change of sign of the effective scattering. This occurs when the first resonance point falls within approximately $\pm 0.5°$ of the pulse front edge at $-10°$. The principal difference is that electrons become trapped as they interact with the pulse, whereas for lower parallel velocities there were no trapped electrons. When trapping takes place the parallel velocity follows the phase velocity, which decreases as electrons approach the equator, and this results in a positive sign of scattering $<\Delta\alpha_{eq}>$ in Fig. 5.18. Furthermore, as the parallel velocity is increased beyond $1.094\ v_{p\parallel eq}$ the first resonance moves even further down the field line and interactions become small

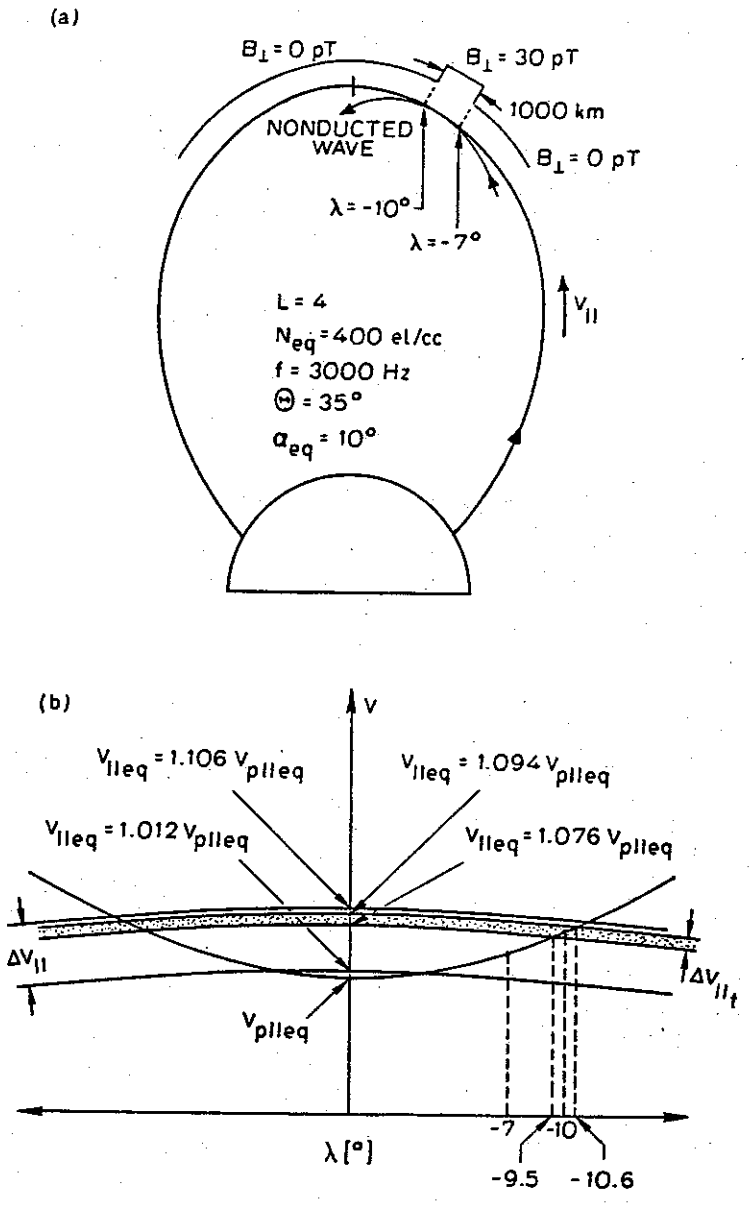

FIGURE 5.17 INTERACTION WITH SPATIAL AMPLITUDE PULSE EXTENDING BETWEEN λ=-10° AND λ=-7°. Shown in (a) is the position of spatial pulse on the field line. The range of affected initial parallel velocities is shown in (b).

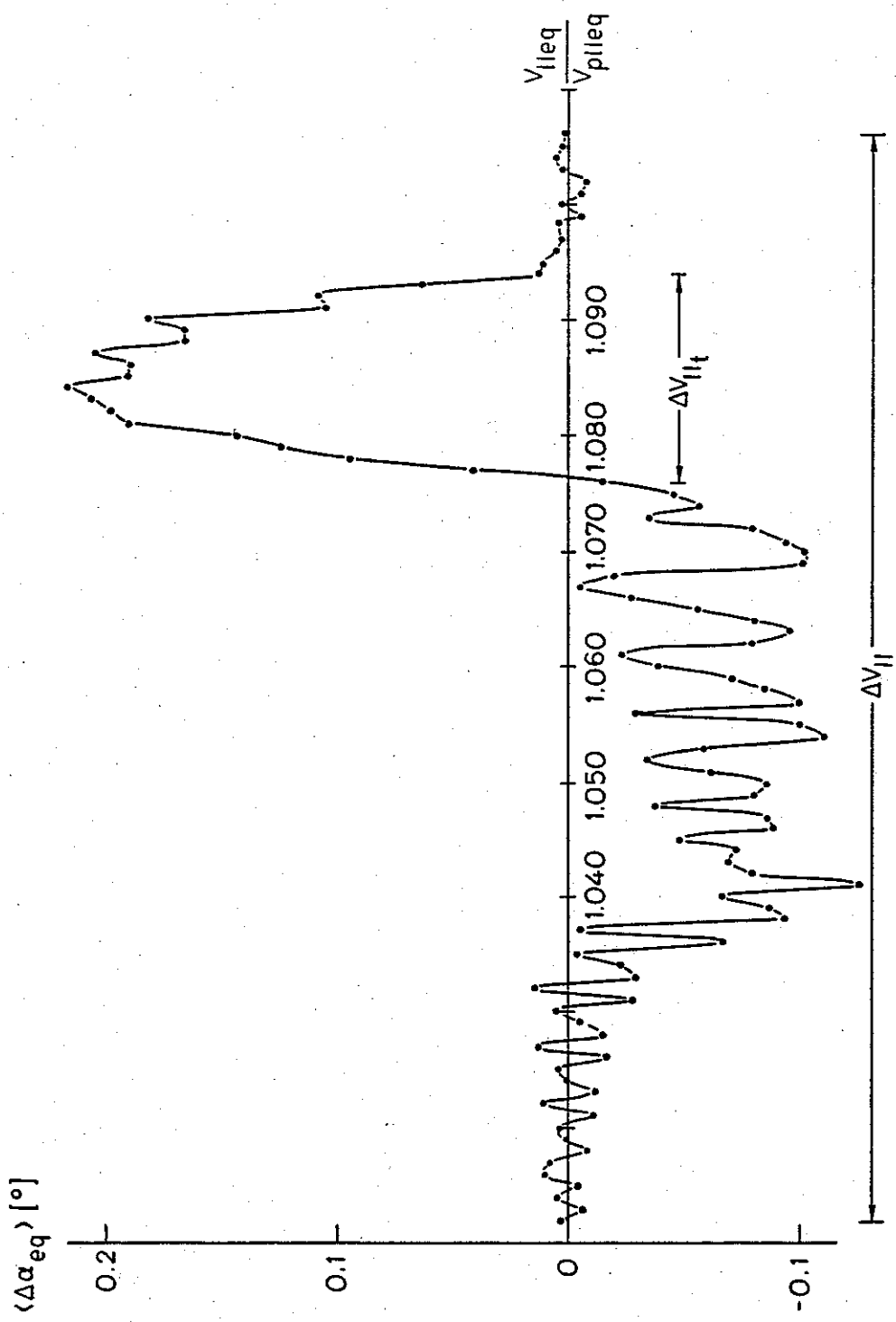

FIGURE 5.18 MEAN SCATTERING FOR INTERACTIONS WITH A SPATIAL AMPLITUDE PULSE EXTENDING BETWEEN λ=-10 AND λ=-7 . Electrons with initial velocities within the $\Delta v_{\|t}$ range are trapped, while electrons with other initial parallel velocities remain untrapped.

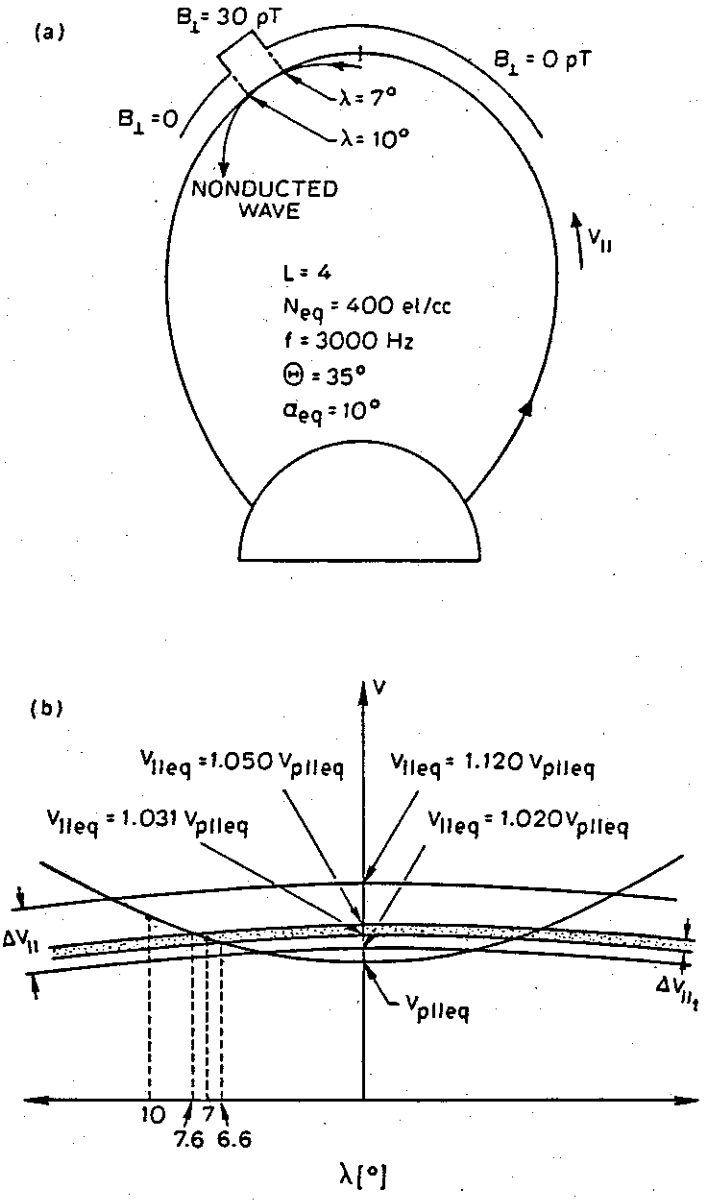

FIGURE 5.19 INTERACTION WITH SPATIAL AMPLITUDE PULSE EXTENDING BETWEEN λ=7° AND λ=10°. The format is the same as that of Fig. 5.18.

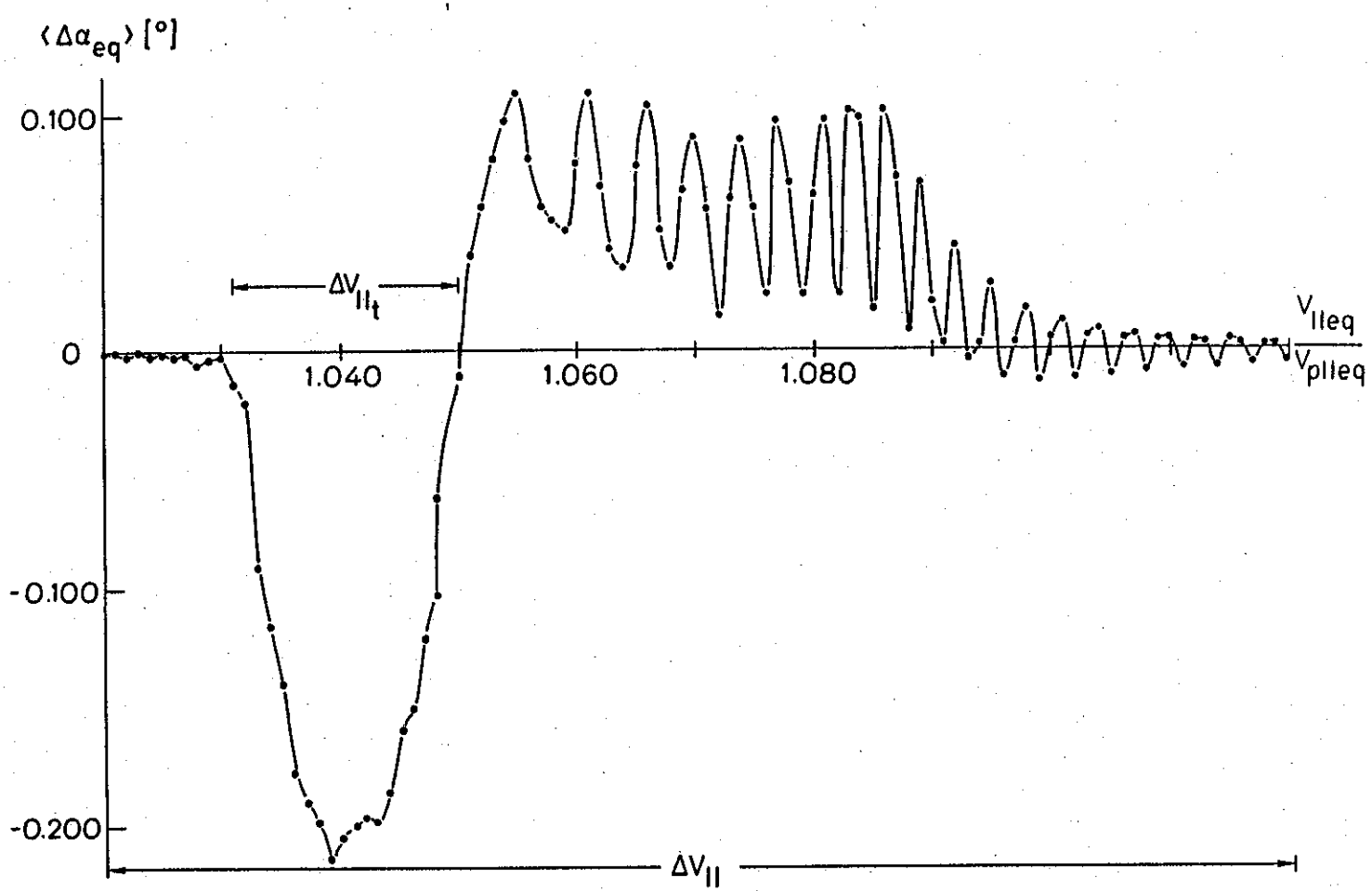

FIGURE 5.20 MEAN SCATTERING FOR INTERACTIONS WITH A SPATIAL AMPLITUDE PULSE EXTENDING BETWEEN $\lambda=7°$ AND $\lambda=10°$. Only electrons with $v_{\parallel}$ in the $\Delta v_{\parallel t}$ range are trapped.

again. The shaded area in Fig. 5.17a indicates the trapping velocity bandwidth Δv_t which is also indicated in Fig. 18. When comparing areas of positive and negative scattering in Fig. 5.18 they turn out to be approximately the same which means that the energy exchange is small.

This example is a good illustration of the different features of the longitudinal resonance interaction. We see that the electron behavior is very dissimilar in cases with and without trapping. Untrapped electrons change their velocity depending on the relative ratio of phase and parallel velocities, while trapped electrons become space bunched and their parallel velocity follows the wave phase velocity.

Figure 5.19 illustrates a similar type of interaction as the one discussed above, only the spatial amplitude pulse is on the other side of the equator. The corresponding scattering results are shown in Figure 5.20. Those results may be explained using the same analysis as the one used in the previous example. The trapping occurs when the first resonance point is close to the pulse front edge at $\lambda = 7°$, although the trapped electron scattering is now negative as the phase velocity increases. The untrapped particle scattering is positive because the phase velocity is smaller than the parallel velocity before the resonance point is reached.

VI. FULL DISTRIBUTION SIMULATIONS

A. INTRODUCTION

In Chapter V we have presented results of single sheet simulations. The purpose of that analysis was to clarify various aspects of the longitudinal resonance process. In this chapter we carry those calculations one step further by increasing the number of test electrons in order to simulate a full distribution. Such calculations are interesting for two reasons:

1) It is possible to calculate a precipitated flux, and
2) It is feasible to estimate wave amplitude changes due to the energy exchange.

In the following examples of full distribution calculations electrons are assumed to interact with a one-sided wave function. As it was already shown in Chapter V, this type of wave function may produce a significant amount of scattering, whereas interactions with narrowband signals (not amplified through gyroresonance) may result in a very small final scattering. Therefore, based on those results, it appears that the constant amplitude CW signals represent a very weak source of precipitation, although those CW waves still may have some amplitude variations around the equator as a consequence of the interaction with electrons.

The energetic electron population is readily described in terms

of an equatorial distribution function f_{eq} $(v_{\parallel eq}, \alpha_{eq})$. From this point on we drop the subscript 'eq', and all quantities represent equatorial values unless specified otherwise. The distribution function is given in $v_\parallel - \alpha$ space because it is a convenient representation which directly shows the pitch angle scattering, $\Delta\alpha$, and it is easy to determine a normalized velocity $v_\parallel/v_{p\parallel}$ which is one of the prime factors affecting the interaction process. The velocity space volume element is then given as $v_\parallel^2 \frac{\sin\alpha}{\cos^3\alpha} d\alpha dv_\parallel d\phi$ [Inan, 1977].

Now we recall results of Figures 5.6 and 5.7 showing the mean scattering of a single sheet as a function of the sheet initial parallel velocity. From those figures it is evident that the trapping velocity range considered is limited to a narrow strip around $v_\parallel = v_{p\parallel}$, while the pitch angle range extends from α_{lc} to α_{max}. The value of α_{max} may be as large as 90°, and specifically in our calculations it may be limited to a slightly lower value due to time averaging in the equations of motion. The angle $\alpha_{lc} = 5.5°$ is the nominal loss cone angle for the dipole field line L = 4, i.e. all electrons with pitch angles lower than 5.5° have mirror points at ionospheric heights (h < 200 km) and are assumed to be lost through precipitation. As already shown in Figs. 5.6 and 5.7, the trapping velocity bandwidth increases with increasing pitch angle due to the effects of the wave magnetic field forces. This trapping velocity bandwidth $\Delta v_{\parallel t}$ is about 0.4% of $v_{p\parallel eq}$ for $\alpha = 10°$, and about 1% of $v_{p\parallel eq}$ for $\alpha = 70°$. Again, it should be noted that this velocity bandwidth refers to the trapped electrons only. The untrapped electrons have a quite different behavior; if the initial parallel velocity is smaller than the lower trapping velocity limit the

scattering is negligible because the wave phase velocity and the parallel velocity of the electron are never matched along the field line. On the other hand, if the initial parallel velocity of an untrapped electron is larger than the upper trapping velocity limit there are always two resonances; at the first resonance scattering is negligible because the wave amplitude is very small, whereas at the second resonance point, where the electron parallel velocity exceeds the wave phase velocity, the untrapped electrons are decelerated. All of the above mentioned classes of electrons are illustrated in Figure 6.1. The scattering of untrapped electrons is much smaller than it is for the trapped electrons, but the interaction velocity range for untrapped electrons is larger than the trapping velocity bandwidth. The effects of trapped and untrapped electrons on the wave amplitude are exactly opposite; the trapped electrons are accelerated and the wave loses energy, whereas the untrapped electrons are decelerated and the wave gains energy. This dissimilar behavior of trapped and untrapped electrons indicates that, in order to calculate a net transfer, it is necessary to consider a wide range of initial parallel velocities of electrons which then requires a very large number of test electrons. While the wave amplitude variation calculations require a large number of test electrons the precipitation calculations may be carried out by considering a significantly smaller number of electrons, because only a certain class of electrons can be scattered into the loss cone, i.e. only trapped electrons with sufficiently small initial pitch angles are precipitated in the ionosphere.

From Fig. 6.1 it is obvious that there is always an $\alpha_{max} < \pi/2$

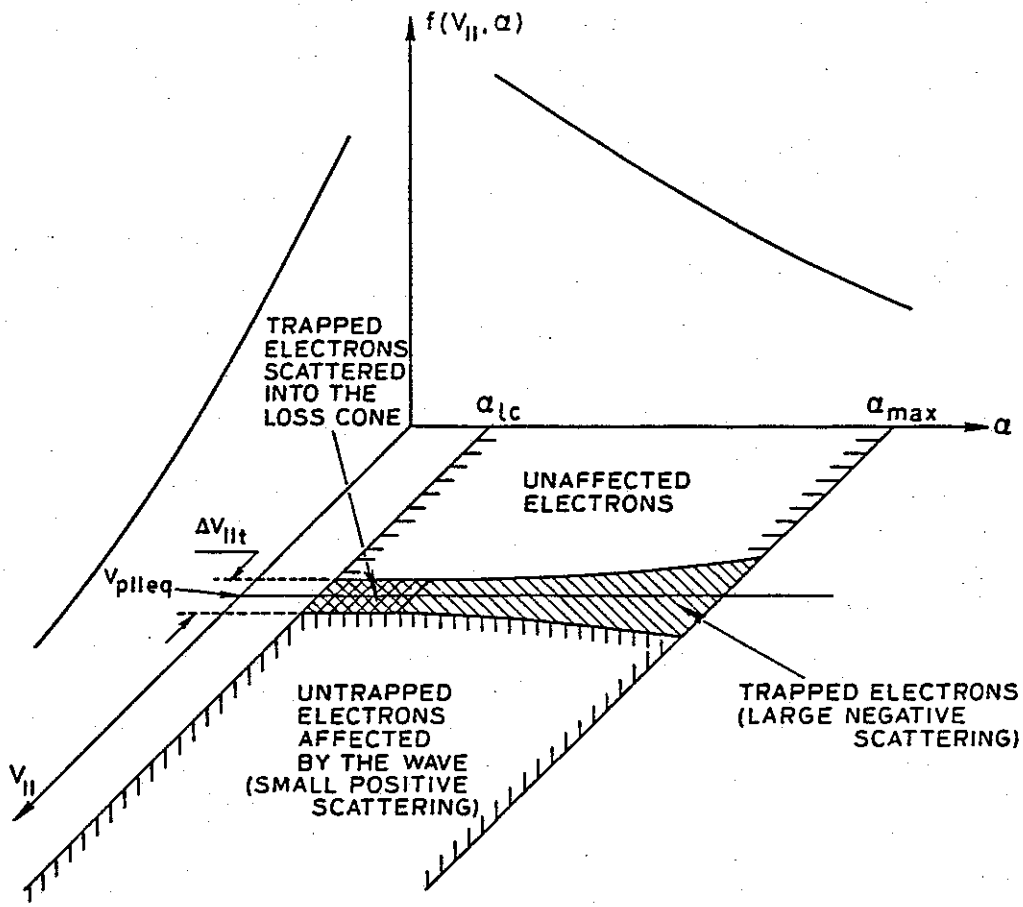

FIGURE 6.1 GENERAL DISTRIBUTION FUNCTION. Differently shaded areas indicate the various behavior of electrons as they interact with the variable amplitude wave.

such that electrons with $\alpha > \alpha_{max}$ cannot be scattered into the loss cone. As noted above those scattered electrons must have been trapped, i.e only trapped electrons may have their pitch angles decreased by the amount required for precipitation. Based on the above limits for $v_{\parallel}$ and α it is feasible to define a region in $v_{\parallel} - \alpha$ space (cross-shaded in Fig. 6.1) containing electrons that can be scattered into the loss cone. This region in the $v_{\parallel} - \alpha$ space is further divided into a number of mesh points identified by their $v_{\parallel}$ and α , and this mesh then represents the initial distribution. The number of electrons at each mesh point is equal to twelve, reflecting the fact that electrons are uniformly distributed in phase. Figure 6.2a illustrates the unperturbed distribution function; note that we use the number density of electrons N_E rather than $f(v_{\parallel}, \alpha)$. The number density and $f(v_{\parallel}, \alpha)$ are related through [Inan, 1977]:

$$N_E = 2\pi\, f(v_{\parallel}, \alpha)\, v_{\parallel}^2 \frac{\sin\alpha}{\cos^3\alpha} \Delta v_{\parallel}\, \Delta\alpha \qquad (6.1)$$

Using Eq. 6.1 it is also possible to find the actual number of electrons represented by a single test electron.

During the interactions the initial distribution of electrons (Fig. 6.2a) is perturbed by the wave, and the final distribution is shown in Figure 6.2b. Note that the velocity mesh size is different in Figs. 6.2a and 6.2b, since the energy of the electrons tends to be significantly increased through the interaction process. Beside an overall increase in electron energies, three electrons are scattered into the loss cone. In the next section precipitation fluxes are

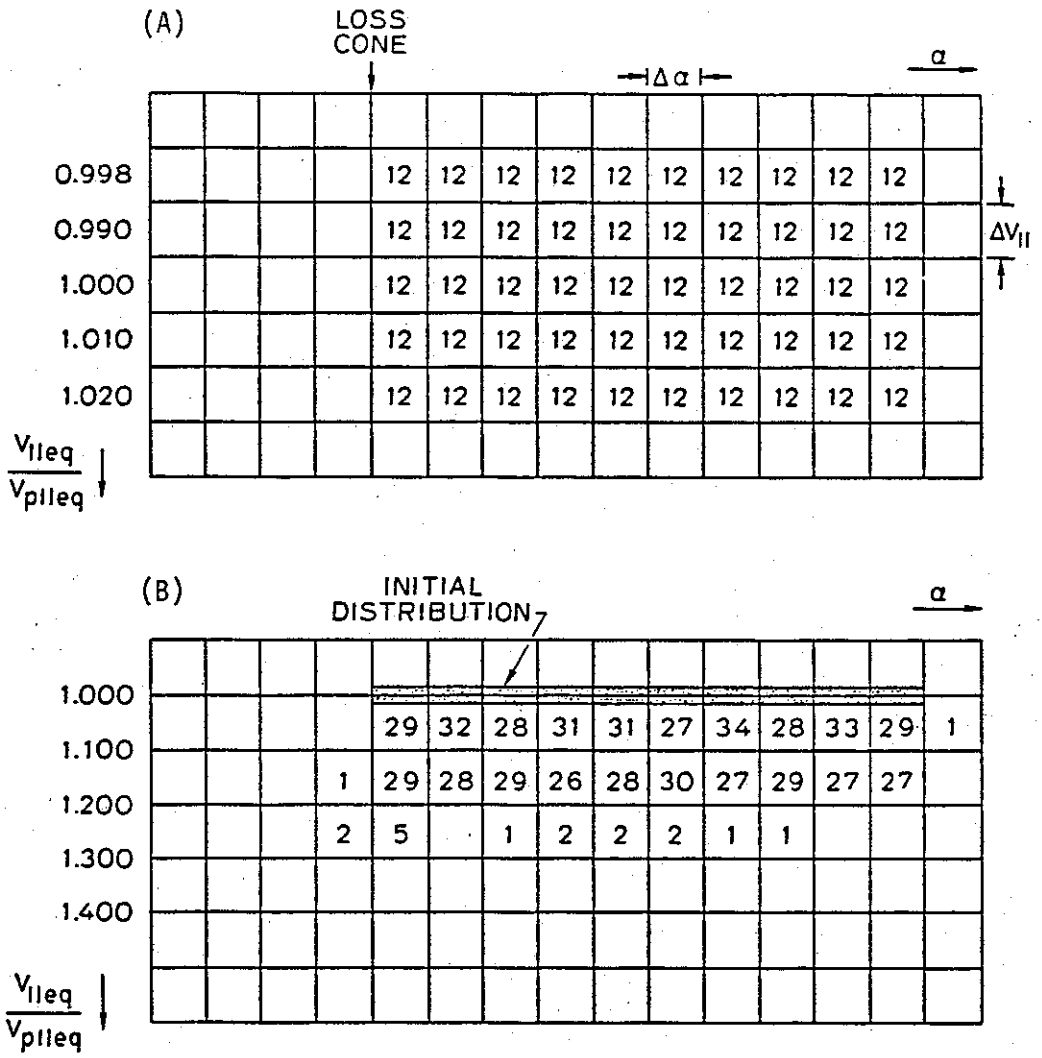

FIGURE 6.2 SIMULATION OF THE DISTRIBUTION FUNCTION. (A) The unperturbed distribution. (B) Perturbed distribution. The numbers in each individual cell indicate the number density of electrons.

computed for three particular cases.

B. PRECIPITATED ELECTRON FLUX

Here we compute the precipitated electron fluxes involving a one-sided wave function, and for three different maximum wave intensities (E_u = 50, 150 and 250 μV/m). The maximum initial pitch angle considered in these calculations is 10°, since there are no electrons with $\alpha > 10°$ scattered into the loss cone even when the electrons interact with a very strong wave, i.e. E_u = 250 μV/m. The initial unperturbed number density function is the same in all three examples, and was already shown in Fig. 6.2a. Furthermore, the distribution function is taken as

$$f(v,\alpha) = \frac{A}{v^4} g(\alpha) \qquad (6.2)$$

where A is a constant and $g(\alpha)$ is some function of pitch angle. In our calculations $g(\alpha)$ is assumed to be an isotropic function given by

$$g(\alpha) = g_1(\alpha) = 1 \qquad \alpha > \alpha_{lc} \qquad (6.3)$$

$$= 0 \qquad \alpha < \alpha_{lc}$$

The following analysis is similar to that presented by Inan [1977], although in his work electron scattering was due to

gyroresonance interactions. First, before computing the precipitation, it is feasible to compute the wave induced pitch angle perturbations given by $f(\alpha)$ which is obtained by integrating $f(v_{\parallel},\alpha)$ over the velocity range of interest. In our examples, involving a 5 kHz wave, it is found that the maximum parallel velocity after the interaction is $v_{\parallel max} = 1.8 v_{p\parallel}$, whereas the minimum parallel velocity is $v_{\parallel min} = 0.98\ v_{p\parallel}$. The equatorial phase velocity $v_{p\parallel}$ for a 5 kHz wave is 11.23 10 m/sec. Thus the pitch angle distribution is given by

$$f(\alpha) = 2\pi \int_{v_{\parallel} = 0.98 v_{p\parallel}}^{v_{\parallel} = 1.8\ v_{p\parallel}} f(v_{\parallel},\alpha)\ v_{\parallel}^2 dv_{\parallel} \qquad (6.4)$$

remembering that electrons are uniformly distributed in initial phase, which results in the factor 2π in Eq. 6.4.

Figure 6.3 shows the normalized pitch angle distribution $f(\alpha)$ as a function of α for different wave intensities. The dashed curves show the initial unperturbed distributions, whereas the solid curves indicate the final distributions. These results show that the longitudinal resonance interaction requires rather strong waves in order to scatter electrons into the loss cone. For a wave with $E_{\parallel}$ = 50 μV/m ($B_{\perp}$= 14 pT) the perturbations are very small, and only a few electrons are scattered below α_{lc}. When the wave amplitude is increased the loss cone starts to fill with electrons, and also electrons with higher pitch angles are scattered down to lower pitch angles. This process is best illustrated in the case of a 250 μV/m wave, where the loss cone is filled with

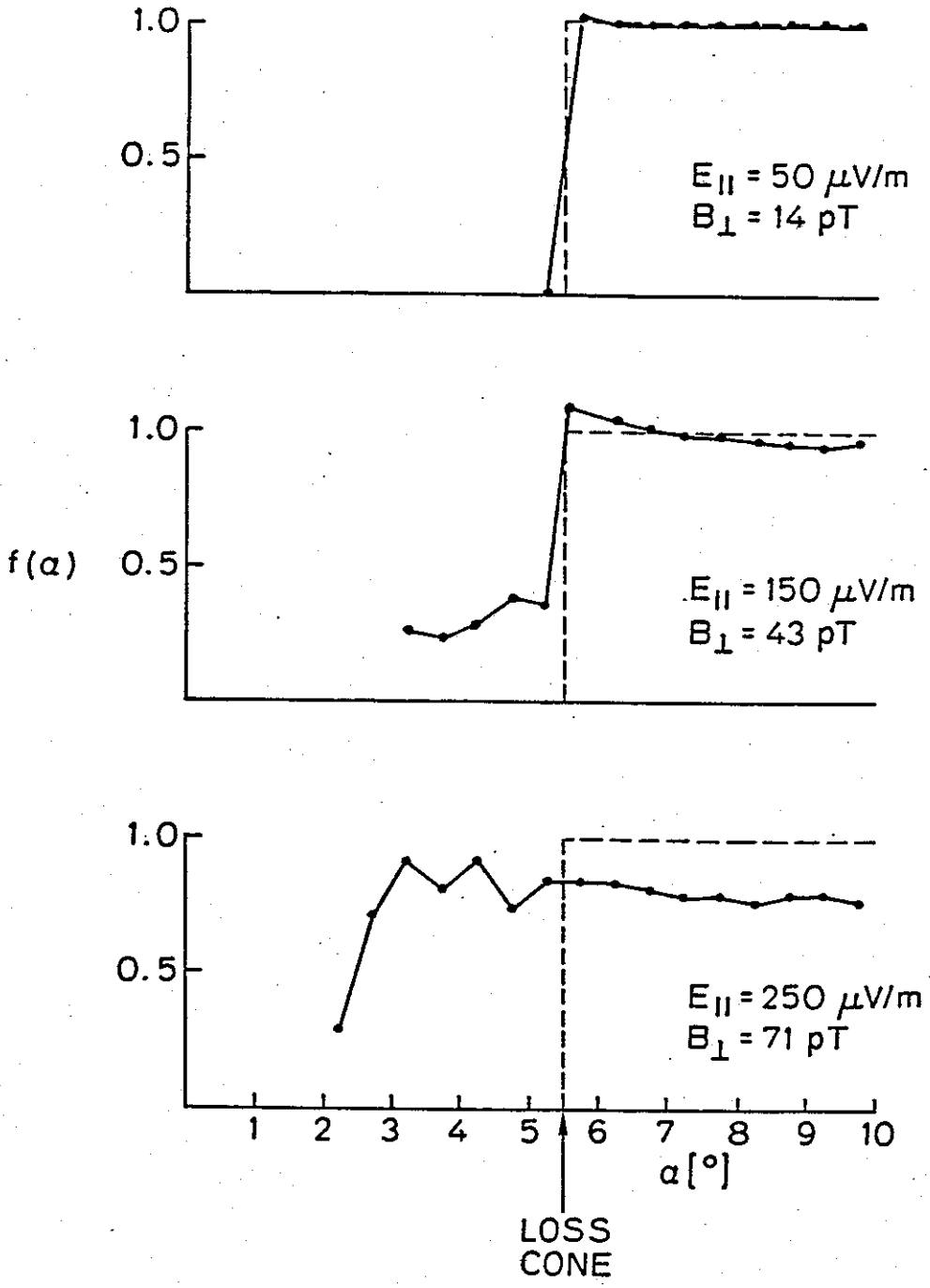

FIGURE 6.3 NORMALIZED ELECTRON DISTRIBUTION f(α). The dashed lines represent the unperturbed distribution. The solid curves represent the perturbed distribution.

electrons having a wider range of initial pitch angles than the electrons reaching the loss cone in the two other cases.

The total number density of electrons precipitated in the velocity range $0.98\ v_{p\parallel}$ to $1.8\ v_{p\parallel}$ is given by

$$N = 2\pi \int_0^{\alpha_{lc}} \int_{0.98v_{p\parallel}}^{1.8v_{p\parallel}} f(v_\parallel,\alpha)\ v_\parallel^2\ \frac{\sin\alpha}{\cos^3\alpha}\, dv_\parallel d\alpha\ L^3(1+3\sin^2\lambda)^{1/2} \qquad (6.5)$$

where the factor $L^3(1+3\sin^2\lambda)^{1/2}$ accounts for the convergence of the field line going from the equator to ionospheric heights. The precipitated energy deposition rate is computed in similar fashion by including the energy weighting factor $\frac{1}{2}\ m\ \frac{v_\parallel^2}{\cos^2\alpha}$ in (6.5) which then yields

$$Q = 2\pi \int_0^{\alpha_k} \int_{0.98v_{p\parallel}}^{1.8v_{p\parallel}} f(v_\parallel,\alpha)\ v_\parallel^2\ \frac{v_\parallel^2}{\cos^3\alpha}\ 1/2m\frac{v_\parallel^2}{\cos^2\alpha}\, dv_\parallel d\alpha\ L^3(1+3\sin^2\lambda)^{1/2} \qquad (6.6)$$

The integrals in Eqs. 6.5 and 6.6 are easily evaluated by a numerical integration. For the three examples considered the normalized energy deposition rate, defined as $Q_N = Q/A$ where A is defined in Eq. 6.2, are:

$E_\parallel = 50\ \mu V/m$	$Q_N = 0.9652 \cdot 10^{-14}$ erg/cm^2/sec
$E_\parallel = 150\ \mu V/m$	$Q_N = 0.8129 \cdot 10^{-12}$ erg/cm^2/sec
$E_\parallel = 250\ \mu V/m$	$Q_N = 0.3565 \cdot 10^{-11}$ erg/cm^2/sec

To compute the total energy deposition it is necessary to evaluate the constant A. This can be done by computing the total number density N_E in el/cc in the specific velocity range 0.98-1.8 $v_{p_{\parallel}}$. In this case

$$N_E = 2\pi \int_0^{\pi} \int_{0.98v_{p_{\parallel}}}^{1.8v_{p_{\parallel}}} \frac{A}{v^4} v^2 \sin\alpha \, dv \, d\alpha \qquad (6.7)$$

The above integral yields

$$A = 2\times10^8 \, N_E \qquad (6.8)$$

Finally, to compute A it is necessary to estimate N_E from the reported measurements. From Schield and Frank [1970] we find that N = 1 el/cc in the 1-2 KeV range and that the number density varies as v^{-4} with velocity (E^{-2} with energy). In our case the electron energies are 300-1000 eV which results in N_E = 10 el/cc, since the number density increases with decreasing electron energy. Substituting N_E = 10 el/cc in Eq. 6.8 we find that $A = 2\times10^9$.

The next step is to compute the absolute energy deposition rates by multiplying the normalized rates Q_N by the constant A. The results are shown below:

$E_{\parallel}$ = 50 μV/m $Q = 1.94\times10^{-5}$ erg/cm^2/sec

$E_{\parallel}$ = 150 μV/m $Q = 1.66\times10^{-3}$ erg/cm^2/sec

$E_{\parallel}$ = 250 μV/m $Q = 7.40\times10^{-3}$ erg/cm^2/sec

The above values indicate that the fluxes precipitated by a 5 kHz wave, which is amplified at the equator through the gyroresonance interaction, are rather small, especially when compared to those computed for gyroresonance interactions. Results for the gyroresonance process calculated by Inan [1977] indicate flux levels of 0.01-0.2 erg/cm^2/sec for a 10 pT wave. Note that 10 pT corresponds to $E_{\parallel}$ = 30 μV/m for $\theta = 30^\circ$ and f = 5 kHz. Thus, the scattering efficiency is considerably higher for the gyroresonance than it is for the longitudinal resonance.

C. ENERGY EXCHANGE AND BALANCE

From the analytical and numerical studies it is evident that the scattering of electrons is always associated with energy transfer, i.e. if electrons gain energy then the wave is attenuated, or if electrons lose energy then the wave is amplified. Also, a large scattering is always associated with a large energy exchange. Such behavior constitutes another major difference between the longitudinal and the gyroresonance processes; namely, electrons can be scattered significantly through the gyroresonance interactions with a very small amount of energy transfer. This is explained by the fact that in gyroresonance it is the momentum transfer that causes pitch angle

changes, whereas the energy remains almost unchanged [Inan, 1977].

The total energy balance calculations for the longitudinal resonance process are extremely complicated as they involve a large number of electrons. As indicated in Fig. 6.1 the electrons with parallel velocities close to the wave phase velocity become trapped which then results in scattering from -0.2° up to -6° for pitch angles from 10° to 70°, respectively. The scattering of untrapped electrons is smaller and positive, about 0.05-0.1° on the average. However, only a fraction of the electron population becomes trapped, while the number of untrapped electrons is much larger. From the sample calculations it was estimated that the upper velocity limit for untrapped electrons can be as high as 1.30 $v_{p\parallel}$, i.e. even if the initial parallel velocity of the electron is $v_\parallel = 1.30\ v_{p\parallel}$ the electron is still scattered more than ±0.005°. The scattering of ±0.005° represents a practical threshold of resolution for the numerical integration method used in our simulations. This resolution limit was found by setting $E_\parallel = 0$ μV/m, i.e. computing only the adiabatic motion of the electrons and comparing the initial and the final pitch angles. Theoretically, the difference between these two pitch angles should be zero, whereas the numerical results have shown ±0.005 fluctuations, which are than used as the limit of accuracy (resolution). These fluctuations are primarily due to the integration scheme, which uses linear interpolation. Returning to the energy exchange problem, it is evident that both trapped and untrapped electrons play important roles, and it is rather difficult to find an exact solution to this problem as the number of electrons involved is very large.

However, it is possible to estimate the energy transfer as follows; let us consider the example of Fig. 5.7a (solid curve) showing scattering as a function of the initial parallel velocity for a fixed initial pitch angle $\alpha = 10°$. This curve can be replotted substituting energy changes for pitch angle changes and also expanding the velocity range. Note that these results must be weighted by an appropriate function to account for different number densities at different velocities. This weighting function is assumed to have a v^{-2} characteristic (Eq. 6.1). Figure 6.4 shows both unweighted and weighted energy transfer, i.e. the average energy gain (loss) per electron with a given initial parallel velocity, as well as the weighting function (dashed curve). Now it is possible to use a numerical integration to estimate the total energy balance for this particular case.

The total energy exchange is given as

$$\Delta E = \int_{E_1(0.99v_{p\parallel})}^{E_2(1.03v_{p\parallel})} dE \qquad (6.9)$$

where ΔE represents the total energy exchanged through the longitudinal interaction with electrons whose initial parallel velocities are in 0.99–1.03 $v_{p\parallel}$ range, and all those electrons have the same pitch angle $\alpha = 10°$. The quantity dE gives the weighted amount of energy exchanged per electron at a particular parallel velocity, and it is shown in Fig. 6.4. The final result of the above integration is $\Delta E = 0.03$ eV. Though this number is obtained using only twelve electrons it is evident that

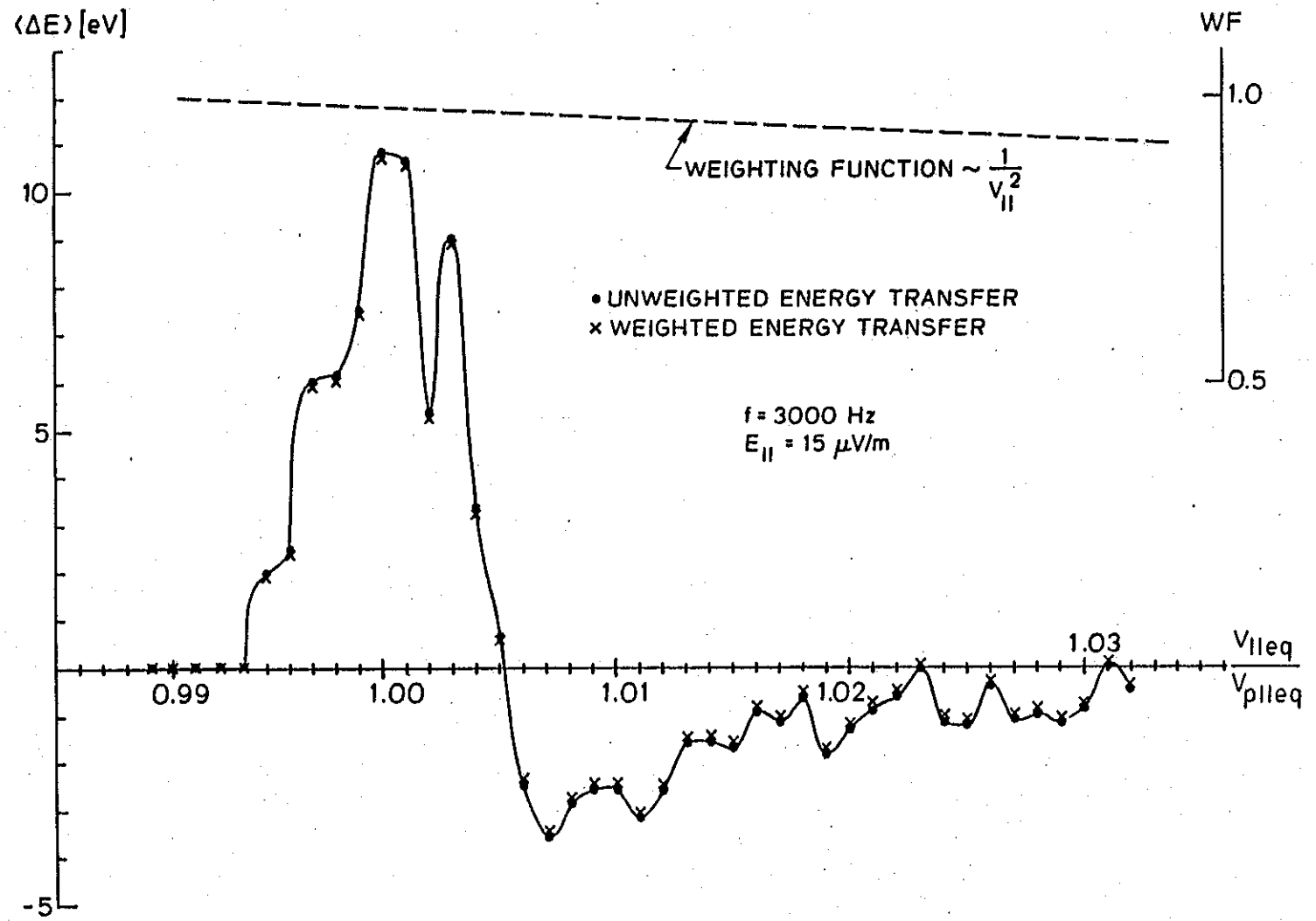

FIGURE 6.4 ENERGY TRANSFER FROM WAVE TO ELECTRONS FOR THE CW SIGNAL INTERACTION. The energy transfer is shown as a function of electron parallel velocity, and positive <ΔE> indicates that electrons gain the energy.

the total energy exchange at the particular pitch angle is very small even when the actual number of electrons is much larger.

To compute the overall energy balance similar calculations should be done for other pitch angles. A rough estimate using Figs. 5.6 and 5.7 indicates that the total energy transfer is very small, since the positive and negative scattering cancels out, i.e. the total area underneath $<\Delta\alpha_{eq}>$ curve is approximately zero.

Summarizing, it appears that both the precipitation and wave amplitude amplification (attenuation) for our sample case are small. Thus, it may be very difficult to observe the presence of this type of longitudinal interaction using ground observations. Another possibility for detection would be to use satellite borne particle detectors and to measure a relatively sharp depletion of electron density around $v_{\parallel} = v_{p\parallel}$. However, the problem is that particle detectors measure energies and pitch angles rather then parallel velocities and pitch angles. Note that the problem arises from the fact that the narrow range of parallel velocities which are affected (and wide range of pitch angles) maps into a wide range of energies (and pitch angles).

For example, if the parallel velocity equals the phase velocity, $v_{\parallel} = v_{p\parallel}$, and pitch angles vary from 5° to 70°, the corresponding electron energies vary from E_o to $E_o(1+\tan^2 70°)/(1+\tan^2 5°) = 8.48\ E_o$, where E_o is the energy of the electrons with 5° pitch angle. Beside the above mentioned spreading effect, which tends to dilute the effects of the longitudinal resonance when measured on an energy basis, the particle detector resolution itself may pose a problem. The typical

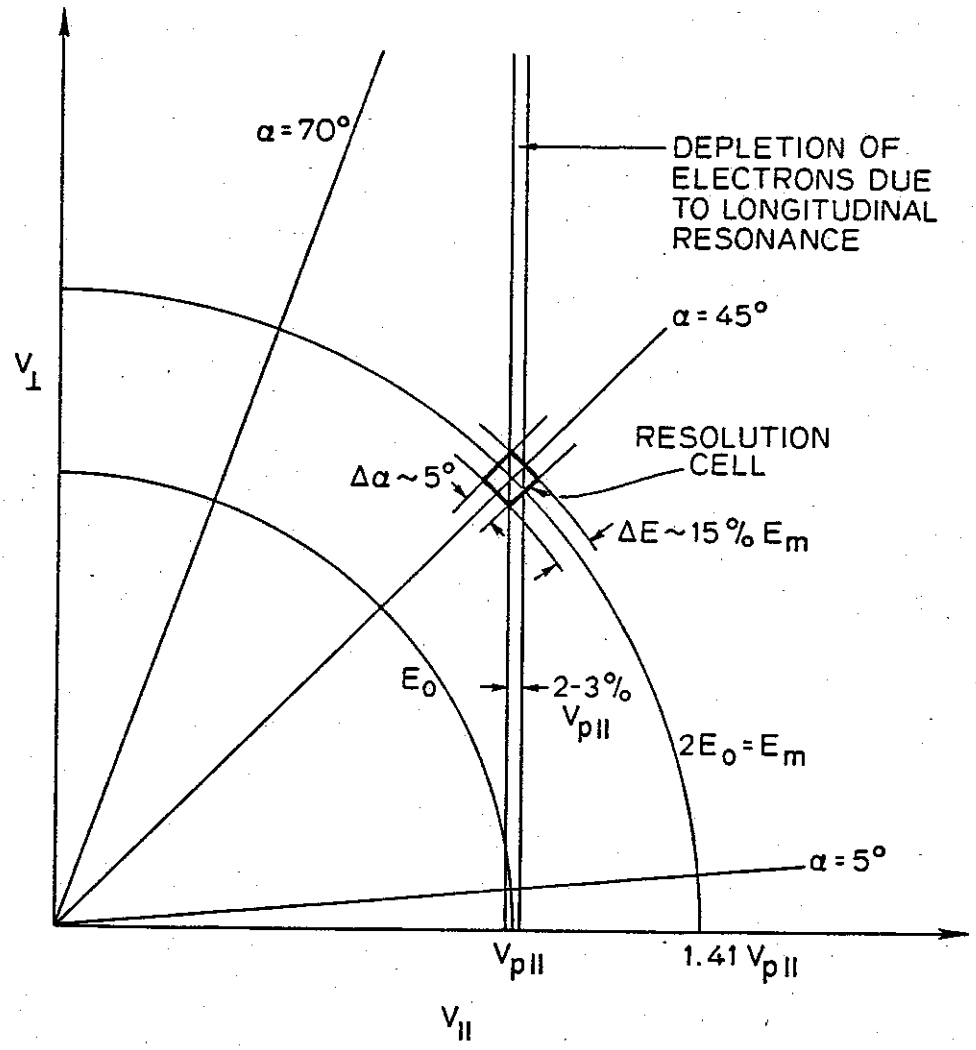

FIGURE 6.5 PARTICLE DETECTOR RESOLUTION AND DETECTION OF LONGITUDINAL RESONANCE EFFECTS. The effects of the resonance interactions are best seen as a depletion of electrons around $v_{\parallel} \simeq v_{p_{\parallel}}$.

resolution of particle detectors is about 2.5°- 5° in pitch angle, and about 15% in E_o, where E_o is the energy of interest. For example, if we want to measure the density of electrons with energy $E_m = 2E_o$, and pitch angle $\alpha = 45°$, the corresponding resolution cell would be as shown in Figure 6.5. On the other hand, the longitudinal resonance will tend to remove electrons from a narrow velocity band around $v_{p\parallel}$, leaving a depletion region in the distribution (Fig. 6.5). The width of the depletion region is very small, so that it occupies only about 30% of the resolution cell, as indicated in Fig. 6.5. Therefore, even if we remove all of the electrons from this depletion region, the particle detector would see only a 30% decrease in the number of electrons within the resolution cell. We recall from Chapter V that longitudinal resonance interactions, involving moderate amplitude waves, result in trapping of only about 30% of the electrons that satisfy the resonance condition (we considered only the trapped electrons, because only those electrons undergo sufficient change in $v_\parallel$ to be moved from one resolution cell to another). Thus the maximum total depletion factor for the resolution cell is estimated to be about 10%. On the other hand, typical particle detector measurements (e.g. Kimura at al., 1982) indicate large temporal variations of the electron flux, approaching an order of magnitude in intervals as short as 50 sec. For that reason the particle detector sensitivity is reduced, because it becomes very difficult to distinguish between variations due to spatial changes in particle distribution and wave induced variations. Thus, present particle detectors are probably not capable of detecting perturbations of the electron distribution due to longitudinal resonance interactions.

VII. APPLICATIONS TO MAGNETOSPHERIC PHENOMENA

Although it was found that the scattering efficiency of the longitudinal resonance process is small, it is possible that the bunching effects of the process may have important magnetospheric applications. In this chapter we consider applications of the longitudinal resonance to the generation of whistler precursors and to the generation of broadband VLF hiss. We also discuss the size of the internal electric field created in the bunching process.

A. GENERATION OF WHISTLER PRECURSORS

Whistler precursors are discrete rising tone emissions that precede two-hop whistlers, starting shortly (0.1-0.3 sec) after the one-hop delay. The precursor may consist of one or more discrete emissions. For the particular measurements of August 2, 1973, the number of emissions varied from one to seven. Figure 7.1 illustrates three typical cases of precursors showing both one-hop whistlers (recorded at Siple, Antarctica), and precursors with corresponding two-hop whistlers (recorded at Roberval, Canada). There is no precursor in Fig. 7.1b, illustrating the fact that not all whistlers propagating on the same path trigger a precursor. Figure 7.1d depicts a single emission precursor, while Fig. 7.1f shows a multi-emission precursor.

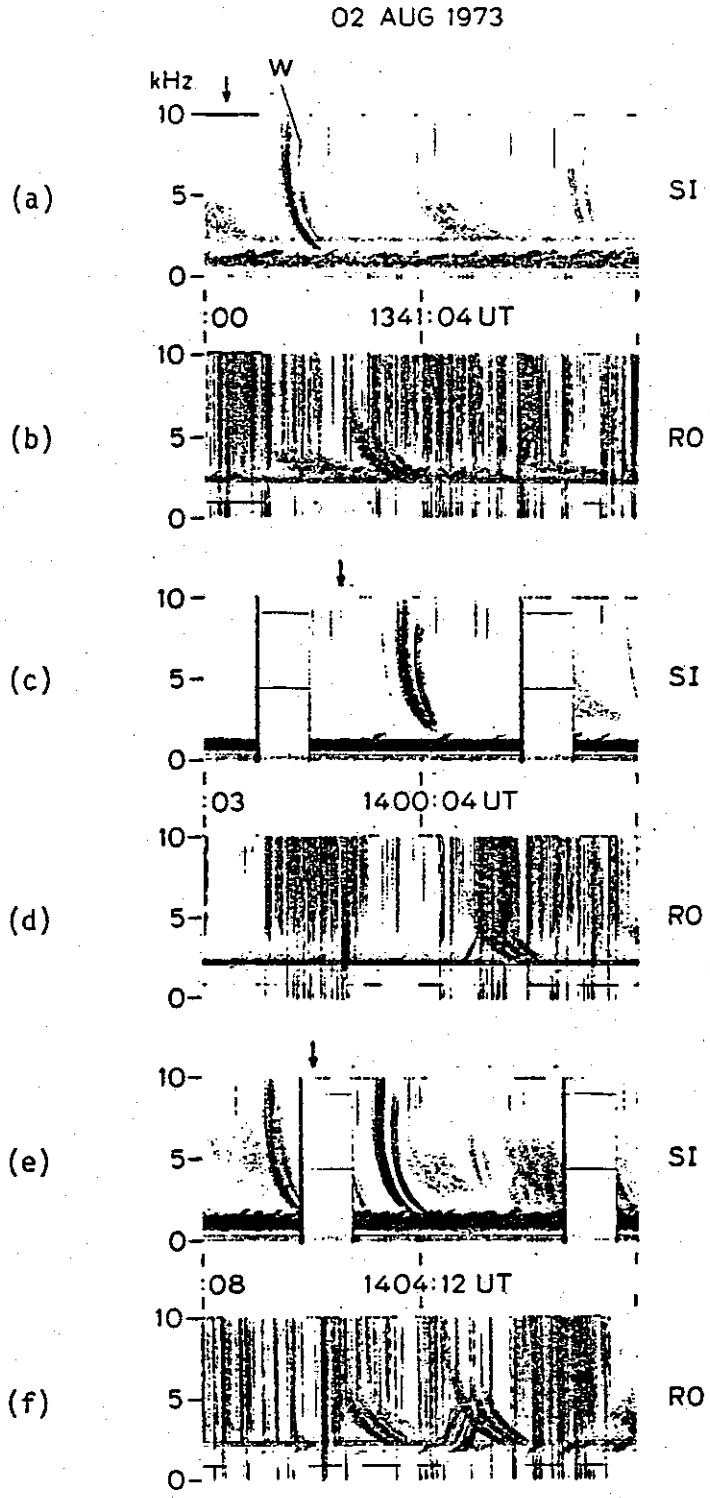

FIGURE 7.1 SPECTROGRAMS OF WHISTLER PRECURSOR EVENTS RECORDED AT SIPLE/ROBERVAL CONJUGATE STATIONS. The causative spheric is marked with an arrow, and the whistler component which triggers the precursor is marked by a W. (b) shows no precursor, (d) shows a single emission precursor, and (f) shows a multi-emission precursor event.

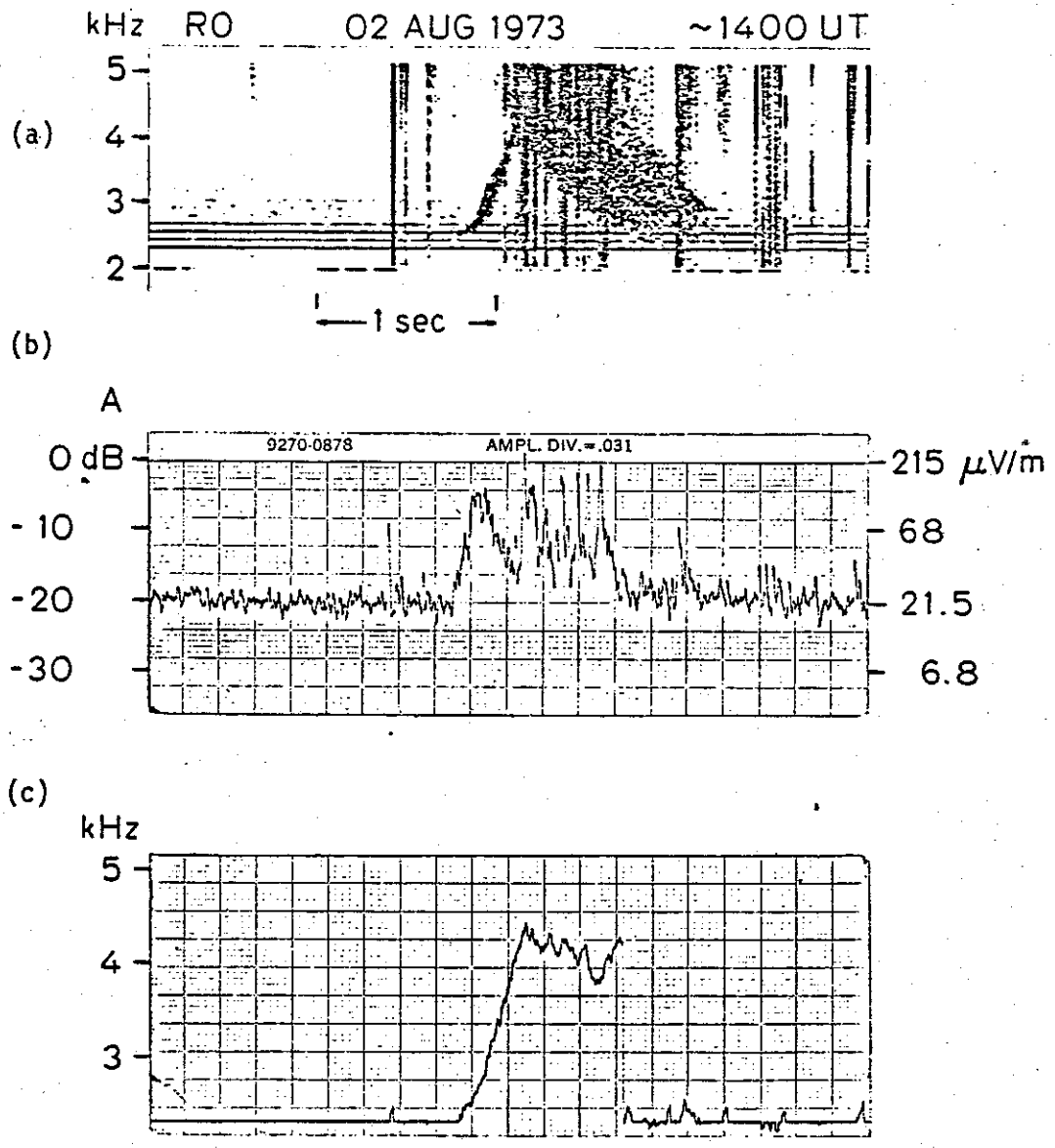

FIGURE 7.2 EXPANDED SPECTROGRAM OF THE PRECURSOR AT 1400 UT FROM FIGURE 7.1. (b) shows the corresponding amplitude variation in a 300 Hz bandwidth, and (c) indicates the rate of frequency change of the frequency-tracking filter used.

These particular data were analyzed by Park and Helliwell [1977], and it was found that the precursors were triggered only by the whistlers propagating in one particular duct, and that the precursors themselves propagated in the same duct. The duct parameters were L = 3.6 and equatorial electron density n_{eq} = 440 el/cc. The center of the plasmapause was located at about L = 4.2 where the equatorial electron density dropped by factor of ten. Figure 7.2 shows an expanded frequency-time spectrogram of the precursor at 1400:03 UT, along with amplitude and frequency changes measured using a frequency-tracking filter. The growth rate deduced from that figure is about 105 dB/sec, and the rate of frequency change is about 6.5 kHz/sec.

Park and Helliwell [1977] have reviewed different proposed generating mechanisms for precursors, including the hybrid mechanism suggested by Helliwell [1965] and Dowden [1972]. This is based on the presence of hybrid whistlers, which first propagate in the earth-ionosphere waveguide to the conjugate hemisphere and than return through the magnetosphere and trigger precursor emissions. Other mechanisms include one proposed by Reeve and Rycroft [1976] in which the nonducted whistler is reflected in the conjugate hemisphere at the lower hybrid resonance (LHR) frequency, and is then deflected by the plasmapause such that it enters the duct near the equator, triggers the precursor through the gyroresonance, and then leaves the duct. A third mechanism involving a nonlinear multiple wave interaction known as parametric decay has been suggested by Reeve and Boswell [1976].

Considering various precursor mechanisms for the Aug. 2, 1973 case, the hybrid-whistler hypothesis can be immediately excluded because

there was no evidence of hybrid whistlers. The mechanism suggested by Reeve and Rycroft [1976] requires special propagation conditions which are difficult to apply to multi-component precursors with a wide range of starting frequencies (~1 kHz for the example shown in Figure 7.1f). Furthermore, the L-shell values of the duct and the plasmapause differed by more than the 0.15 required by their model. Finally, the parametric decay mechanism cannot explain the multicomponent precursors; hence Park and Helliwell [1977] have suggested a new mechanism.

The new mechanism is illustrated in Figure 7.3 and its time sequence is described below:

a) A lightning impulse in the northern hemisphere produces a whistler propagating toward the equator.

b) The whistler wave train signal and the energetic electrons streaming toward the equator interact with one another through the longitudinal resonance process.

c) Due to the longitudinal interaction, electrons become space bunched, which then temporarily increases the electron flux within a certain range of parallel velocities.

d) This enhanced electron flux reaches the equator while the whistler signal that caused the bunching continues to travel toward the southern hemisphere.

f) After crossing the equator the enhanced electron flux interacts with northward traveling power line harmonic (PLH) waves through the gyroresonance process. The enhancement of the electron flux is sufficient to lower the threshold of this interaction below the level required for triggering of an emission by one or more lines of PLH

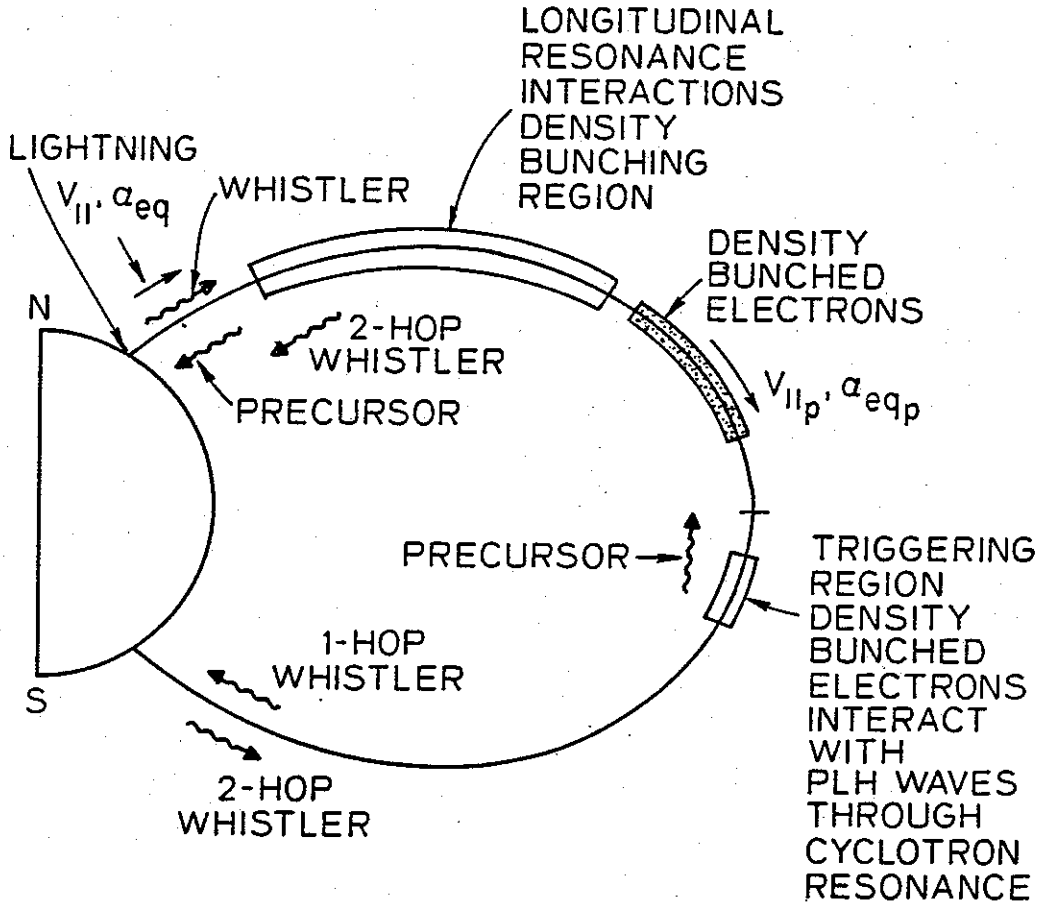

FIGURE 7.3 SCHEMATIC ILLUSTRATION OF THE WHISTLER PRECURSOR GENERATION MECHANISM. See the text for details.

waves. These emissions travel toward the northern hemisphere.

g) While the triggered emission (precursor) travels toward the northern hemisphere, the one-hop whistler reaches the conjugate point in the southern hemisphere, where it is reflected. It then travels back to the northern hemisphere.

h) The precursor reaches the northern hemisphere followed by a two-hop whistler, resulting in a frequency-time spectrograms similar to those depicted in Fig. 7.1.

The detailed timing of this process was worked out by Park and Helliwell [1977] and it was shown that this mechanism can explain different properties of the Aug.2, 1973 precursors such as variable starting frequency, multicomponent emissions and variable starting time. However, there are some special requirements that have to be met in order for this mechanism to work. First, the enhancement of the electron flux achieved through longitudinal resonance must be large enough and should last about 200 ms, so as to provide both the threshold for triggering through gyroresonance as well as the temporal growth time required for emission generation. Second, the PLH waves (which obviously must be present for this mechanism to work) must have amplitudes such that they approach the triggering threshold level.

PLH activity appeared from time to time in the August 2, 1973 case; during some intervals it dominated the VLF spectrum. Park and Helliwell [1977] found that the PLH propagated in the same duct with the precursor; this suggests that PLH waves were present at the time of the precursor observations and, when not detected, were probably close to the threshold for triggering emissions through cyclotron resonance.

As already stated the gyroresonance triggering mechanism will work only if the electron density perturbations achieved through the longitudinal resonance result in an electron flux increase which lasts at least ~200 ms. The 200 msec requirement is associated with a typical temporal growth time [Stiles and Helliwell, 1977], i.e. a typical delay from onset of temporal growth to emission triggering. This flux increase can be achieved, in principle, through electron bunching. We have shown in Chapter V that the longitudinal resonance interaction results in significant space bunching, which in our particular case of a monochromatic signal was about 180%, i.e. the electron density was enhanced roughly by factor of two at $v_{\parallel} = v_{p_{\parallel}}$, with the density enhancement decreasing for other parallel velocities.

However, in order to explain multi-component precursors it is necessary to increase the electron flux over a relatively wide range of parallel velocities. At each velocity the flux increase should last for about 200 msec. To illustrate this process we consider a multi-component precursor consisting of two emissions with starting frequencies f_1 = 2 kHz and f_2 = 3 kHz, and assume that those emissions are triggered at the equator, although the triggering location must be slightly off the equator to account for the rising frequency-time characteristics. From the gyroresonance condition at the equator $f(1+ v_{\parallel eq}/v_{p_{\parallel}eq}) = f_H$ the parallel velocities at which the flux must be increased are $v_{\parallel eq1}$ = 76.6 10^6 m/s and $v_{\parallel eq2}$ = 57.1 10^6 m/s, where we used f_{Heq}= 18.7 kHz and f_{peq} = 188.8 kHz. Thus the whistler interacting with the energetic electrons must be able to produce an increased flux at those two velocities for 200 msec. We also recall from Chapter III

that the parallel velocities $v_{\parallel 1}$ and $v_{\parallel 2}$ vary along the field line as indicated in Fig. 3.11, and that the electrons with higher pitch angles mirror closer to the equator.

Next we recall that the longitudinal resonance condition is given as $v_\parallel = v_{p_\parallel} = c\, f^{1/2}(f_H - f)^{1/2}/f_p$, which yields the resonance frequency $f = 1/2 \left(f_H \pm [f_H^2 - 4(v_\parallel f_p/c)^2]^{1/2}\right)$ (the plus sign gives $f > f_H/2$, where the waves become unducted, so we can disregard that solution). The resonance frequency changes as we change the parallel velocity. For example, if we consider electrons with $v_{\parallel eq_1}$ and $v_{\parallel eq_2}$ and assume $\alpha = 10^\circ$, their parallel velocities at 50° latitude are $v_{\parallel 1} = 0.30\ v_{\parallel eq_1} = 22.9\ 10^6$ m/s and $v_{\parallel 2} = 0.30\ v_{\parallel eq_2} = 17.1\ 10^6$ m/s, and the corresponding resonant frequencies are $f_1 = 2.65$ kHz and $f_2 = 2$ kHz. Thus a whistler train of appropriate frequency range can interact with electrons with different parallel velocities, such that when those velocities are mapped back to the equator they satisfy the gyroresonance condition at different frequencies. If the perturbations of the electron flux at those different velocities are large enough and last long enough (~200 msec), they could result in emission triggering at those frequencies. This would then provide a basis for explaining the generation of multi-emission precursors.

We want first to illustrate that the flux perturbation at a given parallel velocity (actually in a narrow range of about 1% around that velocity) can last longer than 200 msec. In order to do that we recall the results for the interaction with a spatial pulse from Chapter V. From Figs. 5.17, 5.18, 5.19, and 5.20 we see that a 1000-km-long spatial pulse can trap electrons in a narrow band of velocities ($\simeq 2\%$),

and that those electrons beside being trapped, i.e. space bunched, undergo pitch angle scattering on the order of a few tenths of a degree. Although this spatial pulse is stationary and monochromatic, the results from that analysis can be related to the whistler train if we consider the whistler train to be composed of segments of approximately constant frequency. We consider one of those segments with frequency f = 2 kHz; the group velocity of that segment at 50° latitude (L = 3.6) is about 30 10^6 m/s , and if it interacts with electrons for about 2000 km (this is comparable to the length of the spatial pulse considered in Chapter V) the total interaction time is about 70 msec. On the other hand, as long as an electron is trapped it does not matter if the trapping signal is a stationary amplitude pulse (not moving along the field line) or a moving segment of a whistler. If the length of the interaction region in the two cases is comparable, the trapping and scattering effects should also be comparable.

This segment of the whistler is therefore capable of increasing the flux in a narrow band of parallel velocities, but this increased flux should last at least 200 msec at the equator in order to provide the basis for emission triggering. The total duration of the flux perturbation depends on the latitude at which the resonance takes place, and on the pitch angle of the electrons involved. For example, if we want the triggered emission to start at 3 kHz it is necessary to increase the electron flux in a narrow band of velocities around $v_{\parallel} = v_{\parallel eq_2}$, as noted above. However, electrons with $v_{\parallel} = v_{\parallel eq_2}$ will have different pitch angles at the equator, and will thus mirror at different latitudes (see Fig. 3.10). For $\alpha = 10°$ the mirror point is at 53°

latitude, while for $\alpha = 50^\circ$ the mirror point is at 20° latitude. Thus our whistler segment at 2 kHz, as it travels toward the equator (from higher latitudes toward lower latitudes), first encounters electrons with $\alpha = 10^\circ$ at about 50° latitude (the time of this encounter is the reference time $t = 0$). As noted earlier, if the interaction lasts for about 70 msec, it should be sufficiently long time to bunch the electrons. During those 70 msec both wave and electrons move from about 50° to about 48° latitude. After the interaction is over it takes about 0.43 sec for the bunched electrons to reach the equator, or essentially the travel time from 48° latitude to the equator. When the electrons arrive at the equator they have $v_\parallel = v_{\parallel eq2}$ (we have neglected the parallel velocity changes due to the interaction, as it is assumed that the scattering is small). Furthermore, as our whistler segment gets closer to the equator it interacts with electrons with progressively higher pitch angles. The arrival time at the equator for those electrons with higher pitch angles can be calculated using the above described method. For $\alpha = 50^\circ$ the interaction occurs at 20° latitude, and those electrons arrive at the equator at $t \simeq 0.69$ sec (0.5 sec for whistler travel time from 50° to 20° latitude, ~0.1 sec for the interaction, and 0.18 for particle transit from 20° to the equator). Thus the perturbation at the equator would last about $t = 0.69 - 0.43 = 0.26$ sec, which is sufficient for the development of emission triggering. Computations for the whistler segment with $f = 2.65$ kHz indicate that the corresponding flux perturbation lasts about 210 msec. Therefore it is found that the electron flux perturbation may last long enough and may cover a sufficiently wide range of parallel frequencies.

Note that similar computations were done by Park and Helliwell [1977], but without consideration of the interaction time.

As noted earlier in Chapter V, this perturbation (space bunching) is associated with an amplitude threshold of the waves driving the longitudinal resonance. This suggests that one could measure the amplitudes (on the ground) of whistlers with and without precursors, and therefore test for the presence of the threshold. Such amplitude measurements were made on one-hop whistlers recorded at Siple, Antarctica, and propagating at L = 3.6 on August 2, 1973. The data were taken at two frequencies, 4000 Hz and 4600 Hz, using a bandpass filter with Δf = 300 Hz. This provided the temporal resolution needed to distinguish a particular whistler component connected with precursor generation from other multipath components. The results of those measurements are shown in Figure 7.4 as amplitude vs. time diagrams. The whistlers without precursors are indicated by crosses, the whistlers with single emission precursors are indicated by circles, and the whistlers with multicomponent precursors are indicated by squares, where the numbers above the squares represent the number of individual emissions forming a single precursor event.

Figure 7.4 shows that the amplitudes of the one-hop whistlers decreased, on average, from -15 dB (0 dB level corresponds to 100 μV/m) to about -22 dB for f = 4600 Hz. For f = 4000 Hz the average amplitude decreased from -13 dB to about -17 dB in the same period of time between 1335 UT and 1415 UT. This overall decrease of the whistler amplitudes is most likely a result of increased absorption in the ionosphere because of transition from nighttime to daytime conditions (sunrise time

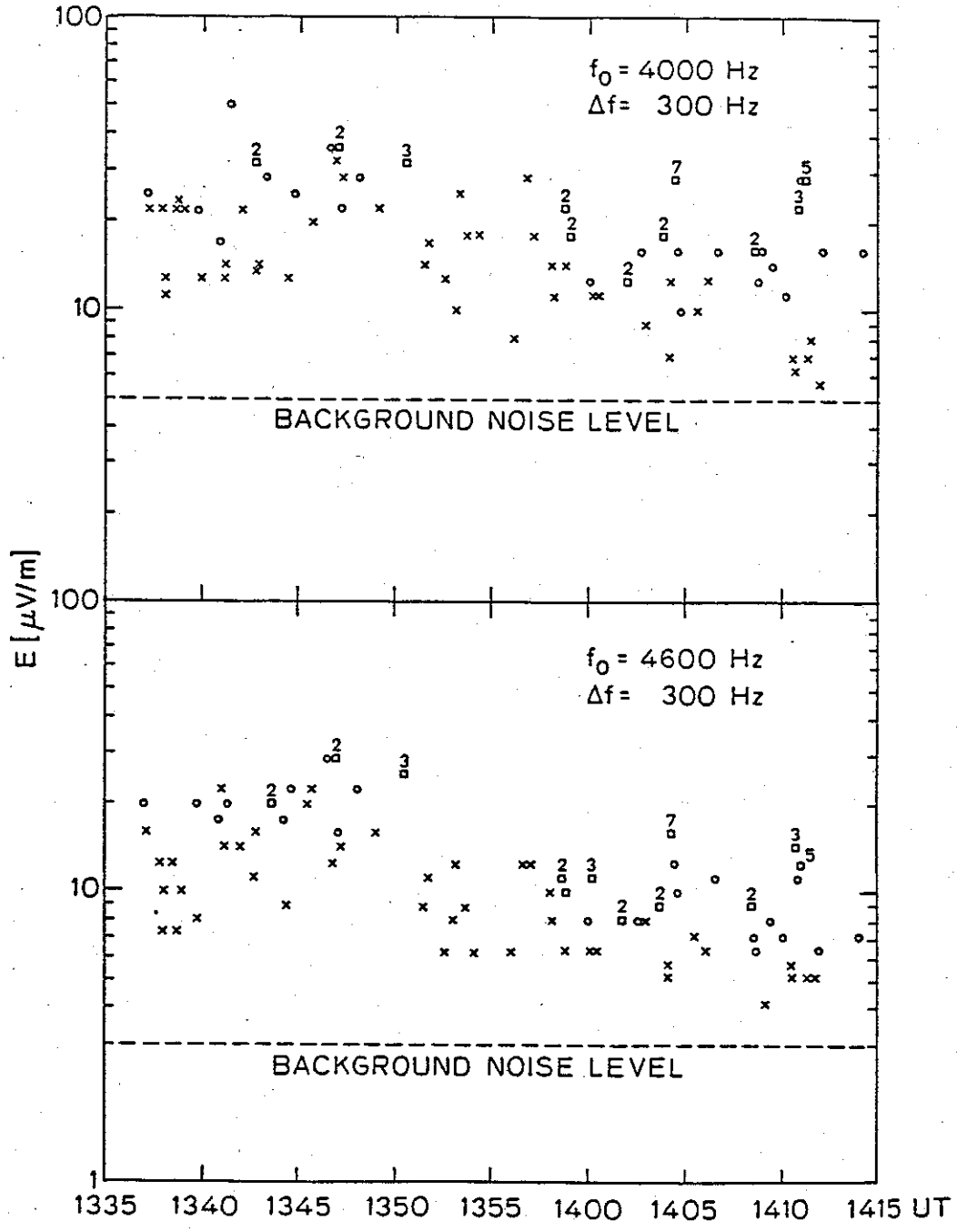

FIGURE 7.4 AMPLITUDE OF WHISTLER COMPONENTS ASSOCIATED WITH THE PRECURSOR ACTIVITY OF AUGUST 2, 1973. For symbol explanation see the text.

was around 1400 UT). Helliwell [1965] has shown that there is a significant increase in the ionospheric absorption at VLF for the night-day transition, and that the amount of the absorption increases rapidly with increasing frequency. This prediction is consistent with the above observations; the amplitude level at 4000 Hz drops about 4 dB, whereas the amplitude level at 4600 Hz drops about 7 dB. If we further assume that the maximum ionospheric absorption occurs in the D region at about 100 km altitude [Helliwell, 1965] it is possible to estimate the duct exit point using the path L value as one coordinate and sunrise time at 100 km altitude as the second coordinate. From Fig. 7.4 we see that the amplitudes of the whistlers start to decrease around 1355 UT which is then assumed to indicate the beginning of sunrise effects. On the other hand calculations show that for sunrise times of 1355 UT and 1405 UT at 100 km altitude, the terminator reaches the latitudes of 71°S and 72°S, respectively. This period of time (1355-1405 UT) is the time when the whistler amplitudes are rapidly decreasing (Fig. 7.4), suggesting that the latitude of the whistler duct exit point was between 71°S and 72°S. Because the whistler duct was on L = 3.6, we can find where this line intercepts the above latitudes; the result is shown in Figure 7.5. The estimated location of the duct exit point lies in the north-west direction from Siple Station, at a distance of about 490 km for 71°S latitude, and about 830 km for 72°S latitude.

A more important feature of Fig. 7.4 is the presence of a threshold level that a whistler amplitude must exceed in order to trigger a precursor. This amplitude threshold is most clearly seen between 1335 and 1350 UT. As found earlier in Chapter V, such behavior

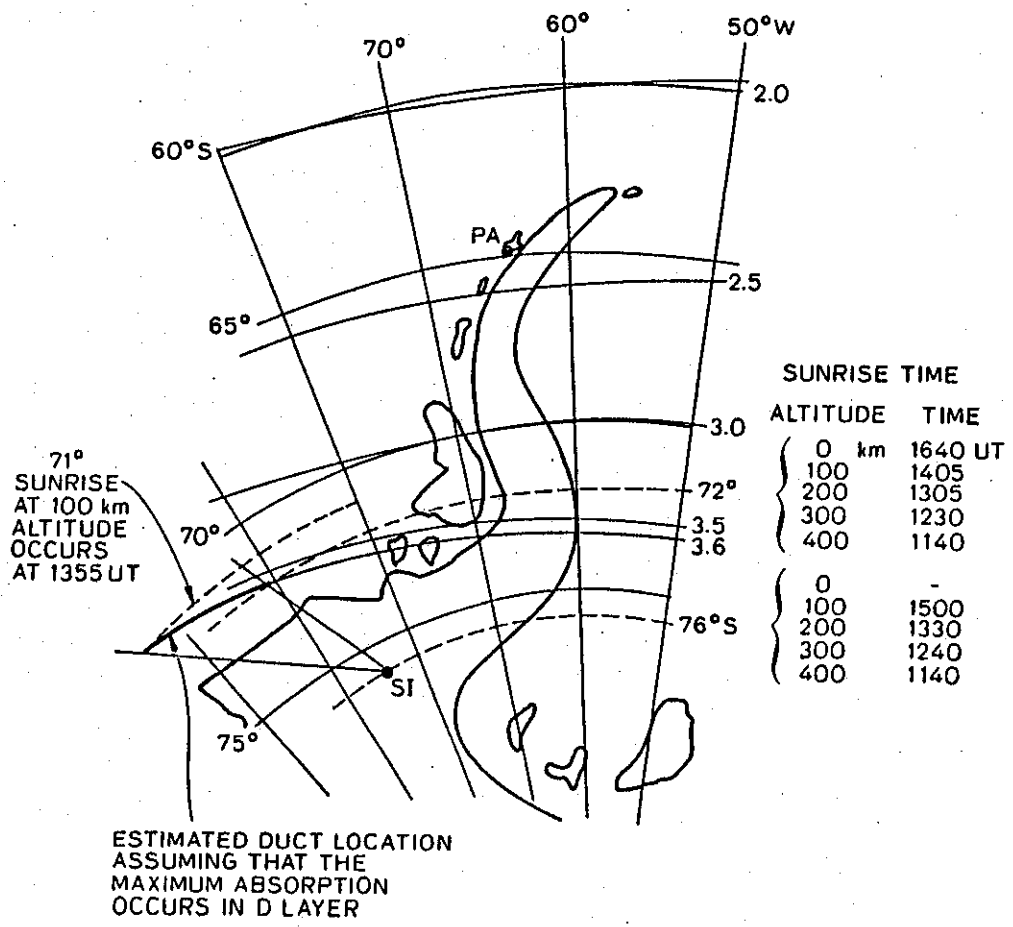

FIGURE 7.5 ESTIMATED LOCATION OF THE WHISTLER DUCT EXIT POINT FOR THE PRECURSOR EVENTS OF AUGUST 2, 1973.

is one of the characteristics of the longitudinal resonance interaction, which then supports the precursor generation mechanism suggested by Park and Helliwell [1977]. We note that the apparent gap in the precursor activity between 1350 and 1400 UT is artificial. At least five precursor events were observed at Roberval, but it was not possible to measure the corresponding amplitudes of the one-hop whistlers due to the operation of a VLF transmitter at Siple (receiver preamplifier muted).

In the next period of time, between 1400 and 1415 UT, the precursor activity still exhibited a threshold, although not as clearly as before. The presence of many multicomponent precursors indicates favorable triggering conditions for the gyroresonance interaction between electrons and PLH waves. This is supported by the level of spontaneous magnetospheric emissions, which increased sharply around 1400 UT, and strong PLR (power line radiation) which was observed for a period of a few minutes.

The data show that the precursor generation was associated with an amplitude threshold in the driving whistler, but the model suggested by Park and Helliwell [1977] also requires that the space bunching produced by the one-hop whistler be sufficient for triggering emissions. As it was found earlier, the space bunching process can roughly double the electron density (flux). According to Helliwell and Inan [1982] who proposed a feedback model to explain VLF growth and discrete emission triggering in the magnetosphere (through gyroresonance), a doubling of the electron flux is usually sufficient to result in the triggering of emissions. In their model the loop gain G is directly proportional to the electron flux. For $G<1$ the system acts like an amplifier, while for

G>1 the system becomes unstable and can generate emissions. Therefore, a doubling of the flux could easily boost the loop gain G to a value larger than unity and thus result in triggering.

Thus the precursor generating mechanism suggested by Park and Helliwell [1977] appears to be supported by the results found for the longitudinal resonance, including both the amplitude threshold and the level of the density bunching.

In the next section we discuss some other aspects of the longitudinal resonance interaction that may be important in other magnetospheric processes.

B. VLF HISS

One of many magnetospheric processes for which the generating mechanism is not certain is VLF hiss, most often observed on the ground as relatively broad band (several kilohertz) noise. VLF hiss often shows no discrete structure, having the appearance on a spectrogram of band-limited white noise. This type of spectrum is characteristic of auroral and plasmaspheric hiss, whereas mid-latitude hiss usually shows some kind of discrete structure. Therefore, the hiss generating mechanism must be such that it can explain the generation of relatively wideband signals, and also account for the observed amplitudes of such signals.

An electron propagating in a dielectric medium does not radiate as long as its velocity remains less than the phase velocity in that

medium; if the electron velocity is larger than the phase velocity we have a case of Cerenkov radiation. The two situation are depicted in Figure 7.6, and we note that the electron radiates at only one angle when $v_{\parallel} > c/\sqrt{\varepsilon_r}$. However, in the case of a dispersive medium different frequencies are radiated in different directions, as shown in Figure 7.7. In the magnetosphere the radiated frequencies are within the VLF range. Thus if the amplitude of the Cerenkov radiation is large enough it could account for the hiss generation. It should be noted that the condition for Cerenkov radiation is exactly the same as the condition for longitudinal resonance, i.e. the electron velocity must match the phase velocity (in the direction of electron travel) in a particular medium.

In the magnetospheric case it can be shown that there are in general two Cerenkov frequencies radiated at each angle, and that the radiation condition is not met when the parallel velocity exceeds the critical velocity $v_{\parallel_c}$ [Brice, 1964]. The critical velocity corresponds to propagation in the Gendrin mode, which was defined in Section III.B. As noted earlier, the broadband nature of Cerenkov radiation makes it interesting as a possible source of VLF hiss, and it was considered by many authors [Ellis, 1959,1960; Dowden, 1960; McKenzie, 1963; Liemohn, 1965; Mansfield, 1967; Seshadri,1967; Jorgenson, 1968; Lim and Laaspere, 1972; Taylor and Shawhan, 1974]. However, all of the power density calculations fell short of explaining the observed power density of VLF hiss, indicating that incoherent Cerenkov radiation is not sufficiently strong to account for VLF hiss. For this reason other mechanisms were suggested which are still based on the Cerenkov radiation, but in which

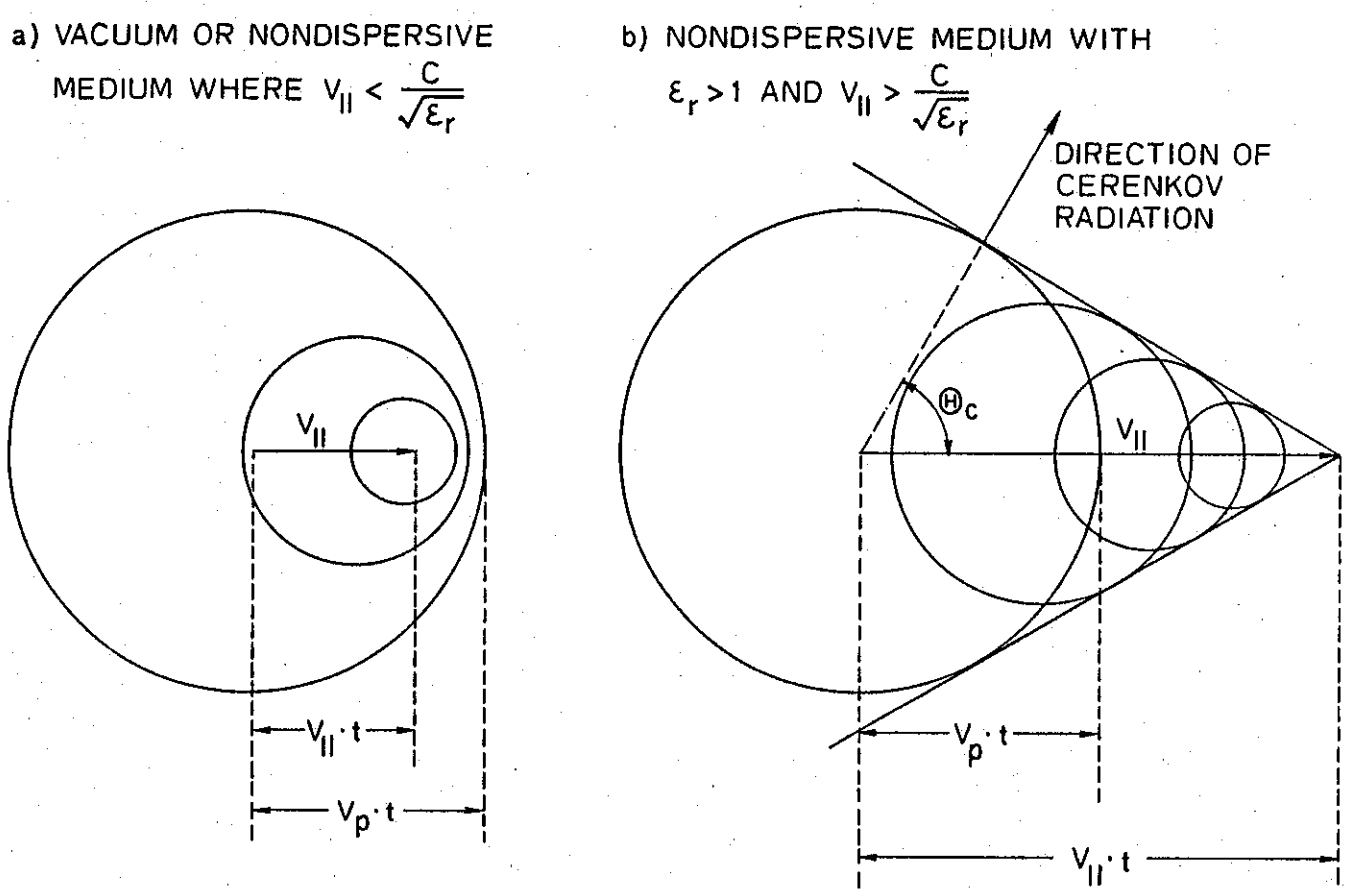

FIGURE 7.6 CERENKOV RADIATION CONDITIONS IN A NONDISPERSIVE MEDIUM. (a) $v_{II} < c/\sqrt{\varepsilon_r}$ and (b) $v_{II} > c/\sqrt{\varepsilon_r}$

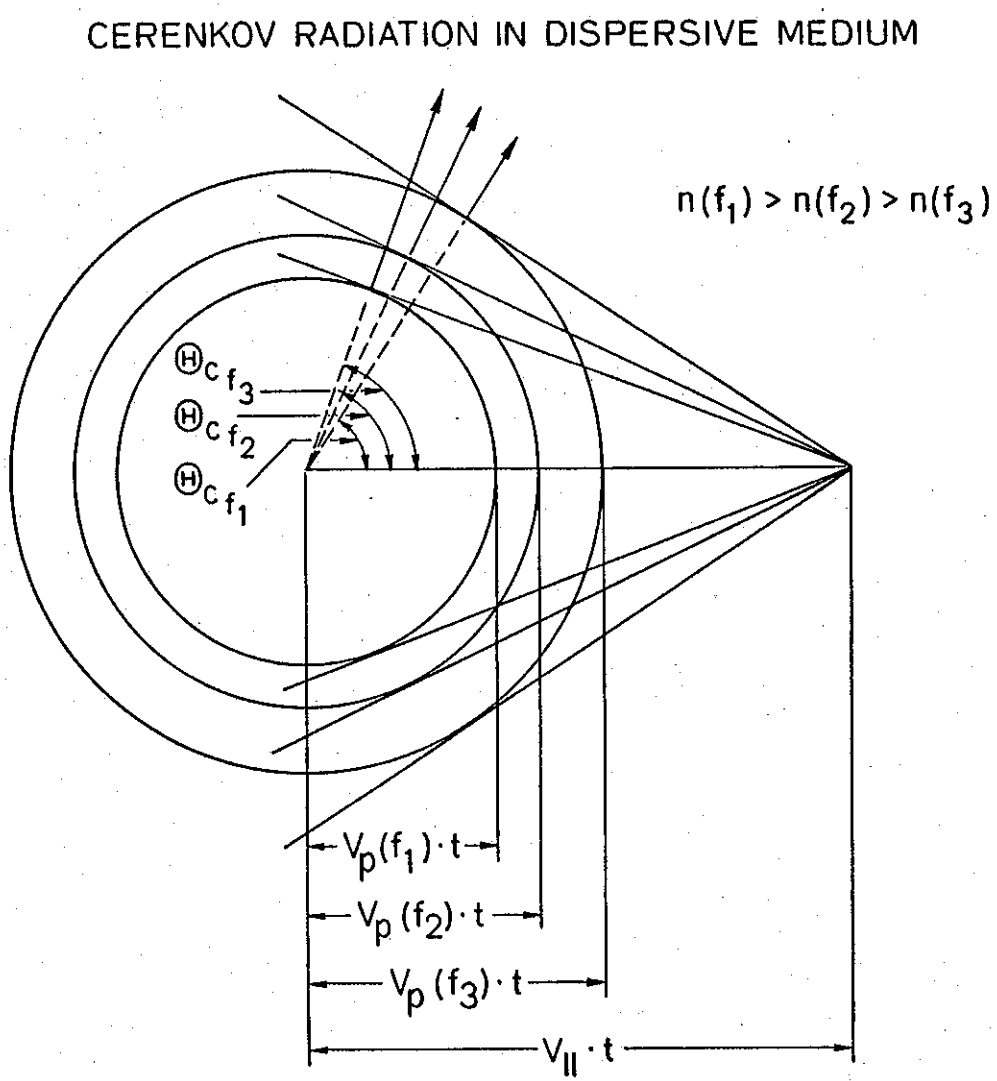

FIGURE 7.7 CERENKOV RADIATION IN A DISPERSIVE MEDIUM. In this case different frequencies are radiated at different angles.

radiation is either coherent [Taylor and Shawhan, 1974], or amplified through interaction with an electron beam [Swift and Kan, 1975; Maggs, 1976]. In the case of the coherent radiation it is assumed that the radiation from n electrons is in phase, resulting in $P = n^2 P$, where P is the power radiated by each electron. On the other hand, if all n electrons radiate incoherently (random phase) the total radiated power is given by $P = nP$.

Due to the n^2 dependence, a relatively small number of electrons radiating coherently could produce power levels which are in agreement with the measurements. Thus the problem is to identify a process that could result in electron bunching such that the bunch dimensions are much less than a wavelength (smaller dimensions mean greater coherence). As already shown, the longitudinal resonance interactions may produce such bunches of electrons, and it may be speculated that the radiation coherence needed to explain VLF hiss is created in the following way: (i) first a strong signal bunches a significant number of electrons (stronger waves would produce better coherence), and (ii) the bunched electrons become detached from the bunching wave. The detachment may be due to difference in phase and group velocity, as is the case for the whistler mode where the phase and the group velocity are always different (except for $f = f_H/2$). For example, consider a pulse with $f < f_H/2$ so that $v_g > v_{p_\parallel}$. Electrons trapped by this pulse will have $v_\parallel \simeq v_{p_\parallel}$, but because the wave energy propagates with $v_g > v_\parallel$, those electrons slide backwards through the pulse, and eventually emerge from the tail end of the wave packet. Such a blob of electrons could radiate coherent Cerenkov radiation.

However, it remains to be seen how long this blob of electrons remains bunched, because it may contain electrons with different pitch angles and different parallel velocities. For the moment let us assume that all electrons have the same parallel velocity, but different pitch angles which means that they have different variations of parallel velocity as required by their adiabatic motion. Thus, for a given spread in pitch angle it may be determined how long it takes the separation between the low and high pitch angle electrons to become larger than the wavelength, which than destroys the radiation coherence. The sample calculations have shown that the coherence time for a given initial spread in pitch angles depends strongly on the latitude where the electrons become detached from the bunching wave, i.e. on the latitude at which their motion begins to be entirely governed by the static magnetic field. For example, assuming the initial range of pitch angles to be from $\alpha = 10^\circ$ to $\alpha = 20^\circ$, and detachment at 20° latitude (electrons are moving toward the equator), it takes only about 1 msec before the separation between 10° and 20° electrons becomes larger than one wavelength. On the other hand, if the detachment occurs at 1° latitude (for the same initial range of pitch angles) it takes about 0.2 sec for the same process to occur. Note that after 0.2 sec the electrons reach 4° latitude, but on the other side of the equator.

A blob of electrons created through the longitudinal resonance interaction and with a spread in pitch angle only could radiate coherently for a substantial period of time (few tenths of second). However, the electrons within a blob have slightly different parallel velocities, e.g. a typical spread in parallel velocity is about 400

km/sec (Figs. 5.10 and 5.15). Thus it will take only about t = 2/400 = 5 msec for those electrons to become separated more than a wavelength at the equator, assuming the wavelength to be 2 km at the equator. From this result it is evident that spreading due to the finite range of parallel velocities occurs much faster than the spreading due to a finite range of pitch angles, and that the life time of the blob is about one hundredth of a second. We also note that the blob of electrons could further be dispersed due to interaction with other waves.

Thus it is possible that the short life time during which the blob can radiate coherently, together with the fact that there may not be many electrons within a single blob, makes the radiated power level insufficient to account for the observations. However, there could be more than one blob formed through the above described process, which could further enhance the radiation (as long as the radiation from different blobs does not interfere). Even stronger radiation effects could probably be achieved if the velocity of the electron blob equals the critical velocity, because in that case all radiated frequencies satisfy the Gendrin condition given in Chapter II. The enhancement of radiation is expected because for the Gendrin mode the ray direction is field aligned for all radiated frequencies, and the group velocity is independent of the wave frequency so that wave packets radiated at different frequencies travel together [Helliwell, private communication].

Another explanation for VLF hiss generation is based on amplification of incoherent Cerenkov radiation through the wave-beam interaction where the beam provides for the 'bump-on-tail' distribution.

As mentioned earlier, a distribution function which has a positive slope, as is the case for the bump-on-tail distribution, may result in Landau growth.

C. COMMENTS ON THE INTERNAL FIELDS OF THE BUNCH

At this point we should note that space bunching always gives rise to an internal electric field through the Poisson equation. This electric field will then act to debunch the electrons, as it opposes the wave bunching field. Although this effect can be neglected in test particle simulations where the number of electrons is small, it may become important depending on the actual flux of particles. We have shown that significant bunching occurs for a parallel electric field around 50 μV/m and higher, so that we choose 5 μV/m as the limit for the internal field, i.e. we assume that internal fields up to 5 μV/m do not significantly affect the bunching process. Using the 5 μV/m field we can find an electron density N that is needed to produce that field. In Chapter IV we showed how the twelve test electrons are uniformly distributed in phase before the interaction, and in Chapter V (Fig. 5.15) we showed that the same electrons are compressed in phase space, i.e. space bunched. The typical compression is about 90° in phase, or 500 m assuming λ = 2 km.

At the same time each single test electron actually represents a large number of electrons in the real distribution, i.e. each test electron represents a sheet of electrons. Thus the question is, if we

have twelve initially equidistant sheets of electrons, and we displace those sheets so that the total displacement is 500 m, what is the maximum electron density for which the internal field (due to the compression of the sheets) does not exceed 5 μV/m? It turns out that this computation is rather simple, and the electron density is given as [Buneman, 1980]

$$N = -\frac{\varepsilon_o E}{e\,\Delta s} \qquad (7.1)$$

where E is our maximum allowable internal field (negative), and Δs the total displacement of the sheets. Using E = 5 μV/m, Δs = 500 m, and $\varepsilon_o = 8.854\ 10^{-12}$ we find N = 0.55 el/m^3 which is the maximum allowable density, i.e. densities larger than this produce internal fields stronger than 5 μV/m, which can reduce the bunching effects. When the density of the electrons is known we can relate it to the electron flux as discussed below.

It was shown that trapping occurs in a narrow range of parallel velocities centered around the wave phase velocity, so we use 1% as a typical value. The next step is to compute the actual number of electrons in that velocity range, and then to compare with the previously computed N = 0.55 el/m^3 . The electrons are assumed to have an initial energy of 300 eV and $\alpha = 10^o$, so that the corresponding parallel velocity is $v_{\parallel} = 9.654\ 10^6$ m/s. In that case the total number of electrons, within 1% velocity range around $v_{\parallel}$, is given as (assuming an isotropic distribution in pitch angle)

$$N = 2\pi \int_0^{\pi} \int_{v_1}^{v_2} \frac{A}{v^n} v^2 \sin\alpha \; dv \; d\alpha \qquad (7.2)$$

where A is a constant that can be deduced from the flux. It can be shown [Inan, 1977] that for E = 1keV and $\alpha = 90°$, $A = 2\phi$, where ϕ is the differential energy spectrum for 1 keV electrons with $\alpha = 90°$. Note that this relationship between ϕ and A holds only for a v^{-4} distribution, and it is necessary to use a different relation for other distributions. Thus, substituting for A in Eq. 7.2, and integrating we have ($n \neq 3$)

$$N = 4\pi A \left(- \frac{v^{-n+2+1}}{n-2-1} \right) \Bigg|_{v_1}^{v_2} \qquad (7.3)$$

whereas for n = 3 we have

$$N = 4\pi A \ln v \Big|_{v_1}^{v_2} \qquad (7.3a)$$

and Table 7.1 shows the results for various values of the differential flux ϕ (1 keV, $\alpha = 90°$) and various values of n (the constant A is given as $\frac{m^2}{2}\left[\frac{2}{m}\right]^{n/2}\phi$ where m is the electron mass).

Thus, from Table 7.1 we can find the values of n and ϕ for which the electron density is lower than 0.55 el/m^3, i.e. we see when it is possible to have bunching without creating a strong internal electric field which may significantly decrease the bunching effects. Also note that only the trapped electrons contribute to the internal field.

Flux (el $cm^{-2} sr^{-1} s^{-1}$ kev)	n	A	N (el/m^3)
10^8	3	$1.3\ 10^{-7}$	$1.3\ 10^{-3}$
10^8	4	$2\ 10^8$	21658
10^8	5	$2.9\ 10^{23}$	$3.1\ 10^5$
10^8	6	$4.4\ 10^{38}$	$6.8\ 10^{10}$
10^4	3	$1.3\ 10^{-11}$	$1.3\ 10^{-7}$
10^4	4	$2\ 10^4$	2.17
10^4	5	$2.9\ 10^{19}$	31
10^4	6	$4.4\ 10^{34}$	$6.7\ 10^6$
10^2	3	$1.3\ 10^{-13}$	$1.3\ 10^{-9}$
10^2	4	$2\ 10^2$	0.02
10^2	5	$2.9\ 10^{17}$	0.31
10^2	6	$4.4\ 10^{32}$	$6.7\ 10^4$

TABLE 7.1 Total number of electrons within 1% velocity bandwidth for 300 eV electrons as a function of flux and various distribution functions.

Because most of the flux measurements are made at higher energies the exact fluxes and distributions at lower energies are uncertain, but as those data become available Table 7.1 can be used as a guide to determine if the bunching of the electrons is affected by the internal fields. Present measurements indicate that the flux can be on the order of 10^3 to 10^9 , and the exponent n can vary between 3 and 5 [Kimura, 1982; Shield and Frank, 1970].

We have presented two examples in which longitudinal resonance

interactions may play an important role, along with an analysis of the limiting electron flux for the bunching. We conclude our discussion with a summary and suggestions for future work.

VIII. CONCLUSION AND SUGGESTIONS FOR FUTURE WORK

A. SUMMARY

We have analyzed the nonlinear longitudinal resonance interactions between energetic electrons and coherent VLF waves in the magnetosphere. The longitudinal resonance, which may result either in wave growth or wave damping, and also causes space bunching of energetic electrons, was numerically simulated using time averaged nonlinear equations of motion. The simulations were done for single electrons, sheets of electrons, and a full distribution of electrons. Those studies, done for different types of wave functions, have shown how the the wave forces modify the electron trajectories, and that the trajectory perturbations result in nonlinear pitch angle scattering. The nonlinear pitch angle scattering variations have been studied for a wide range of the initial pitch angles, wave amplitudes, cold plasma densities and wave normal angles. It was found that there are two basic groups of electrons, trapped and untrapped, where the trapped electrons, in contrast to the untrapped electrons, are trapped in the potential well formed by the wave. The trapped electrons cause the space bunching which increases the electron flux at certain parallel velocities.

The nonlinear scattering for the longitudinal resonance is found to be much smaller compared to that for the gyroresonance interactions, indicating a higher efficiency for the gyroresonance process. This is

so because the scattering for gyroresonance is achieved through the conversion of perpendicular momentum of the electron into parallel momentum with very small energy exchange between the wave and electrons, while the scattering for the longitudinal resonance is solely based on the energy exchange. Due to the smaller scattering efficiency a full distribution simulation produced only small precipitated fluxes, i.e. for moderate strength VLF waves the precipitation due to the longitudinal interactions is below the detectable level of about 0.01 ergs/cm^2/sec.

In a study of magnetopsheric applications we found support for a mechanism proposed by Park and Helliwell [1977] to explain whistler precursors. We conclude that the longitudinal resonance is a likely candidate to drive a process in which a whistler wave perturbs the particles along a field line through longitudinal resonant bunching. This bunching has the effect of creating an enhancement, near the equator, of particle flux in a particular parallel velocity range. The enhancement is of sufficient amplitude and duration to permit a gyroresonance interaction with wave activity such as power line harmonics. We find that the longitudinal resonance is not at first look a likely process for creating coherence in Cerenkov process of hiss generation, but that features of the longitudinal resonance may merit further study in this direction. Also presented was an analysis of the limiting electron flux for the bunching, i.e. we estimated the electron density at which the internal fields of the bunch may become large enough to affect the bunching process.

B. SUGGESTIONS FOR FUTURE WORK

In our presentation we have shown the results of computer simulation of the nonlinear longitudinal resonance interactions with constant frequency whistler mode waves in the magnetosphere. This work could be further extended as described below:

i) We have indicated in Chapter V that both the wave amplitude ($E_{\parallel}$) and the wave normal angle are treated as though they are constant quantities. It was said that this approximation will be valid as long as the interaction region is small, but there may be cases where it is necessary to include effects due to the variation of those quantities. The wave amplitude can be computed as a function of position using a standard WKB approach, while the wave normal angle variations can be calculated using a ray tracing analysis. Those additional computations could either be done separately and entered as data, or they could be added to the existing code.

ii) Another extension of the present work could deal with CW pulse signals propagating along the field line. In this case it should be realized that the wave group and parallel velocities have in general different values (except for the Gendrin mode) which poses additional problems. It can be easily visualized that an electron trapped in the wave potential well, i.e. an electron whose parallel velocity is very close to the wave phase velocity, has to slide either backward or forward through the wave packet when the group velocity is either smaller or larger than the phase velocity, respectively; for $f < f_H/2$

the whistler mode group velocity always exceeds the phase velocity. In the case of a CW pulse signal it would also be possible for electrons to enter the wave packet from both ends, depending on the ratio of their parallel velocities and the group velocity of the pulse.

From the above discussion it is obvious that this problem would require significant changes in the present program, but could also reveal some additional features of the longitudinal resonance.

iii) Another extension of the work presented here would be to investigate the longitudinal interaction for the case of variable frequency pulse signals. In this case the calculations would have to take into the account the fact that different frequencies of the signal interact with different electrons, and also at different locations along the field line. It should be feasible to investigate the behavior of whistlers interacting with energetic electrons by approximating the whistlers with an appropriate number of segments of linearly changing frequency, as was done in the discussion of the precursor.

iv) It was noted earlier that the wave amplitude may be significantly changed due to the interaction, especially in a full distribution simulation. Although in our particular case in Chapter VI it was found that the total energy exchange is small, it will change for other distribution functions. For example, if we assumed a v^{-6} instead of a v^{-4} dependence, there would be many fewer electrons at higher parallel velocities, as the weighting function would change from v^{-2} to v^{-4} (see Fig. 6.4). In this case there would be more energy transferred from the wave to the trapped electrons compared to the energy transferred from the untrapped electrons to the wave, and the final

result would be wave attenuation. Thus in cases like this it may become necessary to include an energy feedback term that accounts for the amplitude changes. However, for a single particle simulation this feedback effect is very small and can be omitted.

APPENDIX A: USEFUL IDENTITIES

Below is the list of identities used in the derivation of time averaged equations of motion, as well as the derivation of an approximation for the $\langle qv_y \mathcal{B}_x \rangle$ term for small θ.

$$\cos(\gamma - \eta\sin\phi) = \cos\gamma\cos(\eta\sin\phi) + \sin\gamma\sin(\eta\sin\phi)$$

$$\sin(\gamma - \eta\sin\phi) = \sin\gamma\cos(\eta\sin\phi) - \cos\gamma\sin(\eta\sin\phi)$$

$$\cos(\eta\sin\phi) = J_0(\eta) + 2J_2(\eta)\cos(2\phi) + 2J_4(\eta)\cos(4\phi) + \ldots$$

$$\sin(\eta\sin\phi) = 2J_1(\eta)\sin(\phi) + 2J_3(\eta)\sin(3\phi) + 2J_5(\eta)\sin(5\phi) + \ldots$$

$$\int_0^{2\pi} \cos(\gamma - \eta\sin\phi)\, d\phi = J_0(\eta)\cos\gamma$$

$$\int_0^{2\pi} \sin\phi\cos(\gamma - \eta\sin\phi)\, d\phi = J_1(\eta)\sin\gamma$$

$$\int_0^{2\pi} \cos\phi\cos(\gamma - \eta\sin\phi)\, d\phi = 0$$

$$\int_0^{2\pi} \sin(\gamma - \eta\sin\phi)\, d\phi = J_0(\eta)\sin\gamma$$

$$\int_0^{2\pi} \sin\phi\sin(\gamma - \eta\sin\phi)\, d\phi = -J_1(\eta)\cos\gamma$$

$$\int_0^{2\pi} \cos\phi\sin(\gamma - \eta\sin\phi)\, d\phi = 0$$

The $\langle qv_y \mathcal{B}_x \rangle$ term (Eq. 2.62) is given as

$$\langle qv_y \mathcal{B}_x \rangle = -qE_{\parallel} J_1(\eta) \sin\gamma \, \rho_z \frac{v_\perp k \cos\theta}{\omega}$$

For small θ $\sin\theta \simeq \theta$, $\cos\theta \simeq 1$, and $\tan\theta \simeq \theta$ so that $\eta = \frac{\omega}{\omega_H} \tan\theta \tan\alpha$, as already found in Section II.C. Furthermore, we note that

$$\frac{v_\perp k \cos\theta}{\omega} = \frac{v_\perp \frac{n\omega}{c}}{\omega} \cos\theta = \frac{v_\perp}{v_{p\parallel}} ,$$

and that near the resonance $v_{p\parallel} \simeq v_\parallel$ so that

$$\frac{v_\perp k \cos\theta}{\omega} = \frac{v_\perp}{v_{p\parallel}} = \tan\alpha .$$

Therefore, $\langle qv_y \mathcal{B}_y \rangle = -qE_{\parallel} \sin\gamma \tan\alpha \rho_z J_1(\eta)$, and for small θ

$$J_1(\eta) = \frac{\eta}{2} = \frac{\omega \theta \tan\alpha}{2\omega_H}$$

Also, for small θ, ρ_z is given as

$$\rho_z = \frac{1}{\omega/\omega_H} \frac{1 - \omega/\omega_H}{1 + \omega/\omega_H} \frac{1}{\theta} .$$

Substituting for $J_1(\eta)$ and ρ_z in the expression for $\langle qv_y \mathcal{B}_x \rangle$, the final result is

$$\langle qv_y \mathcal{B}_x \rangle \simeq -qE_{\parallel} \sin\gamma \tan^2\alpha \frac{1 - \omega/\omega_H}{2(1 + \omega/\omega_H)}$$

```
      C       ANGLES ARE IN RADIANS EXCEPT IN INPUT AND OUTPUT
              DIMENSION Z(3000),PHI(3000),BZ(3000),WN(3000),VP(3000)
              DIMENSION FDAT(20),ENDAT(10),ALPDAT(10),KTEMP(40)
              DIMENSION BESEL(2),ETA(3000),BMULT(3000)
              DIMENSION RKDZ(3000),RKDZL(3000),CTHG(3000)
              DIMENSION AMPLOW(3000),AMPLHI(3000)
              COMMON DVPA,EQALD,ALGRD,VPA,FVPA(400),SDIST,ALEQ,A,SVPA,FDIST(18
             1 0,400),EQAL,FPDIST(180),PI,EM,EL,RPHI,VPE,E,EV,KMAX,VMIN,VPMAX,
             2 ALMIN,ALMAX,ALDC(12),R,RO,VPAEQ,EPA,EVDC(12),IG,EPAG(3000)
              COMMON/BLOCK1/ KFDIST(180,400),IFDIST(180,20)
              COMMON/BLOCK2/ SFDIST(180),IIAS,IIAF,NVG,ALFALO,ALFAHI
             1 ,ALFA(35),JLO,JHI
              COMMON/BLOCK3/ TC(400,12),CARGU(400,12),VPHA(400,12)
             1 ,VPARA(400,12),ENER(850,12),PBCARGU(505,12),P3VPH(505,12),
             2 PBVPA(505,12),TMIN,TMAX,TR(12),TTRACE(12),INDEX(12),
             3 MLO,MHI,MSTEP,TEN(850),TPB(505),DISTAN(850),DISTAN1(505)
      C
      C       Z=ARC LENGTH, PHI=INVARIANT LATITUDE,
      C       BZ=(1/B)*DB/DZ, WN=WAVE NUMBER K, VP= PHASE VELOCITY
      C
      C       IREAD IN ALL NECESSARY DATA
      C
      C       CHOOSE GENDRIN MODE OR NOT (IG=1 OR IG=0)
              READ(5,350) IG
        350   FORMAT(I2)
              READ(5,350) ICONT99
              READ(5,350) ICONT88
      C
      C       COLLISIONLESS MODEL OR DIFUSSION MODEL (ICLM=1 OR ICLM=0)
      C       GET MODEL PARAMETERS TE,XIO,XIH,XIHE,ENEQ
      C
              READ(5,351) ICLM,POWER,TEMP,XIO,XIH,XIHE,ENEQ
        351   FORMAT(I2,6F10.5)
      C
      C
      C
      C
      C       THE WAVE AMPLITUDE IS DIFFERENT IN THE CASE OF GENDRIN MODE
      C       THAN IT IS IN NON-GENDRIN CASE. GENDRIN MODE WAVE INTENSITY IS
      C       BW WHILE NON-GENDRIN MODE WAVE INTENSITY IS LABELED EPA.
      C       THE PROPER SETTING OF WAVE INTENSITIES IS DONE IN FOLLOWING WAY:
      C       1) GENDRIN MODE
      C       WAVE INTENSITY IS BW=CONST*2**IBW WHERE IBWLO<IBW<IBWHI.
      C       IBWLO AND IBWHI ARE READ FROM INPUT CARD DECK. AT THE SAME TIME
      C       EPA IS NOT USED WHICH IS ACCOMPLISHED SETTING IELO=IEHI=1
      C
      C       2) NON-GENDRIN MODE
      C       WAVE INTENSITY IS EPA=CONST*2**IE WHERE IELO<IE<IEHI.
      C       AT THE SAME TIME GENDRIN MODE IS SUPPRESED USING IBWLO=IBWHI=1
      C
              READ(5,352) IBWLO,IBWHI,IELO,IEHI
        352   FORMAT(4I2)
      C
      C       FREQUENCY ITERATION
      C       ENTER THE NUMBER OF DIFFERENT WAVE FREQUENCIES AND THEY WILL BE READ
      C       FROM INPUT CARD DECK
      C
              READ(5,350) INFREQ
              DO 1013 ICNT=1,INFREQ
              READ(5,353) FDAT(ICNT)
       1013   CONTINUE
        353   FORMAT(F10.5)
      C
      C       READ L VALUE AND ANGLE BETWEEN K&B0 (THETA)
      C
              READ(5,354) EL,THETA
        354   FORMAT(2F10.5)
```

```
      C
      C       DEFINE DIRECTION OF PROPAGATION
      C       IWD=1 --> POSITIVE DIRECTION
      C       IWD=-1 --> NEGATIVE DIRECTION
      C
              READ(5,350) IWD
      C
      C       PARAMETERS ALONG FIELD LINE PRINTED IF ICONT1=1
      C
              READ(5,350) ICONT1
      C
      C       FULL DISTRIBUTION USED IF IFULL=1, ADIABATIC APPROXIMATION USED
      C       BEYOND RESONANCE POINT IF IADIA=1, DIFFUSION COEFFICIENTS
      C       COMPUTED IF IDIFF=1
      C
      C       PROGRAM CAN TRACE EITHER A SINGLE PARTICLE OR GIVEN DISTRIBUTION
      C       GIVEN BY THE DISTRIBUTION FUNCTION FDIST(VPARALEL,ALFAEQ).
      C
      C       1) SINGLE PARTICLES TRACING
      C       TO DO SINGLE PARTICLE TRACING IT IS NECCESSARY TO SPECIFY ITS
      C       PARALLEL VELOCITY AND EQUATORIAL PITCH ANGLE.
      C       THIS IS DONE DEFINING TWO PARAMETERS: IV (LOOP 206)
      C       AND IA (LOOP 204).
      C       GIVEN RANGE IV[IVS,IVF] PARTICLE VELOCITY IS GIVEN AS
      C       VPAI=VMIN*(1+(IV-1)/100)*1.05 AND PITCH ANGLE IS READ FROM
      C       INPUT CARD DECK USING IA AS POINTER WITH RANGE [IAS,IAF].
      C
      C       2) FULL DISTRIBUTION TRACING
      C       IN THE CASE OF FULL DISTRIBUTION ALL DATA CONCERNIG SINGLE PARTICLE
      C       WILL BE NEGLECTED. THE INITIAL DISTRIBUTION IS GIVEN BY THE NUMBER
      C       OF BINS IN VELOCITY AND PITCH ANGLE RANGE.
      C       NUMBER OF VELOCITY BINS IS READ AS INPUT DATA (NVG) SAME AS PITCH AN
      C       RANGE [IIAS,IIAF].
      C
              READ(5,355) IADIA,IFULL,IDIFF
        355   FORMAT(3I2)
      C
              IF(IFULL.EQ.1) GO TO 1015
              READ(5,352)IVS,IVF,IAS,IAF
              DO 1014 ICNT1=IAS,IAF
              READ(5,353) ALPDAT(ICNT1)
       1014   CONTINUE
              GO TO 1016
       1015   READ(5,341) NVG,IIAS,IIAF,VRANGE,VINITL
        341   FORMAT(3I2,2F10.5)
       1016   CONTINUE
              IF(IFULL.EQ.1) IVS=1
              IF(IFULL.EQ.1) IVF=1
              IF(IFULL.EQ.1) IAS=1
              IF(IFULL.EQ.1) IAF=1
      C
      C       PRINT PHASE ANGLE YES=1, NO=0
              READ(5,363) ICONT2,MLO,MHI,MSTEP,TMIN,TMAX
        363   FORMAT(4I2,2F10.5)
      C
      C       READ THE STARTING LATITUDE WHERE TRACING SHOULD BEGIN
      C
              READ(5,353) SRPHID
      C
      C       READ WAVE AMPLITUDE INFORMATION
              READ(5,350) IGROW
              READ(5,358) XPHIOD,XLEN,XAMPL
        358   FORMAT(3F10.6)
              READ(5,350) ICONT5
              READ(5,350) ICONT25
              READ(5,353) XMAX
              READ(5,353) VDELTA
```

```
      C
      C
      C        ITERATE FOR BW IN GENDRIN MODE. IF GM IS NOT USED SET IBW=1,1
               WRITE(6,7007) IG,ICLM,TEMP,XIO,XIH,XIHE,ENEQ
       7007    FORMAT(2I3.5F10.5)
               WRITE(6,7008) IBWLO,IBWHI,IELO,IEHI,INFREQ,FDAT(1)
       7008    FORMAT(5I3,F10.5)
               WRITE(6,7009) EL,THETA,IWD,ICONT1,IADIA,IFULL,IDIFF
       7009    FORMAT(2F10.5,5I3)
               WRITE(6,7010) IVS,IVF,IAS,IAF,ICONT2,SRPHID,ALPDAT(1)
       7010    FORMAT(5I3,2F10.5)
               DO 210 IBW=IBWLO,IBWHI
               BW=3.75E-12*2**IBW
               DO 208 IEF=1,INFREQ
               F=FDAT(IEF)
      C
      C-----------------------------------------------------------------
      C        DEFINE ALL NEEDED CONSTANTS
      C
               E=1.6021E-19
               C=2.9978E8
               PI=3.1416
               RO=6.37E6
               PHIO=ATAN(SQRT(EL-1.))
               A=3.1415927/180.
               EM=9.1066E-31
               DZ=1.E4
               R1=7.37E6
               CTH=COS(THETA*A)
               STH=SIN(THETA*A)
               OM=2.*PI*F
               BOLTZ=1.3805E-16
               EMI=9.1066E-28*1837.
               G1=9807.67*RO*RO/R1/R1
               OMS=(PI/12./3600.)**2
      C-----------------------------------------------------------------
      C
      C        TEST PROGRAM FOR FULL DISTRIBUTION
               IF(ICONT88.EQ.0) GOTO 713
               WRITE(6,3958)
       3958    FORMAT(////'TEST BESSEL FUNCTION COMPUTATIONS'//)
               ARG=0.
               CALL BESJR(ARG,1,BESEL,IER)
               WRITE(6,3956) ARG,BESEL(1),BESEL(2)
       3956    FORMAT(3F12.4)
               ARG=1.
               CALL BESJR(ARG,1,BESEL,IER)
               WRITE(6,3956) ARG,BESEL(1),BESEL(2)
        713    CONTINUE
      C
      C-----------------------------------------------------------------
      C        DENSITY MODEL DATA ARE READ FROM INPUT CARD DECK
      C        COMPUTE PF(PLASMA FREQUENCY), FH (GYROFREQ.) AND RIND(REFRACTIVE
      C        INDEX) ALONG GIVEN FIELD LINE USING QL APPROXIMATION.
      C        ALSO COMPUTE WN(WAVE NUMBER IN MAG. FIELD DIRECTION) AND VP(PHASE
      C        VELOCITY IN MAG. FIELD DIRECTION).
      C        Z(N) AND PHI(N) GIVE POSITION ALONG THE LINE.
      C        WN AND VP ARE DIFFERENT FOR GENDRIN AND NON-GENDRIN MODES.
      C
      C
               HH=BOLTZ*TEMP/EMI/G1*1.E-2
      C        SCALE HEIGHTS ARE CONVERTED TO METERS
               HHE=HH/4.
               HO=HH/16.
               GPHEQ=R1-R1*R1/RO/EL-OMS/2./G1/RO/EL*((RO*EL)**3-R1**3)
               ENFAC=XIH*EXP(-GPHEQ/HH)+XIHE*EXP(-GPHEQ/HHE)+XIO*EXP(-GPHEQ/HO)
               ENFAC=ENEQ/SQRT(ENFAC)
               N=1
```

```
      Z(N)=Ø.
      PHI(N)=Ø.
      R=RO*EL
      CDEL=1.
      BZ(N)=Ø.
      FP=SQRT(8Ø.6*ENEQ*1.E6)
      FH=8.736E5/EL**3
      RIND=FP/SQRT(F*(FH*CTH-F))
C     VP(N) IS PHASE VELOCITY IN MAG FIELD DIRECTION
C     IF GENDRIN MODE USED THAN NEXT LINES EXECUTED, OTHERWISE
C     GO TO 11
C
      IF( IG .NE. 1 ) GO TO 11
      VP(N)=C/2.*FH/FP
      CTHG(N)=2.*F/FH
      WN(N)=2.*PI*F/VP(N)/CTHG(N)
      EPAG(N)=C*BW*F/FP*SQRT(1.-4.*F*F/FH/FH)
      GO TO 12
   11 VP(N)=C/RIND/CTH
      WN(N)=RIND/C*2.*PI*F
   12 RKDZ(N)=Ø.
C
C     NEXT LOOP (LABEL 1Ø) COMPUTES ALL MEDIUM PARAMETERS ALONG GIVEN
C     FIELD LINE
C
   1Ø N=N+1
      Z(N)=Z(N-1)+DZ
      PHI(N)=PHI(N-1)+DZ*CDEL/R
      CPHI=COS(PHI(N))
      SPHI=SIN(PHI(N))
      R=RO*EL*CPHI**2
      SRF=SQRT(1.+3*SPHI**2)
      CDEL=CPHI/SRF
      SDEL=2.*SPHI/SRF
      BZ(N)=3./R*(SPHI*CPHI*CDEL/SRF/SRF+SDEL)
C     BZ IS DELTA B OVER DELTA Z DIVIDED BY B
      Z(N)=RO/2./SQRT(3.)/COS(PHIO)**2*(ALOG(SQRT(3.)*SPHI+SRF)
     1 +SQRT(3.)*SPHI*SRF)
      GPH=R1-R1*R1/R-OMS/2./G1/RO/EL*(R**3-R1**3)
      EN=XIH*EXP(-GPH/HH)+XIHE*EXP(-GPH/HHE)+XIO*EXP(-GPH/HO)
      EN=SQRT(EN)*ENFAC
      IF(ICLM.EQ.1) EN=ENEQ*(RO*EL/R)**POWER
      FP=SQRT(8Ø.6*EN*1.E6)
      FH=8.736E5*(RO/R)**3*SRF
      RIND=FP/SQRT(F*(FH*CTH-F))
      FACT1=1-(FP/F)**2
      FACT2=1-FP**2/(F**2-FH**2)
      FACT3=(FH/F)*FP**2/(F**2-FH**2)
      IF(IG.NE.1) GO TO 14
      VP(N)=C/2.*FH/FP
      CTHG(N)=2.*F/FH
      WN(N)=2.*PI*F/VP(N)/CTHG(N)
      RIND2=(FP/F)**2
      STHG2=1-CTHG(N)**2
      STHG=SQRT(STHG2)
      EPAG(N)=C*BW*F/FP*SQRT(1.-4.*F*F/FH/FH)
      RKDZ(N)=(WN(N)+WN(N-1))/2.*DZ*CTHG(N)+RKDZ(N-1)
      GO TO 15
   14 WN(N)=RIND/C*2.*PI*F
      VP(N)=C/RIND/CTH
      RKDZ(N)=(WN(N)+WN(N-1))/2.*DZ*CTH+RKDZ(N-1)
      CTHG(N)=CTH
      RIND2=RIND**2
      STHG2=STH**2
      STHG=STH
```

```
263          15    IF (VP(N).GT.VP(N-1)) VPMAX=VP(N)
269                BMULT(N)=FACT3/(RIND2-FACT2)*(RIND2*STHG2-FACT1)/RIND2
270            1   /STHG/CTHG(N)
271                ETA(N)=WN(N)*STHG/FH
272                NMAX=N
273                IF (R.GT.RO) GO TO 10
274      C         ALL PARAMETERS COMPUTED
275                N=0
276                RPHI=SRPHID*A
277           46   N=N+1
278                IF(ABS(RPHI).GT.PHI(N)) GOTO 46
279                INDMAX=N
280                RKDZL(N)=0.
281           47   N=N-1
282                RKDZL(N)=(WN(N+1)+WN(N))/2.*DZ*CTH+RKDZL(N+1)
283                IF(N.GT.1) GOTO 47
284                DO 48 N=1,NMAX
285           48   RKDZ(N)=RKDZ(N)+RKDZL(1)
286      C---------------------------------------------------------------------
287      C
288      C         TO PRINT PARAMETERS ALONG FIELD LINE ICONT1=1
289      C
290                IF(ICONT1.NE.1) GO TO 6000
291                I=0
292       6002     N=I*10+1
293                IF(N.GT.NMAX) GO TO 6000
294                PHID=PHI(N)/A
295                WRITE(6,6001) PHID,Z(N),EPAG(N),VP(N),CTHG(N),WN(N)
296       6001     FORMAT(F10.2,5E12.4)
297                I=I+1
298                GO TO 6002
299      C---------------------------------------------------------------------
300      C
301       6000     CONTINUE
302      C
303      C         THIS CODE WILL BE EXECUTED IF VARIABLE AMPLITUDE WAVE
304      C         IS USED PROGRAM
305                IF(IGROW.NE.1) GO TO 8061
306                XPHIO=XPHIOD*A
307                XSTART=RO/2./SQRT(3.)/COS(PHIO)**2*(ALOG(SQRT(3.)*SIN
308            1   (XPHIO)+SQRT(1.+3.*SIN(XPHIO)**2))+SQRT(3.)*SIN(XPHIO)*
309            2   SQRT(1.+3.*SIN(XPHIO)**2))
310                XEND=XSTART+XLEN*1000.
311                DO 8032 I=1,3000
312                AMPLOW(I)=0.
313       8032     CONTINUE
314                DO 8033 I=1,3000
315                AMPLHI(I)=0.
316                IF((PHI(I).GT.0.12217).AND.(PHI(I).LT.0.17453)) AMPLHI(I)=45.E-6
317       8033     CONTINUE
318       8061     CONTINUE
319      C
320      C         AMPLITUDE DATA STORED
321      C
322      C
```

```
C
C       INITIALIZE FINAL DISTRIBUTION FUCTION TO Ø IF FULL DISTRIBUTION
C       IS USED IN PROGRAM.
C       THE INITIAL DISTRIBUTION IS SET UP ACCORIDINGLY TO NVG FOR VELC
C       BIN AND IIAS AND IIAF FOR PITCH ANGLE BIN.
C       THE FINAL DISTRIBUTION BINS ARE COMPUTED FOR VELOCITY TO GIVEI
C       THE BEST RESOLUTION AND FIXED FOR PITCH ANGLE (Ø.5 DEGREE IN
C       Ø-9Ø RANGE)
C
        IF (IFULL.EQ.Ø) GO TO 43
C       J FOR ALPHA GOES FROM 1-18Ø
C       NVG IS NUMBER OF GRIDS IN VPARALLEL IN INITIAL DIST FUNCT
        DVPA=VP(1)*VRANGE/(NVG+1)
        K=1
        FVPA(1)=Ø.25*VP(1)
   4Ø   K=K+1
        FVPA(K)=FVPA(K-1)+DVPA*1Ø
        IF(FVPA(K).LT.(VP(1)*3.24)) GOTO 4Ø
        KMAX=K
        DO 42 K=1,KMAX
        DO 41 J=1,18Ø
        IF(K.LT.21) IFDIST(J,K)=Ø
        KFDIST(J,K)=Ø
   41   FDIST(J,K)=Ø.
   42   CONTINUE
   43   CONTINUE
C
C
C       PARTICLE TRACING STARTS
C       ITERATE FOR WAVE INTENSITY
C       FOR GENDRIN MODE WAVE INTENSITY IS SPECIFIED BY
C       MAGNETIC COMPONENT NEAR BEGINNING OF PROGRAM.
C       NEXT DO LOOP SHOULD HAVE ONLY ONE LOOP (IBWLO=IBWHI=1)
        DO 2Ø7 IE=IELO,IEHI
        EPA=45.E-6
        IF (ICONT25.EQ.Ø) GOTO 4Ø8Ø
        EPA=1.E-6*XMAX
 4Ø8Ø   IF(EPA.EQ.Ø) IMAX=1
        IF (EPA.NE.Ø) IMAX=12
C       FOR GENDRIN MODE EPA IS REPLACED BY EPAG(1) FOR OUTPUT PRINTING
        IF (IG.EQ.1) EPA=EPAG(1)
        VFMIN=1.E16
C
C       INITIALIZATION OF PLOTTING DATA ARRAYS
C
        IF(ICONT2.EQ.Ø) GOTO 1721
        DO 1716 I=1,12
 1716   TR(I)=1ØØ.
        DO 1717 I=1,85Ø
        DO 1761 J=1,12
        ENER(I,J)=-1.
 1761   CONTINUE
 1717   CONTINUE
        DO 1718 I=1,12
        DO 1719 J=1,5Ø5
        IF(J.GT.4ØØ) GOTO 172Ø
        TC(J,I)=1.E36
        CARGU(J,I)=1.E36
        VPHA(J,I)=1.E36
        VPARA(J,I)=1.E36
 172Ø   PBCARGU(J,I)=1.E36
        PBVPH(J,I)=1.E36
        PBVPA(J,I)=1.E36
 1719   CONTINUE
 1718   CONTINUE
```

```
388             DO 1762 I=1,85Ø
389             IF(I.GT.5Ø5) GOTO 1763
39Ø             TPB(I)=1.E36
391             DISTAN1(I)=1.E36
392      1763   TEN(I)=1.E36
393             DISTAN(I)=1.E36
394      1762   CONTINUE
395      1721   CONTINUE
396             VFMAX=Ø.
397             JCOUNT=Ø
398             EOTOT=Ø.
399             EFTOT=Ø.
4ØØ             ALFALO=1.E1Ø
4Ø1             ALFAHI=Ø.
4Ø2             IF(IFULL.EQ.Ø) VINITL=1.
4Ø3             VMIN=VINITL*VP(1)
4Ø4     C       ITERATE FOR PARTICLE VELOCITY
4Ø5     C       IVS AND IVF ARE VELOCITY RANGE DATA FOR SINGLE PARTICLE TRACING
4Ø6             IF (IFULL.EQ.1) IVF=IVS
4Ø7             DO 2Ø6 IV=IVS,IVF
4Ø8             VPAI=VMIN*(1.1Ø2+IV*Ø.ØØ1)
4Ø9             IF (ICONT25.EQ.Ø) GOTO 4Ø81
41Ø             VPAI=VP(1)*VDELTA
411      4Ø81   IIVS=1
412             IF(IFULL.EQ.Ø) NVG=Ø
413             IIVF=NVG+1
414             IF (IFULL.EQ.Ø) IIVF=IIVS
415             DO 2Ø5 IIV=IIVS,IIVF
416             VPAII=VMIN+DVPA*(IIV-1)
417             IF((IIV.EQ.IIVS).AND.(IFULL.EQ.1)) VSTART=VPAII
418             IF((IIV.EQ.IIVF).AND.(IFULL.EQ.1)) VEND=VPAII
419             IF (IFULL.EQ.1) SVPA=VPAII
42Ø             IF (IFULL.EQ.Ø) SVPA=VPAI
421     C       ITERATE FOR EQUATORIAL PITCH ANGLE
422     C       IAF AND IAS ARE PITCH ANGLE RANGE DATA FOR SINGLE PARTICLE TRACING
423             IF (IFULL.EQ.1) IAF=IAS
424             DO 2Ø4 IA=IAS,IAF
425             ALEQI=ALPDAT(IA)
426     C       IIAS AND IIAF ARE PITCH ANGLE RANGE FOR FULL DISTRIBUTION
427             IF(IFULL.EQ.Ø) IIAF=1
428             IF(IFULL.EQ.Ø) IIAS=1
429             IF (IFULL.EQ.Ø) IIAF=IIAS
43Ø             ALMIN=5.25+Ø.5*IIAS
431             ALMAX=5.25+Ø.5*IIAF
432             DO 2Ø3 IIA=IIAS,IIAF
433             ALEQII=5.25+Ø.5*IIA
434             IF (IFULL.EQ.1) ALEQ=ALEQII
435             IF (IFULL.EQ.Ø) ALEQ=ALEQI
436             IF (IFULL.EQ.Ø) WRITE (6,998) ALEQ
437     C       ALEQ IS IN DEGREES
438       998   FORMAT(1H1,' EQ PITCH ANGLE=',F7.3/)
439     C       ITERATE FOR BETA
44Ø             DO 2Ø2 I=1,IMAX
441             BETAD=3Ø.*I-3Ø.
442             BETA=BETAD*A
443     C       STARTING LATITUDE IS INPUT DATA
444             RPHI=SRPHID*A
445             SPHI=SIN(ABS(RPHI))
446             CPHI=COS(ABS(RPHI))
447             SRF=SQRT(1.+3.*SPHI**2)
448             S=RO/2./SQRT(3.)/COS(PHIO)**2*(ALOG(SQRT(3.)
449          1  *SPHI+SRF)+SQRT(3.)*SPHI*SRF)
45Ø             IF (RPHI.LT.Ø) S=Ø.-S
451             TANS=TAN(ALEQ*A)**2
452             FHRAT=SQRT(1.+3.*SPHI**2)/CPHI**6
453             VPA=SVPA*SQRT(1.+TANS-FHRAT*TANS)
454             SVPE=SVPA*TAN(ALEQ*A)
455             VPE=SVPE*SQRT(FHRAT)
```

```
456             EO=EM/2.*(VPE*VPE+VPA*VPA)
457             EVO=EO/E
458             IF(IFULL.EQ.1) GOTO 135
459             IF(I.NE.1) GOTO 135
460             IF(ICONT25.EQ.1) RATIO=VDELTA
461             IF(ICONT25.EQ.0) RATIO=VPAI/VMIN
462       135   CONTINUE
463             IF((I.EQ.1).AND.(IFULL.EQ.0)) WRITE(6,7051) SRPHID
464      7051   FORMAT(' TRACING STARTS AT ',F6.2,' DEGREES LATITUDE')
465             IF(IGROW.EQ.1) EPA=XAMPL
466             IF((IFULL.EQ.0).AND.(I.EQ.1)) WRITE(6,999) EL,ENEQ,F,SVPA,EVO,EPA
467          1  ,VPA,VP(1),RATIO
468       999   FORMAT (' EL=',F5.2,3X,'EQ DEN=',F6.1,'CM-3',3X,'FREQ=',-3PF6.3,
469          1  'KHZ',3X,'EQ PAR VEL=',0PE10.3,' M/SEC',3X,'INIT ENERGY=',E12.6,
470          2  ' EV',3X,'EPA=',E10.4,'V/M'/' VPA=',E11.4,'M/S',3X,
471          3  ' EQ PHASE VEL=',E11.4,'M/S',3X,'RATIO(VPAR/VPHASE)=',F7.5)
472             IRDONE=0
473             IRDON=0
474             IT1=0
475             IT2=0
476             IC=0
477             IND=0
478             IC2=0
479             IMDONE=0
480             IMIRR=0
481             T=0.
482             DT=0.0001
483             IT=0
484             N=1
485       100   N=N+1
486             IF (ABS(S).GT.Z(N)) GO TO 100
487             NU=N
488             NL=N-1
489             IF(I.EQ.1) WRITE(6,49) INDMAX,NL,NU
490        49   FORMAT(//3I5//)
491             VPHASE=IWD*(VP(NL)+(VP(NU)-VP(NL))*(ABS(S)-Z(NL))/(Z(NU)-Z(NL)))
492             IF (VPA.GE.(VPHASE*IWD)) ITEST=1
493             IF (VPA.LT.(VPHASE*IWD)) ITEST=-1
494       110   BZF=(BZ(NU)-BZ(NL))*(ABS(S)-Z(NL))/(Z(NU)-Z(NL))+BZ(NL)
495             IF(S.LT.0.) RKDZ1=RKDZL(NL)
496             IF(S.GE.0.) RKDZ1=RKDZ(NL)
497             IF(S.LT.0.) RKDZ2=RKDZL(NU)
498             IF(S.GE.0.) RKDZ2=RKDZ(NU)
499             RKF=IWD*(RKDZ1+(RKDZ2-RKDZ1)*(ABS(S)-Z(NL))/(Z(NU)-Z(NL))
500          1  )
501             IF (S.LT.0.) BZF=-1*BZF
502             CARG=OM*T-RKF+BETA
503             IF((IGROW.EQ.1).AND.(S.LE.0.)) EPA=AMPLOW(NU)
504             IF((IGROW.EQ.1).AND.(S.GE.0.)) EPA=AMPLHI(NU)
505             IF(ICONT99.EQ.0) GOTO 3708
506             COSINE=CTH
507             IF(IG.EQ.1) COSINE=(CTHG(NU)+CTHG(NL))/2.
508             TERM1=VPE*(WN(NU)+WN(NL))/2.*COSINE/F/2./PI
509             ARG=(ETA(NU)+ETA(NL))/2.*VPE
510             CALL BESJR(ARG,1,BESEL,IER)
511             TERM3=BESEL(1)*(1-TERM1*(BMULT(NU)+BMULT(NL))/2.*BESEL(2)
512          1  /BESEL(1))
513             GOTO 3709
514      3708   TERM3=1.
515      3709   CONTINUE
516             IF( IG .NE. 1 ) GO TO 5000
517             EPAF=EPAG(NL)+(EPAG(NU)-EPAG(NL))*(ABS(S)-Z(NL))/(Z(NU)-Z(NL))
518             VPAT=VPA-VPE**2/2.*BZF*DT-E/EM*EPAF*TERM3*COS(CARG)*DT
519             GO TO 5001
```

```
520      5000    VPAT=VPA-VPE**2/2.*BZF*DT-E/EM*EPA*TERM3*COS(CARG)*DT
521      5001    ST=S+(VPAT+VPA)/2.*DT
522              NUO=NU
523              IF (ABS(ST).LE.ABS(S)) GO TO 101
524              NU=NU-1
525       102    NU=NU+1
526              IF (ABS(ST).GT.Z(NU)) GO TO 102
527              NL=NU-1
528              GO TO 104
529       101    NL=NL+1
530       103    NL=NL-1
531              IF (ABS(ST).LT.Z(NL)) GO TO 103
532              NU=NL+1
533       104    CONTINUE
534              BZS=(BZ(NU)-BZ(NL)
535              IF(S.LT.0.) RKDZ1=RKDZL(NL)
536              IF(S.GE.0.) RKDZ1=RKDZ(NL)
537              IF(S.LT.0.) RKDZ2=RKDZL(NU)
538              IF(S.GE.0.) RKDZ2=RKDZ(NU)
539              RKS=IWD*(RKDZ1+(RKDZ2-RKDZ1)*(ABS(ST)-Z(NL))/(Z(NU)-Z(NL)
540            1 ))
541              IF(ST.LT.0.) BZS=-1*BZS
542              CARG=OM*T-0.5*(RKF+RKS)+BETA
543              IF(ICONT99.EQ.0) GOTO 3715
544              COSINE=CTH
545              IF(IG.EQ.1) COSINE=(CTHG(NU)+CTHG(NL))/2.
546              TERM1=VPE*(WN(NU)+WN(NL))/2.*COSINE/F/2./PI
547              ARG=(ETA(NU)+ETA(NL))/2.*VPE
548              CALL BESJR(ARG,1,BESEL,IER)
549              TERM3=BESEL(1)*(1-TERM1*(BMULT(NL)+BMULT(NU))/2.*BESEL(2)
550            1 /BESEL(1))
551              GOTO 3716
552       3715   TERM3=1.
553       3716   CONTINUE
554              IF(IG.NE.1) GO TO 5005
555              EPAS=EPAG(NL)+(EPAG(NU)-EPAG(NL))*(ABS(ST)-Z(NL))/(Z(NU)-Z(NL))
556              VPAT=VPA-VPE**2/4.*(BZF+BZS)*DT-E/EM*(EPAF+EPAS)
557            1 /2.*TERM3*COS(CARG)*DT
558              GO TO 2400
559       5005   VPAT=VPA-VPE**2/4.*(BZS+BZF)*DT-E/EM*EPA*TERM3*COS(CARG)*DT
560       2400   IF(IG.EQ.1) EPATEM=(EPAF+EPAS)/2.
561              IF(IG.NE.1) EPATEM=EPA
562              IF(ICONT99.EQ.0) GOTO 3726
563              TERM2=VPAT*(WN(NL)+WN(NU))/2.*COSINE/F/2./PI
564              TERM4=BESEL(2)*(BMULT(NU)+BMULT(NL))/2.*(1-TERM2)
565              VPE=VPE+VPAT*VPE/4.*(BZS+BZF)*DT+E/EM*TERM4*COS(CARG)*DT
566            1 *EPATEM
567              GOTO 3727
568       3726   VPE=VPE+VPE*VPAT/4.*(BZS+BZF)*DT
569       3727   CONTINUE
570              SC=S+(VPA+VPAT)/2.*DT
571      C       CHECK FOR EQUATOR CROSSING
572              IF ((SC*S).GT.0) GO TO 2401
573              CALL EQCONV
574              IF(IFULL.EQ.0) WRITE(6,2402) T,EV,EQALD,IRDONE
575       2402   FORMAT (' EQUATOR XING',3X,'T=',F7.4,3X,'ENERGY=',E8.3,'EV',
576            1 3X,'EQ PITCH ANGLE=',F6.3,3X,'NO OF RESONANCES=',I3)
577              IRDONE=0
578       2401   CONTINUE
579      C       FIND MIRROR POINT
580              IF (IMDONE.EQ.1) GO TO 2500
581              IF ((VPA*VPAT).LT.0) IMIRR=1
582              IF (IMIRR.NE.1) GO TO 2500
583              CALL EQCONV
584              IF (IFULL.EQ.0) WRITE (6,253) H,RPHID,S,T,EV,EQALD
585        253   FORMAT (' MIRROR POINT',3X,'H=',E12.5,' KM',3X,'PHI=',F7.3,3X,
586            1 'S=',E12.5,3X,'T=',F7.4,3X,'ENERGY=',E8.3,'EV',3X,
587            2 'EQ PITCH ANGLE=',F6.3 )
588              IMDONE=1
589              GO TO 312
```

```
590      2500    VPA=VPAT
591              ENGY=EM/2./E*(VPE*VPE+VPA*VPA)
592              ERROR=ENGY-EO/E
593              AL=ATAN(VPE/VPA)
594              IF(ABS(SC).LE.ABS(ST)) GO TO 105
595              NU=NU-1
596       106    NU=NU+1
597              IF (ABS(SC).GT.Z(NU)) GO TO 106
598              NL=NU-1
599              GO TO 108
600       105    NL=NL+1
601       107    NL=NL-1
602              IF (ABS(SC).LT.Z(NL)) GO TO 107
603              NU=NL+1
604       108    CONTINUE
605              NUO=NU
606              S=SC
607              RPHI=(PHI(NU)-PHI(NL))*(ABS(S)-Z(NL))/(Z(NU)-Z(NL))+PHI(NL)
608              IF (S.LT.0.) RPHI=0.-RPHI
609              RPHID=RPHI/A
610              R=RO*EL*COS(RPHI)**2
611              H=(R-RO)/1000.
612              VPHASE=IWD*(VP(NL)+(VP(NU)-VP(NL))*(ABS(S)-Z(NL))/(Z(NU)-Z(NL)))
613     C        FIND RESONANCE POINT
614              IF ((VPA*IWD).LT.0) GO TO 250
615              IF (((VPA-VPHASE)*ITEST).LE.0) GO TO 251
616              GO TO 250
617       251    CONTINUE
618              IF((IFULL.EQ.0).AND.(IRDON.EQ.0)) TR(I)=T
619              IRDON=IRDON+1
620              IF(IFULL.EQ.1) GOTO 137
621              CARGD=CARG/A
622       139    IF(ABS(CARGD).LT.360.) GOTO 138
623              IF(CARGD.GT.0.) CARGD=CARGD-360.
624              IF(CARGD.LT.0.) CARGD=CARGD+360.
625              GOTO 139
626       138    IF(CARGD.LT.0.) CARGD=CARGD+360.
627       137    CONTINUE
628              IF((IFULL.EQ.0).AND.(IRDONE.EQ.0)) WRITE(6,252) VPHASE,R,RPHID,S,T
629          1   ,CARGD
630       252    FORMAT (' RESONANCE VEL=',E12.5,5X,'AT R=',E12.5,5X,'PHI=',F7.3,
631          1   5X,'S=',E12.5,5X,'T=',F7.4,3X,'BETA=',F7.2)
632              IRDONE=IRDONE+1
633              ITEST=0-ITEST
634       250    CONTINUE
635              T=T+DT
636     C        THE NEXT CARD ,GO TO 300, BYPASSES WRITING OF PHASE ANGLE
637     C
638     C        SAMPLING OF PLOT DATA
639     C
640              IF((ICONT2.EQ.0).OR.(IFULL.EQ.1)) GOTO 1732
641     C
642     C        RESONANCE POINT SAMPLING
643     C
644              IF(T.GT.5.0) GOTO 1732
645              IT=IT+1
646              IF(IT.LT.20) GOTO 1726
647              IF(ABS((VPA-VPHASE)/VPA).GT.0.10) GOTO 1729
648              IF((T-TR(I)).GT.0.20) GOTO 1729
649              CARGD=CARG/A
650       1727   IF(ABS(CARGD).LT.360.) GOTO 1728
651              IF(CARGD.GT.0.) CARGD=CARGD-360.
652              IF(CARGD.LT.0.) CARGD=CARGD+360
653              GOTO 1727
```

```
654      1728    IC=IC+1
655              IF((IC.LT.1).OR.(IC.GT.4ØØ)) WRITE(6,1741) I,T,IC
656      1741    FORMAT(/' FIRST RESONANCE ERROR (BAD INDEX)',I5,F1Ø.5,I5)
657              IF((IC.LT.1).OR.(IC.GT.4ØØ)) GOTO 1726
658              TC(IC,I)=T
659              CARGU(IC,I)=CARGD
66Ø              VPHA(IC,I)=VPHASE/1ØØØ.
661              VPARA(IC,I)=VPA/1ØØØ.
662      1729    IT=Ø
663     C
664     C        ENERGY SAMPLING (EVERY 6 MSEC)
665     C
666      1726    IT1=IT1+1
667              IF(IT1.LT.6Ø) GOTO 173Ø
668              IND=INT(T*1ØØØ/6)+1
669              IF((IND.LT.1).OR.(IND.GT.85Ø)) WRITE(6,1742) I,T,IND
67Ø      1742    FORMAT(/' TOTAL ENERGY ERROR (BAD INDEX)',I5,F1Ø.5,I5)
671              IF((IND.LT.1).OR.(IND.GT.85Ø)) GOTO 173Ø
672              ENER(IND,I)=ENGY
673              IF(I.EQ.1) DISTAN(IND)=PHI(NL)/A
674              IF((I.EQ.1).AND.(S.LT.Ø.)) DISTAN(IND)=-1.*PHI(NL)/A
675              IT1=Ø
676      173Ø    CONTINUE
677     C
678     C        PHASE BUNCING DETECTION (TMIN<T<TMAX)
679     C
68Ø              IF((T.LT.TMIN).OR.(T.GT.TMAX)) GOTO 1732
681              IT2=IT2+1
682              IF(IT2.LT.2Ø) GOTO 1732
683              IC2=IC2+1
684              IF((IC2.LT.1).OR.(IC2.GT.5Ø5)) WRITE(6,1743) I,T,IC2
685      1743    FORMAT(/' PHASE DATA ERROR (BAD INDEX)',I5,F1Ø.5,I5)
686              IF((IC2.LT.1).OR.(IC2.GT.5Ø5)) GOTO 1732
687              CARGD=CARG/A
688      1778    IF(ABS(CARGD).LE.36Ø.) GOTO 1779
689              IF(CARGD.LT.Ø.) CARGD=CARGD+36Ø.
69Ø              IF(CARGD.GT.36Ø.) CARGD=CARGD-36Ø.
691              GOTO 1778
692      1779    CONTINUE
693              PBCARGU(IC2,I)=CARGD
694              PBVPH(IC2,I)=VPHASE/1ØØØ.
695              PBVPA(IC2,I)=VPA/1ØØØ.
696              IF(I.EQ.1) TPB(IC2)=T
697              IF(I.EQ.1) DISTAN1(IC2)=PHI(NL)/A
698              IF((I.EQ.1).AND.(S.LT.Ø.)) DISTAN1(IC2)=-1.*PHI(NL)/A
699              IT2=Ø
7ØØ              IF(IRDONE.GT.1Ø) INDEX(I)=1
7Ø1              IF(IRDONE.LE.1Ø) INDEX(I)=Ø
7Ø2      1732    CONTINUE
7Ø3              IF (T.GT.1Ø) GO TO 2Ø9
7Ø4     C        TEST FOR DETRAPPING.  IF PARTICLE VEL DIFFERS FROM WAVE VEL BY
7Ø5     C        MORE THAN SPECIFIED AMOUNT, NO INTERACTION IS ASSUMED AND ALL
7Ø6     C        PARTICLE PARAMETERS CALC FROM ADIABATIC THEORY
7Ø7              IF (IADIA.EQ.Ø) GO TO 31Ø
7Ø8              IF ((VPA*IWD).GT.Ø.AND.IRDONE.GT.Ø.AND.(ABS(VPHASE-VPA)/VPHASE).
7Ø9          1   GE.Ø.2) GO TO 311
71Ø       31Ø    IF (R.LT.(RO+1.E5))  GO TO 2Ø1
711              GO TO 11Ø
712       2Ø1    CONTINUE
713              CALL EQCONV
714              IF (IFULL.EQ.Ø) WRITE (6,4ØØØ) H,RPHID,S,T,EV,EQALD
715      4ØØØ    FORMAT ( 'LANDING POINT',3X,'H=',E12.5,' KM',3X,'PHI=',F7.3,3X,
716          1   'S=',E12.5,3X,'T=',F7.4,3X,'ENERGY=',E8.3,'EV',3X,
717          2   'EQ PITCH ANGLE=',F6.3 )
718              GO TO 312
719       311    CALL EQCONV
```

```
720          IF (IFULL.EQ.0) WRITE (6,313) H,RPHID,S,T,EV,EQALD
721      313 FORMAT (' DETRAP POINT',3X,'H=',E12.5,' KM',3X,'PHI=',F7.3,3X,
722         1 'S=',E12.5,3X,'T=',F7.4,3X,'ENERGY=',E8.3,'EV',3X,
723         2 'EQ PITCH ANGLE=',F6.3 )
724      312 IF (IFULL.EQ.1) CALL DFUNC
725      C   IF PARTICLE CROSSES EQUATOR, IRDONE PRINTED HERE IS COUNTED
726      C   FROM EQUATOR CROSSING.
727          IF(IFULL.EQ.0) WRITE(6,314) BETAD,IRDONE
728      314 FORMAT(' BETA=',F7.2,5X,'NO OF RESONANCES=',I3/)
729          ALDC(I)=EQAL
730          EVDC(I)=EV
731          EOTOT=EOTOT+EVO
732          EFTOT=EFTOT+EV
733          IF(VPAEQ.LE.VFMIN) VFMIN=VPAEQ
734          IF(VPAEQ.GE.VFMAX) VFMAX=VPAEQ
735          IF(EQALD.GT.ALFAHI) ALFAHI=EQALD
736          IF(EQALD.LT.ALFALO) ALFALO=EQALD
737          JCOUNT=JCOUNT+1
738          TTRACE(I)=T
739      202 CONTINUE
740          IF (IFULL.EQ.0.AND.IDIFF.EQ.1) CALL DIFCO
741          IF((ICONT2.EQ.1).AND.(IFULL.EQ.0)) CALL PLOTTING
742      203 CONTINUE
743      204 CONTINUE
744      205 CONTINUE
745      206 CONTINUE
746          IF (IFULL.EQ.1) CALL SUMARY
747          IF(IFULL.EQ.1) WRITE(6,3200) VSTART,VEND,VFMIN,VFMAX
748     3200 FORMAT(////' DISTRIBUTION FUNCTION PARAMETERS'///
749         1 ' SVPAMIN=',E10.4,' SVPAMAX=',E10.4,' FVPAMIN=',E10.4,
750         2 ' FVPAMAX=',E10.4//)
751          IF(IFULL.EQ.1) DVPA1=DVPA*10
752          IF(IFULL.NE.1) GOTO 3504
753          WRITE(6,3300) DVPA,DVPA1
754     3300 FORMAT(/' INITIAL VEL. BIN=',E10.4,' FINAL VEL. BIN='
755         1 ,E10.4)
756          K1=INT((VFMIN-FVPA(1))/DVPA1)+1
757          K2=INT((VFMAX-FVPA(1))/DVPA1)+1
758          J1=INT(ALMAX*2)+2
759          WRITE(6,3510) JCOUNT
760          IF(JHI.LT.35) GOTO 617
761          WRITE(6,3505)
762     3505 FORMAT(/' FINAL DISTRIBUTION (# OF PARTICLES PER CELL)')
763     3510 FORMAT(////' TOTAL NUMBER OF TRACED PARTICLES WAS=',I6//)
764          DO 3501 K=K1,K2
765          DO 3502 J=1,J1
766          PITCH=J*0.5-0.25
767          WRITE(6,3503) PITCH,K,KFDIST(J,K)
768     3502 CONTINUE
769     3501 CONTINUE
770     3503 FORMAT(F10.4,I4,' # OF PARTICLES=',I4)
771      617 CONTINUE
772          WRITE(6,3610)
773     3610 FORMAT(//' INITIAL DISTRIBUTION AFTER SCATTERING'/)
774          DO 3603 K=1,20
775          DO 3604 J=1,J1
776          IF(K.GT.(NVG+1)) GOTO 3606
777          PITCH1=J*0.5-0.25
778          WRITE(6,3605) PITCH1,K,IFDIST(J,K)
779     3604 CONTINUE
780     3603 CONTINUE
781     3605 FORMAT(F10.4,I4,' NUMBER OF PARTICLES=',I4)
782     3606 CONTINUE
783          DIFEN=EFTOT-EOTOT
784          WRITE(6,3640) DIFEN
785     3640 FORMAT(/' TOTAL ENERGY EXCHANGE (EV)=',E10.4)
```

```
      C
      C        FULL DISTRIBUTION TABLE
      C
               IF((JHI-JLO).GT.32) GOTO 601
               DO 602 J=1,32,2
        602    ALFA(J)=J*0.5-0.25
               WRITE(6,603) (ALFA(J),J=1,32,2)
        603    FORMAT(1H1,'EQUATORIAL DISTRIBUTION FUNCTION (# OF PARTICLES)'
           1   /' VPARALEL (KM/SEC)',50X,' PITCH ANGLE (DEG)'
           2   /8X,16F6.2/9X,32('  I'))
               IF(K1.GT.1) K1=K1-1
               IF(K2.LT.400) K2=K2+1
               DO 604 K=K1,K2
               VEL=FVPA(K)/1000.
               DO 606 J=1,33
        606    KTEMP(J)=KFDIST(J,K)
               WRITE(6,605) VEL,(KTEMP(J),J=1,33)
        605    FORMAT(1X,F8.0,'-- ',33(I2,' '))
        604    CONTINUE
        601    CONTINUE
      3504     CONTINUE
        207    CONTINUE
               IF(IGROW.NE.1) GOTO 9003
               WRITE(6,8201)
      8201     FORMAT(/' WAVE AMPLITUDE DATA')
               WRITE(6,8081) XSTART,XEND,XLEN,XAMPL
      8081     FORMAT(/' START=',E12.4,' END=',E12.4,' LENGTH=',F10.3,' AMPL='
           1   ,E12.4)
               PHI1=PHI(NTOP)/A
               PHI2=PHI(NBOT)/A
               WRITE(6,9020) PHI1,PHI2
      9020     FORMAT(/' ABSOLUTE VALUES OF STARTING AND ENDING LATITUDE ARE:
           1   ',F10.5,3X,F10.5)
               IF(ICONT5.EQ.1) GO TO 9002
               GO TO 9003
      9002     CONTINUE
               WRITE(6,9004)
      9004     FORMAT(/' WAVE AMPLITUDE DATA')
               DO 9005 II=1,3000,10
               WRITE(6,9006) II,Z(II),AMPLOW(II),AMPLHI(II)
      9006     FORMAT(I5,3X,3(E12.4,3X))
      9005     CONTINUE
      9003     CONTINUE
        208    CONTINUE
               GO TO 210
        209    WRITE (6,3001)
      3001     FORMAT (///' INTEGRATION TIME EXCEEDS 10 SEC LIMIT')
        210    CONTINUE
               STOP
               END
```

```
836     C
837             SUBROUTINE PLOTTING
838             COMMON/BLOCK3/ TC(400,12),CARGU(400,12),VPHA(400,12),
839           1 VPARA(400,12),ENER(850,12),PBCARGU(505,12),PBVPH(505,12)
840           2 ,PBVPA(505,12),TMIN,TMAX,TR(12),TTRACE(12),INDEX(12)
841           3 ,MLO,MHI,MSTEP,TEN(850),TPB(505),DISTAN(850),DISTAN1(505)
842             DIMENSION SAVE(350),XX1(850),XX2(400),XX3(400,2),XX4(400),
843           1 TLO(12),THI(12)
844             TMAXI=0.
845             DO 1 J=1,12
846             IF(TTRACE(J).GT.TMAXI) TMAXI=TTRACE(J)
847           1 CONTINUE
848             DO 2 J=1,12
849             DO 3 I=1,400
850             IF((INT(TC(I,J)*100000)-INT(TR(J)*100000)).EQ.0) INDEX(J)=I
851           3 CONTINUE
852           2 CONTINUE
853             WRITE(6,6) TMAXI
854           6 FORMAT(///' PLOTTING ROUTINE STARTED'//' MAXIMUM TRACING TIME='
855           1 ,F10.5)
856             DO 10 J=1,12
857          10 WRITE(6,11) J,TR(J),TTRACE(J)
858          11 FORMAT(' PARTICLE#',I2,' FIRST RES.=',F10.5,' END=',F10.5)
859     C
860     C       FILL UP ENERGY ARRAY
861             DO 20 J=1,12
862             DO 21 I=1,850
863             IF(ENER(I,J).LT.0.) ENER(I,J)=ENER((I-1),J)
864          21 CONTINUE
865          20 CONTINUE
866     C
867     C               SUM ENERGIES FOR ALL PARTICLES
868     C
869             DO 22 I=1,850
870             TEMP=0.
871             DO 23 J=1,12
872          23 TEMP=TEMP+ENER(I,J)
873             ENER(I,1)=TEMP/1000.
874          22 ENER(I,2)=ENER(I,1)/ENER(1,1)
875             WRITE(6,24) ENER(1,1),ENER(850,1)
876          24 FORMAT(' TOTAL ENERGY DATA'//' INITAL ENERGY (EV)',E12.4/
877           1 ' FINAL ENERGY (EV)=',E12.4)
878     C
879     C
880     C       SET UP TIME ARRAY
881     C
882             II=INT(TMAXI*1000/6)+10
883             DO 60 I=1,850
884             IF(I.LE.II) GOTO 61
885             TEN(I)=1.E36
886             ENER(I,1)=1.E36
887             ENER(I,2)=1.E36
888             GOTO 60
889          61 TEN(I)=I*0.006
890          60 CONTINUE
891     C
892     C       PLOT ENERGY VS. TIME (DISTANCE)
893     C
894     C
895     C       DEFINE CURVE WINDOW
896     C
897             KK=1
898          50 FORMAT(' THIS IS STEP',I3)
899     C
900             CALL AGSETF('GRID/LEFT.',0.10)
901             CALL AGSETF('GRID/RIGHT.',0.90)
902             CALL AGSETF('GRID/BOTTOM.',0.10)
903             CALL AGSETF('GRID/TOP.',0.85)
```

```
      C
      C        DEFINE BACKGROUND
      C
               CALL AGSETI('BACKGROUND.',3)
      C
      C        TURN ON WINDOWING
      C
               CALL AGSETI('WINDOWING.',1)
      C
               CALL AGSETF('LABEL/NAME.','L')
               CALL AGSETI('LINE/NUMBER.',100)
               CALL AGSETP('LINE/TEXT.',' ENERGY (KEV)$',1)
               CALL AGSETF('X/MINIMUM.',0.0)
               CALL AGSETF('X/MAX.',TMAXI)
               CALL AGSETI('BOTTOM/MAJOR/TYPE.',1)
               CALL AGSETF('BOTTOM/MAJOR/BASE.',0.5)
               CALL AGSETI('BOTTOM/MINOR/SPACING.',4)
      C
               CALL AGSETF(11HLABEL/NAME.,1HB)
               CALL AGSETI('LINE/NUMBER.',-100)
               CALL AGSETP(10HLINE/TEXT.,11HTIME (SEC)$,1)
      C
      C        LOAD TEMP ARRAYS WITH DATA
               DO 63 I=1,850
         63    XX1(I)=ENER(I,1)
      C
               CALL EZXY(TEN,XX1,850,22HTOTAL ENERGY VS. TIMES)
      C
               DO 64 I=1,850
         64    XX1(I)=ENER(I,2)
      C
               CALL AGSETF('LABEL/NAME.','L')
               CALL AGSETI('LINE/NUMBER.',100)
               CALL AGSETP('LINE/TEXT.','E/E0$',1)
      C
               CALL EZXY(TEN,XX1,850,27HNORMALIZED ENERGY VS. TIMES)
      C
      C
      C        RESET X AND REDEFINE 'NICE'
      C
               CALL AGSETF('X/MAX.',1.E36)
               CALL AGSETI('X/NI.',0)
      C
      C        PLOT ENERGY VERSUS LATITUDE
      C
               CALL AGSETF('X/MIN.',1.E36)
               CALL AGSETF('X/MAX.',1.E36)
               CALL AGSETF(11HLABEL/NAME.,1HB)
               CALL AGSETI('LINE/NUMBER.',-100)
               CALL AGSETP(10HLINE/TEXT.,19HLATITUDE (DEGREES)$,1)
               CALL EZXY(DISTAN,XX1,850,31HNORMALIZED ENERGY VS. LATITUDES)
      C        PLOT RESONANCE DATA
      C
               XMAXI=0.
               XMINI=1000.
               DO 65 J=1,12
               DO 66 I=1,400
               IF(TC(I,J).GT.1000.) GOTO 67
         66    TC(I,J)=(TC(I,J)-TR(J))*1000.
         67    THI(J)=TC((I-1),J)
               IF(THI(J).GT.XMAXI) XMAXI=THI(J)
         65    CONTINUE
               DO 68 J=1,12
               TLO(J)=TC(1,J)
               IF(ABS(TLO(J)).LT.ABS(XMINI)) XMINI=TLO(J)
```

```
      68    WRITE(6,69) J,TLO(J),THI(J)
      69    FORMAT(' RESONANCE #',I3,'TMIN=',F15.4,'TMAX=',F10.4)
            XMAXI=INT(XMAXI/10.)*10.
            XMINI=INT(XMINI/10.)*10.
            IF(ABS(XMINI).GT.200.0) XMINI=-200.0
            WRITE(6,130) XMINI,XMAXI
     130    FORMAT(/' RESONANCE TIME WINDOW'/' TMIN=',F10.4/' TMAX='
           1  ,F10.4//)
C
C           SET XMIN AND XMAX
C
            CALL AGSETI('X/NI.',-1)
            CALL AGSETF('Y/MIN.',0.0)
            CALL AGSETF('Y/MAX.',360.0)
            CALL AGSETI('LEFT/MAJOR/TYPE.',1)
            CALL AGSETF('LEFT/MAJOR/BASE.',60.0)
            CALL AGSETI('LEFT/MINOR/SPACING.',5)
            CALL AGSETF('X/MI.',XMINI)
            CALL AGSETF('X/MA.',XMAXI)
C
C
C           DO PHASE PLOTS
C
            CALL AGSETF('LABEL/NAME.','L')
            CALL AGSETI('LINE/NUMBER.',100)
            CALL AGSETP('LINE/TEXT.','PHASE (DEGREES)$',1)
C
            CALL AGSETF('LABEL/NAME.',1HB)
            CALL AGSETI('LINE/NUMBER.',-100)
            CALL AGSETP(10HLINE/TEXT.,12HTIME (MSEC)$,1)
C
C
C           SET BOTTOM AXIS PARAMETERS
C
            CALL AGSETI('BOTTOM/MAJOR/TYPE.',1)
            CALL AGSETF('BOTTOM/MAJOR/BASE.',50.0)
            CALL AGSETI('BOTTOM/MINOR/SPACING.',4)
C
C
C
C
            DO 103 J=1,12
            DO 102 I=1,850
            XX1(I)=1.E36
     102    ENER(I,1)=1.E36
            ICNT=1
            ENER(ICNT,1)=CARGU(ICNT,J)
            XX1(ICNT)=TC(ICNT,J)
            ICNT=2
            DO 104 I=2,400
            DIFF=ABS(CARGU((I-1),J)-CARGU(I,J))
            IF(DIFF.LT.180.0) GOTO 105
            ENER(ICNT,1)=360.0+CARGU(I,J)
            IF(CARGU(I,J).GT.CARGU((I-1),J)) ENER(ICNT,1)=CARGU
           1  (I,J)-360.0
            XX1(ICNT)=TC(I,J)
            ICNT=ICNT+1
            ENER(ICNT,1)=1.E36
            XX1(ICNT)=TC(I,J)
            ICNT=ICNT+1
            ENER(ICNT,1)=CARGU((I-1),J)-360.0
            IF(CARGU(I,J).GT.CARGU((I-1),J)) ENER(ICNT,1)=CARGU((I-1),J)
           1  +360.0
            XX1(ICNT)=TC((I-1),J)
            ICNT=ICNT+1
```

```
1034        105   ENER(ICNT,1)=CARGU(I,J)
1035              XX1(ICNT)=TC(I,J)
1036        104   ICNT=ICNT+1
1037              CALL EZMXY(XX1,ENER,850,1,850,15HPHASE VS. TIMES)
1038        103   CONTINUE
1039              CALL AGSETF('Y/MINIMUM.',1.E36)
1040              CALL AGSETF('Y/MAXIMUM.',1.E36)
1041    C
1042    C
1043    C
1044              CALL AGSETF('LEFT/MAJOR/TYPE.',1.E36)
1045              CALL AGSETF('LEFT/MAJOR/BASE.',1.E36)
1046              CALL AGSETF('LEFT/MINOR/SPACING.',1.E36)
1047    C
1048    C
1049    C         PLOT VP AND VPA VS. TIME
1050    C
1051              CALL AGSETF('LABEL/NAME.','L')
1052              CALL AGSETI('LINE/NUMBER.',100)
1053              CALL AGSETP('LINE/TEXT.','VELOCITY (KM/SEC)$',1)
1054    C
1055              DO 72 J=1,12
1056              DO 73 I=1,400
1057              XX2(I)=TC(I,J)
1058              XX3(I,1)=VPHA(I,J)
1059              XX3(I,2)=VPARA(I,J)
1060         73   CONTINUE
1061              CALL EZMXY(XX2,XX3,400,2,400,18HVELOCITY VS. TIMES)
1062         72   CONTINUE
1063    C
1064    C         PLOT PHASE BUNCHING
1065    C         SET X,Y AND LABELS
1066    C
1067              CALL AGSETF('Y/MI.',40.0)
1068              CALL AGSETF('Y/MA.',320.0)
1069              CALL AGSETI('BOTTOM/MAJOR/TYPE.',1)
1070              CALL AGSETF('BOTTOM/MAJOR/BASE.',0.05)
1071              CALL AGSETI('BOTTOM/MINOR/SPACING.',4)
1072    C
1073    C
1074              CALL AGSETF('LABEL/NAME.','L')
1075              CALL AGSETI('LINE/NUMBER.',100)
1076              CALL AGSETP('LINE/TEXT.','PHASE (DEGREES)$',1)
1077    C
1078              CALL AGSETF('LABEL/NAME.',1HB)
1079              CALL AGSETI('LINE/NUMBER.',-100)
1080              CALL AGSETP(10HLINE/TEXT.,11HTIME (SEC)$,1)
1081    C
1082              DO 450 J=1,12
1083              DO 401 I=1,850
1084              IF(I.GT.505) GOTO 402
1085              IF(INDEX(J).EQ.0) ENER(I,J)=1.E36
1086              IF(INDEX(J).EQ.1) ENER(I,J)=P8CARGU(I,J)
1087              GOTO 403
1088        402   ENER(I,J)=1.E36
1089        403   CONTINUE
1090        401   CONTINUE
1091        450   CONTINUE
1092              DO 410 I=1,850
1093              IF(I.LE.505) XX1(I)=TPB(I)
1094              IF(I.GT.505) XX1(I)=1.E36
1095        410   CONTINUE
1096              TMINI=TMIN
1097              TMAXII=TMIN+0.1
```

```
1098            DO 200 I=1,20
1099            IF(TMAXII.GT.TMAXI) GOTO 201
1100            CALL AGSETF('X/MIN.',TMINI)
1101            CALL AGSETF('X/MAX.',TMAXII)
1102            CALL EZMXY(XX1,ENER,850,12,850,15HPHASE VS. TIMES)
1103            TMINI=TMINI+0.1
1104      200   TMAXII=TMAXII+0.1
1105      201   CONTINUE
1106    C
1107    C       RESET X
1108    C
1109            CALL AGSETF('X/MAX.',TMAX)
1110            CALL AGSETF('X/MIN.',TMIN)
1111            CALL AGSETF('BOTTOM/MAJOR/TYPE.',1.E36)
1112            CALL AGSETF('BOTTOM/MAJOR/BASE.',1.E36)
1113            CALL AGSETF('BOTTOM/MINOR/SPACING.',1.36)
1114    C
1115    C       PLOT VPA&VPHASE VS. TIME
1116    C
1117            CALL AGSETF('Y/MI.',1.E36)
1118            CALL AGSETF('Y/MA.',1.E36)
1119            CALL AGSETF('LABEL/NAME.','L')
1120            CALL AGSETI('LINE/NUMBER.',100)
1121            CALL AGSETP('LINE/TEXT.','VELOCITY (KM/SEC)$',1)
1122            CALL AGSETF('LABEL/NAME.',1HB)
1123            CALL AGSETI('LINE/NUMBER.',-100)
1124            CALL AGSETP(10HLINE/TEXT.,11HTIME (SEC)$,1)
1125            DO 110 I=1,850
1126            IF(I.LE.505) XX1(I)=TPB(I)
1127            IF(I.GT.505) XX1(I)=1.E36
1128      110   CONTINUE
1129            DO 111 J=1,2
1130            DO 112 I=1,850
1131      112   ENER(I,J)=1.E36
1132      111   CONTINUE
1133    C
1134            DO 113 J=1,12
1135            DO 114 I=1,505
1136            ENER(I,1)=PBVPA(I,J)
1137      114   ENER(I,2)=PBVPH(I,J)
1138            CALL EZMXY(XX1,ENER,850,2,850,18HVELOCITY VS. TIMES)
1139      113   CONTINUE
1140    C
1141    C
1142    C       PLOT VELOCITY VS. LATITUDE
1143    C
1144            DO 400 I=1,850
1145            IF(I.LE.505) XX1(I)=DISTAN1(I)
1146            IF(I.GT.505) XX1(I)=1.E36
1147      400   CONTINUE
1148            CALL AGSETF('X/MAX.',1.E36)
1149            CALL AGSETF('X/MIN.',1.E36)
1150            CALL AGSETI('X/NI.',0)
1151            CALL AGSETF('LABEL/NAME.',1HB)
1152            CALL AGSETI('LINE/NUMBER.',-100)
1153            CALL AGSETP(10HLINE/TEXT.,19HLATITUDE (DEGREES)$,1)
1154    C
1155            DO 300 J=1,12
1156            DO 301 I=1,505
1157            ENER(I,1)=PBVPA(I,J)
1158      301   ENER(I,2)=PBVPH(I,J)
1159            CALL EZMXY(XX1,ENER,850,2,850,22HVELOCITY VS. LATITUDES)
1160      300   CONTINUE
1161            CALL AGSETI('X/NI.',-1)
```

```
1162     C
1163     C        PLOT EACH PHASE CHANGE SEPARATELY
1164     C
1165              CALL AGSETF('LABEL/NAME.','L')
1166              CALL AGSETI('LINE/NUMBER.',100)
1167              CALL AGSETP('LINE/TEXT.','PHASE (DEGREES)$',1)
1168              CALL AGSETF('LABEL/NAME.',1HB)
1169              CALL AGSETI('LINE/NUMBER.',-100)
1170              CALL AGSETP(10HLINE/TEXT.,11HTIME (SEC)$,1)
1171              CALL AGSETF('X/MI.',TMIN)
1172              CALL AGSETF('X/MA.',TMAX)
1173              CALL AGSETF('Y/MIN.',0.0)
1174              CALL AGSETF('Y/MAX.',360.0)
1175              CALL AGSETI('LEFT/MAJOR/TYPE.',1)
1176              CALL AGSETF('LEFT/MAJOR/BASE.',60.0)
1177              CALL AGSETI('LEFT/MINOR/SPACING.',5)
1178              DO 122 J=1,12
1179              DO 121 II=1,850
1180              XX1(II)=1.E36
1181       121    ENER(II,1)=1.E36
1182              ICNT=1
1183              ENER(ICNT,1)=PBCARGU(ICNT,J)
1184              XX1(ICNT)=TPB(ICNT)
1185              ICNT=2
1186              DO 123 I=2,505
1187              DIFF=ABS(PBCARGU((I-1),J)-PBCARGU(I,J))
1188              IF(DIFF.LT.180.0) GOTO 124
1189              ENER(ICNT,1)=360.+PBCARGU(I,J)
1190              IF(PBCARGU(I,J).GT.PBCARGU((I-1),J)) ENER(ICNT,1)=
1191            1 PBCARGU(I,J)-360.0
1192              XX1(ICNT)=TPB(I)
1193              ICNT=ICNT+1
1194              ENER(ICNT,1)=1.E36
1195              XX1(ICNT)=TPB(I)
1196              ICNT=ICNT+1
1197              ENER(ICNT,1)=PBCARGU((I-1),J)-360.0
1198              IF(PBCARGU(I,J).GT.PBCARGU((I-1),J)) ENER(ICNT,1)=
1199            1 PBCARGU((I-1),J)+360.0
1200              XX1(ICNT)=TPB(I-1)
1201              ICNT=ICNT+1
1202       124    ENER(ICNT,1)=PBCARGU(I,J)
1203              XX1(ICNT)=TPB(I)
1204       123    ICNT=ICNT+1
1205              CALL AGSETF('Y/MI.',0.0)
1206              CALL AGSETF('Y/MA.',360.0)
1207              CALL EZMXY(XX1,ENER,850,1,850,15HPHASE VS. TIME$)
1208       122    CONTINUE
1209              WRITE(6,101)
1210       101    FORMAT(///' ALL DONE !!')
1211              RETURN
1212              END
1213     C
1214     C
1215              SUBROUTINE EQCONV
1216     C
1217              COMMON DVPA,EQALD,ALGRD,VPA,FVPA(400),SDIST,ALEQ,A,SVPA,FDIST(18
1218            1 0,400),EQAL,FPDIST(130),PI,EM,EL,RPHI,VPE,E,EV,KMAX,VMIN,VPMAX,
1219            2 ALMIN,ALMAX,ALDC(12),R,RO,VPAEQ,EPA,EVDC(12),IG,EPAG(3000)
1220              SF=SQRT(1.+3.*SIN(RPHI)**2)
1221              WPA=EM/2.*VPA*VPA
1222              WPE=EM/2.*VPE*VPE
1223              EV=(WPA+WPE)/E
1224              WPEEQ=WPE/SF/(RO*EL/R)**3
1225              WPAEQ=WPA+WPE-WPEEQ
1226              VPAEQ=SQRT(2.*WPAEQ/EM)
1227              EQAL=ATAN(SQRT(WPEEQ/WPAEQ))
1228              EQALD=EQAL/A
1229              RETURN
1230              END
```

```
1231     C
1232             SUBROUTINE DFUNC
1233     C
1234             COMMON DVPA,EQALD,ALGRD,VPA,FVPA(400),SDIST,ALEQ,A,SVPA,FDIST(18
1235           1 0,400),EQAL,FPDIST(180),PI,EM,EL,RPHI,VPE,E,EV,KMAX,VMIN,VPMAX,
1236           2 ALMIN,ALMAX,ALDC(12),R,RO,VPAEQ,EPA,EVDC(12),IG,EPAG(3000)
1237             COMMON/BLOCK1/ KFDIST(180,400),IFDIST(130,20)
1238     C       IDENTIFY SLOT FOR FVPA AND EQALD
1239             J=INT(EQALD/0.5)+1
1240             ALGRD=J*0.5-0.25
1241             K=INT((VPAEQ-FVPA(1))/DVPA/10)+1
1242             KFDIST(J,K)=KFDIST(J,K)+1
1243             K1=INT((VPAEQ-VMIN)/DVPA)+1
1244             IF((K1.LT.1).OR.(K1.GT.20)) GOTO 4
1245             IFDIST(J,K1)=IFDIST(J,K1)+1
1246           4 CONTINUE
1247             IF (ALEQ.GE.5.5) SDIST=(COS(ALEQ*A)/SVPA)**4
1248             IF (ALEQ.LT.5.5) SDIST=0.
1249             FDIST(J,K)=FDIST(J,K)+SDIST/12.*(FVPA(K)/SVPA)**2*SIN(ALGRD*A)
1250           1 /SIN(ALEQ*A)*(COS(ALEQ*A)/COS(ALGRD*A))**3
1251             RETURN
1252             END
1253     C
1254             SUBROUTINE SUMARY
1255     C
1256             COMMON DVPA,EQALD,ALGRD,VPA,FVPA(400),SDIST,ALEQ,A,SVPA,FDIST(18
1257           1 0,400),EQAL,FPDIST(180),PI,EM,EL,RPHI,VPE,E,EV,KMAX,VMIN,VPMAX,
1258           2 ALMIN,ALMAX,ALDC(12),R,RO,VPAEQ,EPA,EVDC(12),IG,EPAG(3000)
1259             COMMON/BLOCK2/ SFDIST(180),IIAS,IIAF,NVG,ALFALO,ALFAHI
1260           1 ,ALFA(35),JLO,JHI
1261             EMIN=EM/2.*VMIN*VMIN
1262             EMAX=EM/2.*VPMAX*VPMAX
1263             EFMIN=EM/2.*FVPA(1)*FVPA(1)
1264             EFMAX=EM/2.*FVPA(KMAX)*FVPA(KMAX)
1265             EVMIN=EMIN/E
1266             EVMAX=EMAX/E
1267             EVFMIN=EFMIN/E
1268             EVFMAX=EFMAX/E
1269             IF( IG .NE. 1 ) WRITE(6,50)EPA
1270             IF(IG .EQ. 1) WRITE(6,51) EPAG(1)
1271          51 FORMAT(1H1,' EQ PAR E FIELD FOR GENDRIN MODE=',E10.4,' V M-1'//)
1272          50 FORMAT (1H1,' PARALLEL WAVE ELECTRIC FIELD=',E10.4,' VOLT M-1'//)
1273             WRITE (6,6)
1274           6 FORMAT (' INTEGRATION RANGE'//)
1275             WRITE (6,5) VMIN,EMIN,EVMIN
1276           5 FORMAT (' MIN INITIAL VEL=',E10.4,' M SEC-1',3X,E10.4,' JOULES',
1277           1 3X,E10.4,' EV'/)
1278             WRITE (6,4) VPMAX,EMAX,EVMAX
1279           4 FORMAT (' MAX INITIAL VEL=',E10.4,' M SEC-1',3X,E10.4,' JOULES',
1280           1 3X,E10.4,' EV'/)
1281             WRITE (6,3) FVPA(1),EFMIN,EVFMIN
1282           3 FORMAT (' MIN FINAL VEL=',E10.4,' M SEC-1',3X,E10.4,' JOULES',
1283           1 3X,E10.4,' EV'/)
1284             WRITE (6,2) FVPA(KMAX),EFMAX,EVFMAX
1285           2 FORMAT (' MAX FINAL VEL=',E10.4,' M SEC-1',3X,E10.4,' JOULES',
1286           1 3X,E10.4,' EV'/)
1287             WRITE (6,1) ALMIN,ALMAX
1288           1 FORMAT (' INITIAL PITCH ANGLE RANGE=',2F6.2,3X,' DEGREES'/)
1289             DO 60 J=1,180
1290             SFDIST(J)=0.
1291          60 FPDIST(J)=0.
1292             DO 11 J=1,180
1293             DO 10 K=1,KMAX
1294          10 FPDIST(J)=2.*PI*FDIST(J,K)*FVPA(K)**2*DVPA*10+FPDIST(J)
1295          11 CONTINUE
1296             K4=NVG+1
```

```
1297            DO 100 J=IIAS,IIAF
1298            PITCH3=J*0.5+5.25
1299            DO 101 K=1.K4
1300            IF(PITCH3.GT.5.5)  DIST=(COS(PITCH3*A)/(VMIN+DVPA*(K-1)))**4
1301            IF(PITCH3.LE.5.5) DIST=0.
1302            SFDIST(J+11)=2.*PI*DIST*(VMIN+DVPA*(K-1))**2*DVPA+SFDIST(J+11)
1303       101  CONTINUE
1304       100  CONTINUE
1305    C       FINAL PITCH ANGLE DISTRIBUTION FUNCTION
1306            WRITE (6,20)
1307        20  FORMAT(////' FINAL PITCH ANGLE DISTRIBUTION'//' PITCH ANGLE',5X,
1308          1 'NORM DIST FUNCT',8X,'INIT NORM DIST FUNCT'//)
1309            JLO=INT(ALFALO*2)
1310            JHI=INT(ALFAHI*2)+1
1311            IF((IIAS+11).LT.JLO) JLO=IIAS+11
1312            IF(JHI.LT.(IIAF+11)) JHI=IIAF+11
1313            DO 21 J=JLO,JHI
1314            ALGRD=J*0.5-0.25
1315        21  WRITE(6,22) ALGRD,FPDIST(J),SFDIST(J)
1316        22  FORMAT(F7.2,8X,E12.4,8X,E12.4)
1317    C       PRECIPITATED PARTICLE AND ENERGY FLUX
1318            JLOSS=INT(5.25/0.5)+1
1319            PFLUX=0.
1320            EFLUX=0.
1321            DO 31 J=1,JLOSS
1322            DO 30 K=1,KMAX
1323            EQAL=(J*0.5-0.25)*A
1324            ACCUM=FDIST(J,K)*FVPA(K)**2*SIN(EQAL)/COS(EQAL)**3*DVPA
1325          1 *10*0.5*A
1326            PFLUX=PFLUX+ACCUM
1327        30  EFLUX=EFLUX+ACCUM*0.5*EM*(FVPA(K)/COS(EQAL))**2
1328        31  CONTINUE
1329    C       CONVERT FLUXES TO IONOSPHERIC VALUES AT 100 KM
1330            PHII=ATAN(SQRT(6370.*EL/6470.-1.))
1331            FAC=SQRT(1.+3.*SIN(PHII)**2)*EL**3
1332            PFLUX=PFLUX*FAC
1333            EFLUX=EFLUX*FAC
1334            EVFLUX=EFLUX/E
1335            WRITE (6,40) PFLUX,EFLUX,EVFLUX
1336        40  FORMAT (//' PRECIPITATION FLUX=',E10.4,' M-2 SEC-1'//' ENERGY FLUX
1337          1 =',E10.4,' JOULE M-2 SEC-1    OR  ',E10.4,' EV SEC-1')
1338    C       FLUXES ARE NORMALIZED TO F=V**-4
1339            RETURN
1340            END
```

```
      C
            SUBROUTINE DIFCO
      C
            COMMON DVPA,EQALD,ALGRD,VPA,FVPA(4ØØ),SDIST,ALEQ,A,SVPA,FDIST(18
           1Ø,4ØØ),EQAL,FPDIST(18Ø),PI,EM,EL,RPHI,VPE,E,EV,KMAX,VMIN,VPMAX,
           2 ALMIN,ALMAX,ALDC(12),R,RO,VPAEQ,EPA,EVDC(12),IG,EPAG(3ØØØ)
      C     ALDC IS IN RADIANS,ALEQ IN DEG
            S=Ø
            S2=Ø
            CS=Ø
            CS2=Ø
            SS=Ø
            SCS=Ø
            SE=Ø.
            DO 1Ø I=1,12
            S=S+(ALDC(I)-ALEQ*A)/12.
            S2=S2+(ALDC(I)-ALEQ*A)**2/12.
            CS=CS+(COS(ALDC(I))-COS(ALEQ*A))/12.
        1Ø  CS2=CS2+(COS(ALDC(I))-COS(ALEQ*A))**2/12.
            SD=S/A
            S2=SQRT(S2)/A
            WRITE(6,2Ø) S,SD,S2,CS,CS2
        2Ø  FORMAT(//' DEL AL=',E1Ø.4,' RAD  OR  ',F8.3,' DEG',3X,'DEL AL R
           1MS=',E1Ø.4,' DEG',3X,'DEL COS AL=',E1Ø.4,3X,'DEL COS AL SQ=',
           2 E1Ø.4)
            DO 11 I=1,12
            SS=SS+(ALDC(I)-S-ALEQ*A)**2/12.
        11  SCS=SCS+(COS(ALDC(I))-COS(S+ALEQ*A))**2/12.
            SS=SQRT(SS)/A
            WRITE (6,21) SS,SCS
        21  FORMAT (' REFERENCE CHANGED TO AVE SCATTERED PITCH ANGLE',5X,
           1 'DEL AL RMS=',E1Ø.4,5X,'DEL AL COS SQ=',E12.4)
            DO 3Ø I=1,12
        3Ø  SE=SE+EVDC(I)/12.
            WRITE(6,31) SE
        31  FORMAT(' AVE FINAL ENERGY=',E12.6,' EV')
            RETURN
            END
```

REFERENCES

Angerami, J. J., and J. O. Thomas, Studies of planetary atmospheres, 1, the distribution of electrons and ions in the earth's exosphere J. Geophys. Res., 69, 4537, 1964.

Bell, T. F., Wave particle gyroresonance interactions in the earth's outer ionosphere, Tech. Rept. No. 3412-5, Radioscience Lab., Stanford Electronics Labs., Stanford Univ., Stanford, Ca., 1964.

Brice, N. M., Traveling-wave amplification of whistlers, Tech. Rept. No. 7, Radioscience Lab., Stanford Electronics Labs., Stanford Univ., Stanford, Ca., 1961.

Brice, N. M., Discrete VLF emissions from the upper atmosphere, Tech. Rept. No. 3412-6, Radioscience Lab., Stanford Electronics Labs., Stanford, Ca., 1964.

Brinca, A. L., On the stability of obliquely propagating whistlers, J. Geophys. Res., 77, 3495, 1972.

Budden, J. G., Radio Waves in the Ionosphere, Cambridge University Press, Cambridge, England, 1961.

Buneman, O., Class notes for Introduction to Plasma Physics, Stanford University, 1980.

Burtis, W. J., Magnetospheric Chorus, Tech. Rept. No. 3469-3, Radioscience Lab., Stanford Electronics Labs., Stanford, Ca., 1974.

Burtis, W. J., Magnetospheric chorus: Amplitude and growth rate, J. Geophys. Res., 80(22), 3265, 1975.

Dowden, R. L., Geomagnetic noise at 230 kc/s, Nature, 187, 677, 1960.

Dowden, R. L., Theory of generation of exospheric very low frequency noise (hiss), J. Geophys. Res., 67, 2223, 1962.

Dowden, R. L., Trigger delay in whistler precursors, J. Geophys. Res., 77, 695, 1972.

Ellis, G. R. A., Low-frequency electromagnetic radiation associated with magnetic disturbances, Planet. Space Sci., 1, 253, 1959.

Ellis, G. R. A., Directional observations of 5-kilohertz radiation from the earth's outer atmosphere, J. Geophys. Res., 65, 839, 1960.

Gallet, R. M., and R. A. Helliwell, Origin of very low frequency emissions, J. Res. Nat. Bur. Stand., 63D, 21, 1959.

Gurnett, D. A., A satellite study of VLF hiss, J. Geophys. Res., 71, 5599, 1966.

Gurnett, D. A., and L. A. Frank, VLF hiss and related plasma observations in the polar magnetosphere, J. Geophys. Res., 77, 172, 1972.

Helliwell, R. A., Whistlers and Related Ionospheric Phenomena, Stanford University Press, Stanford, Calif., 1965.

Helliwell, R. A., A theory of discrete VLF emissions from the magnetosphere, J. Geophys. Res., 72, 4773, 1967.

Helliwell, R. A., and U. S. Inan, VLF wave growth and discrete emission triggering in the magnetosphere: A feedback model, J. Geophys. Res., to be published in 1982.

Helliwell, R. A., J. P. Katsufrakis, T. F. Bell and R. Raghuram, VLF line radiation in the earth's magnetosphere and its association with power system radiation, J. Geophys. Res., 80, 4249, 1975.

Inan, U. S., Non-linear gyroresonant interactions of energetic particles

and coherent VLF waves in the magnetosphere, Tech. Rept. No. 3414-3, Radioscience Lab., Stanford Electronics Labs., Stanford, Ca., 1977.

Inan, U. S., and T. F. Bell, The plasmapause as a VLF wave guide, J. Geophys. Res., 82, 2819, 1977.

Inan, U. S., and S. Tkalcevic, Nonlinear equations of motion for Landau resonance interactions with a whistler mode wave, J. Geophys. Res., 87, 2363, 1982.

Jorgensen, T. S., Interpretation of auroral hiss measured on Ogo 2 and at Byrd station in terms of incoherent Cerenkov radiation, J. Geophys. Res., 73, 1055, 1968.

Kennel, C. F., and H. E. Petschek, Limit on stably trapped particle fluxes, J. Geophys. Res., 71, 1, 1966.

Kennel, C. F., and R. M. Thorne, Unstable growth of unducted whistlers propagating at an angle to the geomagnetic field, J. Geophys. Res., 72, 871,1967.

Kimura, I., Effects of ions on whistler mode ray tracing, Radio Sci., 1, 269, 1966.

Kimura, I., H. Matsumoto, T. Mukai, K. Hashimoto, T. F. Bell, U. S. Inan, R. A. Helliwell, and J. P. Katsufrakis, Exos-B/Siple station VLF wave-particle interaction experiments: 1. General description and wave-particle correlation, J. Geophys. Res., to be published.

Kumagai, H., K. Hashimoto, and I. Kimura, Computer simulation of a Cerenkov interaction between obliquely propagating whistler mode waves and an electron beam, Phys. Fluids, 23, 184, 1980.

Liemohn, H. B., Radiation from electrons in magnetoplasma, Radio Sci., 69D, 741, 1965.

Lim, T. L., and T. Laaspere, An evaluation of Cerenkov radiation from auroral electrons with energies down to 100 eV, J. Geophys. Res., 77, 4145, 1972.

Maggs, J. E., Coherent generation of VLF hiss, J. Geophys. Res., 81, 1707, 1976.

Mansfield, V. N., radiation from a charged particle spiraling in a cold magnetoplasma, Astrophys. J., 147, 672, 1967.

McKenzie, J. F., Cerenkov radiation in a magneto-ionic medium (with applications to the generation of low-frequency electromagnetic radiation in the exosphere by the passage of charged corpuscular streams), Phil. Trans. Roy. Soc. London, Ser. A, 255,585, 1963.

Nunn, D., Wave particle interaction in electroptatic waves in an inhomogeneous medium, Planet. Space Sci., 6, 291, 1971.

Nunn, D., The sideband instability of electrostatic waves in an homogeneous medium, Planet. Space Sci., 21, 67, 1973.

Northrop, T. G., The Adiabatic Motion of Charged Particles, New York, Interscience Publishers, 1963.

Palmadesso, P. J., Resonance, particle trapping, and Landau damping in finite amplitude obliquely propagating waves, Phys. Fluids, 15, 2006, 1973.

Park, C. G., Methods of determining electron concentrations in the magnetosphere from nose whistlers, Tech. Rept. No. 3454-1, Radioscience Laboratory, Stanford Electronics Labs., Stanford University, Stanford, Calif., 1972.

Park, C. G., and R. A. Helliwell, Whistler precursors: A possible catalytic role of power line radiation, J. Geophys. Res., 82, 3634, 1977.

Ratcliffe, J. A., The Magneto-Ionic Theory and Its Applications to the Ionosphere, Cambridge University Press, Cambridge, England, 1959.

Reeve, G. D., and R. W. Boswell, Parametric decay of whistlers -- A possible source of precursors, Geophys. Res. Lett., 3, 405, 1976.

Reeve, C. D., and M. J. Rycroft, A mechanism for precursors to whistlers, J. Geophys. Res., 81, 5900, 1976.

Schield, M. A., and L. A. Frank, Electron observations between the inner edge of the plasma sheet and the plasmasphere, J. Geophys. Res., 75, 5401, 1970.

Seshadri, S. R., Cerenkov radiation in a magnetoionic medium, Electronics Lett. 3, No. 6, 271, 1967.

Seshadri, S. R., Fundamentals of Plasma Physics, American Elsevier Publishing Co., New York, 1973.

Smith, R. L., Propagation characteristics of whistlers in field-aligned columns of enhanced ionization, J. Geophys. Res., 65, 815, 1960.

Stiles, G. S., and R. A. Helliwell, Stimulated growth of coherent VLF waves in the magnetosphere, J. Geophys. Res., 82, 523, 1977.

Stix, T. H., Theory of Waves in Plasma, McGraw-Hill, New York, 1962.

Swift, D. W., and J. R. Kan, A theory of auroral hiss and implications on the origin of auroral electrons, J. Geophys. Res., 80, 985, 1975.

Taylor, W. W. L., and S. D. Shawhan, A test of incoherent Cerenkov radiation for VLF hiss and other magnetospheric emisions, J. Geophys. Res., 79, 105, 1974.